1-1-2003

An investigation of droplets and films falling over horizontal tubes

Jesse David Killion
Iowa State University

An investigation of droplets and films falling over horizontal tubes

by

Jesse David Killion

A thesis submitted to the graduate faculty

in partial fulfillment of the requirements for the degree of

MASTER OF SCIENCE

Major: Mechanical Engineering

Program of Study Committee:
Srinivas Garimella, Major Professor
Richard H. Pletcher
James C. Hill

Iowa State University

Ames, Iowa

2003

Graduate College
Iowa State University

This is to certify that the master's thesis of

Jesse David Killion

has met the thesis requirements of Iowa State University

Signatures have been redacted for privacy

TABLE OF CONTENTS

ABSTRACT

Liquid films falling over horizontal-tube banks are frequently utilized in absorption heat pumps, heat-driven systems that provide an environmentally and economically attractive alternative to conventional CFC-based vapor compression cycles in certain applications. The widespread application of these systems has faced crucial hurdles due to the lack of a flow-mechanism based, experimentally validated theory for the binary-fluid absorption heat and mass transfer in falling films. This present work aims to advance the understanding of the behavior of falling films in horizontal-tube banks.

A review of the literature was conducted in three areas: mathematical modeling of falling-film absorption, experimental investigations on the performance of horizontal-tube falling-film absorbers, and the dynamics of droplet formation and impact. It was shown that, although mathematical models of falling-film absorption have grown increasingly sophisticated, even the most recent models make significant simplifications regarding the assumed flow patterns and are not capable of reliably predicting absorber performance. It was concluded that a pressing need for the continued progress in this area is improved understanding of the details of the flow patterns, and in particular, the behavior and role of droplets. The experimental investigations into falling-film absorption on horizontal tubes revealed that, though many parameters such as tube diameter and spacing affect absorption rates, the fundamental mechanism by which they do is not well understood. Experimental investigations also pointed to the fact that understanding the film and droplet behavior is key to capturing the effects of the various parameters on performance. A review of droplet formation and impact studies revealed that there are many relevant techniques recently developed for modeling the details of droplet behavior. However, only axisymmetric cases, such as the formation of droplets from capillaries and jets, are generally considered in the literature. Thus the three-dimensional nature of the problem considered here represents an extension to this body of literature.

Flow visualization experiments were conducted on two horizontal-tube banks with water and aqueous Lithium-Bromide flowing in droplet mode using a high-speed, high-resolution digital imaging system. Qualitative analysis of the resulting images identified many of the common features and also illustrated differences between the current case and the axisymmetric cases considered in the literature including droplet stretching along the underside of the tubes and saddle wave formation upon droplet impact. A digital image analysis routine was developed to generate mathematical representations of the shape and location of the liquid-vapor interface throughout a sequence of video frames. This allowed the estimation of droplet volume and surface area versus time. The results showed that both the volume and surface area between tubes steadily rise to a maximum value at the moment of impact, after which steep declines in both occur as the primary droplet joins the film around the tube. After the initial steep decline, a period of slower decay of the thinning liquid bridges

and satellite droplets was shown to be a period when the surface area to volume ratio increases significantly.

Computational models utilizing the Volume-of-Fluid technique were developed and validated for 2D axisymmetric cases and the 3D case of horizontal tubes. The 2D models captured some of the characteristics observed in the flow visualization, but overall qualitative and quantitative agreement was only fair. The three dimensional model of droplet formation under a horizontal tube showed better qualitative and quantitative agreement with the experimental results. Many of the characteristic features, including the elongation of the drop during early formation and the saddle wave generated upon impact were well predicted by the model. Some differences could be observed in the predicted break-up of the liquid bridge. Suggestions for areas of improvement were also given.

ACKNOWLEDGEMENTS

There are many people without whom I would not have been able to complete this thesis; this list is far from exhaustive. I certainly thank my major professor, Dr. Srinivas Garimella, for his tireless guidance, encouragement and insight throughout this and other projects. He has proven to be a sage and devoted mentor. I would be remiss if I did not thank Vikas Patnaik, Kenneth Schultz and the absorption technology group at Trane. They were generous enough to donate the LiBr used in the testing, host me for a visit to see and ask questions about their operations, and respond to several follow-up inquiries. I am grateful for their assistance. I also thank Donald Knarr, Peter Schmitz and Ronald Jones of Motion Engineering for their patience and willingness to help me enter the world of high-speed imaging. I thank Timothy Ernst for his assistance with rendered drawings. I thank my committee members for their time and thoughtful reviews and for the many hours I spent in their classes and struggling with the homework they assigned; their efforts are greatly appreciated. Finally, I thank my family and friends, in particular my mom and dad, Joan and David Killion, and Mirelle Syrja for their love, support and encouragement; I couldn't have done this without them.

This work was funded in part by an NSF Career Grant awarded to Dr. Garimella and in part by an ASHRAE Graduate Student Grant-in-Aid Award.

NOMENCLATURE

Bo	Bond number (see Equation 2.20, 2.25)
C	Molar concentration [kmol/kmol]
Ca	Capillary number (see Equation 2.24)
C_P	Specific heat [kJ/kg-K]
D	Diameter [m]
D_{AB}	Binary diffusion coefficient [m^2/s]
Fr	Froude number (see Equation 2.26)
g	Gravitational acceleration [m/s^2]
h_a	Heat of absorption [kJ/kg, kJ/kmol]
htc	Heat transfer coefficient [W/m^2K]
I	Mass specific enthalpy [kJ/kg]
k	Thermal conductivity [W/m-K]
Le	Lewis number = D_{AB}/α
m	Mass [kg]
$\dot{m}$	Mass flux [kg/m-s]
Nu	Nusselt number = htc D/k
Oh	Ohnesorge number (see Equation 2.23)
Pr	Prandtl number = $\mu/\alpha\rho$
Q	Heat transfer rate [W]
r	Radius [m], radial coordinate
Re	Reynolds number (defined throughout paper)
T	Temperature [K or °C]
t	Time [s]
u	Stream-wise velocity [m/s]
v	Axial velocity or velocity [m/s]
We	Weber number (see Equation 2.24)
x	Axis coordinate [m]
y	Axis coordinate [m]
z	Axes, axial coordinate [m]

Greek Symbols

Γ	Solution mass flux [kg/m-s]
α	Thermal diffusivity [m^2/s], volume fraction [m^3/m^3]
β	Lamella scale factor (see Equation 2.29)
δ	Film thickness
μ	Viscosity [kg/m-s]
ρ	Density [kg/m^3]
σ	Surface tension [N/m]

Subscripts

0	Initial
1	Species 1
2	Species 2
a	Absorber
A	Species A
b	Bulk
B	Species B
c	Condenser, coolant, critical
e	Evaporator
eq	Equilibrium
f	film
g	Generator
i	Impact
in	Inlet
int	Interface
L	Liquid
o	Outer
out	Outlet
v	Vapor

1 INTRODUCTION AND BACKGROUND

The discoveries of recent years have brought significant focus to the development of thermal systems that reduce the environmental impact of space-conditioning machines. According to the most recent Buildings Energy Databook (Office of Energy Efficiency and Renewable Energy, 2003), buildings account for 37% of the total US primary energy consumption, 11% of which (4.0 quads = 4.0×10^{15} Btu = 11.72×10^{11} kWh) is used for space cooling. Combined, the building heat transfer processes (space heating, cooling, water heating and refrigeration) consume 20% (19.8 quads) of the total US primary energy consumption (Office of Energy Efficiency and Renewable Energy, 2003). The potential environmental impacts of the systems utilized in these processes are two-fold. Firstly, since about 75% of the energy used is derived from combusting fossil fuels (Office of Energy Efficiency and Renewable Energy, 2003), there is a significant release of *greenhouse gases* that is essentially proportional to the total energy consumption. Any improvements in the efficiencies of these systems that result in a decrease in energy consumption will lead to a commensurate decrease in the release of greenhouse gases such as CO_2. Secondly, the refrigerants employed in vapor-compression cycles (which currently account for over 99% of the energy consumed for space conditioning), in addition to having a significant global warming potential as greenhouse gases, are also suspected to act as catalysts that *destroy stratospheric ozone* (Takle, 2003), a crucial component of the atmosphere which protects living organisms from deadly ultraviolet (UV) radiation. One free chlorine atom from a CFC refrigerant can destroy up to 100,000 ozone molecules because the chlorine atom remains free after the reaction. Thus, moving from CFC-based space-conditioning systems to systems that utilize environmentally benign refrigerants may help ameliorate the ozone depletion problem.

Absorption heat pumps are environmentally sound and energy-efficient alternatives to CFC-based space-conditioning systems; they provide a means of achieving improved energy utilization (decreased greenhouse gas emissions) while eliminating the need for potentially ozone-depleting refrigerants. Instead of using electricity or shaft work to drive the cycle, absorption systems can utilize so-called waste heat from other thermodynamic cycles such as power generation systems. At the exit of a power generation cycle, the combustion products contain a significant amount of energy, however the availability is generally too low for cost-effective use in further power generation. Absorption heat pumps are ideally suited to recover a significant portion of this waste heat energy, thus improving energy utilization by both recovering energy that would have otherwise been wasted and reducing the demand for electricity or shaft energy. In doing so, absorption systems provide economically valuable commodities: either space conditioning or refrigeration, or thermal energy at a higher temperature (temperature boosting/amplification) (Herold *et al.*, 1996). However, while absorption heat pump concepts are thermodynamically attractive and use environmentally benign fluids, their widespread application has faced crucial hurdles due to the lack of a flow-mechanism

based, experimentally validated theory for binary-fluid absorption heat and mass transfer in falling films (Meacham and Garimella, 2002), described further below. Most absorption systems available today are economically practical only for large-scale applications such as hospitals, universities, and industrial sites. Systems developed to be effectively utilized in new applications such as Integrated Energy Systems (IES, also known as Building Cooling Heating and Power, BCHP, and Combined Heat and Power, CHP) could have a profound positive effect on the environmental impact of space-conditioning (Jalalzadeh-Azar, 2003).

1.1 Application Description: The Absorber in Absorption Heat Pumps

The most critical component that determines the overall cost, size, and performance of an absorption heat pump is the absorber; the most effective absorber designs utilize a bank of cooled horizontal tubes over which a binary liquid film falls and absorbs the entering refrigerant vapor. As will be shown in subsequent sections through a review of the literature, current understanding of the complex coupled momentum, heat, and mass transfer problem of absorption on films falling over horizontal tubes is only rudimentary. Improving the understanding of the **motion of the film and droplets** and its effects on the heat and mass transfer processes is the key to developing cost- and energy-efficient absorption heat pump components. The basic configuration and working principles of an absorption heat pump are given below.

The simplest absorption cycle (single-effect) is shown schematically in Figure 1.1. There are thermodynamic advantages of more complex (e.g. double- and triple-effect) cycles, however system cost increases with complexity, and other issues such as corrosion and the requirement of higher temperature heat input also come into play. The book by Herold et al. (1996) and the ASHRAE Handbook (ASHRAE, 1997) provide more information about cycle design and analysis. The basic principle of all absorption systems is the same and is based on the thermodynamic properties of a binary fluid pair (two substances that have a strong affinity for each other and differing volatility). The most common fluid pairs are ammonia/water (NH_3/H_2O) and water/lithium-bromide (H_2O/LiBr); lithium bromide is a compound with ionic bonding like salt. In an ammonia/water system, ammonia is more volatile and thus is the refrigerant and water is the absorbent; in a water/LiBr system, water is the refrigerant and aqueous LiBr is the absorbent.

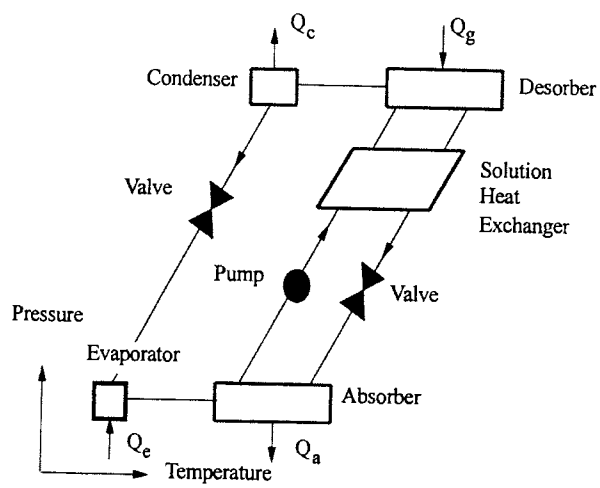

Figure 1.1 Schematic of Single-Effect Absorption Cycle (Herold *et al.*, 1996)

Water/LiBr systems comprise the primary focus of the present work. Figure 1.1 illustrates the four basic components of the cycle: the absorber, the desorber, the condenser, and the evaporator. The temperatures required for heat transfer in the condenser, evaporator, absorber, and desorber are set by external temperatures that essentially fix the temperature/pressure conditions within each of these components based on the fluids employed. The relative positions in Figure 1.1 give an indication of the relative temperatures and pressures within each component. An absorption system conceptually has several components in common with a standard vapor compression cycle; the condenser, expansion valve, and evaporator play the same role. However the compressor is replaced by the absorber, the desorber, a solution pump, a solution heat exchanger, and a solution expansion valve. The basic operation of the cycle can be understood by considering the circuits of the refrigerant and absorbent within the system. Starting at the desorber, a refrigerant-rich solution of refrigerant and absorbent is heated at a high pressure using the heat input to the system (waste-heat, natural gas and solar inputs are also possible). As the mixture is heated, the refrigerant vapor is generated as it preferentially evaporates from the solution mixture and flows into the condenser as a high-pressure, high-temperature vapor leaving a refrigerant-weak liquid solution in the desorber. In the condenser, heat is transferred to the surrounding ambient environment causing the refrigerant to condense. The condensed refrigerant then passes through an expansion valve into the low-pressure evaporator. The change in thermodynamic state through the valve causes the refrigerant temperature to drop and thus heat can be transferred from the air-conditioned or refrigerated space to the refrigerant causing the refrigerant to evaporate. After evaporation, this low-pressure, low-temperature vapor then flows into the absorber. The solution that had been stripped of refrigerant in the desorber by the heating process flows through an expansion valve into the low-pressure absorber where it is typically distributed over a bank of internally cooled tubes as a falling film. Due to the affinity between the absorbent and the refrigerant, the refrigerant vapor will absorb (condense) into the film of refrigerant-weak absorbent solution. At the outlet of the absorber, liquid solution now rich in refrigerant is pumped back up to a high pressure in the desorber. The solution heat exchanger preheats this incoming solution using the flow of hot liquid exiting the desorber. It should be noted that the energy required to pump the liquid is generally less that 1% of the energy required to drive the system (Q_g in Figure 1.1); this contrasts with the energy required to directly compress a vapor (in vapor-compression systems) where the pump-work is the primary energy input.

Several configurations are possible for absorbers; however, gravity-driven films falling over internally-cooled horizontal tubes have significant advantages. First, in H_2O/LiBr systems, the evaporator and absorber operate at an absolute pressure around 1 kPa (0.01 atm). The vapor has a high specific volume at this pressure and any pressure drop associated with flow through the absorber results in an increased evaporator pressure and, therefore, an increased evaporation temperature, which has a negative impact on cycle efficiency and heat transfer. Because falling films are gravity driven, there is no need for an elevated pressure at the inlet of the absorber, thus minimizing the

temperature in the evaporator. Second, a film of liquid has the potential for high heat and mass transfer rates due to the short characteristic length (small film thickness) in the direction of the transfer processes. Third, distribution as a film over a bank of tubes provides a large amount of interfacial surface area between the liquid and vapor and between the liquid and tube walls. Finally, the formation of droplets pendant underneath the tubes, the subsequent detachment, fall, and impact have the effect of mixing the film between each row of tubes as well as generating significant waviness on the film surrounding the tubes, thus augmenting transfer rates versus a smooth laminar film. Consequently, absorbers comprised of internally-cooled horizontal-tube banks are favored in practice due to their ability to provide high transfer rates with minimal pressure drop.

The absorption process causes the temperature and refrigerant concentration of the solution to increase at the interface. The heat released as the vapor is absorbed into the liquid film is removed by the coolant flowing through the tubes. Thermodynamic equilibrium at the interface (a coupled boundary condition), the temperature and heat transfer coefficient within the tube, and the fact that no mass diffusion takes place through the tube walls provide the boundary conditions for the temperature and concentration gradients that drive the heat transfer and mass transfer processes, respectively. Figure 1.2 illustrates representative velocity, temperature, and concentration profiles for the case of smooth laminar flow (for clarity of illustration) around a section of a horizontal tube (note that, as is typically done in practice with H_2O/LiBr systems, the concentration is shown in terms of absorbent concentration which decreases at the interface due to absorption and is essentially 0 in the vapor phase because of the extremely low vapor pressure of LiBr). As noted on the figure, the equilibrium

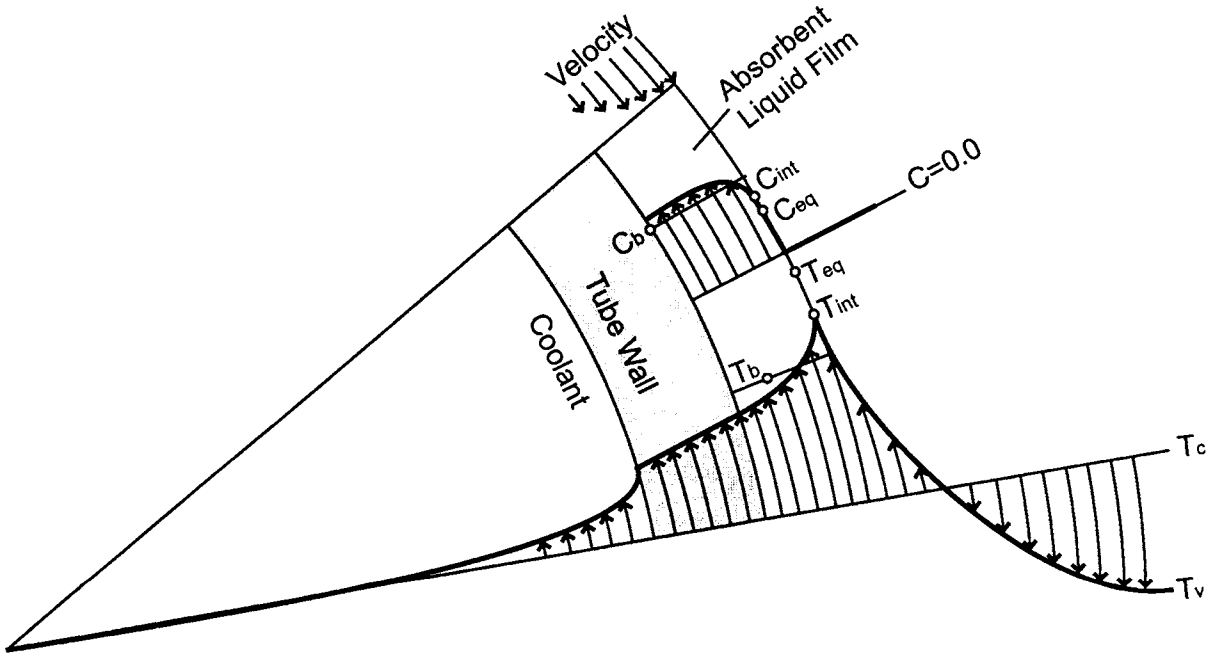

Figure 1.2 Velocity, Temperature, and Concentration Profiles in Smooth Laminar Film Around a Hoirzontal Tube (not to scale), (Killion and Garimella, 2003b)

temperature and concentrations ("eq" subscript) calculated using the local bulk concentration and temperature ("b" subscript), respectively, will differ from the actual conditions at the interface ("int" subscript). The implications of this in determining heat and mass transfer coefficients will be discussed in later sections.

1.2 Motivation

The absorber is a major component in absorption heat pumps. It must perform heat and mass transfer with relatively low driving temperature differences. It has been called the "bottleneck" (Beutler *et al.*, 1996b) in many systems and, thus, is the subject of this research. Improved understanding of the processes inside the absorber component will allow effective designs to be developed for applications that are currently untapped by absorption heat pump machines, which, in turn, could have a significant mitigating impact on the global change problem. Developing this understanding, however, is not trivial; in addition to being coupled by thermodynamic equilibrium at the interface, the heat and mass transfer processes depend heavily on the details of the fluid behavior (flow patterns, interfacial area) in an analogous way to heat transfer in a convection or condensation problem. Thus, ***understanding the flow mechanisms*** within the absorber is a necessary foundation for accurately predicting heat and mass transfer rates Figure 1.3 suggests many of the typical flow features encountered in practice including droplet formation and impact and film waviness. As will be illustrated in the literature review, most absorber models have been developed assuming simplified flow patterns which cannot capture the complex, interrelated effects of absorber design and operating conditions on absorber performance. In addition, experimental results available in the literature frequently appear in conflict because information is reported only at inlets and outlets instead of throughout the absorber, one transfer process is considered without regard for the other, interacting

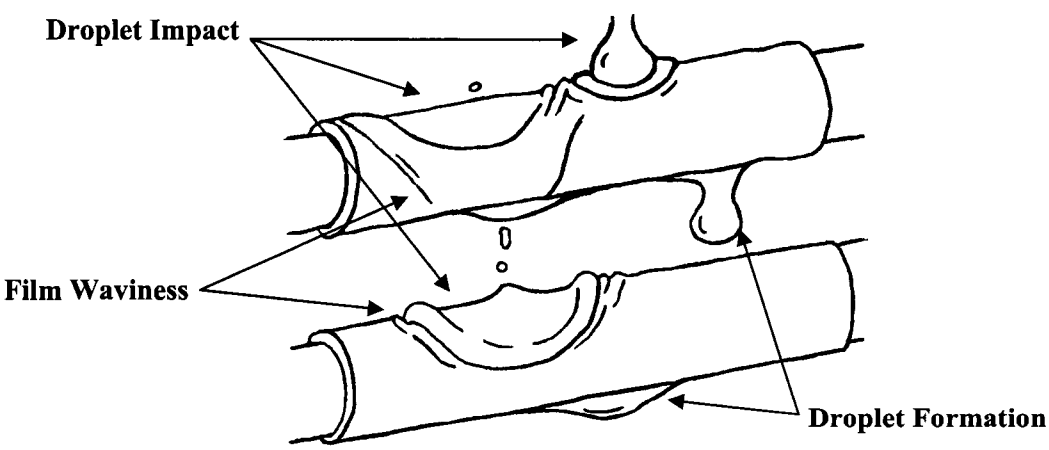

Figure 1.3 Illustration of Flow Patterns Encountered in Horizontal-Tube Absorbers

process parameters are varied one-at-a-time without consideration of combined effects, and the details of the flow patterns are neglected. Before models and empirical understanding can be advanced, a thorough understanding of the flow patterns and their effects on the transfer processes within the absorber must be established.

1.3 Objectives

The scope of the problem outlined above is extensive. To develop a tractable scope for the current project, the following key objectives were established:

- Conduct an extensive critical review of the literature to identify the path of development of models and empirical understanding, the current state-of-the-art, and the key areas where future research should be concentrated. This effort has been reported in Killion and Garimella (2001; 2003c).
- Experimentally identify and analyze overlooked fluid dynamics phenomena using high-speed flow visualization of water and LiBr solutions on a single-column horizontal-tube bank. Some of the results of this effort have been reported in Killion and Garimella (2002; 2003b; 2003a).
- Create and validate transient, laminar, two-phase CFD models of droplets and falling films. This work began with axisymmetric (2-D) models of droplets emerging from capillary tubes, which could be validated with models and experimental data from the literature. A 2-D model more similar to horizontal tubes was then considered, and finally a fully 3-D model of a horizontal-tube bank was developed and compared with the above-mentioned experimental results.

The results of this work are intended to provide an incremental step forward toward the goal of a thorough understanding of falling-film absorption.

2 LITERATURE REVIEW

As the key component, the absorber has received considerable attention in the literature; however, only recently have the role of droplets and the actual flow patterns in horizontal-tube absorbers been considered in any detail (Kirby and Perez-Blanco, 1994; Jeong and Garimella, 2002; Killion and Garimella, 2003b). The next two sections summarize the results of a literature review of both the efforts to mathematically model the absorption process and the attempts to measure process parameters experimentally. A summary of these reviews is presented here. Additional details are available in Killion and Garimella (2001; 2003c).

2.1 Mathematical Modeling of Absorption on Horizontal Tubes

Mathematical modeling of the absorber requires simultaneously solving a coupled heat and mass transfer problem in the presence of complex geometry and flow phenomena. Figure 1.2 shows a simplified representation of absorption on a falling film around a horizontal tube. In general, a large range of film Reynolds numbers may be used in absorbers. Droplet formation, film waviness and turbulence, vapor shear and a variety of other phenomena can complicate the problem through their effects on the fluid dynamics. The film flow direction is generally downward; however the vapor flow and coolant flow directions depend on the design of the absorber. Typically, the coolant is in counter- or cross-flow with the solution for vertical and horizontal tubes, respectively. The vapor migrates toward the liquid, across the interface and into the film; in addition it may be in general co- or counter-flow with the film.

Heat and mass transfer for a differential control volume can be described by the following conservative equations (in two spatial dimensions and one temporal dimension):

$$\rho\left(\frac{\partial i}{\partial t}+u\frac{\partial i}{\partial x}+v\frac{\partial i}{\partial y}\right)=\frac{\partial}{\partial x}\left(k\frac{\partial T}{\partial x}\right)+\frac{\partial}{\partial y}\left(k\frac{\partial T}{\partial y}\right) \tag{2.1}$$

$$\left(\frac{\partial C_A}{\partial t}+u\frac{\partial C_A}{\partial x}+v\frac{\partial C_A}{\partial y}\right)=\frac{\partial}{\partial x}\left(D_{AB}\frac{\partial C_A}{\partial x}\right)+\frac{\partial}{\partial y}\left(D_{AB}\frac{\partial C_A}{\partial y}\right) \tag{2.2}$$

assuming only two species, A and B, exist within the system and the mass densities of the two phases are constant (see (Bird *et al.*, 1960), p. 557). Here i represents the mass specific enthalpy, T the temperature, C the molar concentration of the subscripted species, u and v the velocity components in the x and y directions, and k and D_{AB} is the binary mass diffusivity. The above equations also assume negligible dissipation effects, pressure gradients, transport of mass due to energy fluxes (thermal diffusion or Soret effect, see (Bird *et al.*, 1960)), transport of energy due to mass fluxes (Dufour effect, see (Bird *et al.*, 1960; Delancey and Chiang, 1968)), and transport of energy due to interdiffusion (see (Grossman and Gommed, 1997; Gommed *et al.*, 1999)).

The coupling between these equations is realized through three boundary conditions at the interface between the liquid film and the vapor. First, thermal equilibrium:

$$T_{v,int} = T_{L,int} \tag{2.3}$$

which says that the temperature at the interface must be continuous through the vapor and liquid phase. Second, in almost all cases, investigators assume that vapor pressure equilibrium prevails at the interface; that is, whenever contact is established between the liquid and the vapor, the concentrations at the interface adjust such that the *vapor* pressure of each species in the film at the interface is equal to the *partial* pressure of each species in the vapor at the interface and the temperature of the liquid film at the interface is equal to the temperature in the vapor at the interface. The differences between the equilibrium concentrations at the interface and the bulk concentrations in the two phases induce the concentration gradients that drive the mass transfer processes. This equilibrium boundary condition is typically expressed as:

$$P_v = f\left(T_{L,int}, C_{A,int}\right) \tag{2.4}$$

which relates the interface temperature in the liquid, $T_{L,int}$, and interface concentration in the liquid, $C_{A,int}$, to the vapor pressure, P_V. The function, f, depends on the particular fluids under consideration.

The third coupling boundary condition is an energy balance at the interface. As mass is transported across the interface, it must change phase and join a mixture with different relative concentrations. The change in enthalpy from the vapor state to the solution state (generally called the heat of absorption) is released at the interface causing the interface temperature to rise.

$$h_{abs}\dot{m}_B = k\left.\frac{\partial T}{\partial y}\right|_{int} \tag{2.5}$$

where h_a is the molar specific heat of absorption (a function of P_v, $C_{A,int}$ and $T_{L,int}$) and $\dot{m}_B$ is the molar flux of absorption at the interface. The heat release at the interface generates temperature gradients in both the solution and vapor which drive the heat transfer processes; this can be seen in Figure 1.2. In addition, the temperature of the interface affects the interface concentration through the chemical equilibrium condition; as the temperature increases, the gradients driving the mass transfer processes decrease. Thus, the heat and mass transfer processes are inextricably linked. Summarizing this, Ruheman (1947) wrote "it is not possible to calculate an absorber completely without taking both transfer coefficients into account, however different their initial roles ... may appear to be at the outset".

The earliest efforts to model absorption in falling films that accounted for the coupling of the heat and mass transfer processes, essential where the heat of absorption is significant as in absorption heat pumps, were focused on the idealized situation of water vapor in contact with an aqueous lithium bromide film of uniform thickness with uniform stream-wise velocity on an isothermal vertical plate

(Nakoryakov and Grigor'eva, 1977). Subsequently, investigators have attempted to include more realistic flow characteristics in their models such as parabolic velocity profiles for laminar films, turbulent eddy profiles for turbulent films, and transient film thickness and velocity profiles for wavy-laminar films; however, even the most sophisticated of these models still includes many simplifying assumptions as will be discussed in detail below. Nevertheless, significant work has been done in this area which provides a strong basis for continued development.

Because lithium bromide is essentially nonvolatile, the vapor is pure in the absence of non-absorbable gases and so there is no resistance to mass transfer in the vapor phase. This simplifies the problem somewhat compared to the case of ammonia/water where mass transfer in the vapor phase is not trivial (see (Killion and Garimella, 2001) for a review of models of ammonia/water absorption). Many models of horizontal-tube absorption are essentially adaptations of models developed for vertical-film (flat-plate or tube) absorbers. Also, the history of the modeling effort begins with vertical-films. Thus vertical tube models are included in the review that follows. The models found in the literature generally fall into four groups: laminar smooth film, laminar wavy film, turbulent film, assumed transport coefficients. With assumed transport coefficients, the details of the film motion are assumed implicitly in the form of the correlations for the transport coefficients utilized in the analysis. The case of turbulent films is not particularly applicable when horizontal tubes are utilized. Turbulent films, associated with high mass flow rates of the liquid, are seldom used in practice despite their potentially high transfer coefficients. Other considerations such as maximizing film surface area for a given liquid inventory, maximizing the concentration change in the absorber, avoiding flooding, and maintaining low vapor shear generally preclude their use. Thus, discussion of turbulent films is omitted here; the interested reader may refer to (Killion and Garimella, 2001).

2.1.1 Laminar Smooth Film Assumption

By far, the largest number of models in the literature fall into this category in spite of its extremely limited usefulness. Due to the inherent instability of falling films and/or the presence of droplets, waves invariably develop on the films even at extremely low flow rates. Nevertheless, the smooth film assumption lends itself to mathematically tractable problems that can be solved more readily than more realistic cases. Nakoryakov and Grigoryeva (Grigoryeva and Nakoryakov, 1977; Nakoryakov and Grigoryeva, 1977) consider the case of steady absorption in a smooth laminar film falling down an isothermal, impermeable vertical plate. The list of assumptions they employ is quite long, but many are still currently used and will be enumerated below:

- Temperature equilibrium is instantaneously realized at the liquid-vapor interface, ensuring a continuous temperature field throughout the two phases.
- Vapor pressure equilibrium is instantaneously established at the liquid-vapor interface and prevails along the entire interface. This chemical equilibrium assumption establishes the interface concentrations via continuity of the vapor pressure of each species at the interface

temperature, which is analogous to the enforcement of continuous temperature throughout the two contacting phases.

- All thermophysical properties of the solution and vapor can be considered constant. That is, the effect of temperature and concentration on properties such as thermal conductivity, specific heat, density, viscosity, diffusivity, and the heat of absorption is negligible. This assumption allows, among other things, the terms D_{AB} and k in the governing partial differential equations to be factored out of the differential terms. Equations (2.1) and (2.2) can therefore be simplified to the following form:

$$u\frac{\partial T}{\partial x} + v\frac{\partial T}{\partial y} = \alpha\frac{\partial^2 T}{\partial x^2} + \alpha\frac{\partial^2 T}{\partial y^2} \tag{2.6}$$

$$u\frac{\partial C_A}{\partial x} + v\frac{\partial C_A}{\partial y} = D_{AB}\frac{\partial^2 C_A}{\partial x^2} + D_{AB}\frac{\partial^2 C_A}{\partial y^2} \tag{2.7}$$

- Diffusion and thermal conduction in the stream-wise direction are negligible. This common assumption is well justified by comparing the rate of diffusion/conduction to transport due to motion in the stream-wise direction. Letting the x-direction be the direction of flow, this yields the following simplifications:

$$u\frac{\partial T}{\partial x} + v\frac{\partial T}{\partial y} = \alpha\frac{\partial^2 T}{\partial y^2} \tag{2.8}$$

$$u\frac{\partial C_A}{\partial x} + v\frac{\partial C_A}{\partial y} = D_{AB}\frac{\partial^2 C_A}{\partial y^2} \tag{2.9}$$

- Due to the low velocity associated with absorption, the transverse velocity, v, is negligible, therefore:

$$u\frac{\partial T}{\partial x} = \alpha\frac{\partial^2 T}{\partial y^2} \tag{2.10}$$

$$u\frac{\partial C_A}{\partial x} = D_{AB}\frac{\partial^2 C_A}{\partial y^2} \tag{2.11}$$

- Also, because the anticipated absorption rates are low compared to the solution flow rate, changes in the film thickness are negligible.
- Either the net mass flux in the transverse direction is zero or the concentration of water in the solution is very low. Fick's First Law of Binary Diffusion can be written:

$$\dot{m}_A - C_A(\dot{m}_A + \dot{m}_B) = -\rho D_{AB}\frac{\partial C_A}{\partial y} \tag{2.12}$$

where component A corresponds to lithium bromide and B to water (Bird et al., 1960). However, close examination of the equations reveals that Nakoryakov and Grigoryeva apparently assume:

$$\dot{m}_B = \rho D_{AB} \frac{\partial C_A}{\partial y} \tag{2.13}$$

which is only true if $\dot{m}_A = -\dot{m}_B$ or if $C_A = 1$ and $C_B = 0$. If $\dot{m}_A = -\dot{m}_B$, there is equal and opposite mass flux of lithium bromide and water across the interface, often described as counter- or equimolar-diffusion. If $C_A = 1$ and $C_B = 0$, the film is composed of pure lithium bromide and infinitely dilute in water. Neither of these assumptions is well justified given the solubility limits and low volatility of LiBr. Because of their equivalence, the terms infinite water dilution and equimolar diffusion can used interchangeably.

- The velocity in the laminar film is uniform (see Grossman, 1983; Nakoryakov and Grigoryeva, 1992; Brauner et al., 1989; and Wassenaar and Westra, 1992 for discussion).
- The pressure is constant at all points within the absorber; consequently the interface equilibrium concentration in the film is purely a function of interface temperature. For the range of temperatures encountered, this relationship is approximately linear: $C_i = aT_i + b$; where a and b are constants (see, for example, Grossman, 1983; Ibrahim and Vinnecombe, 1993 for discussion).
- Heat transfer to the vapor is negligible; all the energy released during absorption goes into heating the liquid film (see Habib and Wood, 1990 for discussion). This assumption is questionable since the vapor enters the absorber at a much lower temperature than the solution; however, given the low heat capacity and typically low heat transfer coefficients of the vapor phase, the effect of this assumption on the overall results is probably small.
- The inlet solution concentration and temperature profiles are uniform.

Other ancillary assumptions include complete wetting of the isothermal wall, no shear or surface tension effects at the solution-vapor interface, no buoyancy, natural convection or inertia forces, and no slip or concentration gradients at the wall.

Using these simplifying assumptions, Nakoryakov and Grigoryeva (1977) provide a solution using Fourier separation of variables techniques. Evaluation of the solutions requires the determination of a large number (40-50) of eigenvalues for the series solution to converge. Nevertheless, expressions for temperature and concentration throughout the vertical film, heat transfer at the wall and solution-vapor interface, and average film temperature and concentration are presented. An interesting conclusion of their work is that besides the boundary conditions (solution inlet concentration and temperature, wall temperature, and the equilibrium constants), the solution for this particular case depends only on four non-dimensional parameters:

- the Lewis number, $Le = D_{AB}/\alpha$, which is the ratio of mass diffusivity to thermal diffusivity,
- the Prandtl number, $Pr = \nu/\alpha$, which is the ratio of kinematic viscosity to thermal diffusivity,

- the Reynolds number, $Re = 4u\delta/\nu$, where δ is the film thickness, or Peclet number, $Pe = RePr/4$, and
- the dimensionless group $h_a a/C_P$, where h_a is the heat of absorption, a is a constant from the equilibrium relation (dimension T^{-1}), and C_P is the solution specific heat.

Noting the complexity of using the resulting analytical solution, Nakoryakov and Grigoryeva (1977) also develop approximate solutions. The basis for this method is the use of two more simplifying assumptions. First, it is assumed that the temperature profile in the film is linear, i.e. conduction dominates convection, or $\partial^2 T/\partial y^2 = 0$. Second, the concentration profile is assumed based on an approximate boundary layer solution. As a result, much simpler expressions for the interface and average temperatures and concentrations, and heat fluxes are developed. These solutions are only valid where the preceding two assumptions hold, which is generally far downstream from the inlet, but not so far that the concentration profiles deviate from the boundary layer solutions. By comparing these solutions with the exact analytical solutions as a function of non-dimensional downstream position (Grigoryeva and Nakoryakov, 1977), the authors show that local absorption rates predicted using the approximate method are generally lower than those from the exact solution, and the predicted interface conditions become increasingly divergent closer to the film inlet.

Nakoryakov and Grigoryeva (1980; 1980) also develop a simplified solution that is appropriate for the region near the inlets with a slight modification to the assumed velocity profile: within the thermal boundary layer developing from the isothermal wall, it is assumed that the velocity profile varies linearly but is uniform elsewhere. With these assumptions Nakoryakov and Grigoryeva develop expressions for temperatures, concentrations, and heat and mass fluxes throughout the film from the inlet to the point where the growing boundary layers meet which, the authors suggest, is about 75 times the film thickness for typical operating conditions inside a water-lithium bromide absorber. Beyond this length, the thermal boundary layers from the interface and wall meet and the temperature profile becomes predominantly linear allowing the use of the approximate solutions presented in (Nakoryakov and Grigor'eva, 1977). It is interesting to note that, within the developing boundary layer region, the interface temperature and concentration remain constant at the equilibrium values derived from the inlet conditions.

Later Nakoryakov and Grigoryeva (1992) compare the interface temperatures and concentrations predicted by the previously developed analytical (Grigoryeva and Nakoryakov, 1977) and approximate solutions (Nakoryakov and Grigor'eva, 1977, 1980; Nakoryakov and Grigor'yeva, 1980). Additionally, they compare their results to those of Grossman (1983) which will be discussed in detail later but are essentially an extension of the problem to include a fully developed parabolic velocity profile in the film. In the initial region, all three solutions have the same interface temperature and concentration because the cooling effect of the wall does not reach the interface; the interface conditions are determined by the inlet conditions. Just after the thermal boundary layers meet, the

divergence between the solutions becomes the greatest. Finally, all three solutions converge to the same asymptotic value downstream. Although the differences are not quantified, Nakoryakov and Grigoryeva (1992) claim "the comparison of these results with the exact solutions make it clear that for engineering calculations these simple formulae are quite acceptable."

Nakoryakov and Grigoryeva (1995) relax the assumption that film thickness is constant and allow it to vary with absorbed mass. The problem is again solved in two parts: the developing boundary layer region and the region with a fully developed temperature profile. In the initial region, the solution remains almost unchanged; the interface temperature, and consequently concentration, remain constant while the thermal boundary layers are developing. However, the absorption rate is highest in this region which leads to the highest rate of film thickness growth. Even so, according to the authors, the effect of the film growth on the transport processes is small since the film thickness only changes by a few percent. It is shown that typical film thickness growth is small (<10%) even for relatively large downstream distances. The differences in interface concentration predicted using the approximate solutions with and without variable film thickness are shown to be quite small.

Grossman (1983) uses many of the same simplifying assumptions as Nakoryakov and Grigoryeva (1977). He solves the equations:

$$u\frac{\partial T}{\partial x} = \alpha\frac{\partial^2 T}{\partial y^2} \tag{2.14}$$

$$u\frac{\partial C_A}{\partial x} = D_{AB}\frac{\partial^2 C_A}{\partial y^2} \tag{2.15}$$

for a constant thickness film falling down a vertical adiabatic or isothermal wall. The main difference is that Grossman assumes the fully developed, laminar, Nusselt solution for the velocity profile:

$$u(y) = \frac{3}{2}\bar{u}\left[2\left(\frac{y}{\delta}\right) - \left(\frac{y}{\delta}\right)^2\right] \tag{2.16}$$

where $\bar{u}$ is the average stream-wise velocity. Another condition Grossman uses is that, for the isothermal case, the temperature of the film at the inlet is equal to the wall temperature. Therefore no thermal boundary layer develops from the wall, and the only boundary layer development is inward from the liquid-vapor interface.

Grossman gives some additional justification for two of the assumptions he shares with Nakoryakov and Grigoryeva. He cites justification for using a linearized model for the equilibrium relationship between interface concentration and temperature in a prior work (Grossman, 1982) and states "the validity of the linear relation was checked for two common absorbents, LiBr-H_2O and LiCl-H_2O, and found to be very good under the above limitations for a wide range of temperatures and concentrations". He also points out that the assumption of constant heat of absorption is quite reasonable because its dependence on concentration and temperature is "very weak". This is

presumably because the phase-change enthalpy of the refrigerant at typical absorber pressures, typically around 2500 kJ/kg-K, is the dominant term in the heat of absorption.

Grossman uses both the Fourier method as Nakoryakov and Grigoryeva (1977) and a numerical technique based on finite difference methods. He notes that the assumptions of uniform inlet concentration profile and interface equilibrium together are contradictory and therefore form a discontinuity at the film interface at the inlet. Consequently, he develops a similarity solution that can be used near the inlet (for the range where the thermal effect of the wall does not reach the interface and thus the interface temperature and concentration are constant) where both the numerical and analytical solutions are difficult to obtain similar to Nakoryakov and Grigor'eva (1980; 1980). In his review of heat and mass transfer in falling films (Grossman, 1986), he also points out that in this region, the situation "is adequately described by Higbie's penetration theory, as confirmed experimentally by Emmert and Pigford (1954)." The results of the numerical and analytical solutions are reported to be "in excellent agreement." According to Grossman the assumption of uniform velocity profile leads to a 40% underprediction of the length required to achieve a certain temperature or concentration level (i.e. degree of concentration boundary-layer development) and a 20% deviation in predicted heat and mass transfer coefficients. Grossman (1987) uses essentially the same assumptions as above except that the term for change in energy due to interdiffusion is retained in the governing energy equation. For low Lewis numbers, typical of LiBr systems, the effect of interdiffusion is shown to be small.

Andberg and Vliet (1983) utilize a finite difference formulation to solve the absorption problem for a laminar film falling down a vertical, isothermal wall. Although most of the assumptions are the same as those used by the investigators mentioned above, there are several noteworthy differences. First, the change in energy due to interdiffusion is not neglected. They also assume a fully developed, parabolic stream-wise velocity profile and allow the film thickness, flow-rate and velocity to increase as vapor is absorbed. A coordinate transformation is utilized to fit a "rectangular" solution domain to the thickening film. Interface equilibrium is assumed, but the formulation for this is not linearized as above. Instead, the relationship given in (McNeely, 1979) is used. Andberg and Vliet also give further justification for the assumption that there is no heat transferred from the liquid to the vapor by noting the large difference in the thermal conductivity of the two phases and the fact that the vapor phase generally moves toward the interface as absorption occurs. Comparisons are made with the experimental data of Burdukov et al. (1979). Generally concentrations and temperatures agree within experimental error except close to the solution inlet where the predicted heat and mass transfer rates are the highest. They suggest that the isothermal wall assumption may be inappropriate in this region: "in reality, the heat transfer resistance to the cooling water prevents this high heat flux, and thus the absorption and the change in concentration near the inlet are much more gradual" than predicted.

Andberg and Vliet (1986; 1987a) are perhaps the first to develop a specialized solution for the horizontal tube case. They extend the numerical techniques utilized in the above work to the case of a

bank of tubes using a coordinate system fit to the shape of the film around the tube. The hydrodynamics of the solution flowing over the tubes is treated in great detail but they still make some key assumptions. First, the flow between successive tubes is assumed to be a planar sheet that falls at the speed resulting from free-fall between the tubes. They assume that the flow between tubes does not contribute to the absorption process in any way. Although the authors admit that drop-wise flow or isolated columnar jets between the tubes would be more likely at the solution flow rate considered, they suggest that the planar jet is the best approximation that allows a 2-D solution to the problem. Second, it is assumed that within the planar sheet, the solution is well mixed, resulting in uniform temperature and concentration within the film at the top of each tube. Third, to solve the hydrodynamics of the region where the planar jet transitions to the horizontal tube surface, boundary layer approximations of the Navier-Stokes equations are applied assuming constant properties; it is noted that this turning-jet region accounts for less that 0.1% of the entire solution domain. The thermophysical properties in all other regions depend on the local composition and temperature within the film, although boundary layer forms of the Navier-Stokes equations are still used. Another change justified by the results of their vertical wall model is that the authors neglect the transport of energy due to interdiffusion. Also, the assumption of infinite dilution of water in the film is eliminated by using the expression:

$$\dot{m}_B = \frac{\rho D_{AB}}{C_A} \frac{\partial C_A}{\partial y} \tag{2.17}$$

Results from the models are given for one operating condition with three different solution inlet temperatures (46, 39, and 32°C). The tubes have a 19-millimeter (0.75-inch) OD. The heat transfer model extends through the wall and to a cooling medium (water) with a constant temperature (30°C) and prescribed heat transfer coefficient. The development of velocity, temperature, and concentration profiles are presented along with interface, bulk and wall temperatures and concentrations, and heat and mass fluxes around the tubes. It is noted that the hydrodynamics are quite similar to the classical Nusselt solution and the concentration profiles all generally exhibit the same characteristic shape. The effect of inlet temperature on absorption rate is shown to be significant. At the lowest inlet temperature, the absorption rate near the inlet is approximately an order of magnitude greater than at the highest temperature. The total absorption rate over the whole tube is approximately 80% greater. It is shown that at the highest inlet temperature, significant absorption does not occur until approximately one third of the way around the tube.

Andberg and Vliet (1986; 1987b) suggest a simplified model that retains the key characteristics of the more complex model for horizontal tubes. The Nusselt solution for hydrodynamics, constant thermophysical properties, and a similarity solution for the concentration profile developed from the detailed model are all used to simplify the analysis. The concentration profiles are modeled with a power law approximation for the error function near the liquid-vapor interface. The authors note, as

in the models above that use a similarity solution, that there is "good theoretical basis for using an error function profile near the surface where u ≅ constant." They state that, in terms of overall concentration change within the film, the simplified model results are on average within 3% of the detailed model with a worst case error of 10.5%. Finally, the authors compare their results to data from commercially available absorbers that utilize a geometry similar to that used in the model. An average error of 6.6% is reported based on *overall* concentration change. In a subsequent publication (Cosenza and Vliet, 1990), in which a large amount of experimental data was obtained to validate the above models, fair agreement is reported between the analytical model and experimental data although the analytical model consistently under-predicts the measured data. It should be noted also that in a recent experimental study, Kim et al. (1995) noted that the values of mass diffusivity used by Andberg and Vliet and presumably in much of the literature are significantly higher (up to a factor of 3 depending on concentration) than the values determined by two other experimental studies (Enderby, 1983; Kashiwagi *et al.*, 1985).

Kawae and coworkers (1989) develop a finite difference model of laminar, vertical falling-film absorption which is very similar to that of Andberg and Vliet (1983). The primary difference is that Kawae et al. do not assume constant thermophysical properties (except implicitly in the assumption of film hydrodynamics). They show that allowing for variable properties has a small effect on the results, especially near the inlet where absorption is slow in this case. They find, for instance, that the prediction of total mass absorbed for a 10-meter tall plate is about 5% higher when assuming constant properties.

Brauner et al. (1989) present solutions valid near the inlet region using the similarity technique as in (Nakoryakov and Grigor'eva, 1980; Nakoryakov and Grigor'yeva, 1980). The key difference is that the application of Fick's law of diffusion at the interface is formulated without assuming infinite dilution in the liquid film. Regarding the term which was neglected in Fick's law, Brauner et al. (1988) state, "the convective term ... can be omitted for either $X_A \rightarrow 0$ or $N_{Ay} = -N_{By}$, neither of which holds for the case of hygroscopic condensation. For instance, the minimum molar fraction of water which corresponds to a saturated salt solution of $MgCl_2$, $CaCl_2$, LiBr, NaOH, is about $X_A \cong 0.8$." A comparison with the expressions developed by Nakoryakov and Grigoryeva (1980; 1980) shows significant deviations in temperature and concentration when the *finite* concentration of the film is considered. Brauner et al. show that including this effect leads to predictions of enhanced transfer rates and penetration depth of the concentration boundary layer. An expression for the enhancement factor is also presented.

Brauner (1991) develops new solutions to the vertical laminar film absorption problem for any downstream location for both adiabatic and isothermal wall cases. Her assumptions are the same as those of Grossman (1983) with two significant extensions. First, as in her previous work, the application of Fick's law of diffusion at the interface is formulated without assuming infinite dilution in the water. Second, the film thickness is allowed to vary with absorbed mass; the resulting

transverse velocity component is not neglected. This leads to the following forms of the governing equations:

$$u\frac{\partial T}{\partial x} + v\frac{\partial T}{\partial y} = \alpha\frac{\partial^2 T}{\partial y^2} \tag{2.18}$$

$$u\frac{\partial C_A}{\partial x} + v\frac{\partial C_A}{\partial y} = D_{AB}\frac{\partial^2 C_A}{\partial y^2} \tag{2.19}$$

She substitutes assumed parabolic profiles of temperature and concentration that satisfy the required boundary conditions into the continuity, energy, and species conservation equations. The equations are translated into integral form and numerically integrated. By varying the parameter corresponding to solution concentration, she demonstrates that the solutions for the film temperature, concentration, heat and mass fluxes all change significantly when the concentration of the film is taken into account. Additionally by examining the non-dimensional coefficients of heat and mass transfer, she shows that the heat transfer coefficient is unaffected by the solution concentration and that the modification to the predicted heat transfer is due to the coupling of the heat and mass transfer problems.

van der Wekken and Wassenaar (1988) extend the vertical laminar film problem solved by Grossman (1983) by including a constant temperature cooling medium (representing the case of cross-flow coolant) and coolant heat transfer coefficient, instead of assuming an adiabatic or isothermal wall. They do not assume infinite dilution of the water in the film in their formulation of Fick's law. The rest of their assumptions are identical to (Grossman, 1983). They solve the problem using finite difference methods. Through their parametric studies, the authors show that, the heat and mass transfer coefficients may vary by up to 50% when a parameter such as the non-dimensionalized heat of absorption, Lewis number, coolant temperature or coolant heat transfer coefficient is doubled or increased by an order of magnitude. However, they note that for any realistic problem, these parameters would only vary by "tens of percent" along the film; this leads them to conclude that transfer coefficients predicted using average values of the problem parameters would be sufficient for a design model.

Habib and Wood (1990) create a numerical model for co-current absorption on a laminar, vertical film that includes heat and momentum transfer in the vapor phase. Many typical assumptions are applied including constant film thickness, isothermal wall, and infinite dilution in Fick's Law. The authors include many of the terms typically neglected by other authors in the governing equations (for example Equations (2.1) and (2.2) without the transient terms). They allow for pressure gradients along the absorber and interfacial shear between the two phases, although presumably these terms are very small since the Reynolds numbers for the film and vapor are both 30, and the Nusselt solution for film thickness is used. A unique boundary condition applied by the authors is that the stream-wise gradients in velocity, temperature, and concentration at the exit of the absorber must be zero; no

justification is given for this assumption. The problem is solved using finite difference methods with grid density increasing near the interface. They show that both the temperature in the film and the vapor approach the wall temperature at the absorber exit. The absorption rate along the length of the absorber shows a maximum just after the absorber inlet (presumably where the effect of the wall temperature is first transmitted to the interface) and an exponential decline thereafter. It is shown that as the inlet film temperature is reduced to the wall temperature, the maximum absorption rate increases and its position approaches the inlet. The authors conclude that "the temperature in the gas phase can not be neglected as was suggested by previous investigators" though no quantification of the resulting errors is presented. Furthermore, the authors show very close agreement between their predictions of interface and bulk film concentration along the absorber and those of Andberg and Vliet (1983).

Yang and Wood (1992) also extend the problem solved by Grossman (1983) by allowing the inlet solution temperature to deviate from the temperature of the wall, although they only consider the isothermal wall case. This problem is very similar to the one solved by Andberg and Vliet (1983) and the authors note that they obtain excellent agreement with the results of Andberg and Vliet. However they point out that their formulation of the problem is simplified from the one considered by Andberg and Vliet since the assumptions are essentially the same as those in (Grossman, 1983). They also compare total absorption rate versus downstream position predicted by the model with the authors' previous experimental work. In the experimental data, the film is reported to have waves and the vapor to contain 5% air, two counteracting influences. Perhaps fortuitously, the comparisons reveal that the model predicts the experimental results "reasonably well" except at the lowest film Reynolds numbers.

Hajji and Worek (1992) consider the transient absorption of water vapor into a stagnant film of aqueous lithium bromide. An abridged version of this analysis can also be found in a previous work (Hajji and Lavan, 1990) in which the authors also considered surface tension-driven instabilities. They suggest that the results can be adapted to steady absorption on a falling film over a flat plate by substituting downstream position/stream-wise velocity (x/u) for time (t) in the resulting expressions; presumably this would be analogous to assuming uniform velocity within the film. At the bottom of the film, two boundary conditions are considered: either an isothermal wall, or a constant heat and mass flux wall (which includes adiabatic and impermeable). Using Fourier expansion series methods to solve the problem, the authors show that $Le = 0.015$ provides the best fit to the experimental data for a water-lithium bromide system. It should be noted that Grossman in his review on heat and mass transfer in film absorption (Grossman, 1986) discusses other solutions to absorption on stagnant films. He points out that the solution of Nakoryakov and Grigoryeva (1980; 1980) for coupled heat and mass transfer can be modified for the case of a stagnant film by replacing terms of the form x/u with t. He then points out that the resulting expression for mass transfer coefficient is the same as that obtained from Higbie's penetration theory for isothermal absorption except that the equilibrium

concentration at the interface, which drives the mass transfer, is lowered as a function of the non-dimensional heat of absorption and the Lewis number.

Conlisk (1992; 1993; 1994a) presents the development of a solution to the vertical, laminar film absorption problem employing the Laplace transform technique. His assumptions are essentially the same as Grossman's (1983) except that the film thickness is not required to be constant, the transverse velocity component is not neglected in the species conservation equation although it is neglected in the energy equation, the wall temperature can either be constant or an empirically derived function of downstream position, and infinite dilution of water in the film is not assumed. It is assumed that mass transfer is confined to a boundary layer (i.e. doesn't reach the wall) but this assumption is justified for moderate lengths; for a typical operating condition, Conlisk suggests that this length is about 3-meters, increasing or decreasing with Reynolds number. Conlisk notes that the use of the Laplace transform eliminates the difficulty often encountered in finding solutions at the inlet discontinuity. Considering an expansion series formulation for the film thickness along the absorber, he mathematically demonstrates that, "to a leading order", the film thickness is constant because the mass transfer rate is limited by the physical parameters of the problem. However, his solution for the concentration profile depends on the leading order term for variation in film thickness (absorption rate) which is determined approximately from the inlet and equilibrium conditions for the isothermal case. For the non-isothermal case, a more complex relationship is needed for determining this leading order term of the film thickness variation. Determining the temperature profile requires numerically evaluating a Laplace inversion integral. Conlisk shows that in the region near the inlet where heat transfer is confined to a boundary layer near the interface, a solution similar to the solution for the concentration distribution can be determined which does not require numerical evaluation. In (Conlisk, 1992), he compares the model with experimental data at two operating conditions. The total absorption rate predicted is within 20% of the experimental values, over-predicting the experimental data in both cases. In (Conlisk, 1994a), he concludes that the results suggest "that the use of long tubes to increase heat and mass transfer area is not an efficient means to increase the absorption rate to the tube surface" primarily since the highest absorption rates occur near the inlet. "The implication is that a bank of short tubes operating at lower individual Reynolds numbers will be most efficient for the absorption process." This also corroborates the advantages of horizontal-tube banks stated previously. Assuming that the temperature profile within the film is linear (shown to be a fair assumption at a small downstream length), he develops fully analytical solutions for the problem (Conlisk, 1995a). The total absorption rate at the two operating conditions used for comparison with experimental data is within 1% of the original model. It is shown that at positions very near the film inlet, the prediction of local absorption rate differs greatly between the two models. But because this region is small compared to the length of the tube (1.5 meters in this case) the effect on overall model performance is small. Based on the analytical expressions developed, he shows in (Conlisk, 1995a) that as the initial thickness of the film is reduced, the heat transfer coefficient

increases but the mass transfer coefficient decreases, although no further physical interpretation of why this happens is given. Also, Conlisk notes that the total absorbed mass flux is almost completely independent of the difference between the film inlet and wall temperatures. Presumably this is because the sensible heat load associated with inlet temperature differences is small compared to the heat load of absorption for long absorbers. This conclusion is in sharp contrast to the findings of Andberg and Vliet (1987a) for the horizontal tube case where the film flow length is small.

In (1995b), Conlisk extends his earlier model (Conlisk, 1995a) to include heat transfer to the coolant by including the specific heat, mass flow rate and average heat transfer coefficient of the coolant, as well as wall thickness and conductivity as inputs. Obtaining the solution requires numerical evaluation of two integrals. Comparison with four sets of experimental data reveals that total mass absorption rate is generally predicted within 10%. He also notes that only a 10% increase in absorbed mass is achieved from a four-fold increase in coolant flow rate, and suggests that "attempting to increase the mass absorbed by modifying the coolant-side flow has limited return." This presumably suggests that the process is limited by the diffusion resistance of the falling film.

Ibrahim and Vinnicombe (1993) develop what they call a hybrid method for solving the problem of vertical, laminar film absorption. By combining the analytical solutions proposed by Nakoryakov and Grigoryeva (1980; 1980) near the inlet and along the film interface with a finite difference scheme in other regions of the film, they develop a method that accurately predicts the results of more complex solutions as in Grossman (1983) and van der Wekken and Wassenaar (1988) but requires less computational effort. They also show that linearizing the interface equilibrium condition does not lead to appreciable differences for a practical range of interest. Another interesting conclusion the authors make is that although absorption rates decrease as the heat of absorption increases, the total refrigerant load that could be supplied by a heat pump increases.

Choudhury et al. (1993) examine the problem of absorption in laminar films falling over a horizontal tube in a manner similar to Andberg and Vliet (1987a). However, the film inlet conditions are assumed to be in equilibrium with the vapor. Consequently absorption does not begin until a certain distance around the tube where the heat transfer to the wall is able to reduce the interface temperature. It is shown that their model predicts an optimum solution flow rate which is quite low and depends on tube diameter.

Lu et al. (1996) also develop a model for laminar film absorption over horizontal tubes using the same basic assumptions except that at the top of the tube, the film is assumed to have a velocity equal to the velocity of a body freely falling between the tubes. This assumption neglects momentum losses that would occur upon impact. Results from the model are not presented. Instead, experimental results with one smooth and two different spirally grooved tubes are used to correlate two model coefficients: an effective wetting area coefficient, and a mass transfer enhancement coefficient. The authors suggest that only the spirally grooved tubes at the highest flow rates ($Re = 36$) have complete wetting. The smooth tube wetting coefficient may be as low as 40%. The mass transfer enhancement

for the smooth tube is taken to be identically equal to 1 for all cases. The enhancement factor for the spirally-grooved tubes was calculated to be as high as 8.

Jernqvist and Kockum (1996) solve the problem of vertical laminar film absorption without several of the assumptions commonly found in the literature. For instance, they allow for variable thermophysical properties, developing (laminar) velocity profile, variable film thickness (increasing with absorption), non-linear equilibrium model, energy flux due to interdiffusion, and finite dilution of water in the solution. Although many of these assumptions are relaxed individually in previous models, this is the first attempt to eliminate so many simultaneously. Nonetheless, several assumptions are still employed including no shear at the interface, no heat transfer to the vapor, and an isothermal wall. Also the transverse velocity is neglected in the governing equations. Solutions are obtained using a finite difference formulation (note that the hydrodynamics in the film are simultaneously calculated to account for the variable property effect). One interesting effect of this is that the change in interface velocity with downstream position is a compound effect due to the developing hydrodynamics, the increasing mass flow rate due to absorption, and the changing temperature and concentration in the film affecting the fluid viscosity and density. Comparison with experimental data reveals that the model does not accurately predict the trends in the measured results in all cases. For instance, as film flow rate is increased, the model predicts reduced absorption rates, but the data exhibit an increase in absorption rate. The authors propose a fix based on mixing within the film due to waves. Their discussion of wave effects will be presented in the wavy film section of this paper.

Conlisk and Mao (1996) consider the problem of transient absorption into an initially constant thickness film surrounding a horizontal tube. In this case there is no film inlet to the system, but solutions are time dependent. As time proceeds, the film begins to sag around the tube due to gravity, while simultaneously absorbing vapor; the film thickness varies at each point with time. At the bottom of the tube, surface tension effects are not considered; where a droplet would form, instead a discontinuity occurs limiting the length of time for which solutions are valid as noted by the authors. The authors employ many typical assumptions including constant thermophysical properties, no heat transfer to the vapor, and a linearized interface equilibrium model. Conlisk and Mao note that "absorption is more rapid on the top of the tube where the film is thinning," although it is unclear how this conclusion would be affected by droplet or jet impingement which would normally occur in this region.

A few attempts to solve the coupled equations of heat and mass transfer governing absorption have been made for laminar flow around specialized absorber geometries. Conlisk (1994b) considered laminar flow around a vertical fluted tube which induces tangential velocity due to surface tension effects. Yang and Jou (1995) modeled absorption on a film flowing in a porous media. Conlisk (1996b; 1996a) considered laminar film flow on a vertical tube with “splined fins”.

Table 2.1 contains a summary of the vertical wall models described above. Acronyms are used for the common assumptions to show the progression of attempts to relax assumptions. It should be noted that the tables presented here are not meant to contain a comprehensive list of all assumptions used; rather they primarily display the key assumptions which have been modified and removed by authors over the years. It is clear, even with this partial listing, that no models have been developed without many simplifying assumptions. For instance, many recent models still use the assumption of an isothermal or adiabatic wall. It may be possible, although probably cumbersome, to extrapolate to more realistic wall conditions from these solutions. More useful models should incorporate realistic coolant models since this is a key parameter over which a designer has control. Further discussion of the assumptions can be found in the conclusions section. Table 2.2 summarizes the horizontal tube models. The horizontal-tube case has received less attention in spite of its wide use in absorbers. Currently, the assumptions made to model flow both between and around the tubes are often significant over-simplifications. Thus, this is an area that warrants further development. In general, although they provide valuable insight into the problem, the practical usefulness of laminar-film models is not well established since purely laminar smooth films are rarely encountered in actual absorbers.

2.1.2 Laminar Wavy Film Assumption

As was stated earlier, it is well known that falling films are inherently unstable, even at low Reynolds numbers (see for example (Benjamin, 1957; Fulford, 1964; Kapitza, 1965)). On a vertical film, this instability leads to the growth of waves visible on the film surface even in the absence of any disturbances due to the motion of the vapor. A recent review of the literature on the hydrodynamics of wavy falling films is presented by Miller (1998). Commenting on several key investigations, Miller states "their results imply that all vertical falling films are naturally wavy". In *horizontal-tube banks*, the predominant film waviness occurs as a direct result of the droplets between the tubes since the film flow length is not long enough for large waves to develop due to simple film flow instabilities. Both the detachment from the underside of a tube and the impact on the topside of a tube result in waves on the film. As will be shown, detachment is basically the bifurcation of liquid bridges due to necking as the bridge (also called filament, thread or trail) is stretched behind the falling drop. The point of bifurcation results in a tip with very high curvature. The resulting surface tension forces give rise to fast recoil of the bifurcated filament which causes disturbances (waves) when the impulse reaches the underside of the tube. When a droplet impacts the top of a tube, a characteristic saddle wave is formed which propagates both around and along the tube. More details of this behavior will be given in subsequent sections.

Table 2.1: Summary of Vertical Smooth Laminar Film Absorption Models

Author	Date	Solution Type	Hydrodynamics	Domain	Wall	Other
Nakoryakov and Grigor'eva	(1977a)	analytical (SS)	SFI, USVP, NTV	unrestricted	ISO	CFT, LIEM, EMD, NVHT, CTP, NIE, LFTP
	(1977b)	analytical (ES)	SFI, USVP, NTV	unrestricted	ISO	CFT, LIEM, EMD, NVHT, CTP, NIE
	(1980a,b)	analytical (SS)	SFI, USVP, NTV	film inlet	ISO	CFT, LIEM, EMD, NVHT, CTP, NIE
	(1995)	analytical (SS)	SFI, USVP, NTV	film inlet & downstream	ISO	LIEM, EMD, NVHT, CTP, NIE, LFTP downstream
	(1997)	analytical (ES)	SFI, USVP, NTV	unrestricted	ISO or AD	CFT, LIEM, EMD, NVHT, CTP, NIE
Kholpanov et al.	(1982)	analytical (SS)	SFI, USVP, NTV, vapor shear	film inlet	NA	CFT, LIEM, EMD, NVHT, CTP, NIE
Grossman	(1983)	numerical & analytical (ES, SS near film inlet)	SFI, PSVP, NTV	unrestricted	ISO or AD	CFT, LIEM, EMD, NVHT, CTP, NIE
	(1987)	analytical (SS)	SFI, USVP, NTV	film inlet	NA	CFT, LIEM, EMD, NVHT, CTP
Andberg and Vliet	(1983a)	numerical	SFI, PSVP, NTV	unrestricted	ISO	EMD, NVHT, CTP
	(1983b)	approximate correlation	SFI, PSVP, NTV	unrestricted	ISO	EMD, NVHT, CTP
van der Wekken and Wassenaar	(1988)	numerical	SFI, PSVP, NTV	unrestricted	Isothermal coolant	CFT, LIEM, NVHT, CTP, NIE
Kawae et al.	(1989)	numerical	SFI, PSVP, NTV	unrestricted	ISO	EMD, NVHT
Brauner et al.	(1989)	analytical (SS)	SFI, USVP, NTV	film inlet	NA	CFT, LIEM, NVHT, CTP, NIE
Brauner	(1991)	numerical (SS by inlet)	SFI, PSVP	unrestricted	ISO or AD	CFT, LIEM, NVHT, CTP, NIE
Habib and Wood	(1990)	numerical	SFI, PSVP	unrestricted	ISO	CFT, EMD, CTP, NIE
Yang and Wood	(1992)	numerical	SFI, PSVP, NTV	unrestricted	ISO or AD	CFT, LIEM, EMD, NVHT, CTP, NIE
Hajji and Worek	(1992)	analytical (ES)	Stagnant film	NA	ISO or flux	CFT, LIEM, EMD, NVHT, CTP, NIE
Ramadane et al.	(1992)	numerical	SFI, PSVP, NTV	unrestricted	coolant	CFT, LIEM, EMD, NVHT, CTP, NIE
Conlisk	(1992,3, 1994a)	analytical (LaPlace integrals) & numerical	SFI, PSVP	moderate lengths	fixed temp. profile	LIEM, NVHT, CTP, NIE
	(1995a)	analytical	SFI, PSVP	moderate lengths	fixed temp. profile	LIEM, NVHT, CTP, NIE, LFTP
	(1995b)	analytical	SFI, PSVP	moderate lengths	fixed coolant htc	LIEM, NVHT, CTP, NIE, LFTP
Ibrahim and Vinnecombe	(1993)	hybrid (analytical and numerical)	SFI, PSVP, NTV	unrestricted	fixed coolant htc	CFT, LIEM (tests this assumption), EMD, NVHT, CTP, NIE
Jernqvist and Kockum	(1996)	numerical	SFI, NTV, developing	unrestricted	ISO	NVHT

Legend:

SS = Similarity solution; **ES** = Expansion series; **SFI** = Smooth film interface; **USVP** = Uniform stream-wise velocity profile; **PSVP** = Parabolic stream-wise velocity profile; **NTV** = negligible transverse velocity; **ISO** = Isothermal wall; **AD** = Adiabatic wall; **CFT** = Constant film thickness; **LIEM** = Linear interface equilibrium model; **EMD** = equimolar diffusion at interface; **NVHT** = Negligible vapor-phase heat transfer, **CTP** = Constant thermophysical properties; **NIE** = Negligible interdiffusion effects; **LFTP** = Linear film temperature profile

Table 2.2: Summary of Horizontal Tube Absorption Models

Author	Date	Solution Type	Hydrodynamics	Domain	Wall	Other
Andberg and Vliet	(1986, 1987a,b)	numerical	planar jet, SFI, developing PSVP	film on tube	isothermal coolant	NVHT, NIE
Choudhury et al.	(1993)	numerical	planar jet, SFI, developing PSVP	film on tube	isothermal	NVHT, NIE, CTP, inlet film/vapor equilibrium
Lu et al.	(1996)	numerical	planar jet, SFI, no impact loss	film on tube	isothermal coolant	NVHT, NIE, CTP, empirical wetting and mass transfer enhancement
Conlisk and Mao	(1996)	analytical (LaPlace integrals) & numerical	sagging film, SFI, PSVP	film on tube	isothermal	LIEM, NVHT, CTP, NIE

Legend:
SS = Similarity solution; **ES** = Expansion series; **SFI** = Smooth film interface; **USVP** = Uniform stream-wise velocity profile; **PSVP** = Parabolic stream-wise velocity profile; **NTV** = negligible transverse velocity; **CFT** = Constant film thickness; **LIEM** = Linear interface equilibrium model; **EMD** = equimolar diffusion at interface; **NVHT** = Negligible vapor-phase heat transfer, **CTP** = Constant thermophysical properties; **NIE** = Negligible interdiffusion effects; **LFTP** = Linear film temperature profile

Table 2.3: Summary of Vertical Wavy Film Absorption Models

Author	Date	Solution Type	Hydrodynamics	Domain	Wall	Other
Kholpanov	(1987)	analytical (boundary layer SS)	from stability analysis	near inlet	NA	LIEM, EMD, NVHT, CTP, NIE
Tsvelodub	(1989)	analytical	USVP	near inlet	NA	LIEM, EMD, NVHT, CTP, NIE
Kholpanov	(1990)	analytical	sinusoidal, USVP	near inlet	NA	LIEM, EMD, NVHT, CTP, NIE
Uddholm and Setterwall	(1988)	numerical	Brauner roll waves, PSVP, NTV	unrestricted	isothermal	EMD, NVHT, CTP, NIE
Morioka and Kiyota	(1991)	numerical	sinusoidal capillary waves, PSVP	unrestricted	isothermal	LIEM, NVHT, CTP, NIE
Yang and Jou	(1991,3)	numerical	capillary waves, PSVP	unrestricted	isothermal	EMD, NVHT, CTP, NIE
Sabir et al.	(1996)	numerical	capillary waves, Penev et al. psuedo PSVP	unrestricted	isothermal	LIEM, NVHT, CTP, NIE
Patnaik and Perez-Blanco	(1996)	numerical	Brauner roll waves, PSVP,	unrestricted	isothermal	EMD, NVHT, CTP, NIE

Legend:
SS = Similarity solution; **ES** = Expansion series; **SFI** = Smooth film interface; **USVP** = Uniform stream-wise velocity profile; **PSVP** = Parabolic stream-wise velocity profile; **NTV** = negligible transverse velocity; **CFT** = Constant film thickness; **LIEM** = Linear interface equilibrium model; **EMD** = equimolar diffusion at interface; **NVHT** = Negligible vapor-phase heat transfer, **CTP** = Constant thermophysical properties; **NIE** = Negligible interdiffusion effects; **LFTP** = Linear film temperature profile

The waves that may develop on a falling film are not all alike and those on vertical tubes are significantly different in character to those on horizontal tubes. For the vertical tube case, many investigators have suggested categorization methods based on the non-dimensional Reynolds and Kapitza numbers. A simple classification is proposed by Brauner (1989) who suggests the existence of two primary types of waves: 1) capillary waves which are characterized by their low amplitude, sinusoidal shape, regular frequency, and tendency of the wave-front to be aligned perpendicular to the flow direction (see Figure 2.1), and 2) inertial waves, often called roll waves, which can obtain high amplitudes (several times the underlying film thickness), have a steep wave-front and longer wave-back, may travel as solitary waves with long spans of smooth film in between successive waves (see Figure 2.2). Roll waves may also contain regions of recirculation (Brauner, 1989; Wasden and Dukler, 1989; Jayanti and Hewitt, 1997) that play a role in the transport processes between the film interface and bulk. It is also important to note that wave shape generally travels several times faster than the fluid in the film (this speed ratio is called wave celerity (Brauner, 1989)) and consequently wavy films have a higher mass flow rate than a smooth film with an equivalent mean film thickness. The majority of the mass flow may be carried within the wave shape itself leaving only a fraction of the flow in the thin film substrate between and underneath the waves (Brauner, 1989). Similar studies of the waves formed on horizontal tubes were not found in the literature. Some of the results presented here which elucidate their behavior have been published already (Killion and Garimella, 2003b). As a consequence there are no models in the literature which attempt to predict absorption in films surrounding horizontal tubes in the presence of realistic film waves.

To model the absorption process on vertical tubes in the presence of wavy falling films, investigators typically assume the hydrodynamic solution *a priori*, neglecting the potential influences of the heat and mass transfer processes on film flow. However, several investigators, for example Cosenza and Vliet (1990) and Miller and Keyhani (1999), have noted significant differences in the observed hydrodynamics and surface wetting when absorption is occurring; this is generally attributed to surface tension gradients resulting from uneven absorption over the film surface. It is also typical to neglect the actual development of the waves from an initially smooth film in favor of using an asymptotic steady-state solution. Also, often only a small number of wavelengths are modeled representing a short length of the absorber. Models have been developed for absorption in the presence of both capillary and inertial wavy-laminar films, but in either case most investigators assume that the waves are periodic. Experimental investigations of wavy films reveal that the waves themselves, especially at Reynolds numbers greater than 100, are unstable and often develop into seemingly chaotic three-dimensional patterns (see for example (Morioka *et al.*, 1993)) perhaps requiring a statistical description. The general conclusion of all of these investigations is that the presence of waves significantly enhances the transport processes compared with a laminar film. The exact mechanism attributed to the enhancement and its quantitative value depend on the investigator.

One of the simplest methods for modeling the effect of waves is to assume that a passing wave completely mixes the film, resulting in uniform concentration and temperature profiles at regular intervals corresponding to the characteristic wavelength. This assumption allows laminar film models such as those in (Nakoryakov and Grigor'eva, 1980; Nakoryakov and Grigor'yeva, 1980) for the absorption near the inlet region of a falling-film absorber to be applied to the regions in between each wave. This technique proposed by Kholpanov (1967) is used by Burdukov et al. (1980) and Nakoryakov et al. (1982a; 1982b). They use photography to determine the characteristic wavelength and then assume that the laminar theory for the inlet region holds within each wavelength. Comparison with experimental data shows that this wavy model qualitatively predicts the trends in the experimental data. Jernqvist and Kockum (1996) also assume complete mixing within the film at regular intervals. As was mentioned before, the laminar film predictions of absorption rate decrease with increasing film flow rate, under-predicting the experimental data, which show the opposite trend. The authors show that by increasing the mixing frequency with Reynolds numbers, the model can be made to predict absorption rates closer to the experimental results. Interestingly though, the error in heat transfer rate at the wall, which is over-predicted for even the purely laminar case, is increased when the mixing density is increased. The fact that wall heat transfer rates are over-predicted even when absorption rates are under-predicted may suggest that the assumption of no heat transfer to the vapor is leading to appreciable errors.

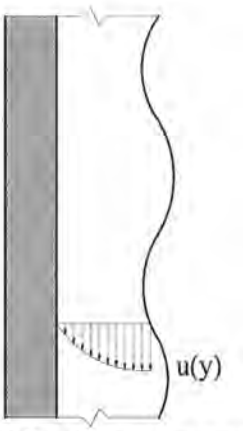

Figure 2.1 Capillary waves

Kholpanov (1987) solves simplified Navier-Stokes equations to determine wave motion; the predicted wave amplitude is shown to agree reasonably well with some experimental data from the literature. By assuming a parabolic stream-wise velocity profile throughout the film, the author then develops a solution for combined heat and mass transfer. Neither the temperature boundary layer nor the concentration boundary layer developing from the interface is allowed to reach the wall; thus the solution is insensitive to wall conditions and valid only near the inlet. Since the transport processes are even more rapid due to the presence of waves, the entry region where absorption is insensitive to wall conditions will presumably be even shorter than for the smooth film case. Kholpanov also considers wavy flow over a rough surface with gas shear using a linear stream-wise velocity profile and flow along the inside of a rotating cylinder. A very similar problem is also considered by Tsvelodub (1989). He

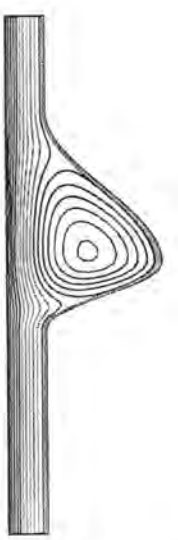

Figure 2.2 Roll waves (Jayanti and Hewitt, 1997)

assumes a constant stream-wise velocity within the boundary layers and develops analytical relationships for heat and mass transfer coefficients in terms of non-dimensional parameters. Kholpanov (1990) analytically develops expressions for coupled heat and mass transfer coefficients for absorption on a wavy film with a purely sinusoidal surface. A constant stream-wise velocity is assumed within the film, and wall conditions are not specified. Wavy film transfer coefficients are expressed as a correction to the laminar film transfer coefficients. The expressions for these corrections are functions of wave amplitude and frequency (or phase velocity), which the author suggests may be determined from experimental data or from approximate expressions presented.

Uddholm and Setterwall (1988) model the absorption process on a vertical isothermal wall where the film exhibits inertial wavy-laminar flow (roll waves). They assume the hydrodynamics within the wave from Brauner et al. (1983; 1985) who divide the roll waves into four sections: wave front, wave back, wave trail, and substrate. Results of photography of falling films allowed Uddholm and Setterwall to develop a correlation for wave frequency based on downstream position. Their experimental results show that near the inlet, the wave frequency may be 20 Hz, but it reduces to about 10 Hz further along the tube as the roll waves develop. The authors consider four different models for the wave frequency: constant 20 Hz waves, constant 9 Hz waves, linearly varying 20–9 Hz waves, and no waves. The predictions of average overall heat transfer coefficients are compared with experimental data from a water-lithium bromide heat transformer. When assuming only low frequency (9 Hz) roll waves, the model over-predicts the experimental data. The other three assumptions under-predict the data by varying degrees. The predicted heat transfer coefficient is between 35 and 120% greater with waves than with a laminar film model.

Morioka and Kiyota (1991) model absorption in the presence of capillary waves. The key assumptions they use are that the film surface is sinusoidal, the stream-wise velocity profile is parabolic, the wave speed and length are determined from a linear stability analysis, but the wave amplitude is arbitrarily assumed to be 30% of the average film thickness to ensure what the authors felt are reasonable velocity profiles within the film. The problem is solved using a finite difference solution on a grid fit to the shape of the wavy film over three wave lengths. Local absorption rates for film Reynolds numbers of 20, 50 and 100 are presented along with the predictions from a smooth film model. Temperature and concentration profiles shown at the wave crests and troughs for a Reynolds number of 20 and 50 demonstrate the development of a "depression" in the concentration profile due to the motion of the waves and the enhanced absorption rates. The authors point out "the absorption mass flux shows a maximum at the troughs of the wave where the film thickness is minimum. At these points, the mass flux is approximately 3 times larger than the smooth flow case." The authors propose that the enhanced absorption rates are due to both the increase in the transverse velocity and the action of the waves effectively exposing and covering sections of an underlying film. They note that their predicted absorption rate is nearly independent of Reynolds number for the range

considered. On average, they report that the absorption rate in wavy films is 70 to 140% higher than for the smooth laminar film case.

Yang and Wood (1991) and Yang and Jou (1993) also consider the problem of absorption on a film with periodic capillary waves, a parabolic velocity profile, and wave velocity and number corresponding to the "most unstable wave" determined by a linear stability analysis. The profile of the film interface is described by a Fourier expansion series, the coefficients of which are determined numerically. The resulting profiles vary with Reynolds number (up to 500), and it is noted that the solution for the wave profile always corresponds to the maximum wave amplitude and minimum average film thickness at any given flow rate. The resulting profiles are not purely sinusoidal, but exhibit shortened wave fronts and elongated wave backs, suggesting characteristics of roll waves; however, the amplitude is much lower than what is normally labeled a roll wave, perhaps due to the linear model used in the stability analysis. A comparison of predicted wave lengths and amplitudes with several sets of experimental measurements from the literature shows fair agreement. The authors develop a numerical solution for absorption using several other assumptions including: constant thermophysical properties, no heat transfer to the vapor, infinite dilution in Fick's law, and an isothermal wall. To speed up the calculation procedure, the results of a smooth film model are used as initial conditions for the wavy film model. The results show that the solution becomes periodic after about the second wave period. Absorption rates predicted with the wavy model are about double the results with a smooth film. It is also shown that absorption rate increases with Reynolds number, the effect diminishing somewhat for higher Reynolds numbers. This trend does not agree with the conclusions of Morioka and Kiyota (1991); the discrepancy may be due to the fact that the hydrodynamic solution of Yang and Wood varies with Reynolds number and is not purely sinusoidal.

Sabir et al. (1996) generate numerical solutions for the problem of absorption on films with capillary waves. They assume the hydrodynamics proposed in (Penev *et al.*, 1968) including a stream-wise velocity profile which the authors point out does not allow for any circulation of liquid within a wave (described as surface renewal). This profile is based on a parabolic function with coefficients that are calculated from a truncated expansion series of sinusoidal functions. The film thickness profile is a similar truncated expansion series of sinusoidal functions. Other assumptions used include: constant thermophysical properties, isothermal wall at solution inlet temperature, linearized interface equilibrium model, and no heat transfer to the vapor. Plots of bulk concentration and temperature against downstream position reveal that initially, the wavy film shows great enhancement over the smooth film assumption. However, further downstream, the results of the two models converge as the limit of absorption is approached. The authors also note that the enhancement of mass transfer appears to be greater than that of heat transfer. They attribute this to the fact that the mass transfer is governed by conditions at the interface where wave effects are strongest, while heat transfer occurs across the entire film and the enhancement near the wall due to the waves is less. The

authors conclude that the enhancement effect is due to the additional transverse velocity components occurring in the wavy flow, not mixing within the waves, although they eliminate the latter possibility purely by assumption.

Patnaik and Perez-Blanco (1996b) model the absorption process on a film with roll waves (Reynolds numbers between 200 and 1000) numerically. The hydrodynamics, specified in (Patnaik and Perez-Blanco, 1996a), are adapted from the work of Brauner (1989) who provides an expression for the length and film thickness of four parts of a roll wave: front, back, trail and substrate. Analysis of video images of falling films of aqueous lithium bromide with Reynolds numbers between 200 and 300 led to identification of a representative 13-Hz wave, which was assumed to be the wave frequency for modeling purposes. Patnaik and Perez-Blanco also assume that the stream-wise velocity profile is parabolic at all points within the film. The interface energy balance is formulated assuming equimolar diffusion, but the authors suggest that compared to the transverse velocity of the film due to the waves, the convective effect of non-equimolar diffusion is negligible. The non-dimensional mass transfer coefficients are shown to be up to almost four times those predicted with a smooth film model. The authors attribute the enhanced transport rates to the transverse components of the film velocity, and their relative phasing with peaks in the stream-wise velocity.

It is worth noting some other significant mathematical investigations into the effect of wavy films on uncoupled heat and mass transfer processes due to their advanced methods of modeling the film hydrodynamics. For instance, Wasden and Dukler (1989; 1990) numerically predict mass transfer rates in the presence of roll waves are 1.5 to 2.5 times the smooth film predictions. The authors note that the significant transverse velocities caused by the waves "in conjunction with recirculation within the large waves ... produce transfer rates for large waves that are several times larger than predicted for quasiparallel velocity fields." This suggests that the assumption of a parabolic stream-wise velocity profile may lead to erroneous results. Jayanti and Hewitt (1997) show that the enhancement of the heat transfer process from roll waves can be almost entirely attributed to the effective thinning of the film (a wavy film transports the same amount of liquid with a thinner average film thickness). It is shown that the heat transfer rate across the film can be closely approximated by assuming that conduction is the only heat transfer mechanism and using the film thickness profile of the wavy film, even in the presence of waves with a large recirculation region. Overall heat transfer coefficients may be increased by up to 35% over a smooth film depending on wave shape. The results of Wasden and Dukler and Jayanti and Hewitt support the conclusion of Sabir et al. (1996) that mass transfer may be enhanced more than heat transfer; however, unlike Sabir et al., they point to the importance of considering the true recirculating nature of roll waves in the absorption process, especially in light of the coupling of the heat and mass transfer processes in absorption.

Table 2.3 contains a summary of the absorption models reviewed here that include a model for film motion in the presence of waves. *It is notable that no horizontal tube models are available that include the effect of film waviness.* Each of these models reviewed predicts significantly increased

absorption rates due to the enhanced mixing effect of waves, underscoring the importance of assumptions about film hydrodynamics. Understanding the details of the behavior of wavy films is still an area that needs significant additional research.

2.1.3 Assumed Transport Coefficients

A distinction can be made between the work reviewed above and the papers in this section. Many investigators have used correlations for heat and mass transfer coefficients derived from experimental work to develop absorption models. These models are primarily used as design tools that are computationally simple. The accuracy depends on how well the correlations represent the actual physical situation.. A common feature of models using assumed transport coefficients is that the governing equations are written in terms of temperatures, concentrations, and velocities that are averaged in the transverse direction for each phase of the system. For instance, the film temperature is taken to be the average temperature of the entire film including the interface, bulk and wall regions. This in essence tacitly assumes the temperature, velocity, and concentration profiles in the correlation for the transport coefficients.

Wassenaar and Westra (1992) consider the *transient* response of a vertical falling-film absorber to step changes in operating parameters such as cooling water temperature, vapor flow rate, and inlet film concentration. They assume that the transient changes do not affect the assumed transport coefficients. The authors point out at least one limitation of this approach is that, in the model, perturbations to the film inlet conditions travel along the absorber at the mean film velocity, whereas the liquid at the interface of even a laminar film travels 50% faster than the mean film velocity. Thus inlet perturbations reach the absorber film outlet later in the model because of the 1-D assumption. But, the authors suggest that the choice of numerical formulation can help overcome this discrepancy by introducing *numerical diffusion*. Other assumptions employed by the authors are very typical: no heat transfer to the vapor, thermodynamic equilibrium at the interface, finite dilution of the water in the film, linearized interface equilibrium model. It is worth mentioning that the equilibrium model, although linearized, is different from most other models because it accounts for the variation of pressure in the absorber, a key feature required for accurately predicting the transient behavior of the system according to the authors. The equation for average film thickness allows for the possibility of laminar, wavy and turbulent flow regimes through the use of constants that must be assumed based on flow rate. Similarly, the choice of appropriate transport coefficients must also be made *a priori*. Parametric studies show that, due to the coupled nature of the problem, the change in system response is not directly proportional to the change in any given parameter. It is shown that the system parameters including absorber pressure, coolant and film outlet temperature, and film outlet concentration respond in different sequences depending on the actual perturbation, and that they may exhibit overshoot before settling to a new steady condition.

Patnaik et al. (1993) utilize a number of different correlations for heat and mass transfer coefficients to develop a simplified model for steady vertical-film absorption that applies to both laminar and wavy-laminar film flow regimes. Their basic assumptions include constant thermophysical properties evaluated at the bulk-averaged temperature and concentration, linear temperature profile within the film, no heat transfer to the vapor phase, and no vapor shear. Different correlations for the falling-film heat and mass transfer coefficients are used in the entrance regions than in the fully developed flow regions. The average film thickness is assumed from Nusselt's solution even in the wavy-laminar condition and the liquid film initially enters in equilibrium with the vapor. The solution is computed numerically along the length of the absorber. The model is used to develop performance charts that present total absorption rate, heat transfer rate, concentration change, film outlet temperature, and outlet subcooling as a function of downstream position for a variety of coolant and solution mass flow rates. These performance charts are proposed to provide a quick absorber design tool for predicting absorber performance, given basic operational conditions. Patnaik and Perez-Blanco (1993) examine the use a modified effectiveness/number-of-transfer-units analysis to develop simplified solutions for vertical falling-film absorbers. By defining several new effectiveness ratios and making a number of assumptions, the authors are able to develop a straightforward relationship between number of absorber transfer units and the defined effectiveness ratios. Key assumptions are: overall heat and mass transfer coefficients are known and constant, the temperature profile within the film is linear (it is shown that this assumption drops out during the solution development), and the relationship between bulk temperature and downstream position is known. An expression for the latter is proposed on the basis of experimental data and the results of other vertical plate models. The authors note that this assumption "needs to be investigated further, and the overall sensitivity of the results to changes in this assumption established." Other assumptions the authors use are fairly common including a linear equilibrium model, no heat transfer to the vapor, and constant thermophysical properties. Using parameters covering a range of reasonable operating conditions for a water-lithium bromide absorber, the authors demonstrate the potential usefulness and simplicity of the method in determining absorber performance.

Kirby and Perez-Blanco (1994) consider the case of absorption around horizontal tubes. They are the first to distinguish the effects of film flow, droplet formation and droplet fall in their model. The absorber is divided into three regions: the film flow region, the droplet formation region, and the droplet fall region. In the droplet formation regime on the underside of the tubes, the average distance between droplets and the average volume of the droplets when they fall are determined from a Taylor instability analysis (Taghavi-Tafreshi and Dhir, 1980). The residence time of the liquid solution in each regime can thus be calculated given an overall mass flow rate. For the droplet fall regime, simple free-fall is assumed, initially from rest. For the film, the Nusselt equations for film thickness and velocity are used. One key assumption about the droplet formation is that, as liquid solution reaches the droplet, it is deposited as a thin spherical shell on the surface of the old droplet

core. Thus the temperature of the liquid solution entering the forming droplet is used to set the driving force for heat transfer and mass transfer (through the equilibrium condition) into the droplet. The authors suggest that this is the "fresh surface" assumption described by Clift et al. (1978). However Clift et al. state that, in the "fresh surface" model, "fresh fluid elements are assumed to arrive at the interface to provide the increase in area." Therefore the interpretation by Kirby and Perez-Blanco seems somewhat questionable. Correlations for the mass transfer coefficients in each of the three regimes are taken from the literature. In the droplet formation region, the best correlation available is a time-averaged empirical expression based upon work with liquid-liquid extraction where droplet formation occurs at the end of nozzles. One of the required parameters for this correlation is the velocity of the liquid in the nozzle, for which the authors apparently substituted some characteristic stream-wise velocity from the film flow regime. Two correlations for heat transfer are used, one for the coolant inside the tubes and one for the falling film. Presumably heat transfer during the droplet formation region is neglected implying that adiabatic absorption takes place in this region. The results suggest that a major portion of the mass transfer takes place in the droplet formation region, while the heat transfer occurs in film flow around the tubes. Additionally, the absorption that takes place between the tubes significantly increases the solution temperature from the bottom of one tube to the top of the next. In a later work (Atchley *et al.*, 1998) they present a more detailed description of the model and compare the results with experimental data for three different tube spacing arrangements. The agreement of overall heat duty, absorbed mass, and heat transfer coefficient is shown to be much better when the space between the tubes is large than when it is small. The authors attribute the differences to the wetting characteristics due to the effect of droplet impact and splashing. The authors also extend the model to tubes with enhanced surfaces by selecting correction factors for the assumed heat and mass transfer coefficients.

Tsai and Perez-Blanco (1998) extend the model of Patnaik et al. (1993) for vertical falling-film absorption to determine the asymptotic limit to absorption performance that could be achieved by active mixing techniques. The authors note that most enhancement techniques, whether active or passive, can be considered as mixing processes. The authors attribute the asymptotic behavior to the fact that "the finite heat transfer coefficients of the absorber wall and the coolant do not allow infinite heat of absorption released to the film" even if resistance to mass transfer is eliminated due to mixing. To establish transfer coefficients applicable to a fully mixed film, the transient problem of transfer into a semi-infinite medium is used. The resulting expressions for transfer coefficients contain the square root of exposure time in the denominator. Thus as mixing frequency is increased, the exposure time is reduced, and the transfer coefficients increase. It is shown that, in theory, an order of magnitude increase in absorption rate is possible over current best practice. As Reynolds number is increased, the asymptotic value of absorption rate increases (with diminishing results) but the concentration difference resulting from this maximum absorption rate decreases. Based on this trend,

the authors suggest that the optimum Reynolds number would be a compromise between these two effects.

Jeong and Garimella (2002) model absorption on a falling film over horizontal-tube banks using a method similar to Kirby and Perez-Blanco (1994). In addition to considering the absorption during film flow, droplet formation and droplet fall, they also consider the effects of incomplete wetting of the tube surfaces by the film and correlate the model in detail using the on- and between-tube temperature measurements of Nomura et al. (1993) which show that the temperature of the liquid decreases as it flows around the tube and increases within pendant drops where essentially adiabatic absorption takes place. The authors use several assumptions including no heat transfer to the vapor, mass transfer is confined to a thin boundary layer near the interface, the temperature difference between the interface and bulk film is constant around the tube, the droplets form as half-spheres under the tube and fall as full spheres between the tubes, and due to internal circulation and short formation times, the temperature within the droplets are uniform. The results compare well with the temperature measurements of Nomura et al. (1993). In addition, the authors showed that the model predicts that the droplets could account for half of the total absorption rate depending on the solution flow rate and wetting ratio. The results of this work, the work of Kirby and Perez-Blanco (1994) and that of Nomura et al. (1993) strongly suggest that understanding the behavior and role of droplets in horizontal-tube absorbers is key to understanding the absorption process. This is also corroborated by other studies of applications using falling films over horizontal tubes such as an evaporative cooler studied by Armbruster and Mitrovic (1998). Armbruster and Mitrovic state that droplet flow mode gives rise to large temperature changes during flow between tubes and that satisfactory agreement between simple correlation methods and experimental results during droplet flow mode is not obtainable.

2.1.4 Conclusions from the Review of Modeling Literature

A large body of work exists in the field of modeling falling-film absorption; however, there appears to be a lack of agreement among authors in several areas and, furthermore, there are still some key deficiencies that can only be addressed through continued enhancement of the existing modeling techniques. The key areas that need further investigation are itemized below:

- **Film hydrodynamics** is an area that clearly needs improved understanding. The often conflicting conclusions of many of the authors clearly show that this key assumption has an extremely large impact on the predicted results. The reasons for adopting a laminar film assumption for the initial work in this area were clear. But given the inherent instability of falling films and the fact that absorbers are often designed specifically to avoid smooth laminar film flow, continuing to use these types of simplifying assumptions is not particularly useful.
- **Hydrodynamics should be considered simultaneously in a coupled manner with the heat and mass transfer processes**, to account for local changes to thermophysical properties due to

absorption. The studies that have attempted to do this have been for smooth-interface, laminar films.

- **Modeling absorption in the presence of wavy film flow** is still an area where more work needs to be done. The existing models make many simplifying assumptions, have had little validation, and generally do not account for the development of the waves along the absorber, for the possibility of fluid recirulation within the wave. Most models also simply assume and impose velocity and thickness profiles within the film rather than deriving them.
- Models for absorption on **horizontal tubes** have not included waves, there are few studies on the **inception and development of waves** on horizontal tubes, and the few studies that consider the role of **droplets** use empirical transport correlations. The literature lacks much useful information on absorption phenomena in pendant forming droplets, but this region may in fact account for a large portion of the total mass transfer in horizontal-tube systems. Additionally, models of horizontal-tube absorbers should include the effect of droplet impact on the top of tubes and the resulting concentration redistribution, non-uniform liquid distribution, and heat transfer enhancement. In general, much more work has been done on vertical film absorption, although horizontal tubes are more widely used in absorber designs.
- Consideration of **surface wetting** limits are rarely incorporated into absorption models and sometimes lead to suggestions for impracticably low film flow rates. When the effect of surface wetting is included, it is usually by empirical correlation with experimental results, not by predictive methods. Physically representative, predictive methods for surface wetting may also require the inclusion of the local thermophysical property variation in the presence of absorption, which requires simultaneous solution with the heat and mass transfer problem, to account for effects such as surface tension gradients formed by preferential absorption. Additionally, fully three-dimensional models may be required to account for the spatially and temporally varying wetting phenomena.
- The **interaction of vapor flow and film flow** has only been included as simple shear forces on a smooth interface, although some of the transport coefficients assumed may, in part, account for this effect. In some instances, it may be warranted to include the vapor-liquid hydrodynamic interaction in more detail, especially in the presence of surface waves.
- There appears to be a general agreement that **vapor pressure equilibrium** prevails at the interface. A linear model of interface equilibrium appears to be reasonable, though not ideal, for most operating conditions in a water-lithium bromide absorber. It may be possible to use more realistic equilibrium models in numerical analyses with the advanced capabilities of today's computers.
- Neglecting **heat transfer to the vapor phase** is a very common assumption. However, some investigators have concluded that heat transfer to the vapor phase is quite important, particularly

in situations with a large temperature difference between the liquid film and vapor and/or high vapor-phase heat transfer coefficients.

- **Simplifications to the governing equations** must be considered carefully. As models begin to include greater detail of spatial variation of parameters, it may be necessary to reevaluate some of the mathematical simplifications that are often made by assuming constant thermophysical properties (including constant total mass density of each phase) and negligible transverse velocities. Additionally, care should be taken, when applying the laws of diffusion, to account for the frame of reference which is used at the interface. This was a point of inconsistency among several authors.
- It is often **difficult to compare the predictions** of different models to each other because of differences in the assumed geometries and operating conditions and the limited amount of predicted data that is typically presented. It would be beneficial if authors presented the results in a more consistent format at a variety of operating conditions, including those used in previous work, and with enough detail that meaningful comparisons could be made. Also, parametric studies are typically done in one-at-a-time fashion from a chosen baseline condition. Investigation of the potential interaction between model parameters has only been done on a limited basis but may shed light on why investigators sometimes come to conflicting conclusions.
- **Experimental validation is very limited** and usually based on overall performance predictions. As was illustrated as early as 1947 by Ruhemann (Ruheman, 1947), significant variations in transfer coefficients can combine to net only slight changes in outlet conditions despite large changes within the absorber. Using overall performance as a basis for evaluating model accuracy masks the real limitations of a model, particularly in cases where the absorption resistance is not the dominant resistance.

It should be noted that this review does not include attempts to model the effects of heat and mass transfer enhancing additives or surfactants that are often an important and required aspect of achieving adequate performance in modern absorbers. There is, in fact, limited literature that attempts to *mathematically* consider this problem (see (Fujita, 1993; Koenig *et al.*, 1999) for example), although there is a significant amount of experimental literature on the subject which is reviewed in the next section. Incorporating the effect of surfactants, which work by altering the surface tension and promoting film waviness, will be important to the applicability of future models.

2.2 Experimental Investigations of Absorption on Horizontal Tubes

A number of investigators have experimentally investigated the problem of water/LiBr absorption on falling films over horizontal tubes. The goal of most of these efforts is to determine how certain system parameters affect the performance of the absorber. Because of the great gains achieved when

using them, much of the research has been conducted with the working fluid containing surfactants and/or with enhanced tube surfaces. Unfortunately though, these efforts have often not addressed the fundamental effects of parameters such as tube diameter and spacing in spite of the fact that the effects of these parameters have not been well established. Moreover, even though the means by which parameters affect the absorption process is by modifying the hydrodynamics of the liquid film, not much flow visualization has been done in conjunction with these experimental investigations. When provisions for visual access have been built into the experimental apparatus, at most one or two still frames and a few sentences describing the investigators' impressions of the flow patterns have been provided in the literature. Notwithstanding these shortcomings, the literature on experimental investigations does contain a significant amount of useful information which has been reviewed by the present author (Killion and Garimella, 2003c). Because of its widespread use and significant impact on the results, the effect of surfactant is impossible to leave out of a discussion of the literature. Thus after introducing the basic experimental techniques, the effect of surfactants is summarized before a systematic examination of several other basic absorber parameters is described.

2.2.1 Typical Experimental Techniques

Although the details of the experimental apparatus used in these types of investigations differ, the general experimental approach is often quite similar and will be described first. Quite often, absorber test stands comprise just a generator and an absorber operating at a single pressure level (typically around 1 kPa) corresponding to the desired evaporator temperature, which eliminates the condenser and evaporator found in a complete absorption heat pump cycle. One notable exception is the apparatus of Kyung and Herold (2002) which comprises an entire single-effect cycle; the advantage claimed of a full system in their case is that the vapor inlet conditions and surfactant circulation within the system are more realistic (Kyung and Herold, 2000; Kyung and Herold, 2002). Systems may run in batch mode where a large amount of solution is prepared to the desired inlet concentration prior to testing by generating water vapor and storing it in another container, or in continuous mode where the vapor generation process occurs at the same time as the testing of the absorption phenomena; see Figure 2.3 for a typical schematic of a continuous-mode, single-pressure apparatus. In either case, the pressure within the system must be lowered by a vacuum pump. Because of the presence of water vapor, the vacuum system typically includes a cold trap upstream of the pump. System leakage rates must be very low to ensure that non-absorbable air does not enter the system. Even low concentrations of air will significantly retard the absorption process, as will be discussed later. The ingression of air is, however, inevitable, and periodic use of the vacuum system purges the non-absorbable gases as is done routinely in commercial machines.

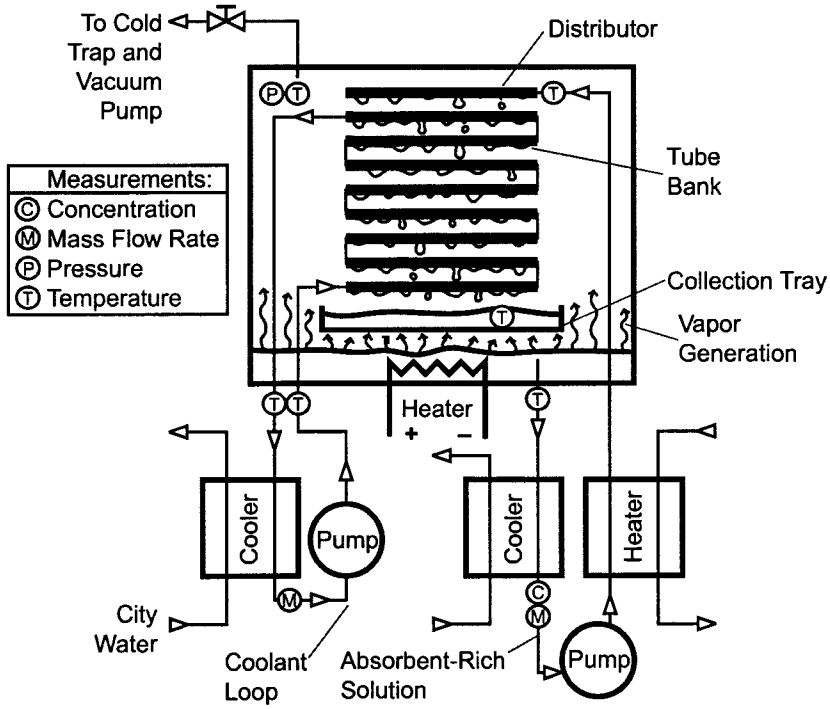

Figure 2.3 Schematic of Typical Single-Pressure, Continuous Mode Test Apparatus with the Vapor Generator Directly Below the Absorber

Vapor generation is typically accomplished with resistance heaters with power output in the range of a few kW depending on the size of the absorber. From the generator, liquid with high absorbent concentration is pumped to the top of the absorber and may also be conditioned en route to achieve the desired inlet temperature. The generated vapor usually enters the absorber near the bottom, often by placing the generator directly beneath the absorber. But counter-current flow is not crucial because the absorbent is essentially non-volatile and thus the vapor-phase is pure and homogeneous in the absence of non-absorbable gases. It is important, however, that the very low density vapor be given ample flow area to reach the absorber to prevent excessive pressure losses. At a nominal pressure of 1kPa, a pressure gradient of just 100 Pa within the absorber will cause a 1.4°C increase in evaporator temperature due to the higher pressure required in the evaporator. Thus a small pressure drop within the absorber can lead to a significant degradation in system performance. The concentrated solution pumped from the generator must be distributed evenly on top of the tube bank. Generally this is accomplished by an array of holes or nozzles that either drip or spray solution onto the topmost tube. The design of this distributor must be done with care to ensure an even initial distribution, see for example (Hu and Jacobi, 1996a). Depending on the solution inlet conditions, adiabatic absorption or generation may occur between the distributor and the topmost tube, which may require compensation in the analysis of the data. Often too, the solution falling off the bottommost tube may be collected before it enters the generator to allow measurement of the conditions at this point.

The coolant circuit presents conflicting requirements. On one hand, a large heat transfer coefficient is desirable so that the controlling thermal resistance is on the absorption side, which suggests that high coolant flow rates would be appropriate. On the other hand, it is also desirable to determine the heat duty of the coolant, which requires accurate measurements of the temperature change, which in turn requires a low coolant flow rate. Typically researchers have used one of two approaches to solve this problem: some use inserts in the tube, thick tube walls (to increase coolant velocity), or some other mechanical enhancement to increase the heat transfer coefficient in the tubes while maintaining a flow rate low enough to accurately measure the temperature change. Others have simply used high coolant flow rates and ignored the heat duty on the coolant side, therefore relying only on the absorption side measurements to deduce the heat duty. The coolant circuit is usually a counter-current, serpentine configuration where the coolant flows through all the tubes in series, although some researchers have utilized a partially or fully parallel flow arrangement.

Other ancillary considerations for a test apparatus include prevention of corrosion, crystallization, and provision for optical access. Since the test apparatus may be frequently modified, exposure to air is inevitable, and aqueous solutions of LiBr or LiCr are corrosive in the presence of oxygen. The use of stainless steel components or copper-nickel tubes helps reduce the corrosion problem, but many researchers still add small amounts (around 0.2-0.3% by weight) of commercially used corrosion inhibitors such as LiOH, $Li_2Cr_2O_7$, or $LiMoO_4$. There is very little documentation on the effect of these on system performance, though presumably it is small. Crystallization is a consideration in any lithium bromide-water or other salt-water absorption system, and start-up and shut-down procedures may need to include provisions to avoid it when testing with high absorbent concentrations. For instance, some researchers add water to the system during the shut-down phase and then purge water during the start-up phase to achieve the desired high solution concentrations without crystallization. Finally, the ability to view the falling film can lead to numerous insights into the phenomena occurring during the absorption process. To facilitate this, many researchers include borosilicate glass sight ports or cylinders in their apparatus.

A variety of standard and non-standard instrumentation is frequently employed in these types of investigations. Thermocouples, thermistors, differential thermopiles, and RTDs are used to measure temperatures of interest, which include, at a minimum, the overall solution and coolant temperature changes (see Figure 2.3). Sometimes temperatures are also measured at intermediate points including coolant temperatures after each pass and solution temperatures on and between the tubes. Standard pressure transducers and flow meters of appropriate ranges are used to monitor the system pressure and the flow rate of the coolant and solution. The flow rate of the refrigerant vapor is usually inferred from other data such as generator power, solution flow rates, concentration and temperature measurements. The determination of concentration is inferred either by extracting a sample and measuring its specific gravity or refractive index, or by measuring of the density of solution streams

using densitometers. In general, it is advisable to have redundant measurement methods due to the uncertainties and the small concentration variation (2-10%) often encountered in these systems.

The raw data collected are rarely useful for direct comparison with other systems. But, the derivation of transfer coefficients from the data presents an interesting problem because the heat and mass transfer processes are coupled. Because the heat released at the liquid-vapor interface is proportional to the mass absorbed, and because the concentration that prevails at the interface depends on the temperature of the interface, *the conditions (temperature and concentration) at the interface are directly dependent on both the heat and mass transfer processes*. Figure 1.2 shows representative concentration and temperature profiles on a section of a film falling over a horizontal tube. Since the actual driving forces in the film and vapor are the differences between the conditions at the interface and those in the bulk, it is impossible to define a driving force and thus a transfer coefficient for one transfer process that is truly independent of the other transfer process. This has led researchers to adopt a fictitious driving force for defining the transfer coefficients. For example, the log-mean-temperature-difference for the heat transfer process is frequently defined as follows:

$$\mathrm{LMTD} = \frac{\left(T_{eq,in} - T_{cw,out}\right) - \left(T_{eq,out} - T_{cw,in}\right)}{ln\left(\left(T_{eq,in} - T_{cw,out}\right)/\left(T_{eq,out} - T_{cw,in}\right)\right)} \tag{2.20}$$

where T_{eq} is the equilibrium temperature based on the *bulk* solution concentration and the absorber pressure. But, due to absorption of water vapor at the interface, the concentration at the interface is not the same as the bulk, and therefore the temperature at the interface will be less than T_{eq} as shown in Figure 1.2. Similarly, the log-mean-concentration-difference is often defined as:

$$\mathrm{LMCD} = \frac{\left(C_{eq,in} - C_{b,in}\right) - \left(C_{eq,out} - C_{b,out}\right)}{ln\left(\left(C_{eq,in} - C_{b,in}\right)/\left(C_{eq,out} - C_{b,out}\right)\right)} \tag{2.21}$$

where C_{eq} is the equilibrium concentration based on the bulk solution temperature and the absorber pressure. Again, the actual concentration at the interface will not reach C_{eq} since the temperature at the interface will be higher than the bulk temperature due to the absorption at the interface. Although these are convenient definitions to use, they add complications to the way the derived transfer coefficients must be interpreted. Because the assumed driving forces are not equivalent to the actual driving forces, the derived transfer coefficients will have undesirable mathematical dependencies on system parameters such as the solution inlet conditions. In a forthcoming paper (Islam *et al.*, 2003), Islam et al. address the challenge of defining transfer coefficients for the case of coupled transport. They develop an expression for evaluating an effective mass transfer coefficient, K_{ef}, which is a function of both the heat and mass transfer coefficients of the falling film. They propose a method for extracting heat and mass transfer coefficients from experimental measurements based on a mathematical model but note that "since the heat and mass transfer processes from the film interface to the bulk solution are coupled, it may be more meaningful to consider K_{ef} as the design variable of

interest." Thus it is clear that transfer coefficients derived based on assumed log-mean-differences must be interpreted and compared with great care.

2.2.2 Absorber Configurations and Operating Conditions

A variety of absorbers are utilized in the experimental investigations reviewed here. The design parameters for each apparatus used in the papers reviewed here (listed according to the paper in which the apparatus is first described) are summarized in Table 2.4.

Table 2.4 Summary of Absorber Designs Used in the Investigations Reviewed Here

Author(s)	Number of Tubes	Tube OD [mm]	Center-Center/ Diameter	Tube Length [mm]	Surface Structure	Coolant
Burdukov et al. (1980)	6	16	1.6	150	smooth	NA, isothermal
Cosenza and Vliet (1990)	5, 3	19.5, 42.2	2	610	smooth	parallel flow
Greiter et al. (1993)	24	15.9	1.375	400	smooth, enhanced	serpentine
Nomura et al. (1993)	13	15.9	1.32	200	smooth	serpentine
Atchley et al. (1998)	6	16	1.79, 2.19, 2.79	280	smooth + 9 enhanced	serpentine
Wang (1996)	NA	15	NA	500	smooth	NA
Wassenaar (1996)	10	12 (5mm ID)	1.0, 1.25, 2.25, 3.0	340	smooth	serpentine
Lu et al. (1996)	8	20, 19	NA	400	smooth, 2 enhanced	serpentine
Nagaoka (1987b)	8	19	NA	250	smooth, 2 enhanced	serpentine
Kyung and Herold (2002)	4, 8	19.1	2.33	360, 460	smooth	serpentine
Range for all authors (typ.)	3 – 24	12 – 42	1.3 – 3.0	150 – 600		

Table 2.5 summarizes the range of operating conditions used in the investigations reviewed here. In some cases the authors did not specify enough detail to determine the values in Table 2.5; these instances are identified with NA (not available). In compiling Table 2.5, the correlations for thermodynamic properties of aqueous LiBr found in the ASHRAE Handbook (American Society of Heating Refrigeration and Air-Conditioning Engineers Inc., 1997) as implemented in Engineering Equation Solver (EES) (Klein and Alvarado, 2000), a commercially available software program, were used to convert the data given by the authors into a standard format. In addition to the solution inlet

Table 2.5 Summary of Operating Conditions Used in the Investigations Reviewed Here

	Coolant		Solution				
Author	**T_{in} [°C]**	**htc [W/m^{2}K]**	**Γ [kg/s-m]**	**T_{in} [°C] (° subcool)**	**C_{in} [wt%] (ΔC_{max})**	**Pressure [kPa]**	**Surfactant (concentration)**
Burdukov et al. (1980)	20	~7700	0.15 – 1.25*	35 (10.6)	57.5 (17.25)	1.33	NA
Cosenza and Vliet (1990)	14.8	~1300 – 2600	0.02 – 0.06	30 (-1–12)	50 – 58 (5-20)	0.8 – 1.33	2EH (500 ppm)
Greiter et al. (1993)	28, 30	5500	0.006 – 0.06	34.8 – 43.8 (-2.4 – 4.0)	40 – 59 (2.8 – 42)	0.46 – 4.63	none, 2EH,octanol, decanol (0-640 ppm)
Nomura et al. (1993)	32	~2250	0.012 – 0.052	55 (-4.7 – 0.7)	62 (9.5 – 12.7)	1.04 – 1.41	none
Atchley et al. (1998)	20–35	~1160–2550	0.009 – 0.029	43.2, 47.3 (~0)	60, 62 (4.2 – 15.5)	0.87	none, 2EH (500 ppm)
Wang (1996)	NA	NA	0.025 – 0.083	50 – 60 (NA)	50–60 (NA)	0.47 – 0.93	NA
Wassenaar (1996)	NA	NA	NA	NA (8 – 54)	NA (NA)	NA	none
Lu et al. (1996)	30, 35	~5400 – 5500	0.013 – 0.021	40, 45 (-1.1 – -2.9)	55, 58 (4.0 – 7.0)	1.07, 1.60	none
Nagaoka (1987b)	28	~6500	0.003 – 0.025	40 (5.1)	58 (9.8)	1.2	none, octanol
Kyung and Herold (2002)	30.0	5400	0.014 – 0.05	37.7 – 52.6 (-5.5 – 5.5)	57, 60 (7.4, 9.2)	1.23, 1.09	None, 2EH
Range for all authors (typ.)	15–35	1100 – 7700	0.003 – 0.08	30–60 (-5 – 12)	50 – 62 (3 – 20)	0.5 – 1.6	0 – 600 ppm

* the definition of Γ used by authors is not clear
** absorbent: LiBr/$ZnBr_2$ (2:1), refrigerant: CH_3OH

temperature and concentration, it is also useful to identify the degree of subcooling and the maximum possible concentration change based on inlet conditions. The degree of subcooling is defined as the difference between the equilibrium temperature and the bulk temperature of the inlet solution; in some cases this value is negative indicating that the solution inlet temperature is above the equilibrium temperature, which presumably leads to flash evaporation at the inlet. The equilibrium temperature is evaluated at the absorber pressure and bulk solution inlet concentration. The maximum possible concentration change is defined as the difference between the inlet concentration and the concentration in equilibrium with the coolant inlet temperature at the absorber pressure. Γ is the film flow rate which is defined as the total mass flow rate of the incoming absorbent-rich liquid divided by twice the tube length (see section on effect of film flow rate). Other reference lengths such as D, πD, etc. have also been used in the literature. In such cases, they have been converted to

the basis stated here to facilitate comparison. The factor of two arises from the fact that the liquid flows around two sides of the tube as it flows from the top to the bottom.

2.2.3 Effects of Surfactant

Surfactants, chemical additives that alter the properties of the liquid-vapor interface, have a profound effect on the absorption process and are widely used in commercial absorbers. It is important to understand their effects before the effects of other parameters are considered because the presence of surfactants not only alters the performance, but also can alter the effects of other parameters (Miller, 1999). The literature contains a great deal of empirical information on the effect of surfactants and some competing theories about how they work; some of these have been reviewed by Ziegler and Grossman (1996). The surfactant in most experimental studies of LiBr-water is 2-ethyl-1-hexanol (2EH), although some use octanol (also called 1-octanol or octyl alcohol). 2EH changes the viscosity and surface tension of aqueous LiBr solutions, but the steady state changes in these properties do not adequately explain the resulting enhancement in absorption rates (Beutler *et al.*, 1996a). Most researchers agree that effective surfactants create significant Marangoni convection (induced by surface tension gradients) that causes mixing of the boundary layers within the film and exposes fresh surface to the vapor. The literature also suggests that the 2EH enhances absorption rates by improving the surface wetting and increasing film instabilities (Cosenza and Vliet, 1990) and by increasing the number of droplets (Ziegler and Grossman, 1996). Hoffman et al. (1996) and Ziegler and Grossman (1996) point out that the trends and theories reported about surfactants by different researchers to date are somewhat conflicting. For instance, Kashiwagi et al. (1985) and others have suggested that Marangoni convection is induced by the presence of so-called surfactant islands. Others (Hozawa *et al.*, 1991; Hihara and Saito, 1993; Ziegler and Grossman, 1996) have proposed that the change in surface tension with LiBr concentration and/or temperature in the presence of surfactant is what causes the instabilities in the liquid film. The numerical analysis of Koenig et al. (1999) suggested that, in addition to the change in surface tension with LiBr concentration and temperature, the diffusivity of the surfactant may be important. Fujita and Hihara (1999) suggested that the effect of temperature may actually be more important than that of concentration for the surfactant octanol. The results in (Kulankara and Herold, 2000; Kyung and Herold, 2002) point to the importance of surfactant in the vapor phase and suggests why additives with low volatility may not enhance absorption rates significantly despite their ability to reduce surface tension. Although the exact details of how surfactants enhance the heat and mass transfer processes is clearly quite complex and still a subject of ongoing research, results in the literature allow some quantification of the overall effect.

Nagaoka et al. (1987b) show that the absorption rate increases by 50% when approximately 250 ppm (by weight) octanol is added to an 8-tube absorber. This percent increase is nearly independent of film flow rate although the total absorption rate in all cases increases with increasing flow rate.

They also present overall heat and mass transfer coefficients that are based on the temperature difference between the bulk film and the coolant, and the concentration difference between the equilibrium concentration at the bulk film temperature and the bulk concentration. The authors' results show that the heat transfer coefficient increases by a factor of 5 to 7 times, and the mass transfer coefficient 8 to 10 times the values without any surfactant. Like the absorption rate, the transfer coefficients also increase with increasing film flow rate. It is not clear why such dramatic increases in transfer coefficients would cause a comparatively moderate increase in total absorption rate; however, this could be due to the choice of driving force definitions. Fujita (1993) reviews some similar results available in the Japanese literature (Inoue *et al.*, 1986a, b, 1987; Nagaoka *et al.*, 1987a). Figures 2.4 and 2.5 contain heat and mass transfer coefficients taken from their results for smooth tubes as well as the enhancement due to surfactant calculated by the present authors. The results show that, although the transfer coefficients increase with increasing film flow rate, the enhancement due to surfactant diminishes somewhat from around 2.4 to 1.9 as the film flow rate increases. Their data also show almost a tenfold improvement in the mass transfer coefficient. The authors attributed this large increase in the mass transfer coefficient to the increase in surface convection along the length of the tube and suggest that further improvements to the absorption rate would require improvements to the coolant-side heat transfer coefficient.

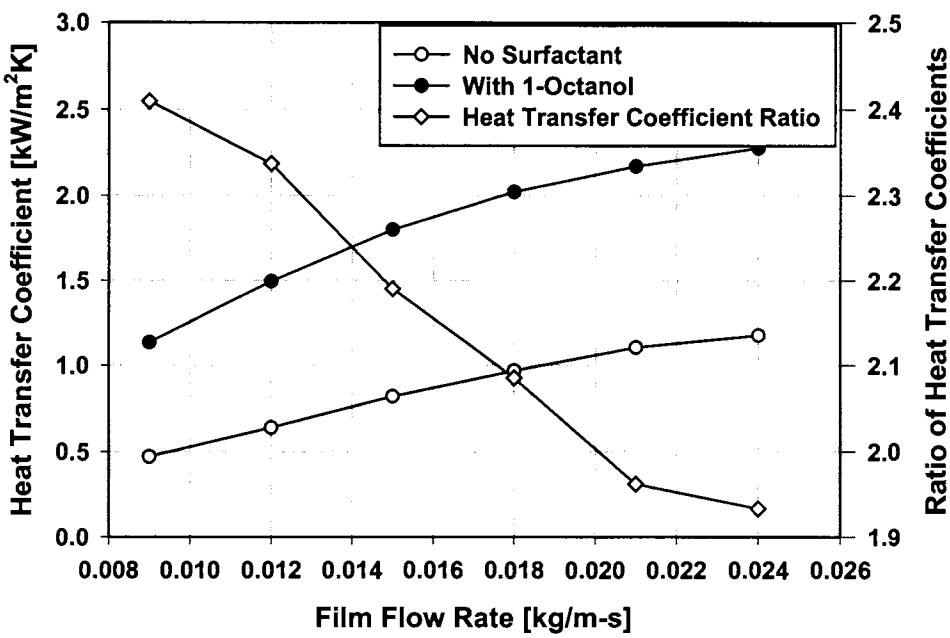

Figure 2.4 Heat Transfer Coefficients With and Without Surfactant, from (Fujita, 1993)

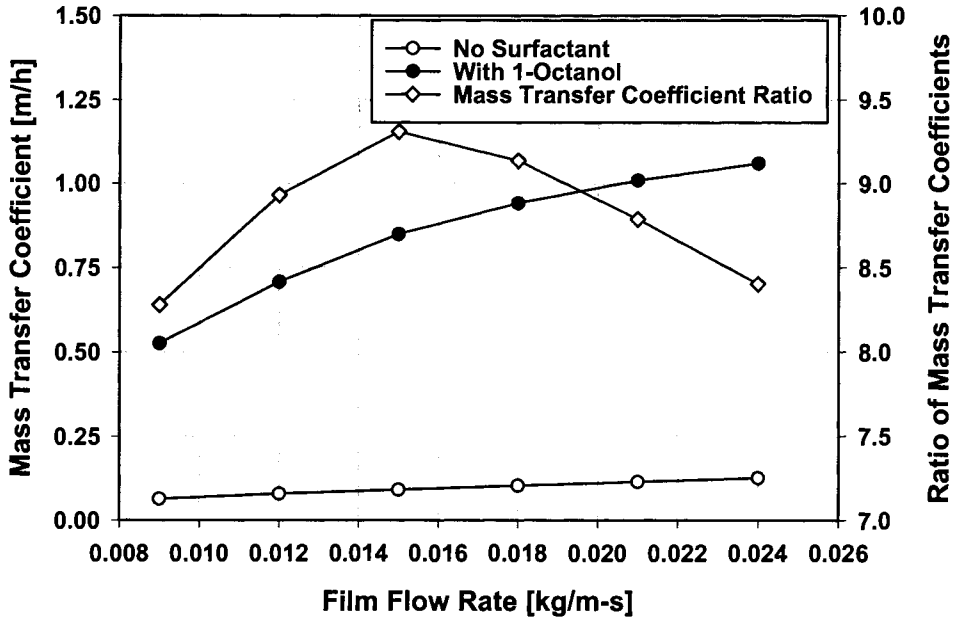

Figure 2.5 Mass Transfer Coefficients With and Without Surfactant, from (Fujita, 1993)

Cosenza and Vliet (1991) compare experiments with about 500 ppm of 2EH to those with "the additive largely removed". They show that the heat transfer coefficient was approximately 3 to 4 times higher with the high concentration of surfactant. They also note that as the film flow rate increases, the enhancement to the heat transfer coefficient from the surfactant decreases, which agrees with the results presented by Fujita (1993) above. They attribute the improvement with surfactant to improved wetting as well as increased interfacial activity. Also, they observe that the effect of surfactant on the film flow is dependent on the presence of absorption (Cosenza and Vliet, 1990). Similarly, Ziegler et al. (1999) show that the heat transfer coefficient increases as the driving temperature difference increases when 2EH is present, which suggests that the enhancement of absorption rates due to the surfactant depends on the rate of absorption. The experimental results of Kyung and Herold (2000; 2002) corroborate these findings and the authors explain that this is a result of the higher delivery rate of vapor-borne surfactant to the film surface associated with higher mass and heat fluxes.

Hoffman et al. (1996) utilize the 24-tube apparatus of Greiter et al. (1993). Complete specification of this apparatus is given by Grossman and Alefeld (1996). "Helical rods" installed inside the tubes provide a very high coolant-side heat transfer coefficient. Results (shown in Figure 2.6) show that the heat transfer coefficient (based on the LMTD defined in Equation 2.20) is improved by about 50% with just 10 ppm of 2EH (note that the volumetric film flow rates specified correspond approximately to the range $0.017 \leq \Gamma \leq 0.044$ kg/m-s). Above 40 ppm, the heat transfer

coefficient is relatively constant. Kim et al. (1996) found very similar behavior with a vertical tube absorber, although the maximum augmentation of the heat transfer coefficient was about 200%. Additionally, Kyung and Herold (2000) and Ziegler et al. (1999) show that almost all of the enhancement associated with 2EH occurs with concentrations as low as a fraction of a ppm. The solubility limit of 2EH in aqueous LiBr is around 50 to 100 ppm (Kim *et al.*, 1996; Kulankara *et al.*, 1999), but varies with concentration and temperature (Kim *et al.*, 1994; Kulankara and Herold, 2002). Even with the apparent uncertainty in the solubility limit in the literature (Yao *et al.*, 1991), the results of Hoffman et al. (1996) indicate that the heat transfer enhancement occurs at concentrations well below the solubility limit. Accordingly, Kulankara and Herold (1999) suggest that the bulk concentration of surfactant is not as relevant as the amount of vapor-borne surfactant delivered to the film interface. The test apparatus used by Hoffman et al. (1996) was enclosed in a glass container, which allowed visual inspection of the film flow patterns. The authors noted that the largest improvement due to the 2EH was in the low film-flow rate cases where the surfactant eliminated the incomplete wetting that occurred when no surfactant was present. They also noted increased horizontal movement of the film on the tubes in the regions of high absorption, which agrees with the observations of Cosenza and Vliet (1990) and others. Finally, they suggest that the effect of surfactant cannot be easily correlated simply with traditional non-dimensional numbers and that understanding the effects requires determining the details of the film flow and droplet formation in the presence of surfactant.

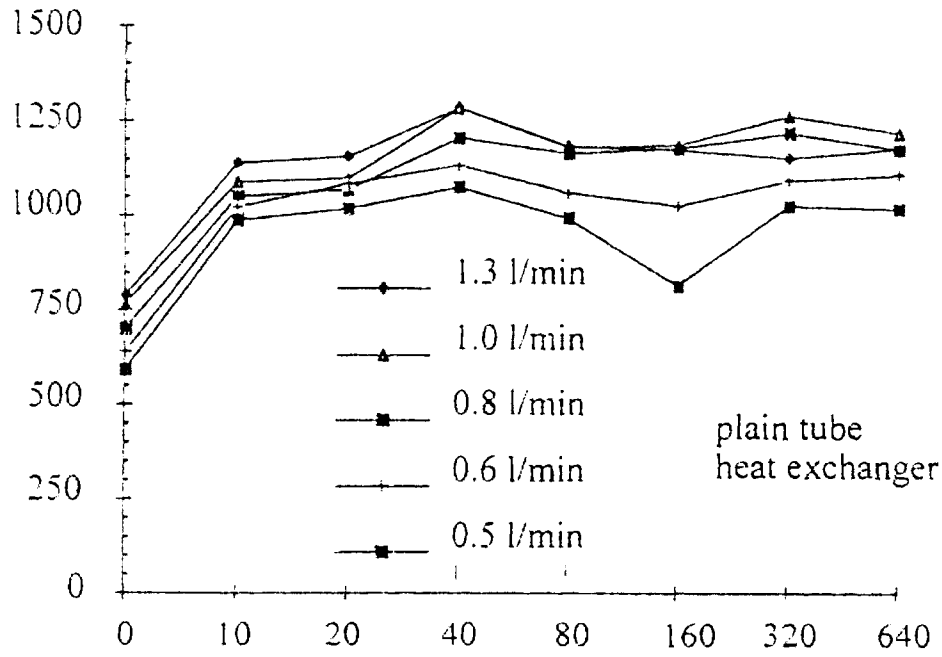

Figure 2.6 Effect of 2EH Concentration on Heat Transfer Coefficient, from (Hoffman *et al.*, 1996)

The results of Hoffman et al. (1996) with 2EH did not show the level of improvement found in the results of Nagaoka et al. (1987b) with octanol. Beutler et al. (1996a) investigated the effect of three surfactants, 2EH, octanol, and decanol, using the same experimental apparatus as Greiter et al. (1993) and Hoffman et al. (1996). The heat transfer coefficients shown in Figure 2.7 illustrate that the improvement with octanol is greater (about 80%) than with 2EH (about 60%) for a nominal operating condition. The improvement with octanol shown in Figure 2.7 is somewhat lower than that reported by Fujita (1993) (Figure 2.4), but the film flow rate is about 0.043 kg/m-s, which is higher than the highest flow rate used by Fujita (1993). Since the improvement in Figure 2.4 appears to be decreasing with increasing film flow rate, these results seem to corroborate each other. This may suggest that the results shown by Fujita (1993) were also influenced by incomplete surface wetting at the low flow rates without surfactant. Beutler et al. (1996a) note that all three alcohols studied lower the surface tension of aqueous LiBr and that this reduction increases steadily up to their respective solubility limits. This trend in surface tension does not, however, adequately explain the trends shown in Figure 2.7. Moreover, they point out that the surface tension is nearly the same with octanol as with decanol at high concentrations. Therefore, they conclude that surface tension reduction is not a sufficient parameter for explaining the absorption enhancement. The theory of Kulankara and Herold (2000) provides one possible explanation of the results shown in Figure 2.7 since the vapor pressure of 2EH and octanol are 12 and 7 times higher than decanol. Unfortunately, Beutler et al. (1996a) do not estimate the mass transfer coefficients, so there is no corroboration of results shown in Figure 2.5.

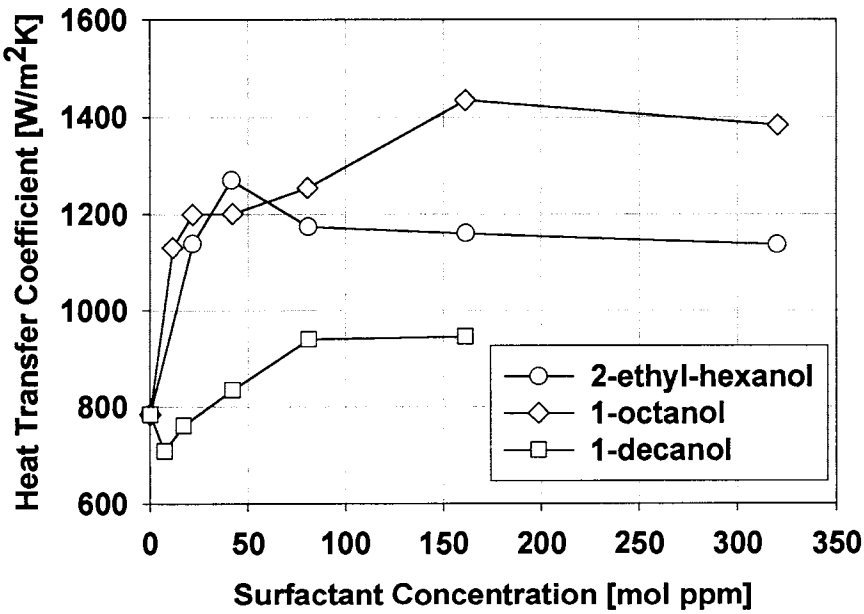

Figure 2.7 **Heat Transfer Coefficient versus Surfactant Concentration for Three Alcohols, from (Beutler *et al.*, 1996a)**

Atchley et al. (1998) and Miller (1999) both investigate the effect of 2EH on absorption over 6 horizontal tubes; these two reports are based on data taken from the same test apparatus. Although their test setup has a comparatively low coolant-side heat transfer coefficient (similar to (Cosenza and Vliet, 1990)), their results corroborate some of the findings mentioned above. In addition, the authors present photographs of the change in flow pattern when 500 ppm 2EH is added. The improvement in heat transfer coefficient due to the addition of surfactant reported by the authors is nominally about 200–300% which is higher than reported above. However, this result is obtained with a lower solution flow rate (0.009 kg/m-s) and a higher inlet LiBr concentration (60-62%) than the previous results. Nagaoka et al. (1987b) showed that the improvement due to surfactant increases as the film flow rate decreases. This trend can also be indirectly seen in some of the results of Atchley et al. (1998) and Miller (1999). Kim et al. (1994) suggest that for a given concentration of surfactant, the surface tension reduction increases as the LiBr concentration increases. Thus, it is plausible that the larger improvement measured by Atchley et al. (1998) and Miller (1999) is a combined result of the lower solution flow rate and higher inlet concentration. By varying the coolant inlet temperature, and thus the total absorption duty, the authors show that without surfactant, the heat transfer coefficient remains nearly constant irrespective of absorber load. However, with surfactant, the heat transfer coefficient increases steadily with increasing absorption rate: the same coupling observed by Ziegler et al. (1999). The authors also observe that the effect of the 2EH on the flow pattern changes with time. The photographs they present show that shortly after the surfactant is introduced, the film exhibits a wavy texture with a large amount of motion in the axial direction of the tube as noted by other investigators (Cosenza and Vliet, 1990; Beutler *et al.*, 1996a; Hoffman *et al.*, 1996). They also show that the behavior of the droplets between the tubes is different; with surfactant there are more droplet formation sites, although the size of the droplets and the trail of solution following them is about the same as with no surfactant. A photograph 16 minutes later shows that the film interface is largely smooth and that the droplets are significantly smaller, spaced closer together, and have much shorter trails than either the case without 2EH or shortly after its introduction. The authors report that the absorber performance during this transient was nearly constant, but provide no explanation for this transient change in the film behavior; although these observations may corroborate the theory of Herold et al. (Kulankara and Herold, 2000; Kyung and Herold, 2002) that the vapor-borne surfactant is important. Other researchers have also noted that the droplets become smaller and more closely spaced in the presence of surfactant (Beutler *et al.*, 1996b; Hoffman *et al.*, 1996).

Kyung and Herold (2000; 2002) use a bank of 4 and 8 horizontal tubes in a complete single-effect absorption heat pump cycle with 2EH. Besides using an entire cycle, they also purposely incline the horizontal tubes 0.45° from horizontal to promote wetting. The authors note that at the low flow rates, there are still dry patches when no additive is present, but because of the inclination, the dry patches continuously move along the tube so that no portion of the surface remains dry for a period of 1 second. The bank of 4 tubes was tested at the same system conditions as the bank of 8 tubes.

Significantly higher heat fluxes were seen in the bank of 4 tubes. For the bank of 4 tubes, the authors show that the heat transfer coefficient enhancement due to the presence of surfactant (100 ppm) was about 67% and independent of solution flow rate. It is plausible that this lack of dependence on the flow rate is due to the improved wetting at low solution flow rates from the tube inclination compared to the results discussed above. With the bank of 8 tubes (which had a lower heat and mass flux), the improvement due to 2EH was reported to be only 20%. This corroborates the fact that the enhancement due to surfactant depends on the absorption rate and also supports the hypothesis about the flow of surfactant to the film surface from the vapor phase. The authors show that the heat transfer coefficient increases with the concentration of 2EH only up to 80 ppm, with further increases in 2EH concentration not affecting the heat transfer coefficient, similar to the findings of (Hoffman *et al.*, 1996).

From the above literature, it is clear that surfactants play a major role in the performance of horizontal-tube absorbers. Visual observations of the film during absorption have identified significant motion in the axial direction of the tubes in the form of wavy rivulets and the change in droplets between the tubes as the predominant mechanism by which the liquid film is agitated and absorption rates increased. In addition to inducing film instabilities, the surfactant has been shown to alter the behavior of the droplets between the tubes which some researchers believe contribute significantly to the overall mass transfer process (Nomura *et al.*, 1993; Kirby and Perez-Blanco, 1994; Atchley *et al.*, 1998; Jeong and Garimella, 2002). However, this basic understanding reveals several areas where more research is needed to further understand and quantify the effect of surfactants on the overall absorption rate, including the quantification of the effects on film waviness, heat and mass transfer coefficients, droplet behavior, the coupling between absorption rate and interfacial instabilities, and surface wetting.

2.2.4 Effects of Absorber Geometry

Primary design features that affect the performance of a horizontal-tube absorber include:

- tube diameter
- vertical space between tubes
- number of tubes per column
- tube surface structure

The effects of these parameters are summarized in Table 2.6 and discussed below. Other parameters such as tube length and number of columns only scale the size of the absorber. These could affect the performance by changing the film flow rate per tube length, which will be discussed in the section on operating conditions. Other practical design considerations that must be considered in a complete design but that will not be discussed here include: vapor flow area (to minimize vapor pressure drop), film distribution method (to ensure even distribution and promote surface wetting), vapor inlet configuration, solution collection, purge system for non-absorbable gases, etc.

Table 2.6 Summary of the Effects of Absorber Geometry

Parameter	Effects
Tube diameter	Cosenza and Vliet (1990) suggest that heat transfer coefficients decrease with increasing diameter
Vertical space between tubes	Wassenaar (1996) suggests that between-tube mixing improves up to 15 mm between tubes. Atchley et al. (1998) and Miller (1999) suggest that results depend on presence of surfactant and wetting may improve with increased tube spacing
Number of tubes per column	Results from Greiter et al. (1993) and Nomura et al. (1993) indicate that the heat transfer coefficient increases further down the tube bank, but absorption rate decreases due to driving force decrease with tube number
Tube surface structure	Most research indicates improved performance with enhanced surface tubes. Wetting and transfer coefficients may both be improved, but results depend on presence of surfactant. The effects on heat transfer coefficients and mass transfer coefficients are often different. Some surface structures may inhibit the augmentation of the mass transfer coefficient due to surfactant by restricting axial motion of the film (Fujita, 1993).

2.2.4.1 Tube Diameter

The literature is remarkably bereft of investigations into the effect of this parameter. The range of tube diameters shown in Table 2.4 is fairly narrow, with most falling between 15 and 20 mm. Cosenza and Vleit (1990) compare the results with a bank of five 20 mm tubes to those with a bank of three 42 mm tubes, both with about 500 ppm 2EH, and suggest the following relationship:

$$Nu_f = 0.30\,Re_f^{0.46}\left(\frac{D}{D_o}\right)^{-0.2} \qquad (2.22)$$

where D_o = 19.5 mm, $Re = 4\Gamma/\mu$, and μ is the viscosity. Although the authors point out the limited basis for this correlation, this relationship suggests that as the tube diameter increases the heat transfer coefficient decreases, although the sensitivity is not great. Because the tube spacing and number of tubes are different between the two test setups, there may be some confounding effect in the results. Nevertheless, this trend seems reasonable considering the effect of droplets and boundary layer development. With a smaller tube, there is less distance for the film to flow between droplet mixing events and so it might be anticipated that smaller tubes would lead to greater transfer coefficients (Cosenza and Vliet, 1990); this is further corroborated by the work of Hu and Jacobi (1996b) (discussed later) who show that during heat transfer to falling films over horizontal tubes, smaller tubes have higher heat transfer coefficients. Also, some investigators (Nomura *et al.*, 1993; Kirby and Perez-Blanco, 1994) have suggested that the droplets contribute significantly to the total mass transfer. For the same total surface area, smaller tubes would lead to more droplets as the fluid flows between the successive tubes in the tube bank, which would contain more tubes due to the smaller surface area per tube. Thus, the relationship in Equation 2.22 seems at least qualitatively correct,

although these plausible interpretations should be confirmed through specifically designed experiments and analyses.

2.2.4.2 Vertical Spacing Between Tubes

Wassenaar (1996), Atchley et al. (1998), and Miller (1999) systematically investigate the effect of tube spacing on the performance of a horizontal-tube absorber. Wassenaar (1996) utilizes a bank of ten 12 mm tubes where the space between the tubes could be varied from 0 to 24 mm (center-center/diameter from 1.0 to 3.0) with a unique binary fluid pair (see Table 2.5). Instead of experimental results, ratios of predicted outlet solution temperature and concentration to measured values are shown. Furthermore, the inlet conditions are not well specified and thus it is difficult to determine the actual inlet conditions as reflected in Table 2.5. The author does state that the amount of subcooling was large "in order to get a sufficient change in temperature and concentration." The testing is performed without any surfactant and the author notes incomplete wetting of the tube and an increase in space between droplets with increasing tube spacing. By comparing results from their model and experiments, the author suggests no mixing occurs between tubes for 0 spacing, an average of no mixing and complete mixing when the space between tubes is 3 mm and complete mixing between the tubes for larger spacing. As shown in Table 2.4, Atchley et al. (1998) and Miller (1999) use a bank of somewhat larger tubes with the space between tubes from 12.7 to 28.6mm ($1.79 \leq$ center-center/diameter ≤ 2.79). Without any surfactant, the authors also observe incomplete wetting of the tube surface, although they point out that the wetting improves as the tube spacing increases due to the higher impact velocities of the droplets, and that no dry spots are observed with the largest tube spacing. At the smallest tube spacing, the authors report bridging or jetting between the tubes. The net result of this behavior is that the heat transfer coefficient, and hence total absorber load, increases with increasing tube spacing for the case with no surfactant. For the range investigated, the improvement in heat transfer coefficient with tube spacing was as high as 60%. With 500 ppm 2EH, however the sensitivity of the absorber performance to tube spacing is much less and not necessarily monotonic; although the largest spacing generally performed marginally better than the rest, the results show that the smallest spacing outperformed an intermediate spacing at most conditions. The authors conclude that the implication of these results for an absorber with tight tube spacing is that if the surfactant degenerates over time, the degeneration in performance may be compounded by the change in flow pattern between the tubes.

2.2.4.3 Number of Tubes per Column

Very little information is available on the effect of the number of tubes in a column on the performance of a horizontal-tube absorber. Greiter et al. (1993) calculate the overall heat transfer coefficient for groups of four tubes within their 24-tube absorber, however, in their results, individual groups are not identified. It does appear that the variation in heat transfer coefficient may be as high

as 35% or more, with the lower tubes having the higher heat transfer coefficients. The authors do not provide any explanation of this result. It should be noted that although there is no surfactant used to obtain these results, the tubes have a knurled surface. It is difficult to estimate whether these results would hold with smooth tubes or with surfactant. Nomura et al. (1993) measure the temperature of the solution on and between each tube in their bank of 13 smooth tubes as well as the coolant temperature after each pass. They do not estimate the heat transfer coefficient, but from an approximate analysis of their data, it appears that the heat transfer coefficient would be nearly constant for all tubes. However, the authors also note that the surface wetting deteriorates significantly from the topmost to bottommost tube. If the reported wetting ratio is taken into account, then their data suggest that the heat transfer coefficient for the wet surface of the bottom tubes is higher than for the wet surface of the top tubes. It is not clear why the heat transfer coefficients would increase with tube number, but the authors note that the absorbed mass per tube *decreases* with tube number because the driving potential decreases down the absorber. Another interesting result shown by Nomura et al. (1993) is that the solution temperature increases significantly (over 2°C on average) between the tubes. Similarly large temperature changes between tubes during droplet flow have also been shown in evaporative coolers utilizing falling films over horizontal-tube banks (Armbruster and Mitrovic, 1998). The authors suggest that this indicates that the droplets between the tubes are cool enough to continue absorbing without heat rejection and thus contribute to the total mass transfer. Finally, Wang (1996) suggests that if the number of tubes is less than four, each tube has a characteristic heat and mass transfer coefficient, but beyond four, the tube-to-tube differences diminish. The author also provides some relationships for the ratios between the transfer coefficients on the first few tubes that are based on the film flow rate, average temperature and concentration on each tube, but it is not clear how these would be applied.

2.2.4.4 Tube Surface Structure

A large amount of research focuses on the use of tubes with complex surface structures such as fins, grooves, or knurls to enhance the performance of horizontal-tube absorbers. Some of this research shows that the enhancement from the surface structure depends on whether surfactants are present (Miller, 1999). Enhancements of around 50% in terms of transfer coefficients are not uncommon, however, some researchers show that certain surfaces may increase the heat transfer coefficient while decreasing the mass transfer coefficient, especially in the presence of surfactant. Much more information is given in (Killion and Garimella, 2003c).

2.2.4.5 Summary of Geometric Effects

Clearly, from the results above, the design of the absorber can have a significant effect on its performance, however the information required to accurately quantify these effects is still lacking. Most of the interpretations provided are qualitative explanations of overall results, rather than

quantitative analyses developed from detailed local measurements of temperatures, concentrations, and the like. Additionally, the effects of individual parameters are not necessarily independent of each other and there has been no systematic investigation addressing these potential interactions. For instance, the presence of surfactants has a large impact on the conclusions one draws about the performance of enhanced tube surfaces. Without surfactant, structured surfaces deliver large improvements in total absorption rate when compared with a smooth tube with the same nominal dimensions. However, when tested in the presence of surfactant, the improved wetting of the structured surface is negligible, and in some cases, the surface structure actually degrades the convective mixing action of the surfactant. It should also be noted that in a significant portion of the literature, only heat transfer coefficients are reported. From the results discussed above, this single parameter does not necessarily correlate well with the actual absorption rate because absorption involves intrinsically coupled heat and mass transfer. Therefore, it is recommended that investigators include measurements that allow the accurate quantification of the mass transfer rate and coefficient as well as the heat transfer.

2.2.5 Effect of Operating Conditions

Perhaps the most commonly studied parameter in falling-film absorption is the film flow rate. It is one of the few independent parameters for component design, although system design considerations dictate overall flow rate and some geometric constraints. In addition to flow rate, the inlet conditions of the concentrated solution, refrigerant vapor, and coolant all influence the performance of horizontal-tube falling-film absorbers primarily through their influence on thermophysical properties and the driving potentials for the transfer processes. These parameters may be independently controlled in a testing situation, however, they may be the result of external constraints such as ambient air and heat source temperatures in an actual heat pump application. Nevertheless, it is important to understand how all of these parameters can affect the absorption process.

2.2.5.1 Effect of Film Flow Rate

Nearly every investigator studies the effect of film flow rate. As described earlier, the film flow rate expressed as the mass flow rate of the incoming absorbent-rich liquid solution divided by two times the length of the tube is the most relevant parameter. The effect of this parameter has been mentioned briefly in the preceding sections. Burdukov et al. (1980) show that the concentration change experienced by the falling film decreases as film flow rate is increased since the absorption rate does not increase in proportion to the film flow rate. However, from a rudimentary analysis of their results, it appears that the transport coefficients do increase monotonically with increasing film flow rate. Nagaoka et al. (1987b) show that the absorbed mass increases with increasing film flow rate for the cases of smooth tubes with and without surfactant, and structured tubes with surfactant.

Additionally, their results suggest that both the heat and mass transfer coefficients increase significantly (from 100 to 300%) with film flow rate for all cases ($0.004 \leq \Gamma \leq 0.02$ kg/m-s). The results shown in (Fujita, 1993) from the same group of researchers show similar trends for an even larger selection of data. Cosenza and Vliet (1989; 1990; 1991) propose the relationship in Equation 2.22 based on testing with smooth tubes and 500 ppm 2EH. This equation suggests that the heat transfer coefficient increases in proportion to the film flow rate raised to the power 0.46. Although there is a significant degree of scatter in their results, this trend is clearly evident. Greiter et al. (1993) state that from their results "there seems to exist no evident correlation between the heat transfer coefficient and the mass flow rate." But, they also point out that, in general, higher film flow rates lead to higher overall heat transfer coefficients. They show, however, that other parameters such as viscosity and surface tension correlate well with the trends in heat transfer coefficients over a wide range of solution flow rates; as surface tension and viscosity increase, the heat transfer coefficients decrease. Beutler, Hoffman, et al. (Beutler *et al.*, 1996b; Hoffman *et al.*, 1996) observe similar behavior. They also point out that the increase in heat transfer coefficient with increasing film flow rate is more pronounced at low flow rates due in part to the change in surface wetting, and that at higher flow rates, the heat transfer coefficients tend to approach an asymptotic maximum. This can be seen, for example, in Figure 2.9. The results of other investigators tend to show similar trends, although the magnitude of the increase with film flow rate varies with each investigator (Isshiki and Ogawa, 1996; Lu *et al.*, 1996; Atchley *et al.*, 1998; Miller, 1999; Kyung and Herold, 2002). Wang (1996) presents plots of average heat and mass transfer coefficient as a function of film flow rate divided by viscosity (a non-dimensional value); these results show a complex variation with this non-dimensional flow rate. At low values, the transfer coefficients increase with increasing flow rate; at intermediate values, the transfer coefficients are nearly constant; and at high values, the transfer coefficients increase again with flow rate. The author explains this behavior in terms of the interaction between incomplete wetting, film thickening, and the onset of wavy film flow. From these results, the author suggests a relationship for the non-dimensional heat transfer coefficient, which varies with the film Reynolds number raised to the power 0.584. It is seldom noted in the literature that increasing the film flow rate also increases the sensible heat load due to the increased heat duty required to cool the liquid film without absorption. The ratio of this sensible heat load to absorption heat load can be substantial. As the film flow rate increases the increases in heat transfer coefficient may not result in real increases in absorption rate, and therefore, cooling or heating rates of the cycle.

2.2.5.2 Effect of Solution Inlet Conditions

The temperature and concentration of the absorbent-rich liquid entering the absorber can influence the absorption process through its departure from equilibrium, its effects on the driving forces for heat and mass transfer, and on thermophysical properties. If the liquid enters in a highly

subcooled state (see Table 2.5), the mass transfer process will start immediately; however, if the liquid enters near equilibrium, enough heat must first be transferred to the cooling medium to depress the temperature at the film interface before significant absorption will begin. Of course, the absorber pressure in part determines the equilibrium conditions, but the pressure is usually determined by the required evaporator temperature and therefore is typically kept within a small range for most applications. Although absorber pressure certainly has an important effect on absorber performance, it is not frequently studied in the literature as an independent variable. Several investigators using the apparatus of Grieter et al. (Greiter *et al.*, 1993; Beutler *et al.*, 1996b; Grossman and Alefeld, 1996; Hoffman *et al.*, 1996) study the effect of the inlet concentration of the liquid film on the heat transfer coefficient. The design of their test stand is such that the inlet concentration is determined by the absorber pressure, so the generation of very low concentration inlet conditions required absorber pressures significantly higher than would typically be used in a real application. It is difficult to say if this pressure variation could have any confounding effect on their results. The authors show that the heat transfer coefficient is strongly influenced by the liquid viscosity and surface tension. The authors note that the viscosity varies over 350% for the range of concentrations that they consider (from 40-59 %wt LiBr, see Table 2.5) (Hoffman *et al.*, 1996). The authors show that the variation of heat transfer coefficient with viscosity is much larger than the variation with film flow rate; the heat transfer coefficients with the lowest inlet concentration are about 8 times higher than those with the highest inlet concentration, whereas for the entire range of flow rates ($0.005 \leq \Gamma \leq 0.045$ kg/m-s) the heat transfer coefficient varied by less than a factor of 3. The authors note that in addition to the increase in viscosity as the inlet concentration increases, the thermal conductivity decreases and the resulting film thickness increases, both of which would reduce the heat transfer coefficient. On the other hand, Kyung and Herold (2000) show that changing the inlet concentration from 57% to 60% has very little effect on the heat transfer coefficient. Thus they suggest that for practical system design, the effect of inlet concentration is small. Besides the inlet concentration, the degree of subcooling is another parameter over which a designer would have control. However, in the literature, there is not much study of this parameter. Kyung and Herold (2002) systematically study the effect of departure from saturation at the inlet, ranging from 5.5°C superheat to 5.5°C of subcooling. Although they note that the heat transfer coefficient and heat transfer rate both decrease with increasing subcooling, they found that the sum of the heat rejection within the absorber and the subcooler remains nearly constant, which suggests that the total absorption rate may be independent of the degree of subcooling. Presumably, in most practical applications, the amount of sensible heat that could be removed before the absorber would be small compared to the total latent heat released during absorption and so, except in certain unique situations, the degree of subcooling would not have a dominant impact on the overall absorption rate. Unfortunately, there is very little information in the literature that reveals the effect of inlet conditions on the mass transfer coefficient or overall

absorption rate, though the effect could be similar to the effect on the heat transfer coefficient mentioned above.

2.2.5.3 Effect of Coolant Temperature and Flow Rate

Most researchers investigating absorption heat and mass transfer attempt to maintain very high coolant-side heat transfer coefficients to ensure that the absorption process is not coolant-side limited. As mentioned previously, this may be accomplished by using high coolant flow rates and/or internal heat transfer enhancements. The inlet coolant temperature is typically chosen to be a nominal value representative of some standard operating condition. The coolant inlet conditions set the limit of the maximum absorption rate or potential outlet subcooling achievable. However, in addition, some researchers show that the coolant-side conditions can have more of an effect than simply altering the driving potentials for the absorption process. Atchley et al. (1998) and Miller (1999) study the effect of coolant-side heat transfer coefficient and temperature and show that the heat transfer coefficients are not necessarily independent of the temperature driving force when surfactants are present. Their results show that, with surfactant present, when the coolant temperature decreases from about 35 to 21°C, the heat transfer coefficients increase by as much as 45%. Ziegler et al. (1999) report a similar trend with surfactant present in amounts from 0.16 to 2.1 ppm and a driving temperature difference from 5 to 12°C. These results suggest that there is an interaction between the effect of the surfactant and the driving temperature difference available for the absorption process itself. In addition, this suggests that other tests conducted with varying coolant flow rates must be interpreted carefully because as coolant flow rate increases, its stream-wise temperature change decreases, thus augmenting the driving temperature difference for the absorption process. The sensitivity of the liquid surface tension to temperature in the presence of surfactants would be an important parameter in determining the effectiveness of surfactants. Since the absorption at the interface also causes steep gradients in the concentration profile, some authors have suggested that the change in surface tension with absorbent concentration may be the key characteristic that determines the effectiveness of surfactants (Hozawa *et al.*, 1991; Hihara and Saito, 1993; Ziegler and Grossman, 1996). An analogous coupling between the mass transfer coefficient and the mass transfer driving potential has not yet been documented in the literature. The authors also show that when there is no surfactant present, the transfer coefficients are nearly constant for the same range of coolant temperatures or driving temperature differences (Atchley *et al.*, 1998; Miller, 1999; Ziegler *et al.*, 1999). Atchley et al. (1998) and Miller (1999) also vary the coolant-side flow rate and thus the heat transfer coefficient, however they do not present the resulting heat transfer coefficients, just the absorber duty. It can be seen that, in a manner similar to the response to coolant temperature, as the coolant-side flow rate is increased, the absorbed mass increases both with and without surfactant. With surfactant, this increase is significantly greater, again suggesting a coupling between the effect of surfactants and the actual rate of absorption.

2.2.5.4 Effect of Non-Absorbable Gases

Great care is taken in LiBr-water absorbers to minimize the presence of any non-absorbable gases such as atmospheric air. Nevertheless, even small concentrations of non-condensing gases can retard the absorption process because they buildup at the liquid-vapor interface due to the bulk flow of the vapor. Cosenza and Vliet (1991) show the effect of air concentration on the total absorption heat flux and solution concentration change. Their results show that at 5% volume concentration, the absorption rate is reduced by about 50% from the value without non-absorbable gases. They note that air concentrations must be maintained below 0.1% to keep the influence of non-absorbable gases on the absorption rate to less than 3%. Beutler et al. (1996c) demonstrate similar results from testing with a hydroxide mixture absorbent. They suggest an exponential relationship between the heat transfer coefficient and the air concentration from their data. This relationship suggests that a 3% drop in film heat transfer coefficient would occur at about 0.2% concentration of air. It is obvious from these results that the presence of even trace amounts of air can have a profound impact on the absorption rate.

2.2.5.5 Summary of Operating Condition Effects

The operating/inlet conditions of an absorber have a significant impact on the absorption rates and to the extent that they can be controlled by a designer, there is some latitude for optimization. The results in the literature provide some quantification of the effects of the various operating parameters; however, there are still some parameters whose effects are not fully quantified, and the interaction between parameters is just beginning to be understood. Some observations about performance effects based on overall measurements are offered, but explanation based on flow mechanisms and local heat and mass transfer phenomena are largely lacking. The investigations required to advance the understanding of these effects have the same requirements outlined in previous sections: detailed understanding of film and droplet hydrodynamics and quantification of the heat and mass transfer rates in systematic and consistent manner.

2.2.6 Conclusions of Review of Experimental Literature

The literature containing experimental results from investigations of absorption of water vapor onto falling films of aqueous absorbent over horizontal tubes has been reviewed in detail. The literature contains a significant amount of information regarding the influence of surfactants, absorber geometry, and operating conditions; however there is still a large opportunity to advance the current understanding. The mechanisms by which surfactants affect the fluid behavior and the absorption process in these systems is still an area of active research. The range of absorber geometries covered in the literature is somewhat limited, but the research does indicate that the diameter, number, and spacing each have an impact on the results. The characterization of these effects is far from complete. The use of structured surfaces has garnered a significant amount of attention in the literature and it

has been shown that even with surfactants, enhanced surfaces appear to provide a substantial enhancement to the absorption process, although the literature shows that in some cases the surface structure can actually degrade the mass transfer coefficient compared to a smooth tube with surfactant. The literature indicates that the inlet conditions of the liquid, vapor, and coolant streams which set the operating conditions within the absorber can have a strong influence on the absorption process both through setting the driving potentials and through their effect on thermophysical properties. Increasing the film flow rate tends to asymptotically increase the absorption rate, although it also decreases the concentration change realized. The film flow rate also influences the fraction of the surface that is wet by the film. In addition, droplet formation frequency and the interaction between neighboring drops during formation and impact can be affected by the film flow rate. The overall sensitivity to film flow rate found in the literature varies significantly between researchers. This is probably due to differences in the baseline condition used as a reference for comparison since the inlet liquid concentration and temperature can have a stronger impact on the absorption rates than the film flow rate. Research also shows that in the presence of surfactants, the transfer coefficients are not independent of the driving potential so the coolant-side conditions can have a greater effect on the process than simply setting one side of the driving potential. Other parameters such as absorber pressure and the presence of non-absorbable gases have an impact on the absorption process, but are not typically considered as parameters which can be used to optimize the absorber performance because they are determined by external constraints.

The literature suggests that the effects on film waviness, axial motion, and droplet formation are important aspects of the mechanism by which surfactants and the various design parameters affect the absorption process, and also that these phenomena may not be independent of the absorption rate. Additionally, the literature suggests that the behavior of the droplets forming between the tubes plays a significant role in the overall absorption process and that surfactants affect the size, frequency, and shape of the droplets. Specific objectives and suggested techniques for future experimental work are given in (Killion and Garimella, 2003c).

2.3 Other Related Literature

The reviews presented above purposefully have a focused scope to provide a comprehensive survey of, and identify areas of need in, falling-film absorption technology. However, for the flow visualization and computational work, there is other related literature that should be noted and used for guidance in conducting the subject research.

2.3.1 Condensation

Condensation on banks of horizontal tubes has been studied a great deal. Nusselt's flat plate laminar film condensation analysis can be extended to horizontal-tube condensation assuming sheet flow between the tubes (Nusselt, 1916). Correlations for the average heat transfer coefficient for a

given number of tubes can then be derived (Incropera and DeWitt, 1990) by assuming that the heat transfer to the sheet between tube and the effect of the acceleration of the falling sheet are negligible. Chen (1961) used boundary layer integral analysis to extend Nusselt's smooth film condensation model to include momentum gain and condensation of the sheet *between* tubes. Chen assumed that the "temperature defect" or degree of subcooling is completely used up in additional condensation during sheet flow of condensate between tubes; thus the liquid is assumed to reach saturation conditions at the top of each tube. Although including these effects leads to higher estimates of the heat transfer coefficient for a bank of horizontal tubes, the estimates still generally underpredict measured results. Incropera and DeWitt (1990) note that the effect of droplets is the most plausible explanation for why experimental results are generally higher than the predictions. Verelst and Berghmans (1981) use a stability analysis to estimate the droplet spacing and estimate a corresponding time/space-averaged film thickness. They examine the predictions of several other models which attempt to include various effects neglected in Nusselt's analysis and show that their model, by including the effect of droplets in the calculation of heat transfer coefficients, achieves the best agreement with a large set of measured heat transfer coefficients. After examining several possible dimensionless groups, they determine that including a Bond number (ratio of characteristic gravitational force to surface tension force) correction provides the most significant improvement to the standard Nusselt analysis. It should be noted that the effect of droplet subcooling is likely to be *more* significant in the case of absorption, especially for the case of aqueous LiBr where the resistance to mass transfer is great. In pure component condensation, the degree of subcooling of the droplets is likely to be less because there is virtually no diffusion resistance to slow the condensation process on the film. However, for binary condensation or absorption where there is a significant resistance to mass transfer, the heat transfer in the falling film can significantly outpace the mass transfer leading to a sizeable degree of subcooling within pendant droplets. Furthermore, the detachment and impact of the drops substantially mixes the film and thus breaks up developing mass-transfer boundary layers thereby enhancing the mass transfer process. In addition, the waves produced on the film can also have a substantial effect: Fujii (1992) in a review illustrates with photographs several different film flow modes that may occur on the surface of the tubes in condensation of binary vapors such as ethanol-water on horizontal tubes. These include dropwise condensation, and three forms of film waviness: streak, ring, and microscopic ripples. By comparing the measured heat transfer coefficients with the laminar film theory, he shows that each of these modes has a sizeable enhancing effect on the Nusselt number. He suggests that the measured effects can be further clarified through observations of the condensation mode.

Hu and Jacobi (1996a) conduct an investigation into the flow modes and transitions between them for falling films of five different fluids over banks of tubes with five different diameters from 9.5 to 22.2 mm and tube spacing from 5 to 50 mm. The authors review several methods for liquid distribution in the literature and suggest a "dummy" tube directly beneath a distribution tube provides

the most consistent, uniform distribution. By observing the flow mode between the tubes (droplet, column, or sheet) at various flow rates for the different fluids and tube arrangements, the authors develop a set of empirical transition criteria. The range of viscosities and tube diameters considered includes those of present study; however, the maximum density was lower (1140 versus 1592 kg/m^3) and maximum surface tension lower (0.068 versus 0.092 N/m) than the conditions in the present study with aqueous LiBr. They suggest relationships for transition Reynolds numbers (ratio of inertia to viscosity forces) based on a modified Galileo number (ratio of viscosity to gravity forces based on the capillary length scale, not tube diameter). The authors note that the transitions exhibit hysteresis: the transition occur at higher Reynolds numbers if the flow rate is increasing than if the flow rate is decreasing. This analysis is useful for determining upper limits for solution flow rate in a horizontal-tube absorber to ensure droplet mode flow between tubes. Hu and Jacobi also study the effect of flow mode on local heat transfer coefficients around the tubes (Hu and Jacobi, 1996b). By surveying the temperature (rotating a tube with embedded thermocouples) of 3 tubes with outer diameters from 15.9 to 22.2 mm during uniform heating (no phase change), the authors were able to show that the time-averaged heat transfer coefficient exhibits significant axial and circumferential variation during droplet flow mode. The droplet impingement points had local heat transfer coefficients up to three times as high as elsewhere on the tube. They also show that the Nusselt number was significantly higher for smaller tubes for all Reynolds numbers investigated during droplet mode, but that tube spacing did not have a significant effect. In a subsequent work (Hu and Jacobi, 1998), the authors demonstrate that for most fluids, the space between droplets decreases with increasing flow rate. They provide correlations for predicting the spacing of droplets and jets which are functions of Reynolds number, modified Galileo number (also sometimes called the Kapitza number), and dimensionless tube diameter. However, they do not provide data for droplet size or frequency.

Cavallini et al. (2001) recently conducted a study of the flow patterns in horizontal-tube banks inside LiBr absorbers. Their apparatus comprised five copper tubes, 16 mm outer diameter, 250 mm long with a tube-to-tube spacing of only 11 mm. They utilized three different concentrations of LiBr ranging from 47.2 to 58.8% LiBr by weight. They provide photographs of the four flow patterns observed: droplet, column, column-sheet, and partial sheet. They note that the presence of absorption did not seem to affect the flow patterns or transitions between them; tests in ambient air appeared the same as tests with more realistic operating conditions. They present flow regime maps in terms of film Reynolds number and a non-dimensional parameter, K which is a function of the Reynolds and Galileo number. These authors show that the transitions between flow regimes agree with the predictions of Hu and Jacobi (1996a) and Armbruster and Mitrovic (1994) although they note that the transition from droplet to column flow between tubes occurs at a slightly lower Reynolds number than predicted; they suggest that this is due primarily to the small tube-to-tube spacing used in their apparatus.

2.3.2 Droplet Formation

The phenomenon of droplet formation has been studied for hundreds of years. According to the review by Eggers (1997), droplet formation was first mentioned in scientific literature in 1686 by Mariotte (1686). Investigating the formation of droplets from fluid jets, Savart (1833), Plateau (1849), and the famous works of Lord Rayleigh (1879a; 1879b) laid much of the foundation for the modern understanding of the formation of droplets. In 1908, Worthington published "A Study of Splashes" which contains 197 remarkable photographs of the coronet splashes that occur when droplets or solids fall onto films or into pools (Worthington, 1908). Work in this field continues today aided by the advent of high performance computers and high-speed, high-resolution video cameras. In addition, due to the inherent natural beauty of droplet formation, the phenomenon has made forays into popular culture with works like the famous milk-drop splash of Edgerton (Edgerton, 1937; Edgerton *et al.*, 1937) and many print and television advertisements (see Figure 2.8). Many empirical/modeling techniques have been developed as a result of experimental investigations into the problem of droplet formation. Some of these are summarized by Kumar and Kuloor (1970), Clift et al. (1978) and Frohn and Roth (2000). A recent review by Eggers (1997) provides an excellent summary of many modern mathematical, experimental, and computation methods utilized to better understand the details of the droplet behavior; Eggers gives special attention to the case of droplets forming from jets or capillary tubes (Figure 2.9 suggests the form of the problem for these cases) and the dynamics of the bifurcation (droplet detachment, bridge breakup, etc.) event. Other reviews covering similar topics can be found in (Bogy, 1979; Yarin, 1993; Middleman, 1995). Axi-symmetric cases have received the vast majority of the attention in the literature. The case of formation under horizontal tubes, however, leads to differences from most of the literature in terms of the overall shape, size, and internal velocity fields of the droplets, especially in the early stages of droplet formation where the extent of the drop in the lengthwise direction of the tube may be several

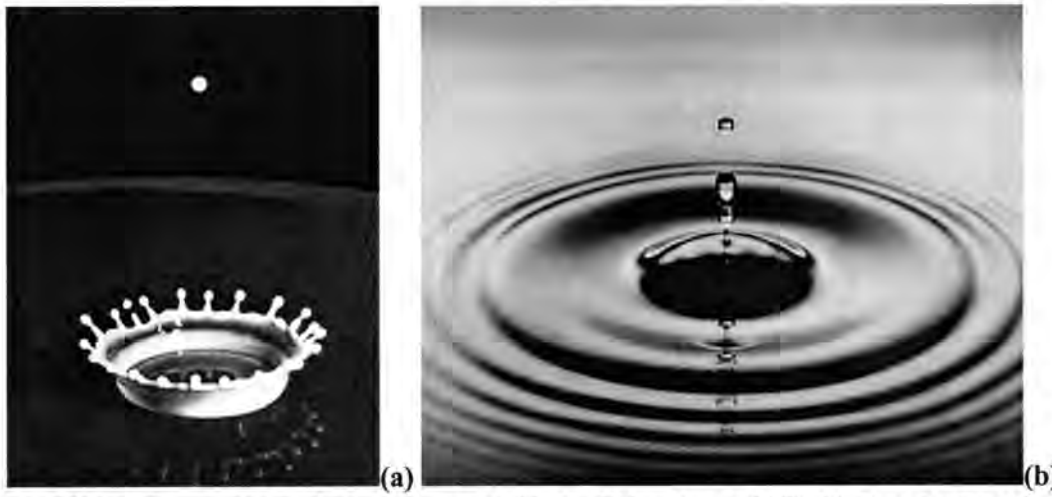

(a) **(b)**

Figure 2.8 (a) Famous Milk-Splash Coronet Photo (Edgerton, 1937) (b) Droplet Photograph Used in Advertising (Stultz and Stultz Photography, 2003)

times its extent in the circumferential direction. In addition, the likelihood of the behavior of one droplet to influence a nearby droplet via impaction and film waviness is high in the case of tube banks, especially as the flow rate is increased. The possibility of this type of interaction doesn't exist in droplet formation from capillary tubes or liquid jets. As will be illustrated in section 3, the disturbances due to droplet interaction can have a profound effect on the behavior of the droplets and film. Despite these differences, the fluid dynamics at the point of bifurcation are almost always axi-symmetrical and independent of the particulars of the setup used to generate the droplets (Peregrine *et al.*, 1990; Eggers, 1997). Thus, even when studied under a different context, advancements in the understanding of the fluid behavior near the pinch point (a point of singularity and zero radius of curvature) are universal and have application to the case of droplet formation under horizontal tubes. In addition, methods for handling free-boundary problems with two phases can sometimes be extended to the more general three-dimensional case.

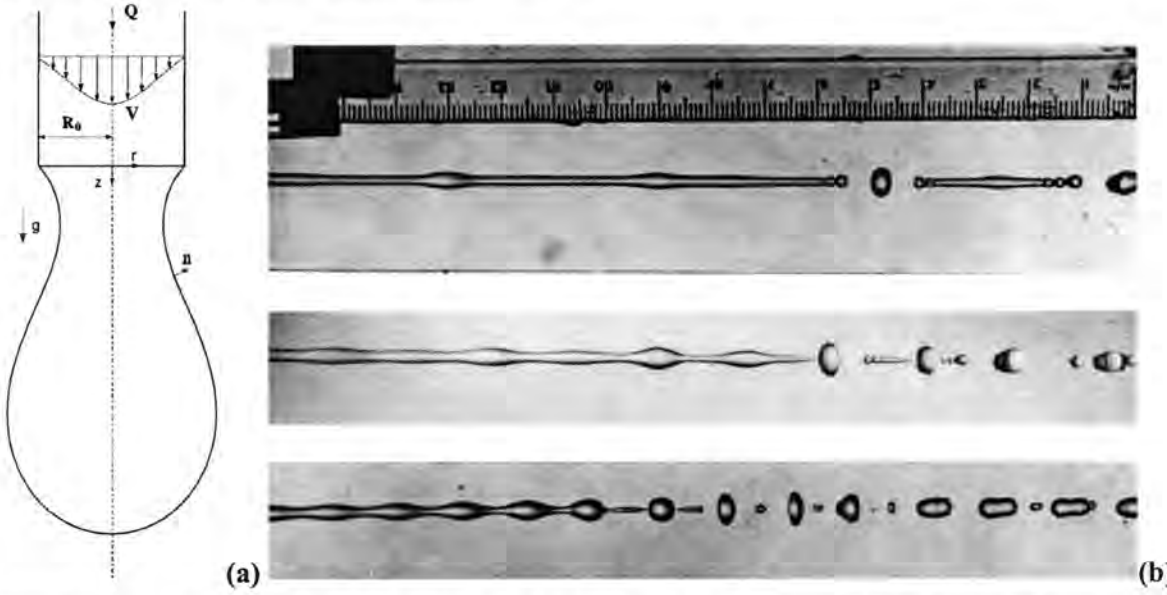

Figure 2.9 (a) Schematic of Droplet Formation from a Capillary Tube, adapted from (Zhang and Stone, 1997), (b) Droplet Formation from the Breakup of Laminar Jets, adapted from (Rutland and Jameson, 1971)

The early works of Edgerton (Hauser *et al.*, 1936; Edgerton *et al.*, 1937) are some of the first to experimentally show the development of droplets from capillary tubes. The shadowgraphs and photographs presented show some of the features of the formation and detachment process for several fluids including water and glycerin and alcohol. These pictures have enough resolution to show that satellite droplets form from the collapse of the liquid bridge between the primary drop and the parent fluid after the bridge breaks from each attachment point (see Figure 2.10a). Also, the strong effect of thermophysical properties, including viscosity and surface tension, on the length, diameter, and stability of the drops and bridge is illustrated. The authors note that "the secondary drop in most

cases vibrates very violently and at first somewhat irregularly." At a low flow rate, a pendant drop essentially assumes a series of equilibrium shapes until the surface tension can no longer support the weight of the drop; equilibrium droplet shape and stability have been considered in the literature (Worthington, 1881; Pitts, 1974; Middleman, 1995; Eggers, 1997). Even at exceedingly low flow rate, the events occurring near the final pinch point or bifurcation proceed at time and length scales that depend almost entirely on fluid properties. It has been shown that the only scales governing the motion at the break are: $t_0 = (r_0^3\rho/\sigma)^{1/2}$ which is on the order of 4 ms for a 2 mm diameter droplet of water (Eggers, 1997) (ρ is the fluid density, σ is surface tension, and r_0 a characteristic length of the droplet), and the viscous length scale, $l_v = \rho\nu^2/\sigma$ (Peregrine *et al.*, 1990) which is only around 140 Å for water (ν is the kinematic viscosity). Peregrine et al. (1990) are perhaps the first to present (and note the self-similarity of) the characteristics of the bifurcation of droplet detachment in enough detail to resolve some of the motion at these very short length and time scales. They present very vivid, magnified photographs of the times before, after, and near the instant of bifurcation for a droplet of water emerging from a 5.2 mm capillary tube (see Figure 2.10b). Many of the features described by Edgerton, Peregrine and their coworkers are also exhibited with droplets forming under horizontal tubes (see section 3): necking and the formation of a thinning liquid bridge or thread between the droplet and the parent liquid above it, a conical point attached to the nearly spherical droplet at the instant of bifurcation, the fast recoil and instabilities exhibited by the broken liquid bridge, and a secondary bifurcation at the opposite end of the liquid bridge leading to the formation of satellite droplets.

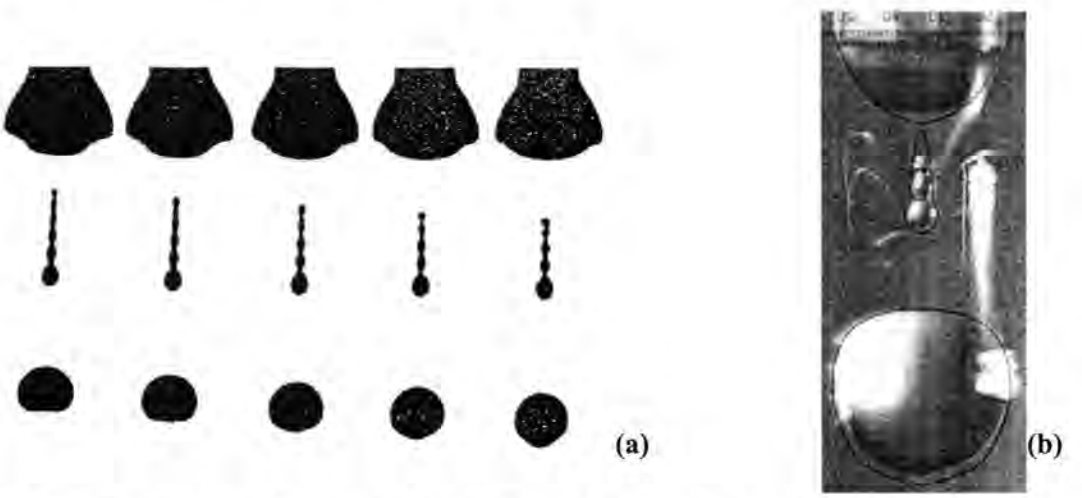

Figure 2.10 **(a) Example Photograph from Hauser, Edgerton, et al. (1936), (b) Example Photograph from Peregrine et al. (1990) shown with Computation Results of Gueyffier et al. (1999)**

Many early investigations of droplet formation were concerned primarily with predicting droplet size and/or the jet length before droplets formed, e.g. (Scheele and Meister, 1968; Kumar and Kuloor, 1970; Heertjes *et al.*, 1971). In the 1970s, the study of so-called "drop-on-demand" droplet generation (drops generated by accelerating an initially quiescent fluid in a capillary tube by the sudden imposition of a pressure pulse of very short duration) received significant attention due to the development of ink-jet printers. However, many of these models neglect the influence of viscosity (Eggers, 1997) and the droplets formed in this case are generally on the order of 25 μm (Middleman, 1995). Due to the complexity of the problem and the ever increasing computation speed of computers, most recent attempts to mathematically analyze droplet formation have relied heavily on numerical techniques. There are, however, still simplifications and innovative techniques that must be employed to make the problems tractable. One major challenge is to efficiently handle/track/capture the free interface between the two phases. The many methods developed for this generally fall into two categories (although hybrid approaches have also been proposed): tracking/capturing the interface on a *fixed grid*, or using a *conformal grid* that is updated to adhere to the shape of the interface at every step. Some time ago, Hyman (1983) provided a review of several of these techniques which include the so-called Marker-and-Cell (MAC) and Volume-of-Fluid (VOF) methods. Other techniques found in the literature include the level-set method (Sussman *et al.*, 1994; Sussman *et al.*, 1998), various front-tracking schemes, e.g. (Unverdi and Tryggvason, 1992a, b; Boulton-Stone, 1993; Blake *et al.*, 1995), free surface capturing techniques (Kelecy and Pletcher, 1997), finite element techniques (Wilkes *et al.*, 1999; Notz *et al.*, 2001), boundary element/integral techniques (Oguz and Prosperetti, 1993; Schulkes, 1994; Zhang and Stone, 1997), and 1-D/slender jet Navier-Stokes approximations (Eggers, 1993; Eggers and Dupont, 1994; Shi *et al.*, 1994; Eggers, 1995; Papageorgiou, 1995; Brenner *et al.*, 1997). Many of these techniques, however, have limitations that make them inappropriate for application to the case studied here. For instance, the 1-D approximations do not predict the size of the droplets or handle internal circulation within the drop well (Wilkes *et al.*, 1999) and would be impossible to generalize to the non-axisymmetric geometry presently considered, most boundary element/integral techniques neglect viscosity (Oguz and Prosperetti, 1993; Schulkes, 1994) or assume Stokes flow (Zhang and Stone, 1997) and cannot arbitrarily handle the rupture and rejoining of interfaces (Schulkes, 1994), similarly, finite element techniques, though accurate, are also difficult to extend beyond the point of bifurcation (Wilkes *et al.*, 1999), free-surface capturing techniques have not been thoroughly developed to include surface tension forces (Kelecy and Pletcher, 1997), and so on. The VOF technique, originally proposed in the mid 1970's by several different investigators (see (Rider and Kothe, 1998)), has proven to be one of the most effective, generally applicable techniques. The VOF method has been advanced by many contributors including (Brackbill *et al.*, 1992; Kothe and Mjolsness, 1992; Kelkar and Patankar, 1994; Brackbill and Kothe, 1996; Gueyffier *et al.*, 1999; Harvie and Fletcher, 2001); it has been successfully extended to three dimensions (Gueyffier *et al.*, 1999; Harvie and Fletcher, 2001), can

appropriately handle surface-tension-driven flow (Brackbill *et al.*, 1992; Brackbill and Kothe, 1996), and moving boundaries (Kelkar and Patankar, 1994). Summaries of the historical development of the VOF method and several other methods of handling free-surface problems are given by Rudman (1997; 1998) and by Rider and Kothe (1998). The number of investigations that have, with varied degrees of success, utilized some implementation of the VOF method is significant and growing rapidly. Some examples will be discussed later. The principle of the VOF method is that a single, scalar value in each computational cell is used to represent the percentage of that cell occupied by one phase. In cells containing only a single phase, the value will be either 1 or 0. In cells through which the phase-interface passes, the value will be between 1 and 0 representing the fraction of the primary phase in that cell. The two main challenges in this method are: 1) to reconstruct the shape of the interface based on the volume of fluid in neighboring cells, and 2) to advect fluid near the interface in such a way that the interface remains sharp (does not diffuse) while rigorously satisfying mass conservation. Methods for handling these challenges are still areas of current research, e.g. (Rudman, 1997; Rider and Kothe, 1998; Rudman, 1998; Gueyffier *et al.*, 1999; Harvie and Fletcher, 2001). Nevertheless, the method has proven to provide reasonable accuracy, is quite economical in terms of memory usage (requiring only one scalar value to be stored for each cell in the solution domain), and has no inherent difficulties when interfaces rupture or coalesce, unlike other methods such as the marker-and-cell or conformal grids, which can exhibit gaps or highly distorted cells when the interface shape becomes complex.

The number of investigations into the dynamics of droplet formation from jets and capillary tubes attests to the formidable nature of the problem. A few of the recent attempts to mathematically model the details of formation from a capillary tube are reviewed next; see Eggers (1997) for a more detailed review of the jet break-up problem, Zhang and Basaran (1995) for a thorough experimental study of the capillary tube problem and Kowalewski (1996) for a thorough experimental study of the jet break-up problem. The axisymmetric, self-similar nature of the bifurcation problem has lead several researchers (Cram, 1983; Keller and Miksis, 1983; Eggers, 1993; Eggers and Dupont, 1994; Shi *et al.*, 1994; Papageorgiou, 1995; Brenner *et al.*, 1997) to seek 1-D models for the fluid dynamics near this point (these approximations also have proven to be reasonably valid for the entire liquid domain in certain instances (Ambravaneswaran *et al.*, 2002)). Without neglecting viscosity or curvature, Eggers and Dupont (1994) numerically solved a 1-D equation derived from simplified Navier-Stokes equations and showed good agreement with the results of Peregrine et al (1990). Brenner et al. (1997) exercised and investigated the implications of the 1-D models and the self-similarity of the dynamics near the pinch point for fluids of various viscosities. Their results suggest that as the viscosity vanishes, the self-similarity breaks down causing a singularity in the curvature at the point of rupture. They investigate the effects of this on the behavior of the recoiling bridge after the rupture. Schulkes (1994) neglected viscous effects and numerically solved the potential flow problem using boundary integrals. The model adequately predicts the results of Peregrine et al. (1990) but

Schulkes found that the singular nature of the problem at the bifurcation led to "severe numerical difficulties." By manually modifying the shape of the interface once the neck radius was sufficiently small, the calculation could be forced to continue past the break point. Zhang and Stone (1997) considered low-Reynolds-number-flow from a vertical capillary tube and also utilized a boundary element/integral analysis but assumed viscous/Stokes flow. They used their model to predict the effect of Bond number, the viscosity ratio between the two phases, capillary number, and the co-axial flow of the ambient phase on droplet volume, break time and length. The non-dimensional parameters, Bo and Ca are defined as follows:

$$Bo = \frac{r_0^2 \Delta\rho g}{\sigma} \qquad (2.23)$$

where $\Delta\rho$ is the density difference between the two phases, r_0 is the outer radius of the capillary tube, σ is the surface tension and, g the acceleration of gravity.

$$Ca = \frac{\mu v_0}{\sigma} \qquad (2.24)$$

where v_0 is the average velocity at the exit of the capillary tube and μ is the viscosity of the liquid phase (other non-dimensional parameters used in the analysis of these systems are summarized in the next section). They showed that the breaking length increases dramatically and the thread diameter decreases as the liquid becomes more viscous, that the time to break decreases with increasing Ca (flow rate), and that the volume of the primary drop decreases with increasing Bo (for a fixed tube diameter). Wilkes, Philips and Basaran (1999) develop a finite element method using a grid that conforms to the liquid phase. They suggest that this method provides a more accurate means of handling interfaces that can "overturn" on themselves, (i.e. develop a dimple or depression after the bifurcation), and bridges the gap between the inviscid model of Shulkes and the Stokes flow model of Zhang and Stone. They discuss the tessellation methods utilized to conform to the highly deformed physical domain. They show that the computed values of length at the time of break agree with their experiments to within 2% over a wide range of viscosities (and thus break-up lengths). It is not clear if this method or that of Zhang and Stone could proceed beyond the break without employing a method like Schulkes (1994). Ambravaneswaran et al (2000) use the 1-D Navier-Stokes approximation of Eggers and DuPont (1994) to investigate the droplet frequency and formation patterns for a series of several hundred drops. This is feasible since the 1-D models are significantly less computationally intensive than other numerical methods. They show that as the flow rate increases, the formation of satellite drops ceases. They also demonstrate numerically and experimentally the existence of alternating "period-2" droplet break-lengths; that is the first, third, fifth, etc. drop break at the one length, while the second, fourth, etc break at another length. In addition, they calculate hysteresis in the flow patterns: the behavior at any given flow rate depends on whether the flow rate had been increasing or decreasing previously. Notz et al. (2001) study the

dynamics of the satellite droplets formed when the liquid thread breaks by simulating the thread as an initially conic section with spherical cap ends. They use the finite element method of Wilkes et al. (1999) which handles overturned interfaces without difficulty. They show that "overturned" shapes are likely in satellite droplets and compare their predictions with very high resolution, high-speed video of a satellite drop. The silhouettes of the numerical and experimental drops exhibit a series of remarkable shape changes and reasonable agreement is shown between the two. Finally, Ambravaneswaran et al. (2002) compare the results of 1-D models with the finite element models of Wilkes et al. (1999) for the case when droplets are formed at larger flow rates than are typically considered with 1-D models. They show that the agreement between the two models depends on the dimensionless parameters defined above and the Weber number (see Equation 2.27 below) and Ohnesorge number (see Equation 2.26 below). In general, when the surface tension force is dominant, the agreement between the two models is good.

As was mentioned above, the VOF method has been successfully applied to numerous problems in droplet formation and impact (discussed in the next section) as well as bubble formation. Some advantages of the VOF method are that it provides one of the more straightforward ways to add interface tracking to an existing single-phase CFD solver, it works for three-dimensional non-axisymmetric problems, no special algorithms are necessary to handle interface rupture or coalescence, and it is computationally economical. Some of its disadvantages are that, until recently (Harvie and Fletcher, 2001), the advection methods could lead to "flotsam" or numerical debris, the interface reconstruction and advection methods could produce slightly jagged interface profiles when the velocity of the interface was not normal to the grid faces, and for an interface reversibly sheared forward and backward the same amount (typical of advection tests for different VOF implementations) the final interface location will show some disagreement or noise when compared with the initial position (see (Rudman, 1997; Rider and Kothe, 1998; Rudman, 1998; Harvie and Fletcher, 2001)). Even with these potential pitfalls, the VOF method has seen widespread implementation in commercial CFD packages. Applications in the literature are too numerous to list comprehensively. It has been validated to predict droplet formation of a viscous fluid in air from the end of a capillary tube (Gueyffier *et al.*, 1999; Zhang, 1999b), jet breakup in liquid-liquid flows (Richards, 1994; Richards *et al.*, 1995), bubble formation and oscillation during the impact of raindrops into deep pools of liquid (Prosperetti and Oguz, 1993), the formation and break-up of crown splashes in droplet impacts on thin liquid layers (Rieber and Frohn, 1999; Gueyffier, 2000), the formation of droplets from a capillary tube surrounded by a viscous medium (Zhang, 1999a), the formation (Oguz and Prosperetti, 1993), rise (Gueyffier *et al.*, 1999) and burst-through (Chen *et al.*, 1997; Yoshikawa *et al.*, 1997; Suzuki *et al.*, 1998) of a bubble in a liquid medium. However, no literature has been found that has attempted to apply VOF techniques to the three dimensional case of modeling the formation of droplets and waves in horizontal-tube, falling-film flow.

2.3.3 Droplet Impact and Film Waviness

The impact of droplets in the case of horizontal tubes and falling films has not received a great deal of attention. However, droplet impact in general is a field that is widely studied. Applications include soil erosion due to rain drops, e.g. (Al-Durrah and Bradford, 1982; Nearing *et al.*, 1986; Nearing and Bradford, 1987), spray coating and painting, e.g. (Groshart, 1985), impact erosion on metal surfaces such as turbine blades, e.g. (Field and Hutchings, 1984), the distribution of pesticides on plant foliage, e.g. (Sundaram and Sundaram, 1991; Sundaram, 1992; Sundaram *et al.*, 1994), filtration of aerosols, e.g. (Dickson and Addlesee, 1984; Douglas and Ilias, 1987; Michaels and Goren, 1987; Wang and Kasper, 1991; Huang and Tsai, 2003), the effect of rain on the environment of bodies of water, e.g. (Blanchard and Woodcock, 1957; Pumphrey and Elmore, 1990; Prosperetti and Oguz, 1993; Kinnell, 2001), spray cooling of hot surfaces, e.g. (Qiao and Chandra, 1998; Healy *et al.*, 2001), deposition of molten metals, e.g. (Kang *et al.*, 1994), and so on. The bulk of the studies can be divided into two groups: impact of droplets onto dry surfaces and impact of droplets into liquid pools. The case of impact onto thin films has received considerably less attention and when studied, the film thicknesses used are generally of the order of the drop size; much thicker than the films considered here. Rein (1993) suggests that in the limit of thin films, "the events become in many respects similar to splashing on solid walls". Furthermore, Levin and Hobbs (1971) report that, in terms of splashing, there is little difference between a dry surface and a wet one except that the time scales are shorter for the wet surface. Weiss and Yarin (1999) showed that if surface tension is sufficiently high to suppress the formation of a crown and thus the possibility of splashing, then their numerical results for impact of droplets onto thin films were similar to those of researchers who had considered dry surfaces. Nevertheless, there are key differences between the two situations. For a dry wall impact, the roughness of the surface and the dynamic (advancing and retreating) contact angle (dependent on the relationship between the surface tension in the three phases (Carey, 1992)) have a strong effect on the splashing and spreading behavior (Rein, 1993; Tropea and Marengo, 1999; Zhuang *et al.*, 1999). In fact Stow and Hadfeild (1981) suggest that the splashing threshold depends more strongly upon surface roughness the smoother the surface is. Many researchers (Hobbs and Osheroff, 1967; Shin and McMahon, 1990; Cossali *et al.*, 1997; Tropea and Marengo, 1999) have shown also that the presence and depth of a shallow liquid layer has a great influence on the outcome of splashing. Additionally, even at low impact velocities, a shock wave develops within the drop and the onset of sideways jetting is strongly determined by the conditions of this shock, see (Rein, 1993) for discussion. The behavior near the initial point/moment of contact is, therefore, strongly dependent on the compressibility of the droplet (Rein, 1993), the elasticity of the wall (Lesser, 1981), the shape of the droplet and the wall (Engel, 1955). Thus the presence of a deformable liquid surface on the film could lead to significant differences in the onset of splashing and the spread of the liquid versus a dry surface.

Still, there is a significant amount of information available in the literature that, carefully considered in light of the precautions above, is relevant to the current work. Rein (1993) has provided a good review of impacts on dry walls and liquid pools. Tropea and Marengo (1999) have also reviewed the impact of droplets on walls and films. In an informative and entertaining review, Prosperetti and Oğuz (1993) have summarized the impact of liquid drops onto liquid surfaces with the objective of understanding the characteristics of sound generated underwater by rain; the results are useful for determining rainfall amounts over large bodies of water.

Throughout the literature, several key dimensionless groups governing droplet impact are often used. These include:

- Impact Reynolds number:

$$\mathrm{Re_i} = \frac{\rho d_0 v_0}{\mu} \tag{2.25}$$

  which is a function of the droplet density, ρ, and viscosity, μ, as well as the diameter, d_0, and velocity, v_0, at the time of impact. Impact Reynolds number expresses the ratio of droplet inertia to viscosity. Note that in the situation considered here, droplets are almost never spherical (discussed later) and so precisely determining the characteristic length is not obvious or trivial. A representative value for this parameter from analysis of high-speed video of aqueous LiBr (discussed later) is $\mathrm{Re_i} = 635$.

- Ohnesorge number:

$$\mathrm{Oh} = \frac{\mu}{\sqrt{\rho \sigma d_0}} \tag{2.26}$$

  which is a function of viscosity, surface tension, σ, and density as well as the droplet diameter. This expresses the ratio of viscous forces to the square root of inertia and surface tension forces. It is equivalent to $\mathrm{We}^{1/2}/\mathrm{Re}$. A representative value for the case considered here with aqueous LiBr is $\mathrm{Oh} = 4.8\times10^{-3}$.

- Weber number:

$$\mathrm{We} = \frac{\rho d_0 v_0^{\,2}}{\sigma} \tag{2.27}$$

  which expresses a ratio of inertia to surface tension forces. It also can be considered to be the ratio of surface tension time scale to convective time scale (Hsiao *et al.*, 1988). This is equivalent to $(\mathrm{Oh} \cdot \mathrm{Re})^2$. For the aqueous LiBr case considered here a value of $\mathrm{We} = 9.2$ is representative.

- Bond number:

$$\mathrm{Bo} = \frac{d_0^{\,2} \Delta \rho g}{\sigma} \tag{2.28}$$

which includes the acceleration of gravity, g. This expresses a ratio of gravitational forces to surface tension forces. For aqueous LiBr under the conditions studied here, a typical value is Bo = 7.4.

- Froude number:

$$Fr = \frac{v_0}{\sqrt{gd_0}} \tag{2.29}$$

which expresses a ratio of inertia forces to gravitational forces. For aqueous LiBr, Fr = 1.1 is typical of the conditions studied here.

Rein (1993) and Mundo et al. (1995) provide several methods for estimating the conditions required for the onset of splashing. Splashing can be defined as any case where the droplet impact leads to the generation of satellite drops. There are two primary methods by which this may occur. The first is from the "fingers" extending from the crown splash, shown for example in Figure 2.8a. This type of splash can occur with deep (Worthington, 1908), shallow (Rieber and Frohn, 1999; Gueyffier, 2000), or no liquid underneath the impact (Yarin and Weiss, 1995). The exact method of instability that leads to the development of the fingers is still not completely understood (Rein, 1993; Rieber and Frohn, 1999), although once created, the breakdown of the fingers into satellite drops ostensibly follows the famous problem studied by Rayliegh: the breakdown of a thin liquid jet into droplets. Although this phenomenon was thoroughly illustrated in the book by Worthington (1908) and made famous by Edgerton (1937), only recently has it received significant attention in the literature (Yarin and Weiss, 1995; Cossali *et al.*, 1997; Thoroddsen and Sakakibara, 1998; Rieber and Frohn, 1999; Weiss and Yarin, 1999; Gueyffier, 2000). Rieber and Frohn (1999) add a random disturbance to the initial velocity of the film and droplet in each discrete volume to obtain "physically reasonable numerical results for the disintegration" of the crown splash. Their results, also featured on the cover of the book by Frohn and Roth (2000), do appear to capture the characteristic fingering, cusping and disintegration illustrated in Figure 2.8a and well-documented in the literature. The second method for generating splash is the so-called Worthington jet, shown for example in Figure 2.8b. This is only formed when the liquid pool is sufficiently deep for a crater to form and collapse (Shin and McMahon, 1990; Weiss and Yarin, 1999; Gueyffier, 2000) although similar behavior is seen with dry surfaces when a droplet rebounds after spreading to a very thin disc-shape (Fukai *et al.*, 1993; Fukai *et al.*, 1995). Several researchers have studied the maximum size of the crater, height of the Worthington jet, and effect of liquid depth (Rein, 1993). It is expected that splashing of this second type could not be observed in the situation considered here due to the thinness of the liquid film. Rein (1993) reviews several criteria for the onset of splashing found in the literature and highlights the relationship of Walzel (1980). This suggests that for a Weber number less than some critical value, We_c, splashing will not occur. The following relationship for We_c based on the Ohnesorge number is claimed to be valid even for thin liquid layers:

$$We_c = 7.9\times10^{10}Oh^{2.8} \quad (2.30)$$

Increasing viscosity and decreasing surface tension would tend to suppress splashing according to this relationship. Rein (1993) cites other researchers have suggested different critical We values for the onset of splashing for droplet impact onto (deep) liquids and the importance of impact Reynolds number. Mundo et al. (1995) suggest that for a K value (see Equation 2.31) less than 57.7, complete deposition of a droplet onto a dry surface will occur without splashing:

$$K = Oh \cdot Re^{1.25} \quad (2.31)$$

For typical conditions considered here, taking the effective diameter of the primary droplet at the moment before impact to be the characteristic length (computed from the volume of liquid below the thinning neck region), the value of We would be 9.6 compared to a We_c of 2.5×10^4 from Equation 2.30. It should be noted that this value of We_c appears exceptionally high compared to other values in the literature; e.g. Reiber and Frohn predict a strong crown splash (Rieber and Frohn, 1999) with We = 250 (a factor of 4 lower than the We_c predicted from Equation 2.30 in their case). From Equation 2.31, a typical value for K is 15.3. Thus for the conditions considered here, one would not expect to see splashing or crown formation but simply droplet spreading upon impact, which is indeed the case, as shown later.

When droplet impact leads to spreading, the thin film formed that propagates away from the point of impact with ever decreasing velocity is called a lamella. It has been noted in the literature that the leading edge of the lamella is generally thickest. The behavior of the lamella leads to another difference between the current case and that of impact on a dry surface. In the case of impact on a dry surface, the lamellae often expand to a maximum diameter and then retract owing to surface tension to an equilibrium shape. In contrast, with a wet surface, the lamellae expand until they are no longer distinguishable features, and on horizontal tubes, expansion in the circumferential direction is limited to the bottom of the tube. Still, there may be some scope for comparing the behavior of lamellae on dry surfaces with the current case; Weiss and Yarin (1999) state that their numerical results of droplet spreading on a thin film exhibits patterns similar to the results of other researchers modeling droplet spreading on dry surfaces. From experiments of droplets impacting dry surfaces with significantly higher Re and We values than occur in the present study, Loehr (1990) suggested the following simple relationship for the growth of the lamella:

$$\beta(\tau) = 1 - exp(-c\tau) \quad (2.32)$$

where the so-called scale factor, $\beta = d_{lamella}/d_0$, the dimensionless time, $\tau = tv_0/d_0$, and c is an empirical value suggested to be around 1 that depends on surface tension and surface roughness. In the case of dry surfaces, the maximum value of β achieved by a droplet has been the subject of several investigations. It is interesting to note that, to model the propagation of the lamella along a dry surface, the standard no-slip assumption must be abandoned to avoid the appearance of infinite forces

(Dussan V., 1979). The literature suggests that a "precursor film" tens to thousands of Angstroms thick precedes liquid spreading alleviating the macroscopic singularity at the contact line (Cazabat and Cohen Stuart, 1987; Middleman, 1995).

When a droplet impacts a liquid surface but does not create a splash or bounce (another well-documented phenomenon which was also observed frequently with the satellite droplets in the experimental work here, see (Reynolds, 1881; Ching *et al.*, 1984; Rodriguez and Mesler, 1985; Zhbankova and Kolpakov, 1990; Rein, 1993)), it is said to "coalesce". It is well known that when the liquid depth is sufficient (typically greater than one droplet radius) a downward-traveling vortex ring is created. According to Rein (1993) this was first studied in detail by Thompson and Newall (1885). Since then many researchers including Chapman and Chritchlow (1967), Rodriguez and Mesler (1988), Sigurdson, Peck and coworkers (Peck and Sigurdson, 1994; Sigurdson and Peck, 1994; Peck and Sigurdson, 1995; Peck *et al.*, 1995), Durst (1996), and Dooley et al. (1997) have studied the details of this vortex creation. Rein (1993) summarizes some of these results and some theories of how the impact and free surface energy of the droplet generate the vorticity. Unfortunately, since the film thicknesses in horizontal-tube falling films are so small, it is unlikely that this phenomenon has much bearing on the current study, although some vorticity may still develop at the leading edge of the lamella as in a boundary layer.

Finally, it should be noted that a significant amount of research has been done on the generation of bubbles during droplet impact. There are several mechanisms by which this may occur including cavitation (Rein, 1993), local aerodynamic distortion of the droplet interface at the point of impact creating a dimple in the drop near impact (Middleman, 1995), entrainment during coalescence (Blanchard and Woodcock, 1957; Esmailizadeh and Mesler, 1986), dynamics of the crater collapse trapping a bubble (Pumphrey and Elmore, 1990; Prosperetti and Oguz, 1993), collapse of a crown splash over a crater formed by the droplet (Worthington, 1908), and so on. The number and size of bubbles generated can vary widely with the generation mechanism. Recent research (Weiss and Yarin, 1999) indicates that entrainment of very tiny bubbles may actually occur as the result of a very small torus jet that develops in the area of high curvature where the drop initially meets the film surface.

2.4 Need for Further Research

From the reviews presented above, it can be seen that despite the significant amount of research work in falling-film absorption published in the literature, there are still many areas where even a basic understanding is still lacking. In particular, understanding the behavior and role of droplets and film waviness has consistently been cited as a critical area for further advancement. The research on droplet formation is a current and exciting field of study with many recent advancements that have been made possible by the ever improving power of modern computers. However, the focus of the research on droplets has focused almost exclusively on axi-symmetric droplets forming either from

the bottom of a capillary tube or other small orifice as in an ink-jet printer, or from the breakdown of liquid jets. Although it has been shown that the local fluid dynamics at the point of bifurcation are virtually independent of the actual method by which the droplets are formed, the overall shape, size, and behavior of the droplets are strongly influenced by the formation method. In addition, most droplet impact studies have considered impact on dry flat plates, deep pools or relatively thick films with the emphasis being on splashing. Thus, the study of the details of droplet formation under and impact onto horizontal liquid-coated tubes at the conditions found in a horizontal-tube absorber would represent a novel and important contribution to the literature. The goal of the research presented below is to advance the understanding of droplet behavior in falling films on banks of horizontal tubes by experimental flow visualization and computational analysis.

3 FLOW VISUALIZATION

Even if one could peer into an operating horizontal-tube absorber, most of the details of the film flow would be obscure to the naked eye because they happen so quickly. Even at the seemingly low flow rates and bulk liquid flow velocities characteristic of falling-film absorption, the entire cycle of a droplet from inception and formation through detachment, fall and impact, occurs in just a few tenths of a second. The complex, interacting features that accompany this evolution, for instance, the propagation of the impulse generated upon droplet impact as waves that travel back up through the droplet and liquid bridge, develop and progress in a matter of milliseconds. These phenomena cannot easily be seen without the aid of high-speed imaging (and some magnification). To enable clear access to the details of the flow of falling films in horizontal-tube banks, experimental flow visualization was conducted on a single-column bank of horizontal tubes in ambient air with films of both water and aqueous Lithium-Bromide using a high-speed, high-resolution digital imaging system. The observed phenomena were first evaluated qualitatively to identify and illustrate the important characteristics and variety of complexities that can occur and are often overlooked in such flows, and comment on the implications of these details. Subsequently, the results were further analyzed quantitatively for comparison with computational results using custom image processing software routines developed in the Matlab (The Mathworks Inc., 2002b) programming environment. What follows is a discussion of the experimental methodology, the qualitative analysis of the observed phenomena and their implications on heat and mass transfer, a review of digital image analysis and mathematical techniques used for the quantitative analysis, a description of the software developed to facilitate the quantitative analysis, and finally, typical results from the quantitative analysis.

3.1 Experimental Setup

Two single-column tube banks were constructed for these experiments (see Figure 3.1); the dimensions are summarized in Table 3.1. The first, tested with distilled water, comprised six horizontal brass tubes 12.7 mm in diameter, approximately 200 mm long with tube center-to-center spacing of 38.1 mm (providing a 25.4 mm tube-to-tube distance). After initial work with this apparatus, the second was constructed to better approximate the geometry typically used in commercial absorbers. It comprised nine copper tubes 15.9 mm in diameter and 500 mm long with a tube center spacing of 31.8 mm (providing a 15.9 mm tube-to-tube distance); it was tested with surfactant-free and corrosion inhibitor-free aqueous Lithium-Bromide (53.44% LiBr by weight). With the primary focus being an understanding of fluid flow, neither apparatus included provision for absorption or heat transfer. The apparatus were surrounded by air at atmospheric pressure and room temperature. No special controls for humidity, temperature, or fluid purity were used since the objective of these tests was primarily to obtain a qualitative understanding.

Table 3.1 Summary of Tube Bank Designs

	Water	Aqueous LiBr
Tube Diameter [mm]	12.7	15.9
Center-to-Center Spacing [mm]	38.1	31.8
Tube-to-Tube Spacing [mm]	25.4	15.9
Length [mm]	200	500

In the first, the tubes were mounted in a cantilever fashion to allow clear viewing from the end as well as the sides. In both cases, the levelness of the tubes was checked with a bubble-in-tube hand-held level. Establishing perfect levelness was not critical; the primary criterion was that the droplets did not preferentially traverse in one direction along the underside of the tubes while they formed. Some researchers (Kyung and Herold, 2000; Shultz, 2001; Kyung and Herold, 2002) have actually found that maintaining a very small inclination (less than a degree) is advantageous for promoting even wetting of the tubes.

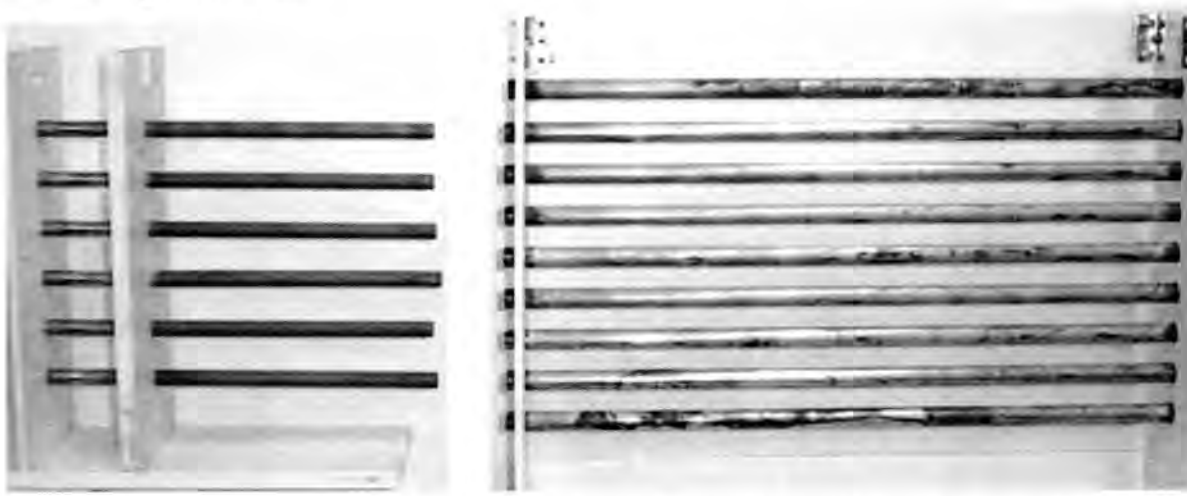

Figure 3.1 Tube Banks (Left: 12.7 mm Brass Tubes; Right: 15.9 mm Copper Tubes)

A pump was used to circulate the liquid first through a rotameter, which both controlled and measured the flow rate, then through a distributor which dispensed liquid along the top of the tube bank. The distributors were designed to promote even distribution of liquid along the length of the tubes. Two slightly different designs were used. Both were based on a tube-in tube design with fluid entering the inner tube. Small holes directed upward were spaced evenly along the inner tube; the relatively high-velocity, high-pressure-drop flow through these holes ensured even axial distribution of the fluid by minimizing "header" effects due to pressure drop along the inner tube. Fluid exiting these small holes flowed into the annulus formed by the two tubes (impinging on the inside of the outer tube), flowed through the annulus around both sides of the inner tube, and finally exited the distributor through a large flow area in the bottom of the outer tube. In this way, the high-velocity

flow through the small holes ensured equal distribution along the length of the tube, but the flow out of the distributor was slow enough not to impart any significant initial velocity to the film. The main functional difference between the two distributors, besides being different sizes and having different hole arrangements, was that, in the first, fluid exited the annulus through a 1 mm wide slot in the outer tube and flowed around a "dummy tube" placed about 1 mm below, while in the second, the bottom half of the outer tube was cut away. Thus, in the first, droplets formed from the underside of the dummy tube, whereas in the second, the droplets formed from the underside of the inner tube (see Fig 3.2). The first distributor was constructed from copper tubes. Six small holes (0.9 mm) were drilled in the 6.4 mm diameter inner tube 25.4 mm apart. The 12.7 mm diameter dummy tube was placed approximately 1 mm below the slot in the 12.7 mm diameter outer tube. Equal flow on both sides of the tube was achieved by rotating the distributor tubes until the droplets fell straight down from the dummy tube. The second distributor was considerably longer (about 500 mm) and machining such a long, straight slot along the outer tube proved to be very challenging. The combination of the weakened tube structure (as the slot was cut) and the forces of the cutting tool led to a slot that was not straight even when the work piece was solidly clamped into a milling machine. From work with the first distributor it was known that, when using a narrow slot, the orientation of the slot with respect to the dummy tube was critical to achieving even flow on both sides and thus droplets that fall vertically and do not "sling" away from the tube column. Therefore, a crooked slot would have been nearly impossible to use. The alternative technique employed was to make the "slot" so large that its influence on the flow was minimal. This was achieved by cutting away almost half of the underside of the outer tube. It was found that this arrangement provided excellent results without a dummy tube and was not highly sensitive to the angular orientation of the outer tube. The second distributor was made from PVC to ease construction. The inner and outer tubes were nominally 15.9 mm outer diameter and 17.7 mm inner diameter respectively. The 16 small holes were spaced 31.8 mm apart and were approximately 1.4 mm diameter.

In both cases flow rates could be increased to the point that liquid columns would begin to form (see Figure 3.3); this was useful for establishing complete tube wetting before a test, but for the testing, the flow rate was kept much lower than this in the droplet flow regime (see Figure 3.3). Typically the film Reynolds number ($4\Gamma/\mu$) was somewhat less than 100. (According to the work of Hu and Jacobi (1996a) the Reynolds number where the droplets would transition to continuous columns is about 425 for water and 740 for aqueous LiBr)

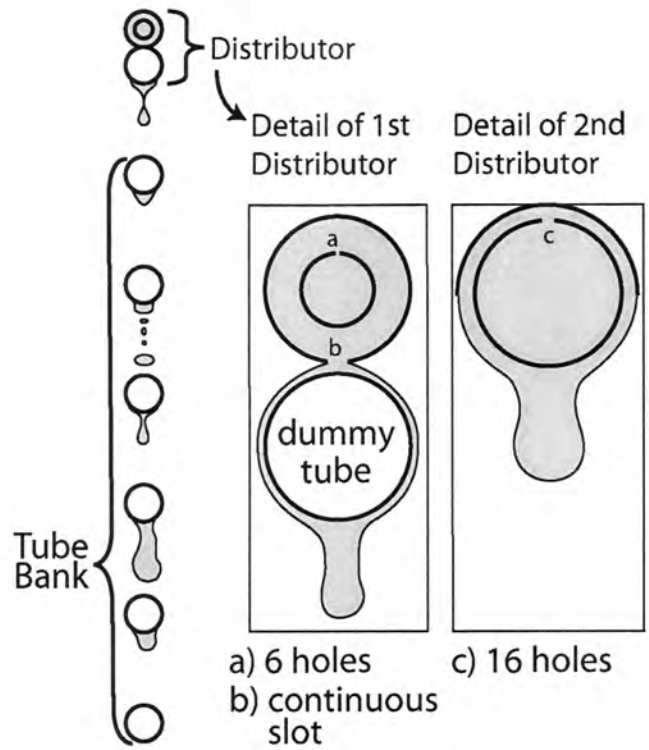

Figure 3.2 Distributor Cross-Section Detail

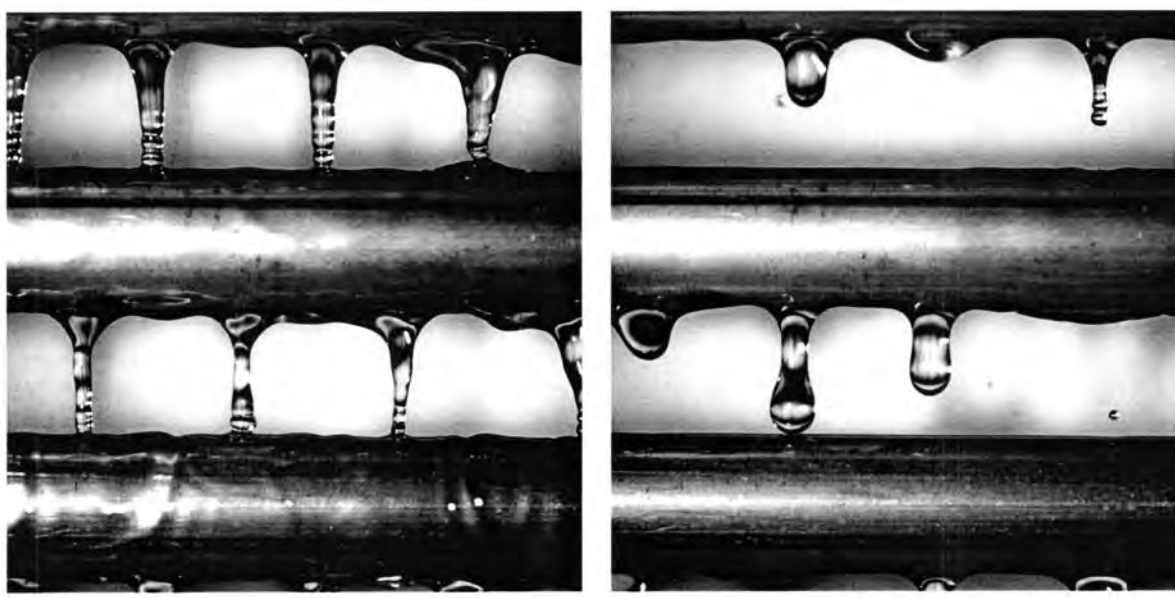

Figure 3.3 Example of Column Flow (left) and Drop Flow (right) Modes with 53.44% LiBr

For the brass tubes used with water, the tube surfaces were prepared by thoroughly cleaning with solvent, polishing using a common metal polishing compound, then heating to promote a thin oxide layer on the surface. This last step improved the wetting of the tube although it did not guarantee complete wetting at the given flow rates, especially near the bottom of the tube bank. As the water flowed over successive tubes in the bank, it tended to cohere, and an initially well-distributed film would form three or four collected streams at the bottom of the bank. This phenomenon has also been observed by other researchers such as Nomura et al. (1993) and is particularly problematic when using water instead of a fluid pair such as water and Lithium Bromide. After some of the testing was completed, to improve the wetting at the bottom of the bank, the tube surfaces were all sandblasted. This significantly improved the wetting of the tubes and reduced the tendency of the water film to form rivulets toward the bottom of the tube bank; however, the resulting dull surface of the tubes obscured the details the film motion in the images. The copper tubes used with the aqueous LiBr were simply cleaned before use. Aqueous LiBr tends to etch the surfaces so after running for a few moments, the surface of the tubes would be bright copper.

Two types of high-speed digital video cameras, both made by Photron (Photron USA Inc.), were used to capture the images of the film. The cameras are operated through an IEEE 1394 computer interface. Frame rates of 500 frames per second (fps) and higher were used with shutter speeds from 1/500 to 1/4000 seconds. At 500 fps, one camera, the Fastcam Ultima 1024 using a color CMOS sensor, could support a resolution of 1024 x 1024 pixels, while the other camera, the Fastcam PCI, yielded a monochrome image with a resolution of 512 x 240 pixels; this second camera was only used for some of the testing with water. The cameras were equipped with enough memory to store 1 second of video which could then be subsequently downloaded and stored as AVI files on a computer hard-drive. A variety of zoom and fixed lenses were used to obtain the desired magnification. An "Omni" light made by Lowel was used for illumination. The 500 watt tungsten/halogen bulb was model "FTK" with an illumination temperature of 3200 K. Using the "Super Spot" parabolic reflector which has a 12° beam angle (defined as the point where the intensity drops to 50% of maximum), the lamp provides 2750 foot-candles (29700 Lux) of illumination at a distance of 1.5 meters. This high level of illumination is required to provide adequate exposure for the high shutter speeds and CMOS sensor used here.

3.2 Departure From Idealized Flow Pattern

As stated in the literature review section, attempts to mathematically model these coupled heat and mass transfer processes on falling films over horizontal tubes have included many idealizing assumptions about the behavior of the film (Killion and Garimella, 2001). Most frequently, the film is considered to be smooth and laminar, droplets between successive tubes are not considered to participate in the absorption process, and the film is assumed to be uniformly distributed along the tube and to start with a well-mixed, uniform concentration and temperature at the top of each tube

(Andberg, 1986; Andberg and Vliet, 1987a; Choudhury *et al.*, 1993; Conlisk and Mao, 1996; Lu *et al.*, 1996). Models of this type are of limited use for system design and optimization, or even for understanding the implications of significant design parameters. What is required for advancing modeling capabilities is a thorough understanding of the flow patterns. These will be illustrated in the next section. The many interactions such as the waves and ripples generated by an impacting drop will be highlighted. It is thought that it is this "non-ideal" behavior of the falling film that directly leads to the relatively high transfer rates achieved in practice.

The discussion is organized as follows:

First, the *formation, detachment, and fall of a droplet* from a relatively undisturbed film will be discussed. Second, the *waves* created on the film due to droplet impact and detachment will be discussed. Even more complex behavior arises when falling and forming droplets interact with each other and with a wavy film. Therefore, the final discussion topic will focus on these *interacting phenomena*, which include, for instance, two droplets impacting near each other at the same time, or the effect of a droplet impacting above a forming droplet. These interactions can generate significant departures from the non-interacting case. Wherever possible, visual evidence of the phenomena discussed will be presented.

3.2.1 Droplet Formation, Detachment and Fall

Droplet formation is a phenomenon related to the Rayleigh instabilities (Carey, 1992). Initial instabilities of the annular film surrounding the tube are driven by surface tension forces similar to the instabilities of cylindrical columns of fluids. As the film thickens at the bottom of the tube and droplet formation sites begin to form near the so-called most dangerous wavelength, buoyancy forces (gravity) take over and amplify the inherent instability. Liquid accumulates at the low spots of the liquid film and gravity begins to pull the forming droplets away from the tube. Unlike the classical instability problems, the liquid and vapor are not initially at rest or uniform velocity in this system, and influences other than the most dangerous wavelength can affect the actual droplet spacing. Most notably, the incidence of a droplet impacting from a tube above frequently leads to a local excess of liquid that initiates a new droplet formation site directly underneath the impact site. Also, when a droplet detaches, a significant portion of the liquid often stays attached to the tube; thus a particular droplet formation site may simply be the artifact of previous droplet formation site giving rise to preferential formation sites, at least on a temporary basis. In addition, axial motion of the liquid on the under-side of the tube due to propagating (and colliding) waves may generate a local excess of liquid that can develop into a formation site. This would be especially true in the presence of absorption with surfactant where axial motion may be significant (Cosenza and Vliet, 1990; Miller, 1999).

Early Formation. A droplet allowed to form relatively undisturbed will exhibit certain common characteristics, although, as in the capillary and jet problems previously reviewed, the details may

vary significantly with thermophysical properties. A droplet forming pendant from a horizontal tube is not axisymmetric but is elongated in the axial direction of the tube in the initial stages of formation due to surface tension forces. In fact, the precursor to a droplet may appear to be a wave on the film along the bottom of the tube that is much longer than the width of a droplet, as shown for water in Fig. 3.4. As liquid continues to arrive at this location from the film surrounding the tube, the amplitude of this wave begins to increase to accommodate the increased volume of liquid (Fig. 3.4b-e). At some point in this process, the wave ceases to appear sinusoidal and begins to adopt the appearance of a forming droplet. Subsequently, the sides of the droplet begin to contract as the liquid is drawn to the lowest point on the wave; the film left on either side reverts to a relatively uniform thickness (Fig. 3.4g). Ostensibly, liquid must be drawn from regions of the tube that encompass a significantly greater length of the tube than just the width of a drop. Thus the formation of the droplets induces some transverse velocity component within the film surrounding the tube. Whether this occurs primarily at the bottom of the tube or around the complete tube circumference is not readily obvious, but it could have the effect of mixing the film.

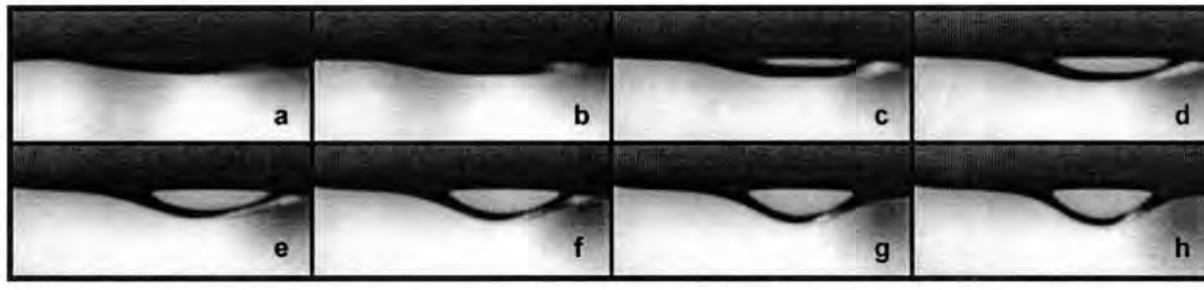

Figure 3.4 Water, Early Formation Site Developing from Long Wave, Side View, 10 ms between frames

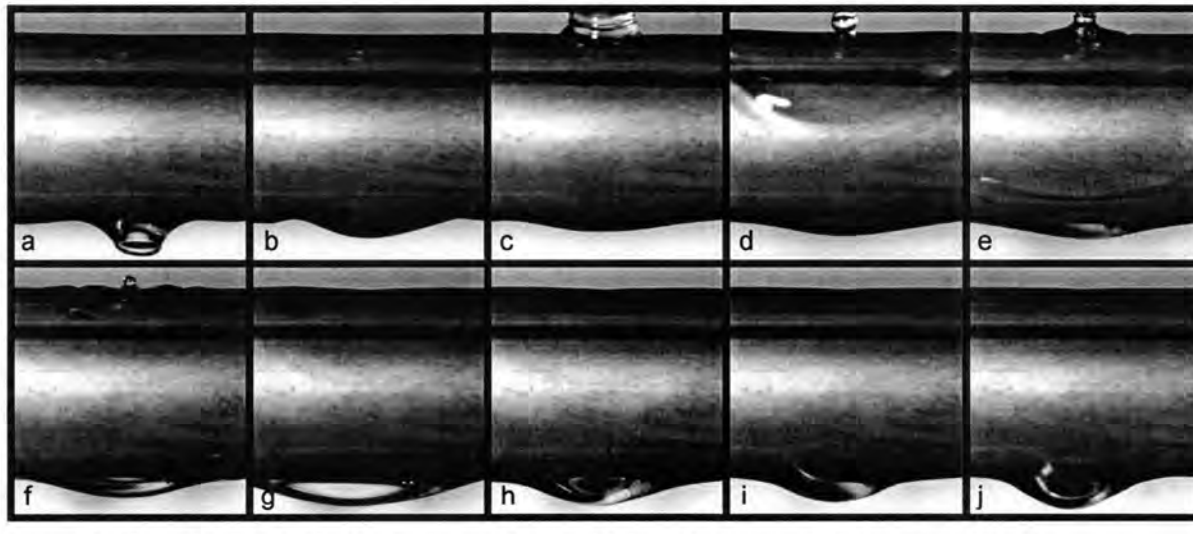

Figure 3.5 LiBr, Early Formation, Effects of Detachment and Impacting Droplet, Side View, 20 ms between frames

Figure 3.5 shows a similar pattern for aqueous LiBr (time between frames is twice as much as Figure 3.4). However, these frames illustrate the effect of a pre-existing and impacting drop on the drop-site formation process. It can be seen in the bottom of Figure 3.5a-d that a significant portion of liquid is recoiling after droplet detachment, leading to a localized excess of liquid. In figure 3.5c, a droplet impacts above this location and the liquid propagates around the tube, arriving around frame f. This adds significantly to the local excess of liquid and the formation site grows in frames f-j in much the same manner as was shown in Figure 3.4. Fig. 3.6a-f shows a similar progression for water, but viewed from the end of the tube looking slightly upward. Again, note that the time between each frame in Fig. 3.6 is double that in Fig. 3.4, and the perspective in Fig. 3.6 results in the viewing of four formation sites simultaneously (although only two finally develop into droplets within the duration shown). Fig. 3.6a-f show that during early development, the droplet formation sites do not change much in width in the horizontal direction perpendicular to the tube axis in spite of the large changes in the lengthwise direction. In fact, Fig. 3.6a-f reveals that the thickness in the circumferential direction may actually decrease during early droplet development, contrary to what occurs in the lengthwise direction.

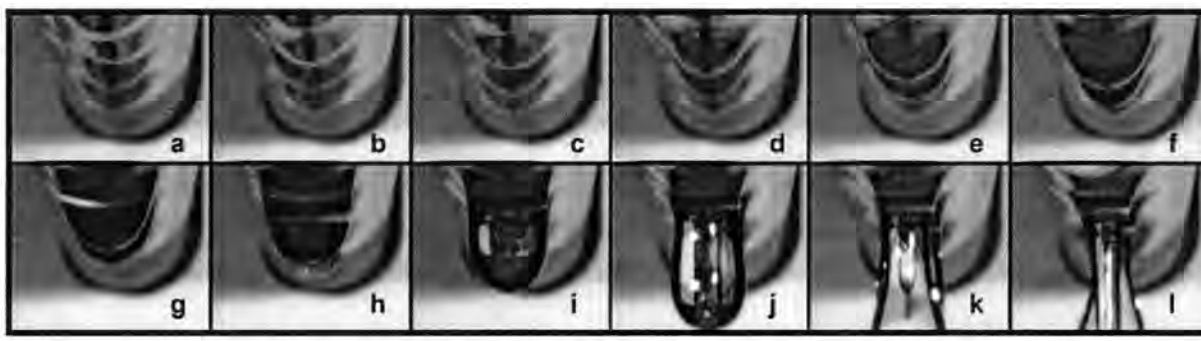

Figure 3.6 Water, Early Formation, End View, 20 ms between frames

Later Formation. As more liquid enters the forming droplet, the distance from the tube to the tip of the droplet continues to increase and the tip of the droplet tends to a spherical cap, a more axisymmetric shape. Fig. 3.7 shows the final stages of droplet development for water after the formation site is well established. Comparing, for instance, Fig. 3.6i and Fig. 3.7g, which both show droplets at nearly the same point in their development, indicates that the tip of the droplet has a nearly spherical cap and somewhat cylindrical sides. In the progression leading up to Fig. 3.6i and Fig. 3.7g, the droplet contracts in the direction of the tube axis. Mass and species redistribution within the droplet is inevitable during this transition, although the mixing in the case of an undisturbed droplet may be relatively low compared to other situations. During the later stages of droplet formation, the surface area of the droplet increases and there are competing theories about how the "fresh" surface develops (Clift *et al.*, 1978). Some have proposed that the increased surface area should be at the conditions of the arriving fluid (Kirby and Perez-Blanco, 1994), others have suggested a surface stretch model where the liquid at the surface effectively remains there throughout the formation

process (Clift *et al.*, 1978), while others suggest that the droplet is well mixed due to the rapidity of the formation process (Jeong and Garimella, 2002). The circulation within the droplet, the characteristics of the fresh surface, and the shape of the drop all have large impacts on the contribution of a forming droplet to the absorption process. It has been shown that this contribution may be a significant portion of the total absorption rate (Nomura *et al.*, 1993; Kirby and Perez-Blanco, 1994; Atchley *et al.*, 1998; Jeong and Garimella, 2002) even though the heat transfer from the droplet to the tube is limited (due to the relatively large thermal resistance between the droplet interface and the tube wall) because the liquid film may be significantly subcooled during its flow around the tube. This will determine the temperature and concentration of the liquid at the surface of the droplet, circulation and the conditions within the droplet itself, and the ever-changing surface area and shape during droplet formation.

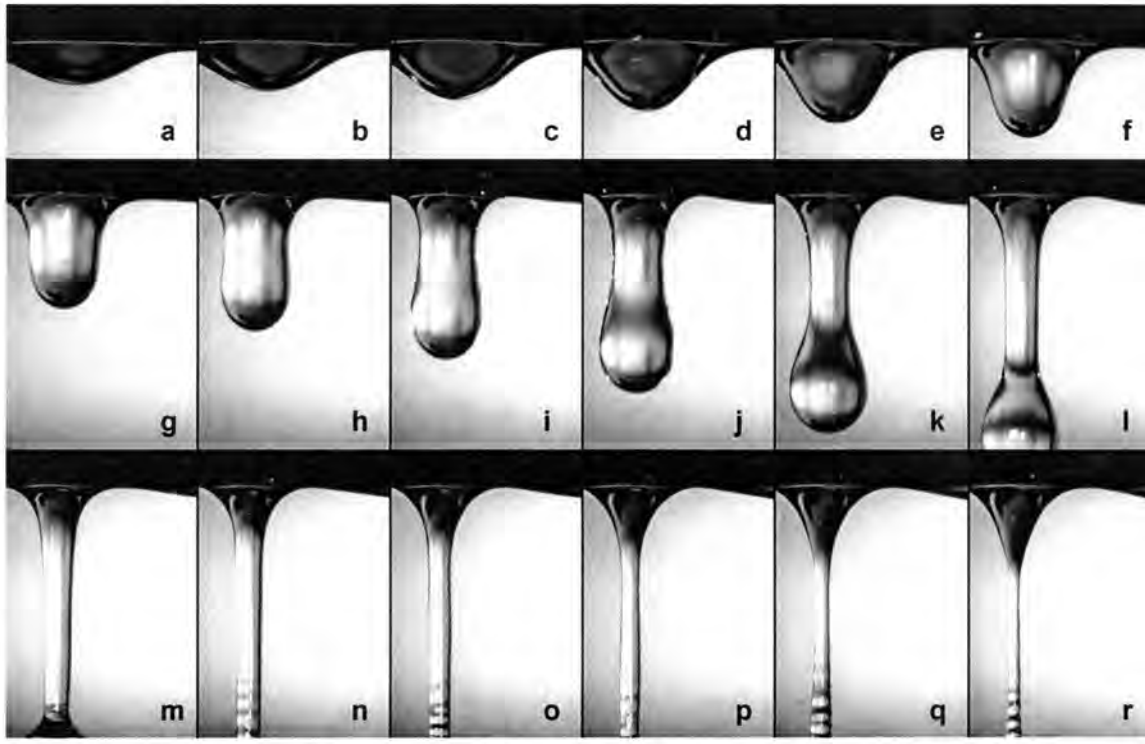

Figure 3.7 Water, Drop Formation, Side View, 10 ms between frames

Detachment and Fall. As the droplet continues to grow and extend away from the tube, the droplet will reach a critical volume beyond which the droplet is unstable (Pitts, 1974). This appears around Fig. 3.7g. When this occurs, gravity force acting on the body of the droplet becomes greater than the surface tension forces acting on the circumference of the droplet, it starts to detach and its downward velocity begins to increases quickly. As gravity accelerates the head of the droplet, the droplet pulls away from the tube faster than new liquid enters from the film. This causes necking and the formation of a liquid bridge between a primary droplet and the film or parent liquid on the tube (see Fig. 3.7h-m where the original pendant droplet is transformed into a large primary droplet

attached to the bottom of a thinning cylindrical filament). This thinning liquid bridge is extended by the motion of the droplet and becomes almost cylindrical (Fig 3.7i), although the end near the bottom is typically thinner than the end near the top before the bridge breaks (e.g. Fig. 3.7m; in Fig. 3.7n-r the end near the droplet is out of the frame of view but breaks before the necking at the top near the base, seen in Fig. 3.7r, occurs). Research has suggested that the presence of surfactants, which modify the surface tension of the liquid, can change or even virtually eliminate the liquid bridge (Miller, 1999). Nevertheless, if a liquid bridge does develop, it exposes a fresh surface for absorption, which has not been considered in models of these systems.

In addition to the development of the liquid filament, several interesting observations can also be made about the progression of the shape of the droplet at the bottom of the filament. During detachment, the droplet itself transitions from a spherical cap to more of a raindrop shape as the surface at its anterior is drawn together by surface tension (Fig. 3.7k). This continued development of the detachment phase is shown in Fig. 3.8. As the bridge continues to thin, the competing surface tension forces eventually break the liquid bridge at a point close to the droplet. At this time, the droplet approaches a spherical shape because the surface tension forces from the liquid bridge are confined to a small area on the surface of the drop (see Fig. 3.8c). Also the thinning filament near the eventual pinch point is approaching a singularity in the equations of motion where "microscopic effects that are outside the realm of hydrodynamics" can determine the actual moment of rupture (Eggers, 1997). The sequence of the impact and detachment events is not always the same. It depends on the thermophysical properties of the system as well as the tube spacing. In the case of aqueous LiBr shown in Fig 3.9, the droplet hits the tube significantly before the liquid filament detaches (frame m). In this case, a temporary liquid bridge is formed between tubes. As this bridge

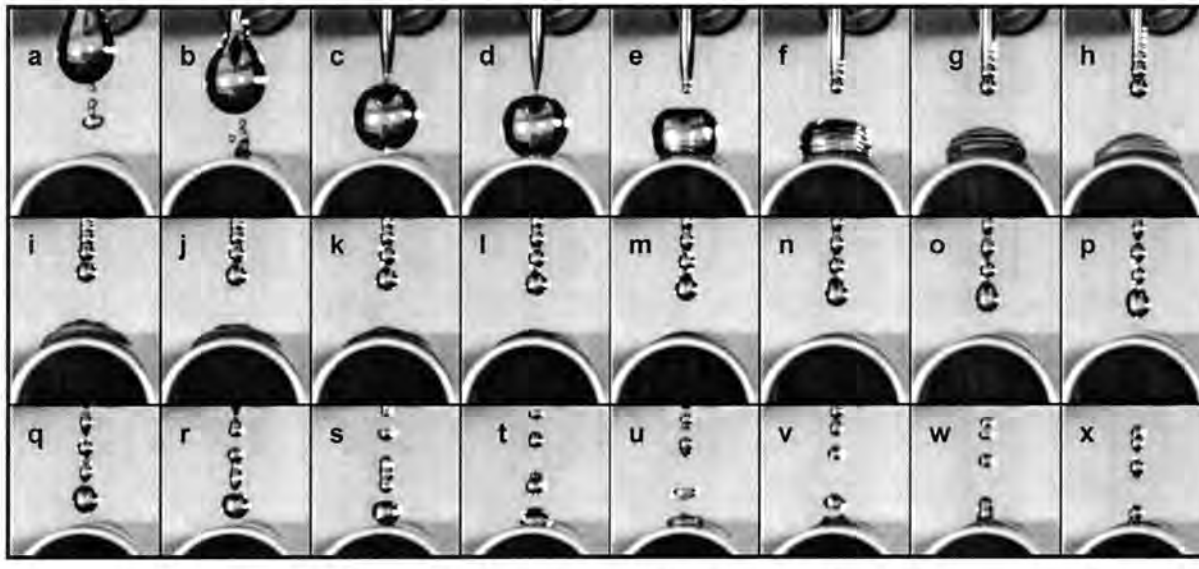

Figure 3.8 **Water, Droplet Fall, Detachment and Impact, End View, a-c 10 ms between frames; c-x 2 ms between frames**

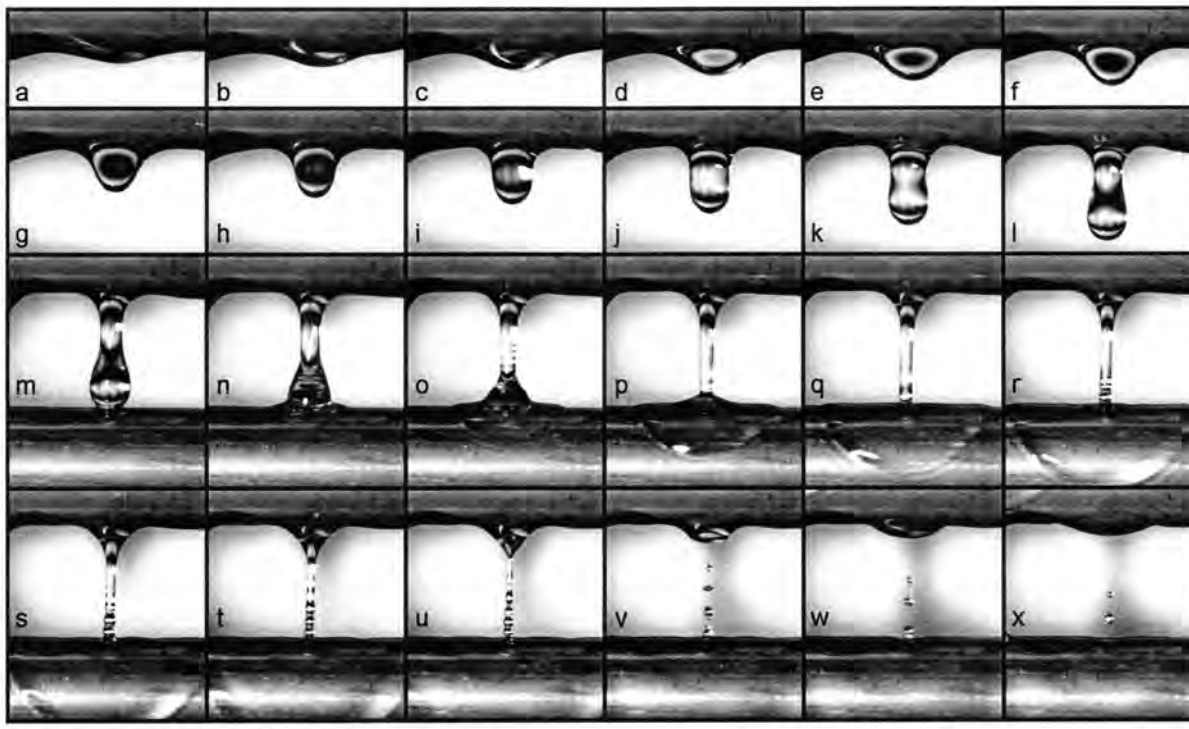

Figure 3.9 LiBr, Droplet Formation, Detachment and Impact, Side View, a-m 10 ms between frames, m-x 6 ms between frames

thins its volume and surface area both decrease, although, as will be shown later, the surface area to volume ratio actually increases. In addition, instabilities from the impact can propagate up the thinning liquid bridge and contribute to the formation of the satellite. The initial break may occur at either the top or bottom of the thinning bridge, but regardless, both events usually happen in rapid succession (Fig 3.9u). The velocity at the point where the liquid bridge breaks is extremely high (Peregrine *et al.*, 1990; Zhang, 1999b; Notz *et al.*, 2001) due to the very small radius of curvature causing extremely high pressure at this point. Eggers (1997) suggests that, as the pinch is approached, the time-scale becomes increasingly small, the radius of the filament approaches zero, the radius of curvature at the pinch approaches zero, and the velocity at the pinch point approaches infinity. The resulting violent (though small scale) rupture and the overall imbalance in surface tension forces after the break leads to a rapid recoil/collapse of the bridge (Figs. 3.8d-e and 3.9u-v) and harmonic distortion (Figs. 3.7n-r and 3.8e-p) which eventually leads to a number of satellite droplets of significantly less volume than the primary droplet (Figs. 3.8q-x and 3.9u-x). The shape oscillations, agglomeration, and path of these satellites have received some attention (Peregrine *et al.*, 1990; Richards *et al.*, 1995; Zhang and Basaran, 1995; Zhang, 1999b; Notz *et al.*, 2001) and can have an effect on absorption rates. For instance, the two middle satellite drops of Fig. 3.8q agglomerate in Fig. 3.8s-t and cause a significant shape oscillation (Fig. 3.8t-w does not fully resolve these motions

in time). Also, it should be noted that during other frame sequences recorded in this study, the breakdown of the liquid bridge into satellite drops was often seen to be more rapid than shown in Fig. 3.8; on the order of less than 10 ms. Although much smaller in volume and surface area than the primary droplet, it is likely that satellite droplets contribute to the absorption process. This is because the method of their formation involves not only the generation of fresh surfaces, but also related high-velocity shape transitions that will mix the fluid within the satellites. The formation of these satellite drops has been largely ignored in studies of absorption.

3.2.2 Droplet Impact and Film Waviness

Although falling films are inherently unstable and will develop waves at almost any Reynolds number (Benjamin, 1957; Fulford, 1964; Kapitza, 1965), films on horizontal tubes typically do not have the required development length for waves to develop from the inherent film instability alone. Nevertheless, film waviness is induced, sometimes with great vigor, due to the action of the droplets both impacting and detaching from the film. Moreover, the absorption process itself can induce film waviness in certain circumstances (Cosenza and Vliet, 1990; Fujii, 1992; Miller, 1999). Waves have been shown to mix the film and increase the transfer of both heat and mass, e.g. (Burdukov *et al.*, 1980; Brauner and Moalem Maron, 1982; Nakoryakov *et al.*, 1982b; Uddholm and Setterwall, 1988; Wasden and Dukler, 1990; Fujii, 1992; Mudawar and Houpt, 1993; Yang and Jou, 1993; Patnaik and Perez-Blanco, 1996b; Jayanti and Hewitt, 1997; Miller, 1998).

Film Waviness Due To Droplet Impact. Fig. 3.8, 3.9 and Fig. 3.10 show in some detail the behavior of the primary droplet and film during the impact phase. The assumption usually employed in models is that the film is completely mixed at the top of the tube and flows smoothly and without axial variations around the tube. These figures clearly show the limitations of this assumption. When the droplet impacts the film, it immediately begins to deform around the tube (Fig. 3.8e-l, 3.9n-t, and 3.10b-f). The spreading lamella wraps around the tube forming a characteristic saddle-shaped wave. At the same time ripples from the impact travel upward through the droplet (Fig. 3.8e-g. 3.9o, and 3.10c), which can affect the dynamics of the bridge if it is still attached. At the exact moment of impact, the theoretical velocities in the liquid are higher than the speed of sound (Rein, 1993) but slow quickly. Throughout the much of its life, though, the saddle-shaped wave travels at a higher velocity than the droplet speed at impact, which can generate smaller ripples in the film substrate ahead of it (Fig. 3.9q-r and 3.10d-f). The propagation speed of the wave slows as it spreads over an increasing portion of the tube surface, and also probably due to viscous effects. Other researchers have shown that the effect of a wave traveling over a substrate is to mix the film underlying film (Uddholm and Setterwall, 1988). The propagating saddle wave therefore probably generates a freshened surface and partially mixed film behind its front. In addition, each satellite droplet creates its own saddle wave (Fig. 3.10i, j), which will have the same effect, although to a lesser extent.

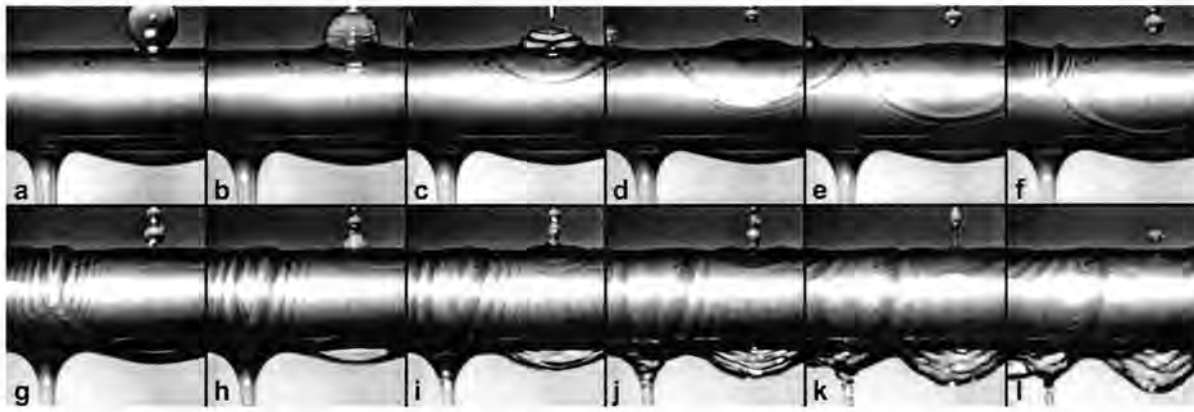

Figure 3.10 Water, Droplet Impact and Film Waviness, Side View, 4 ms between frames

It is also noteworthy that the fluid from the droplet does not all spend the same amount of time on the tube. A significant portion of the liquid from the droplet ends up on the underside of the tube where it can again begin forming a droplet within about 30 ms of impact (Fig. 3.10h-l). Another significant portion is still near the top of the tube at that time and the rest is distributed along the surface of the tube. This is a significant violation of the assumption that the liquid in the droplet will flow uniformly down the sides of the tube. Fig. 3.9 and 3.10 also show the axial flow occurring on the tube. In the Fig. 3.10, two droplets impact at nearly the same time, one out of the field of view to the left. The saddle waves begin to interact (Fig. 3.10e) and give rise to a circumferential ring of liquid that is nearly stationary in the axial direction (Fig. 3.10g-j) leading to locally excess fluid and potentially a droplet formation site. This interaction appears to slow the advancement of the saddle waves as well. It can be seen that the transverse motion of the droplet extends to an area several times the diameter of the droplet (Fig. 3.9t and 3.10l).

Film Waviness Due to Droplet Detachment. The detachment of a pendant drop also causes a disturbance at the bottom of the tube from which it was generated. To a lesser extent than in the impact case, this generates waves on the film above and to the side. This process can be seen in Fig. 3.5a-c and 3.9u-x. At the moment the bridge breaks, the liquid remaining attached to the tube is typically shaped like a stretched triangle (Fig 3.9u). The surface tension forces at the tip of this shape furthest from the tube are unbalanced and the highly curved surface at the tip causes a large pressure gradient within the liquid which leads to a fast recoil of the tip (Fig. 3.9u-w). This leads to capillary waves that propagate back up and along the tube in a saddle shape similar to, but smaller in magnitude than that from a droplet impact. Unfortunately, it is difficult to distinguish the full shape of the wave in most figures due to the lighting conditions (it may also be less pronounced due to the greater thickness of the film under the tube than on top), however the axially moving component is clear. These waves can disturb the formation of neighboring droplets and are likely to affect the mixing in the film.

3.2.3 Complex Interactions

In the examples discussed thus far, some care has been taken to select instances where the behavior of the droplets has proceeded mostly in isolation from the effects of other droplets. However this solitary behavior is infrequent, especially at higher liquid flow rates and tubes lower in the column, where neighboring droplet sites will be almost continuously active. The interactions of forming and impacting droplets with each other are usually transmitted through the waviness generated on the film around the tube. Already, some of these interactions have been shown in Figures 3.5 and 3.10. In Figure 3.5, the early development of a droplet formation site was augmented by the arrival of a significant amount of fluid from a droplet impact above. This is one of the most predominant interaction modes seen in the tube bank. In Figure 3.10, as mentioned above, the waves developed from two droplets impacting near each other collide and the basic structure of both advancing saddle waves was affected (Fig. 3.10f-j). Also shown in this sequence, the droplet formation site on the right-hand-side of the figure (see the progression at the bottom right of each frame), which was in early stages of development, was significantly affected by the arrival of fluid and waves from the droplet impact directly above it. This created a pendant triangular wavy structure on the droplet formation site itself (Fig. 3.10j-l); in many instances this leads to early droplet departure, see Table 3.2. Additionally, the liquid bridge located axially between and underneath the two impacting droplets was also disturbed by the waves from both impacts. This disturbance propagated down the liquid bridge itself and influenced the breakup of the bridge into satellite droplets (Fig. 3.10j-l). The preceding example illustrates just some of the many possible interactions. There are many other possibilities. Some of the more common occurrences are characterized in Table 3.2. It should be noted that these interactions appeared more pronounced in the case of water; this may be due to the lower viscosity, smaller tube diameters, larger tube spacing, or a combination of these. The interactions shown in the table can be most easily characterized by their influence on the droplet formation process. The effect of interactions on the film waviness is certainly as important, but the patterns are generally similar to those shown in Figures 3.9 and 3.10. The vigorous waviness and shape transformations in Table 3.2 suggest that significant mixing is induced, leading to the redistribution of species and thermal energy within the liquid. Other behavior observed but not illustrated in Table 3.2 includes:

- the generation of satellite droplets with upward velocity, some of which bounce off the liquid remaining attached to the underside of the tube
- rapid droplet reformation and detachment from the liquid under the tube after bridge detachment
- swelling and turning (back and forth with respect to vertical) of liquid bridges
- agglomeration of neighboring droplet formation sites
- droplet spinning during freefall
- droplet slinging away from vertical

It was also generally observed that droplets would frequently stagnate at some point in the formation process or form very slowly until another droplet came from above. As soon as the liquid from this impacting droplet arrived, the droplet formation process was greatly accelerated. Thus it seems that a major portion of the liquid may travel around the tubes driven by the momentum of impact, leaving a much smaller portion to flow as a gravity driven film. Once again, this is clearly different from the most commonly used assumption of uniform velocity as a boundary condition at the top of the tube. Thus, one way of viewing the overall fluid flow would be to consider much of the total liquid to flow as droplets that are in effect sliced and slowed by the tubes but never fully formed into a film.

Table 3.2 Examples of Behavior Due to the Interaction of Droplets and Film Waviness

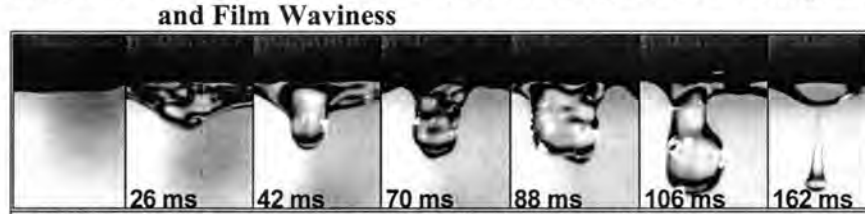

Underside of tube has thin film, droplet impacts above

26 ms)	Forms pendant wavy triangular sheet
42 ms)	Droplet protrudes by momentum from impact
70 – 162 ms)	Undulating, oddly shaped droplet and satellites follow

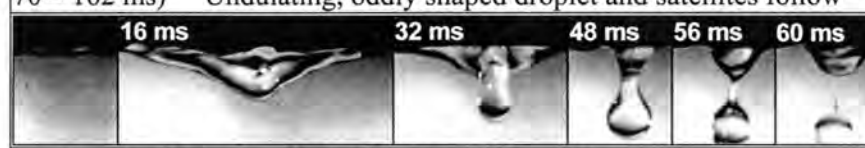

Underside of tube has thick film, droplet impacts above

16 ms)	Pendant wavy sheet
32 ms)	Droplet protrudes
60 ms)	Leads to early droplet detachment with no trail

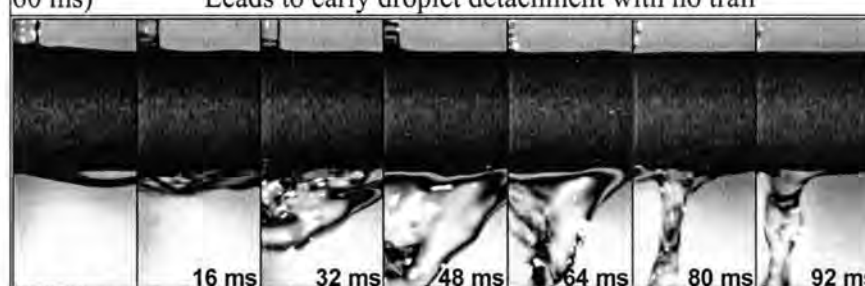

Droplet impacts above and to the left of nascent droplet formation site

32 – 48 ms)	Very large pendant, triangular, wavy sheet formed
64 –92 ms)	Collapses into liquid bridge with helical twisting motion

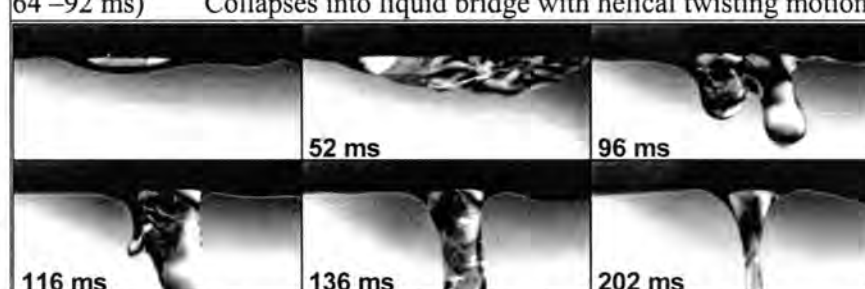

Droplet impacts above and to right of an existing droplet formation site

96 ms)	Double droplet forms
116 ms)	Left droplet absorbed into large liquid bridge
202 ms)	Twisting flow generated in bridge

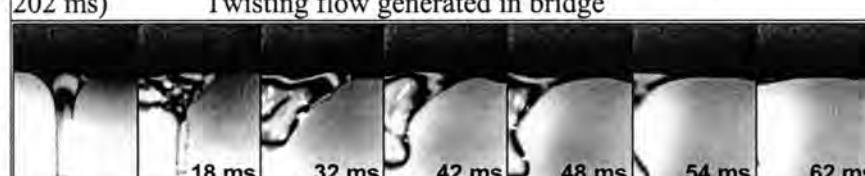

Droplet impacts above and to the left of an existing liquid bridge

18 ms)	Disturbance breaks bridge
32 – 62 ms)	Leads to axial translation of formation site out of frame

3.2.4 Implications and Importance

The high-speed video shown here has revealed some of the complex characteristics of flow around horizontal tubes even at low film flow rates. These include the development of a droplet formation site from the bottom of a smooth film, the progression of shape transitions through the development of the droplets, the stretching of the liquid bridge between the tube and droplet, the thinning and breakup of the liquid bridge and generation of satellite drops, the waves generated upon droplet impact including the characteristic saddle wave; the waves and oscillations generated from droplet detachment and bridge breakup, and various interactions between these individual mechanisms (that lead to secondary flow phenomena with often vigorous undulations). The nature and frequency of these events depend on design parameters such as tube spacing and film flow rate as well as the thermophysical properties of the liquid, especially the fluid viscosity, surface tension and density (compared to the vapor). Some of the characteristics revealed here are common to drop formation from capillary tubes and jet as reviewed previously, especially in the region of bifurcation where the length and time scales do not depend on the geometry of the apparatus. However, significant differences from the axi-symmetrical cases typically studied in the literature were also revealed; in particular the lengthening of the drop along the tube and the interaction of drops and waves.

Fluid properties and absorber design parameters are known to affect the absorption rate, e.g. (Greiter *et al.*, 1993; Atchley *et al.*, 1998; Killion and Garimella, 2003c), but the reason for the effects has yet to be well understood. It is proposed that the influences of such parameters on the absorption rate are manifest in part through their influence on droplet and film behavior. The idealizations of the flow patterns used in the past to mathematically model the heat and mass transfer process on falling films over horizontal tubes have not included these complexities, an omission that has prevented these models from capturing the effects of critical design parameters. In addition, it should be noted that the saddle waves formed by droplet impact do not conform to the models of waves on vertical films that develop due to inherent film instabilities; thus a simple extension of techniques used for vertical wavy films to the horizontal tube case may not be adequate. Therefore it is necessary to consider the details of the droplet and film behavior to advance the state of the art in modeling absorption in these systems. The observations shown here represent an advancement toward that end.

3.3 Digital Image Processing Routines

Digital images of falling films are not particularly difficult to interpret qualitatively with the human eye. However, the information stored is simply a large array of numbers for each frame containing no explicit information about the motion of the droplets and film. Converting these numbers to useful, quantitative metrics that capture some of the features of the observed phenomena is the subject of this section.

3.3.1 Review of Image Analysis and Mathematical Techniques

Digital image processing is a field of immense practical application now that digital communication has become commonplace. There are literally hundreds of textbooks on the subject, e.g. (Besl, 1988; Klinker, 1993; Seul *et al.*, 2000; Russ, 2002). Identification of the shape and position of the interface between the liquid and gas phases in the video is the primary objective of the image analysis methods presented here. The entire image processing procedure was implemented in Matlab (The Mathworks Inc., 2002b) through the development of an interactive graphical user interface (GUI) relying heavily on the image processing toolbox and the spline toolbox. Besl (1988), who developed a sophisticated algorithm for identifying objects and surfaces in so-called range images, notes that "contrast, brightness and color contain surprisingly little explicit geometric information about the 3-D world that we perceive" (p 3). He points out that in order to accurately interpret even a simple image in which a shadow falls across a smooth plane requires "high-level" knowledge about the scene which is described in the image. Whereas humans, who are "remarkably proficient at the qualitative visual inference and perceptual organization processes required for image interpretation regardless of image type and quality", would have no trouble distinguishing the smooth surface through the light and shadowed regions, this would be a challenging task for a computer. Similar problems of shadows, glare, noise and ambiguity exist in the droplet images presented in the previous section. The easiest "image" for the desired analysis would indeed be a range image which, instead of quantifying color at each pixel location, quantifies distance from the sensor; sharp jumps would appear at the location of the interface between liquid and vapor and, in addition, the geometric information required for estimating droplet volume and surface area would already be quantified in the image. However, range images are not frequently used in high-speed imaging, probably due in part to their inherent lack of aesthetics (they contain none of the subtle details of surface texture, highlights, color, etc that make objects appear 3-D in a 2-D image). Another alternative which could ease the task of identifying the interface would be to use backlighting, e.g. (Hauser *et al.*, 1936; Fagerquist, 1996). Backlighting droplets can provide images with high contrast and clearly defined interfaces between the two phases (the droplets generally appear dark and the background light) that can be detected with simple thresholding procedures, but these images suffer from the same lack of aesthetics and lack of quasi-3D information as range images. The final option is to attempt to analyze the aesthetically pleasing images shown in the previous section complete with all of their ever-changing highlights, shadows, glares, and backgrounds. Since finding one algorithm that could handle this process for any general case would be a formidable undertaking, a semi-automated analysis routine was developed. The basic concept is that, after a human identifies the initial region of interest (ROI) in the first frame of a sequence to be analyzed, edge detection algorithms with suitably tunable parameters can then be used to automatically detect the real droplet interface in the ROI in each subsequent frame, with simultaneous human supervision and intervention where necessary to prevent the procedure from going off course. The tunable parameters are not only

various threshold values, but also include the choice of edge detection algorithm itself. This method, which will be explained in more detail in the next section, proved to be quite effective for accurately and quickly identifying the liquid-vapor interface throughout the entire droplet evolution process. The main restriction is that the edge is only valid in the two dimensions contained in the plane normal to the direction of viewing (since only one camera was used; using two synchronized cameras would avail the possibility of reconstructing geometry in three dimensions; note also that no compensation for "perspective" was included in the current analysis). Thus, information about depths and distances out of this plane, such as film thickness/wave height around the tube and the thickness of droplets in direction of view, remain unquantifiable by the current approach.

The process of edge detection is, in practice, a digital filtering process on a 2-D signal. Analogous to how low-, high-, and band-pass filters can be tailored to achieve the desired output from a 1-D signal such as a transient sound-pressure-level trace, 2-D filtering techniques effectively convolve a suitable filter mask with the entire 2-D matrix (Seul *et al.*, 2000). Edge detection is generally accomplished by calculating local gradients in intensity through a differential operator, sometimes applied in the two principal directions of the image separately. Just as differentiation of a time-signal accentuates higher frequency content, the gradient operator on a 2-D signal tends to accentuate high-frequency "pixel noise". Thus, most edge detection filters are a combination of a gradient operator and a smoothing filter, such as a standard Gaussian mask. In addition, the size of the mask is another parameter that can be selected. Frequently a 3x3 matrix is used; thus, the value computed by the filter at any given point is a function of the value at that point and the values at the eight surrounding points (Seul *et al.*, 2000). Other neighborhood patterns include a 4-nearest-neighbor cross, a 5x5 neighborhood with and without the corner points, and so on; larger masks (also called kernels) are less sensitive to noise, but result in less resolution of the edge position (a thicker edge) (Russ, 2002). Of the many edge detection algorithms suggested in the literature (Russ, 2002), empirically, two stood out as having the greatest utility and, for purely pragmatic reasons, were used for approximately 99% of the images analyzed. The Canny algorithm (Canny, 1986) is a computationally efficient method (Russ, 2002) that utilizes two threshold values for detecting "strong" and "weak" edges. The weak edges are only included in the output if they connect to a strong edge. Thus this method is often able to detect weak edges without also including a lot of noise in the output. The Sobel method (Sobel, 1970) utilizes one threshold value but has become one of the most widely used methods (Russ, 2002), no doubt due to its effectiveness and simplicity. This method calculates horizontal and vertical derivatives and then combines them as the square root of the sum of the squares which leads to an orientation-independent result. The final result of the edge detection technique is an array with the value 1 at pixel locations likely to contain an edge and 0 elsewhere. For these detected edge points to be translated into actual geometric information, a method involving splines was employed.

So-called splines have gained popularity in recent years because of their powerful ability to approximate discrete data with smooth mathematical functions. In particular, splines are piecewise-polynomial functions that blend smoothly and can be efficiently stored (as coefficient arrays) and manipulated on computers. Spline functions can be created to *interpolate* between points (the function will pass precisely through the data points), smoothly *approximate* data (minimizing the second derivative while approximating the data to within a set tolerance), define a least-squares fit of arbitrary order, approximate the solution of ordinary differential equations, and more. The order, smoothness, end-conditions and various other parameters are all at the discretion of the user. For a detailed exposition of the development and practical application of splines, see (de Boor, 1978). Cohen et al. (2001) give an introduction to techniques for modeling geometry with splines including some aspects of differential geometry. The algorithms presented by de Boor (1978) have been extended to handle vector-valued splines in the Matlab Spline Toolbox (The Mathworks Inc., 2002a), which was used in this work. The primary motivation for using splines in this case was to generate appropriate and tractable mathematical representations for the positions of the liquid-vapor interface in a sequence of images. It is important to note that cubic smoothing splines have the "smoothest interpolation property" (de Boor, 1978) (p.66), that is, they *uniquely* minimize (approximately) the strain energy for a function passing through a given set of data within the specified tolerance. Since systems having free surfaces with interfacial tension tend toward equilibrium states that minimize the surface energy, i.e. surface area (Carey, 1992) (p29), splines are uniquely suited for describing the shape of the interfaces of such systems. Thus, given a finite set of coordinates defining the position of the interface that inherently contain some noise or uncertainty as any measured data must, the cubic smoothing spline is the "natural" choice for developing a continuous, mathematical definition of the interface. The two-valued (x and y coordinates) cubic smoothing splines thus used were fit through a number of the identified edge pixels and parameterized by the distance between selected edge points. After a calibration step to establish the relationship between pixels and a length scale in the image, the spline representations could be mathematically revolved and integrated to determine their interfacial area and internal volume. This method of revolution is, of course, only valid in regions where the droplet is nearly axi-symmetric. More details on this limitation are given in the following sections. It should also be noted that, since the spline was fit around the entire visible interface, it effectively defines two sides of the same drop. Thus revolving and integrating gives the sum of two estimates of the drop volume and surface area, one from each side. A simple division by two results in the mathematical average of the fit of the two sides. The details of the mathematics involved in the spline revolution process, including sample routines for estimating the error for the case of a sphere of known diameter, are given in Appendix A.

3.3.2 Semi-Automated Droplet Image Processing Program

The droplet image analysis routine (IMAN) was programmed as a graphical user interface (GUI) due to the visual and interactive nature of the analysis process. To facilitate the discussion, a series of screen captures from the GUI will be presented. Figure 3.11 shows a typical screen capture during the analysis of a droplet formation event. By describing the various controls displayed in this figure, the operation of the processing routine should be completely elucidated.

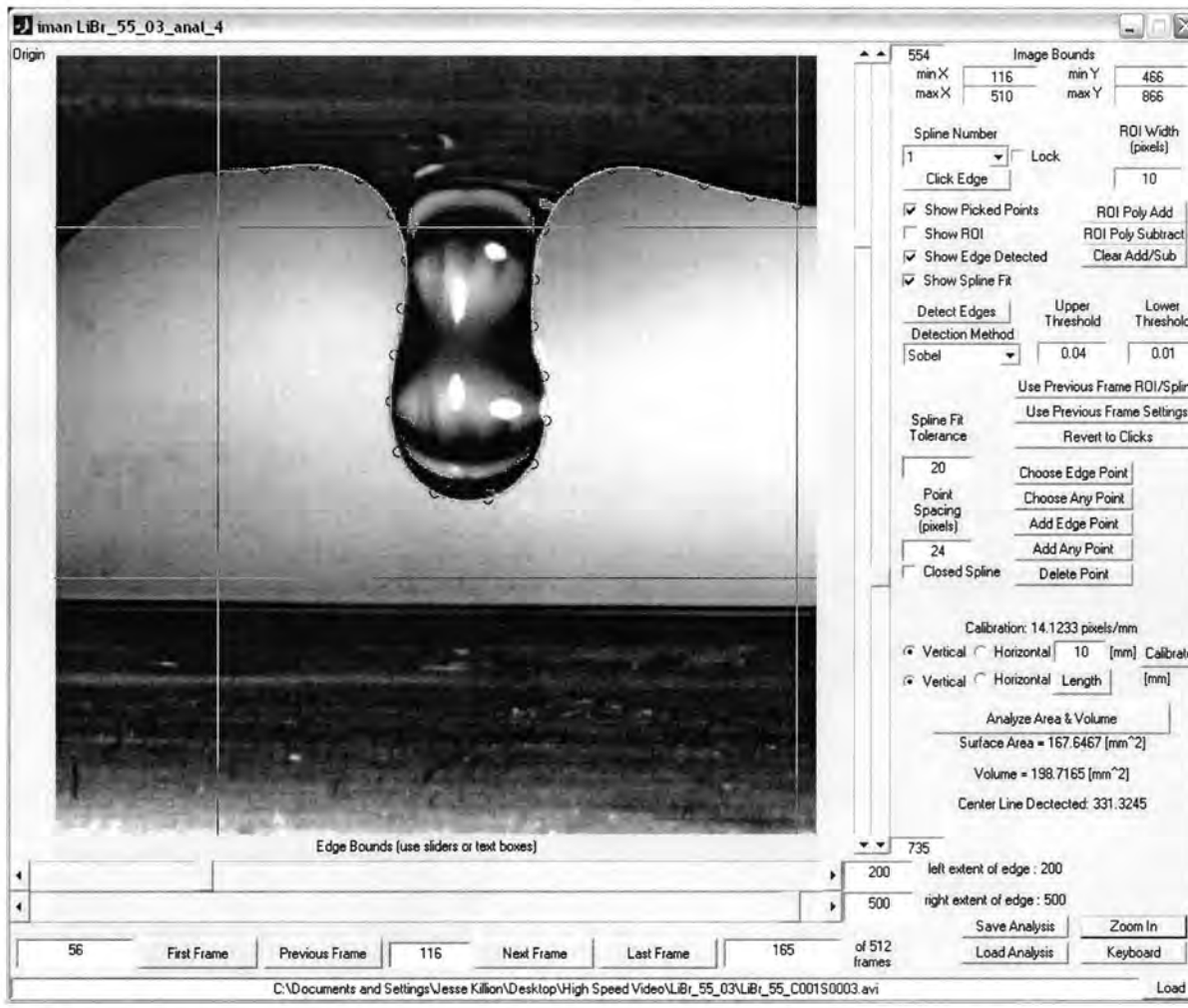

Figure 3.11 Screen Capture of IMAN Image Analysis Program Graphical User Interface

The image of the droplet is shown here with the detected edge points and spline fit superimposed. This example is a frame from the same sequence shown in Figure 3.9. In images, the coordinate origin is in the *upper* left corner, corresponding to the pixel in the first row and first column of the array. Thus the y-axis is reversed from convention. The extent of the first pixel in terms of the coordinate axes is 0.5 to 1.5 such that its center is at (1.0,1.0); in this way the coordinates of the center of each pixel correspond to the row and column index of that pixel in the image array. In

original 1024x1024 image, the field of view included three tubes. The boxes in the upper right corner of the window labeled "Image Bounds" can be used to restrict the extent of the image displayed and analyzed to a subset of the entire image. Due to the reversed y-axis, the "min Y" and "max Y" values correspond to the topmost and bottommost pixels, respectively. Restricting the analysis region speeds up the performance of some of the analysis and display capabilities. This is distinct from zooming (button in lower right corner) which does not affect the extent of the data analyzed. The video (AVI) file may be compressed using virtually any standard CODEC as long as the CODEC is appropriately installed on the computer, (see Matlab help for "aviread"). The name of the original file and the file for storing the analysis are shown along the bottom and top of the display, respectively. Analyses may be saved (button in lower right of window), terminated and restarted at any time without loss of continuity. The arguments passed upon invocation of the program determine what AVI file and analysis file to use. The user may navigate within an AVI file using the buttons and text boxes underneath the image. Values entered into the "First Frame" and "Last Frame" text boxes set the frames which will be displayed when the "First Frame" and "Last Frame" buttons are pressed, respectively. The "Previous Frame and "Next Frame" buttons step through the file one frame at a time; however a desired frame number may be entered directly into the current frame display (between the previous and next buttons) at any time. The sliders underneath and to the right of the image control the position of the two vertical and two horizontal lines seen crossing the image. The current locations of the sliders (in pixels) are displayed in the text boxes near the sliders; the position of the sliders can be set by dragging the slider, clicking in the slider bar, clicking on the slider arrows, or typing a new value into these text boxes. In most cases, error checking is performed upon update of any of the control values. For instance, any input value of the left limit slider is corrected to be less than the value of the right limit slider, decimal values are rounded to integers where necessary, slider values cannot be set beyond the displayed bounds, etc. The function of the sliders is to further restrict the domain of analysis as will be discussed later.

Once the image is displayed appropriately and the first frame of the sequence selected, the analysis begins with the "Click Edge" button. This allows the user to define a region of interest (ROI) in which the program will search for the interface. The user clicks are stored and then fit using a spline. This is truncated to the left and right limits set by the sliders and immediately displayed on the screen. The width of the ROI is determined by the value in the "ROI width" text box, to the right of the "click edges" button. Figure 3.12 shows how the screen might look after this initial step.

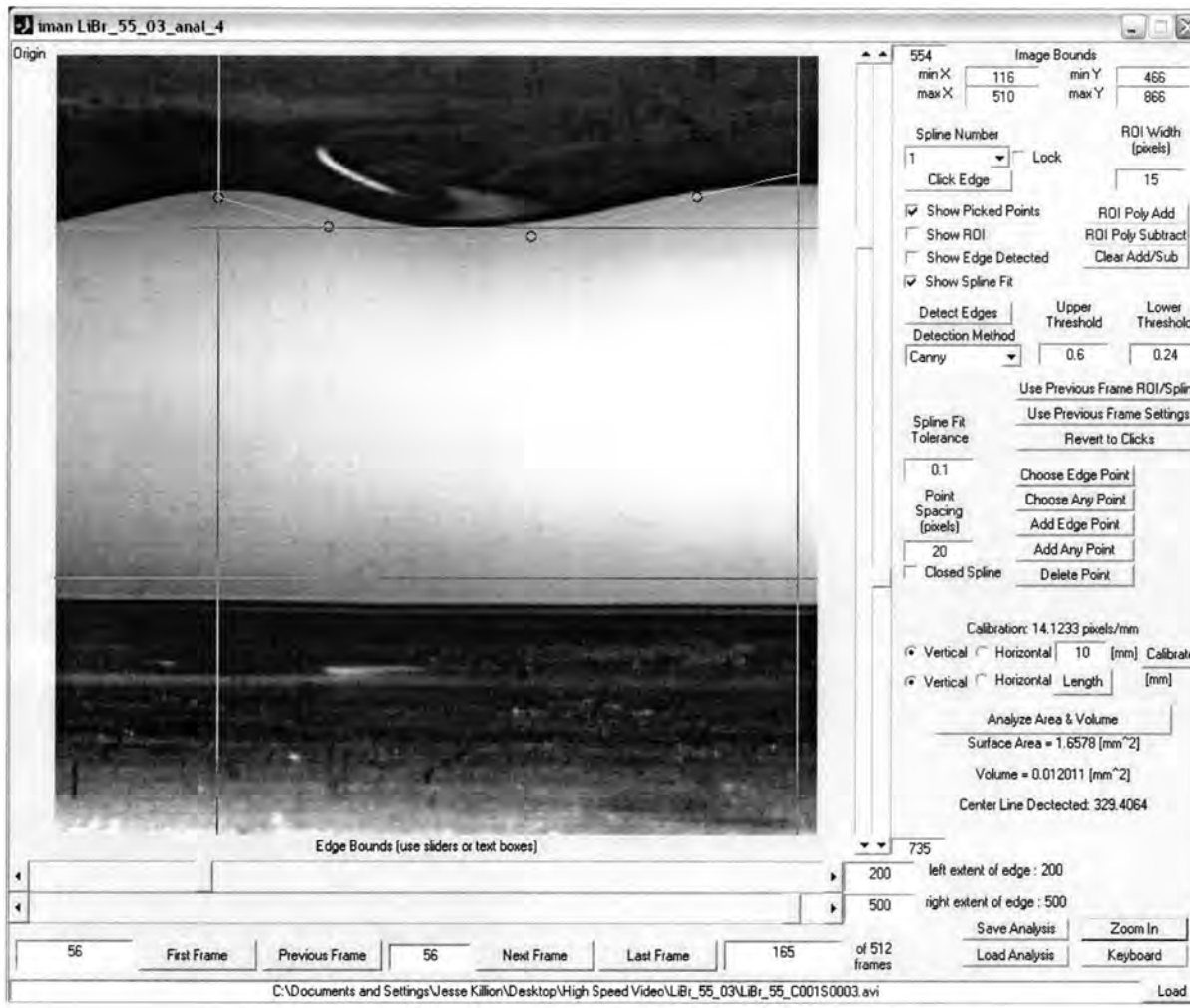

Figure 3.12 Screen Capture of IMAN after Initial User Clicks

The circles designate the locations where the user clicked except that the end points have been corrected. It is advisable to click outside the limits initially. When this is done, a spline is initially fit through all of the clicked points and then used to determine the points at which this spline crosses the left and right limits. These intersection points are substituted for the original clicks outside the limits and the spline is regenerated using these new end points. Note that the curved line displays the spline fit to the clicked points (which is also used to define the ROI). It is perhaps a subtle point, but utilizing the sliders to automatically limit the extent of the analysis minimizes creeping of the detected edge in the horizontal direction along the interface from frame to frame. At any time after this first step, the region of interest can be highlighted by clicking the "Show ROI" check box. The ROI is calculated initially by taking "ROI width" sized steps along the spline and marking the pixels in an "ROI width" by "ROI width" area surrounding each point (including the end point). In addition, the ROI Poly Add and ROI Poly Subtract buttons may be used to add or subtract arbitrary polygonal areas to the ROI using the mouse. Figure 3.13 illustrates the ROI and the Poly Add function.

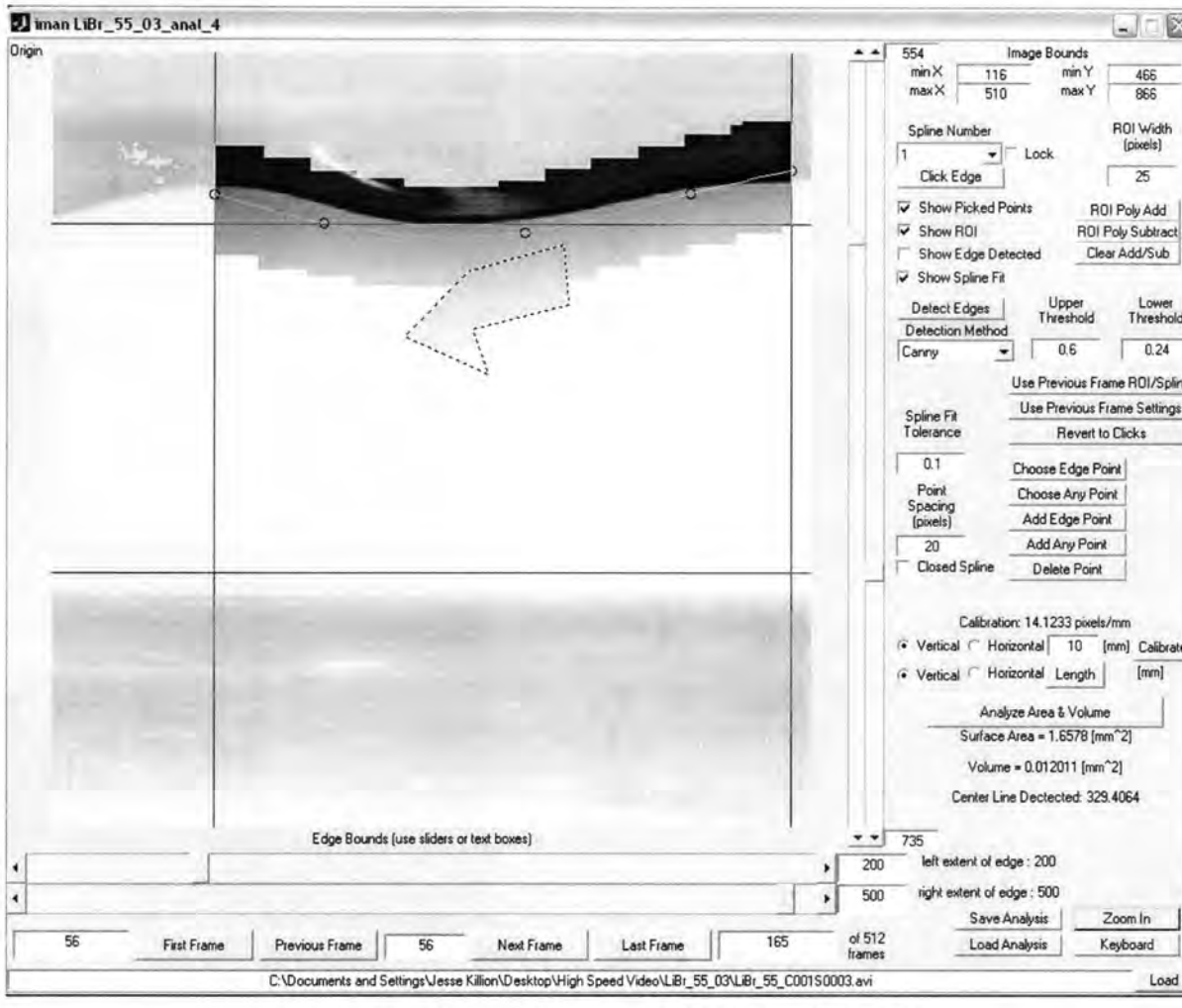

Figure 3.13 Screen Capture of IMAN showing ROI

Once the user is satisfied that the ROI contains the interface, the edge detection method and its associated parameters are set using the dropdown box "Detection Method" and the "Upper Threshold" and "Lower Threshold" text boxes. Once these are set, clicking the "Detect Edges" button performs the desired edge detection (filtration) within the region of interest. At this time a new spline is then fit to the interface. This is done using the old value of the spline fit (either from clicks or from the previous frame) as an initial guess. Starting with the left end-point of the old spline, an exhaustive search of all of the detected edge points is done to determine the one that is closest to the original point. Using the value of the "Point Spacing" text box, another point on the spline is selected "Point Spacing" pixels along the old spline and the closest edge point is found again. This is repeated until the end of the old spline is reached. The selected points are designated with small circles. The calculations involved in this step occur very quickly so there is just a short delay between clicking "Detect Edges" and the update of the display. From the selected edge points,

a new spline is fit using the value of "Spline Fit Tolerance" displayed in the box. At any time, the user may change the point spacing or the tolerance and the edge points will be reselected and/or the spline refit. Figure 3.14 shows the edge detected and fit from the spline shown in Figure 3.13.

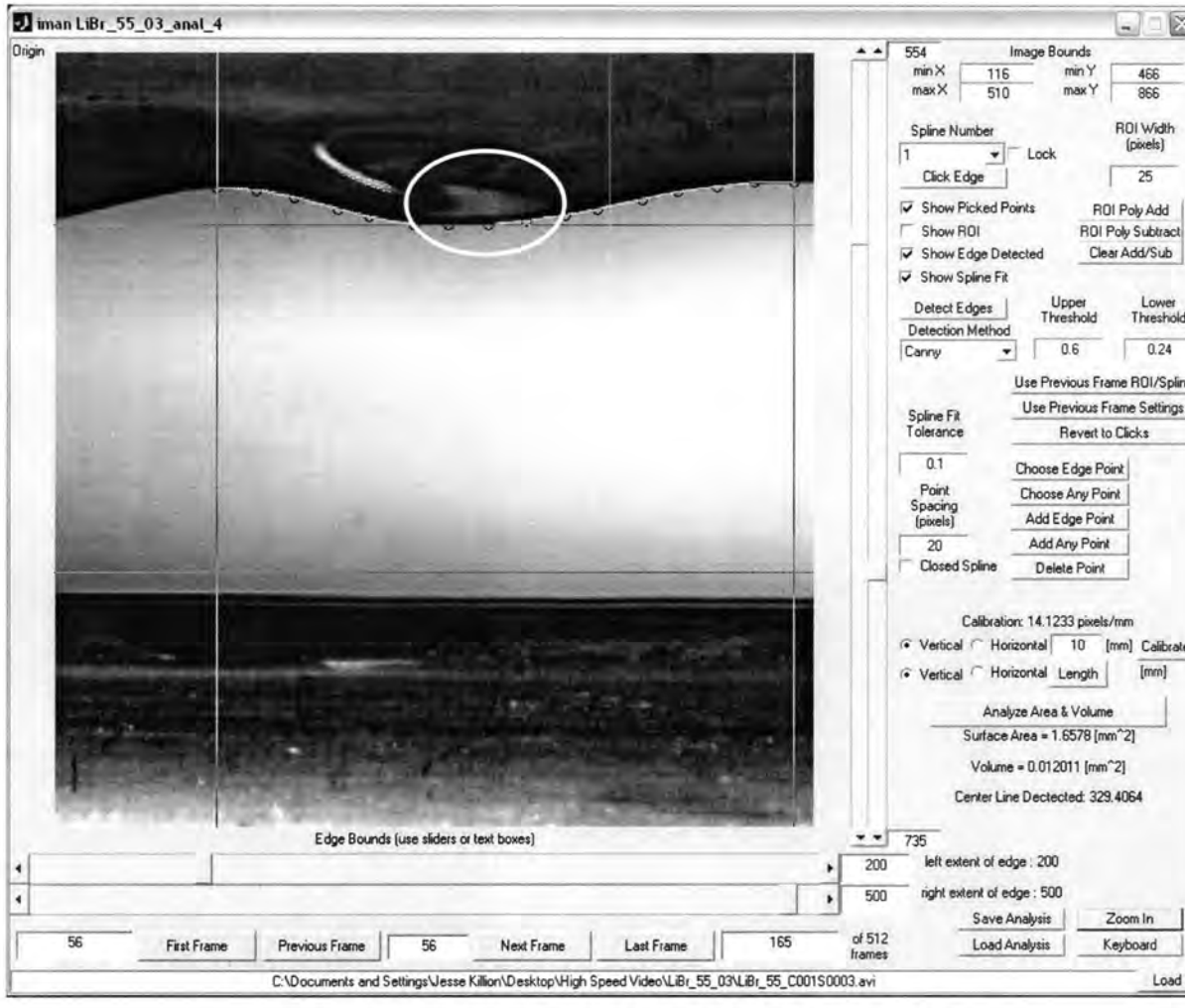

Figure 3.14 Screen Capture of IMAN showing Detected Edge

It is very difficult to distinguish the spline fit (solid line) from the detected edge points (shown as light dots) since the two lie virtually on top of each other. This frame was a particularly easy frame to analyze requiring no tweaking of the thresholds, ROI, selected edge points or spline tolerance. In fact, the next several frames can be automatically processed with no input from the user. Eventually, challenges do arise when glares and shadows coincide with the interface region. For example, the lighter colored area circled in the previous figure begins to intersect the interface about 16 frames after the first frame analyzed. Figure 3.15a shows the edge points detected in this case as white dots in certain pixels. It can be seen that the edge detection routines fail near the tip of the drop in this case where the contrast between the drop and the background is extremely low. IMAN provides

several ways to handle this. In fact, the default automatic fit is perfectly reasonable in this case as there are enough edge points detected that the spline can simply span the gaps (see Figure 3.15b).

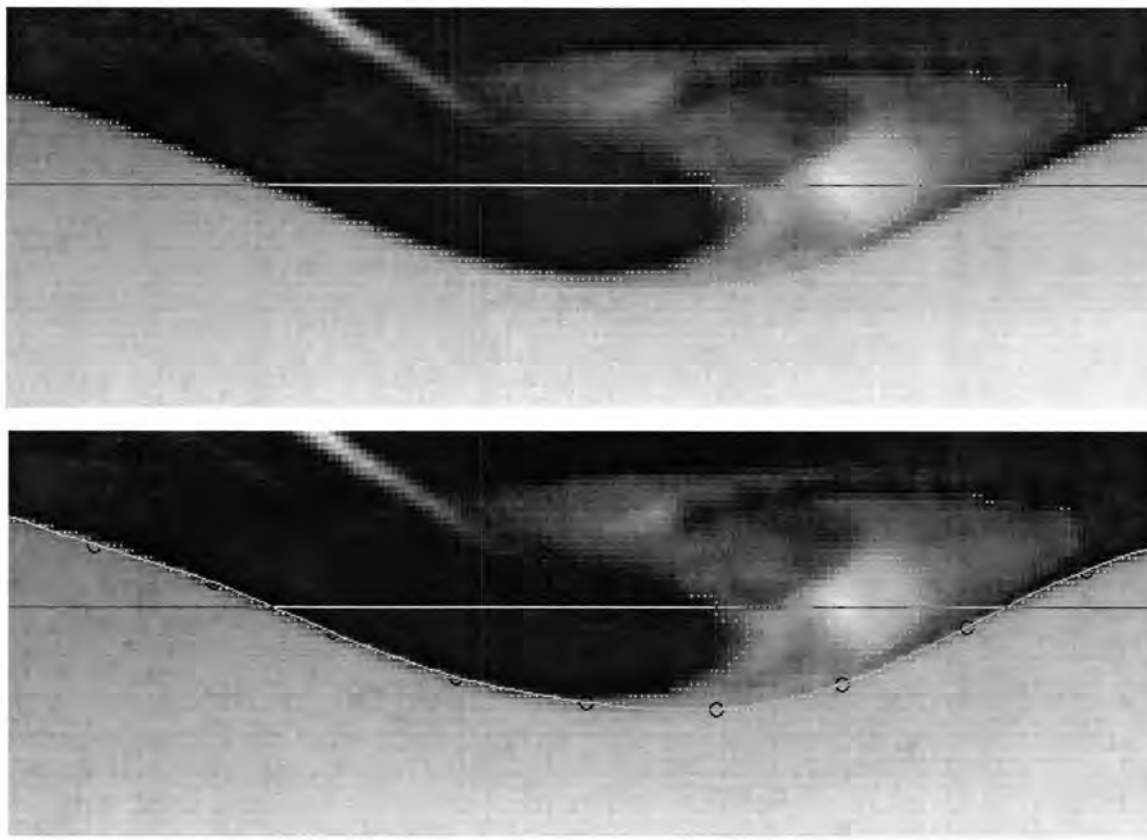

Figure 3.15 Screen Capture of IMAN showing (a) Gaps in Detected Edge near Highlight, and (b) Default Fit

However, in cases where the gaps are more severe or troublesome, there are several methods for manually correcting the edge points chosen. The "Choose Edge Point" button will take a mouse click and modify the nearest control point (circles) to correspond with the detected edge point nearest the click. "Choose Any Point" also modifies the nearest control point; however, the click is not restricted to a detected edge point but can be any pixel in the image. This is particularly useful for dealing with bright glares that tend to "bloom" as seen on the right side of the droplet in Figure 3.11. In those cases, the interface might need to pass directly through a bright spot which contains no detectable edges; the "Choose Any Point" utility suitably handles this issue. In addition there are "Add Edge Point" and "Add Any Point" buttons which operate in an analogous way, except that, rather than modifying the location of an existing control point, one is *added* between the two nearest control points. This is useful in areas of extremely high curvature that may not be automatically resolved with fixed point spacing. Finally, there is also a "Delete Point" button that removes the control point nearest the location the user clicks. The zoom in/zoom off button makes the use of these utilities

considerably easier with high-resolution images. Note that each time a control point is modified, the spline fit is redone and stored.

Whenever a user performs an edge analysis, the values of the various parameters such as spline tolerance, point spacing, edge detection method and thresholds, ROI, etc. are stored for that frame. Clicking to the next (or previous) frame will have one of two effects: if the frame has been previously analyzed, the parameters will all be set to the values used in the analysis of that frame. If the frame has not been analyzed, the settings from the previous frame are maintained and, if the "Detect Edges" button is pressed, the ROI and spline fit from the previous frame are advanced to the current frame to be utilized as the initial guess (similar to how the initial clicks spline was utilized in the first frame). In this way, many frames can be processed in rapid succession without the need for changing settings. This algorithm effectively transmits the "high-level" knowledge imparted by the user on the first frame through each frame of the analysis. Sometimes, however, particularly difficult frames may prompt the user to try several edge detection methods/thresholds. Since the spline and ROI are updated each time the edge is detected, potentially the spline can drift further away from the real interface over the course of several iterations due to the detection of false edges. Several methods are provided for resetting the analysis in this case. First, the "Use Previous Frame ROI/Spline" button simply resets the ROI and initial guess spline based on the analysis of the previous frame. There is also a "Use Previous Settings" button which resets the various analysis parameters to the values used in the prior frame without changing the current spline and ROI. Finally, if none of these methods work, the user can manually click to form the ROI (as in the first frame). Once this is done, the clicked points and ROI are also stored with the frame and retrievable at any time with the "Revert to Clicks" button.

The final aspect of IMAN is the analysis of droplet volume and surface area. Calibration is accomplished by entering a known length in the calibration value, clicking the "Calibrate" button and then, using mouse clicks to designate the extent of the known reference length, e.g the space between tubes. The "horizontal" and "vertical" buttons can be used to restrict the calibration to only the horizontal or vertical component of the button clicks. In the case of horizontal tubes, using the "vertical" tick button, the user can click anywhere along the top and bottom edges of the tubes to establish the reference length. After calibration, clicking the "Analyze Area and Volume" button will perform the revolutions described in Appendix A using the vertical limits set by the vertical slider bars. Great care must be taken in choosing appropriate limits for the revolution analysis because the droplets are not axi-symmetric near the tubes. Revolution of the drop interface shape in the regions that are not axi-symmetric can lead to significant errors in the reported volume and surface area. This will be discussed further in the next section.

After the liquid bridge joining the primary drop to the parent liquid above breaks, several satellite droplets are often formed. To facilitate the analysis of such frames with multiple zones of interest, several splines can be fit on each frame using the "Spline Number" pull down menu. Initially, the

options are "1" and "add". As soon as "add" is selected, the entire storage structure is resized to the new number of splines. Clicking to the next or previous frame will show the last spline analyzed unless the "lock" check box is ticked, in which case the spline number will remain fixed for each frame displayed whether or not that spline exists for the given frame. Note that all analysis parameters are stored for each spline on each frame so that switching spline numbers will update the analysis settings if the selected spline number has been previously analyzed on the current frame. There is a fundamental difference between satellite droplets and a pendant drop: satellite droplets should be characterized by a spline which starts and ends at the same location. To permit this, the "Closed Spline" check box toggles this feature of the spline. When checked, the first point is appended to the end of the list of points and the spline recalculated resulting in a closed loop spline. When unchecked, this point is deleted and the recalculated spline is open on top.

In addition to the basic functionality described above, a utility for querying any length in the image is provided: the "Length" button. This is useful for quickly determining the diameters of droplets, liquid threads and other distances of interest in the images. Finally, the "Keyboard" button temporarily gives the user access to the "handles" structured array that includes all of the information regarding the analysis to that point. Some useful commands are displayed in Matlab's main window when this function is used including instructions for how to export the analyzed surface areas and volumes (summed over all of the spline numbers) to a separate file.

3.3.3 Results

Figure 3.16 shows several analyzed frames for a LiBr droplet (the same droplet shown in Figure 3.9). The horizontal lines show various limits used to analyze the droplet surface area and volume discussed below. The spline fit to the interface is shown as a light solid curve. The times have been adjusted such that the moment of impact (actually the moment when the droplet first crosses the lower boundary) is time 0. The impact event provides a convenient point of synchronization for aligning the results of several analyses. Figure 3.17 shows the results of the analysis of surface area, internal volume, and surface-area-to-volume ratio for the interfaces identified in the sequence. Note that the vertical grid-lines in Figure 3.17 correspond to the frames shown in Figure 3.16. In addition, Figure 3.17 contains schematics of the identified profiles without the underlying image at these same times (only the analyzed region is shown).

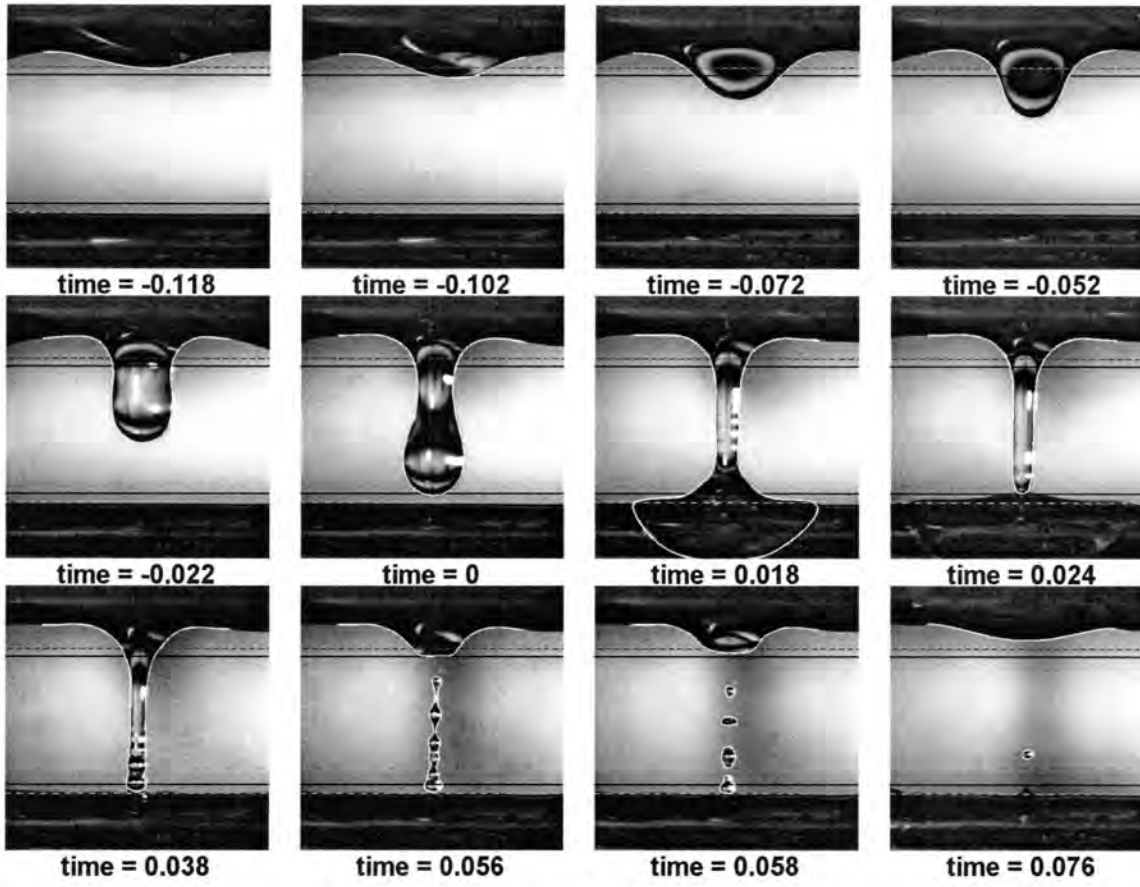

Figure 3.16 Superposition of Video Frames and Analyzed Interfaces for LiBr Droplet

It is critical to restrict the analysis of volume and surface area to the region of axial symmetry in the image. The three curves on each plot in Figure 3.17 illustrate the effect of the upper and lower limits on the analysis of surface area and volume. The solid line illustrates a correct analysis where the upper and lower boundaries used in the analysis contain regions that are primarily axisymmetric; the two broken lines illustrate what happens when the limits are placed too high or too low in the image and will be discussed next. At time –0.118, the droplet just begins to cross the upper boundary that is too close to the tube. Thus the surface area and volume curves for using this boundary (dashed line) begin to rise. The droplet crosses the lower of the two uppermost boundaries just before time –0.102 where the solid line begins to rise. As the droplet grows and pulls away from the tube, it can be seen that the dashed line actually undergoes a region of decreasing volume (and surface area). This is not physically reasonable and reflects the fact that in frame –0.072, the interface at the boundary too close to the top tube is wider than it is at time –0.052. This is the result of the tube stretching the droplet in the lengthwise direction. Since this stretched profile is not axi-symmetric, revolving it overestimates the surface area and volume in the drop because it overestimates the depth of the droplet in the direction of view. This suggests that the lower of the two uppermost limits is a more accurate estimate of the location at which the droplet shape becomes nearly axi-symmetric; the

volume calculated with this boundary is strictly increasing (solid line). It can be seen that during droplet formation and the stages where it pulls away from the tube, the volume and surface area increase to a maximum value just before impact. In reality, the volume does not truly decrease after the impact, as suggested by Figure 3.17, it just leaves the region of interest and is redistributed on the tube surface. However, the lack of rotational symmetry at the impact site makes accurately quantifying the volume and surface area in this region impossible since no detailed information about the film thickness is available.

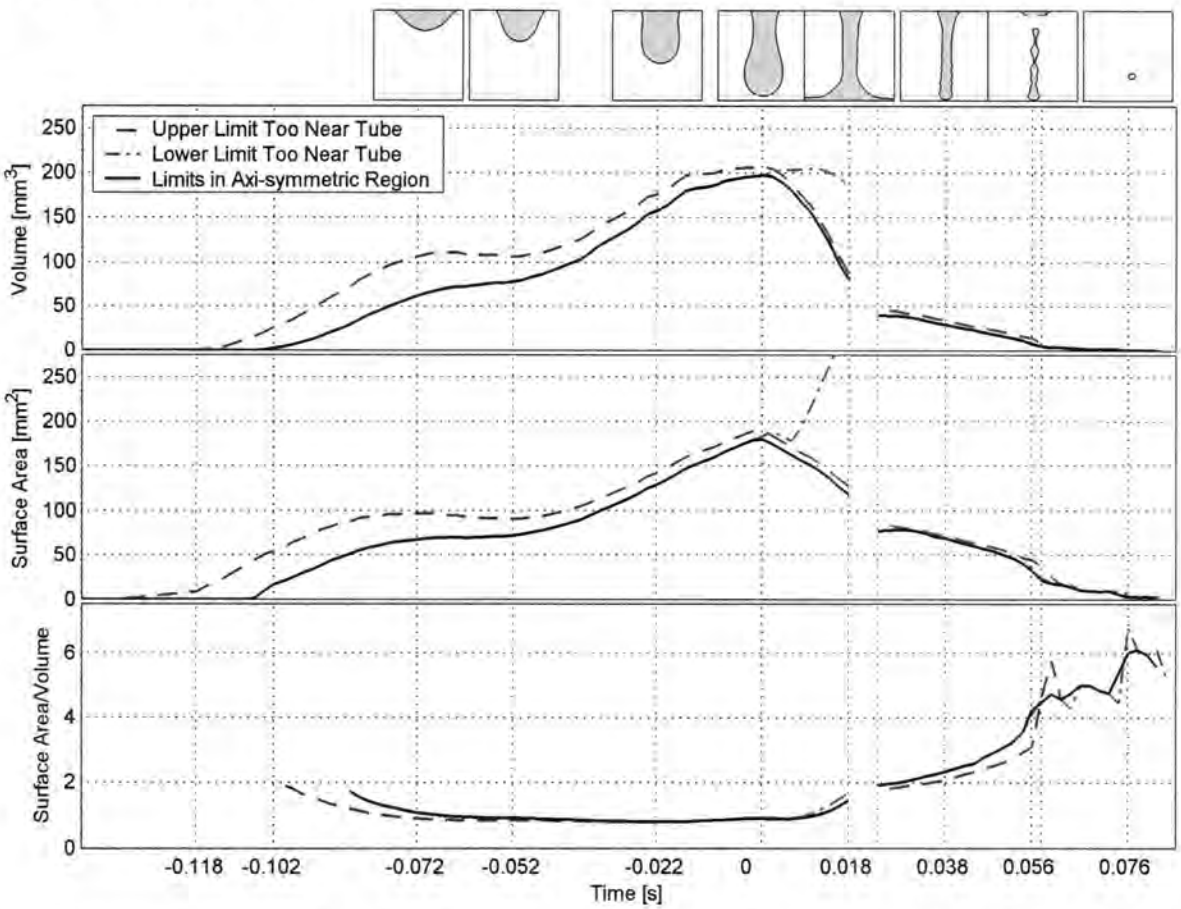

Figure 3.17 Image Analysis Results: Droplet Volume, Surface Area, and Area/Volume Ratio throughout the Entire Droplet Evolution Cycle

The interface tracked after the impact can be forced to follow the spreading lamella (saddle wave) as shown in the profile at time 0.018 in Figure 3.16. There is no particular incentive to do this other than for visual interpretation since the section of the spline depicting the saddle wave should not be included in the calculation of surface area or volume since it is not axisymmetric and it overlaps the tube. However, the dot-dashed line (seen extending to the right of the peaks in the graphs) shows the result of continuing the analysis in this way when the lower limit is beyond the region of axial

symmetry. Actually, the dot-dashed line does provide some physically reasonable insight into the spreading lamella. The calculated surface area of the droplet shoots up shortly after impact while the volume remains relatively constant. However, the spreading lamella does not, in fact, create new surface area since the tube was already wet with film before the droplet arrived; it merely rejuvenates it. Thus the higher of the two bottommost boundaries (solid line) provides a more sensible estimate of the change in surface area after impact (i.e. it begins to decreases sharply at impact as the free surface of the droplet rejoins the film). Tracking the saddle wave with the spline is possible for a few frames after the impact; nevertheless, at some point, the saddle wave becomes undetectable and or/ expands outside of the field of view. This necessitates reinitializing the shape of the spline using manual clicks at a later frame to impart the necessary high-level knowledge to the analysis. The frame at time 0.024 illustrates the reinitialized interface shape. Because the interface at time 0.024 does not extend beyond the lower boundary, there is a slight discontinuity in the plots, represented by the gap from times 0.018 to 0.024 in the plots in Figure 3.17. It is clear that the curves on either side of the gap would intersect, but the connecting curve can not be defined without ambiguity due to the dramatically different shapes at the bottom of the identified interface profiles at times 0.018 and 0.024. What is clear is that shortly after impact, the volume and surface area of the primary droplet is lost to the surface of the tube resulting in a steep decline in both curves. After this, the remaining liquid bridge continues to thin and drain until it breaks and forms satellites. During this process, the volume and surface area of liquid between the tubes continues to decrease, although at a slower rate than was associated with the impact of the primary drop. It is interesting to note that the surface area to volume ratio begins to increase significantly and reaches a maximum with the development of satellite droplets. It can be seen that this ratio exhibits some unsteadiness during the lifespan of the satellite droplets. This is due partly to the shape oscillation of the drops, partly to the sequential impact of the satellite drops, and partly to the increased uncertainty in the calculation of droplet sizes when the whole drop occupies just a small number of pixels. The implication of the rising area to volume ratio is that, although the total surface area and volume is small, satellite drops may absorb significant amount of vapor due to the reduced resistance to heat and mass transfer.

3.4 Summary and Conclusions of Flow Visualization

Using high-speed, high-resolution video, the behavior of falling films over horizontal-tube banks was observed. Particular attention was paid to the behavior of the droplets and film waviness. It was shown that the assumptions typically used in models of these types of systems are grossly violated by the actual flow patterns. In addition, a semi-automated computer routine was developed to analyze the recorded images. The outputs of these routines are smooth mathematical descriptions of the interface, along with estimates of the droplet surface area and volume during the entire evolution cycle of a droplet. These will provide the basis for comparison with the results of computational models discussed in the next section.

Some specific conclusions have already been mentioned, but will be summarized here:

- The behavior of droplets during formation and impact in horizontal-tube banks shares some common features with the axisymmetric cases of formation from a capillary tube and impact on a flat plate, namely: the development of a primary drop with axisymmetric shape and a thinning liquid bridge connecting the primary drop to the parent liquid; the spreading of a liquid lamella after impact that initially travels with a very high velocity but steadily slows; and the formation of oscillating satellite droplets when the liquid bridge breaks.
- There are significant differences from the axisymmetric cases as well, namely: horizontal tubes elongate the droplets in the direction of the tube axis, particularly early in the formation process; lamella spreading is distorted around the tube to form a saddle-wave; and the interaction of neighboring droplets can have a sizeable impact on the details of the behavior of each drop.
- The assumption that films are evenly distributed along the top surface of a tube is strongly violated in the case of droplet flow. Additionally, the momentum of an impacting drop propels a significant amount of liquid around to the underside of the tube very quickly where it can have a strong effect on subsequent droplet formation events. The energy of droplet impact also leads to waviness of the liquid film and significant axial velocity of the film.
- During pendant droplet formation and during the stages where the primary drop pulls away from the tube and a thinning liquid bridge is formed, the surface area and volume of liquid between the tubes steadily increases to a maximum the moment before impact.
- Upon impact, the surface area and volume of liquid between the tubes decreases quickly as the primary droplet is spread over the tube.
- Thinning liquid bridges exhibit a decreasing surface and volume during their lifespan but an increasing surface-area-to-volume ratio. The maximum area-to-volume ratio occurs when the bridge breaks into satellite droplets.

4 COMPUTATIONAL MODELS

The objective of the computation effort described here is to develop a model that accurately captures the flow phenomena observed in the previous section including droplet formation, impact and film waviness. Of the many methods in the literature for modeling this type of two phase system with breaking/coalescing free interfaces, the Volume-of-Fluid (VOF) method was selected for a number of reasons, although there are other methods that could also have been used to accomplish the objective. Section 2.3.2 contains a discussion of the strengths and weaknesses of some the various techniques considered. The key strengths of the VOF method are that it does not require any new solution techniques compared with standard routines that solve Navier-Stokes equations, it is adaptable to any arbitrary, three-dimensional geometry, it does not require any special grid generation techniques and is even suitable for unstructured grids (Youngs, 1982), methods for including surface tension forces are well documented (Brackbill *et al.*, 1992; Brackbill and Kothe, 1996), and it has proven successful in modeling many other types of related flow phenomena.

The objective stated above for the computational work is part of a larger objective described in the introduction to improve the state of the art in performance prediction and efficient design of falling-film, horizontal-tube absorbers. Thus the future utility of this model requires that it be adaptable to include coupled heat and mass transfer as well as potentially complex models for surface tension required to capture the effect of surfactants (discussed in section 2.2.3). Therefore, a commercially available CFD package that has these capabilities *and* grants the user access to primitive variables and a large amount of control over the details of the solution procedure, including implementation of user-defined algorithms and functions, is an ideal environment in which to develop this model. The commercially available package FLUENT (Fluent Inc., 2003) met these criteria and was used for the computations presented here.

4.1 Assumptions and Fluid Properties

The flow was assumed to be laminar throughout the solution domain in all cases considered here. This is a justifiable assumption given the low film Reynolds numbers under consideration (around 100, see section 3.1). Even though bifurcation and impact events can lead to locally high velocities, it is assumed that they do not generate turbulence in a way that would require any special modeling.

The thermophysical properties of the air and the fluid phase (either water for comparison with the literature or aqueous LiBr for comparison with experiments) were assumed to be constant within each phase. These were evaluated at 25°C and 101.325 kPa based on the data in (Keenan *et al.*, 1983) for air and (Haar *et al.*, 1984) for water. For 55%-wt LiBr, the data of (Lee *et al.*, 1990) was used to evaluate the viscosity and a correlation developed by Herold (Klein and Alvarado, 2000) was used to evaluate the density. The surface tension between air and aqueous LiBr was estimated by interpolating the data in (Kulankara and Herold, 2002) which includes a survey of values in the

literature and new experimental data at room temperature and atmospheric pressure. All of these correlations were implemented in the commercially available software program EES (Klein and Alvarado, 2000). Table 4.1 summarizes the properties:

Table 4.1 Summary of Thermophysical Properties Used in Computational Analysis

	Air	Water	55 %-wt LiBr
Density, ρ [kg/m^3]	1.185	997	1592
Viscosity, μ [kg/m-s]	1.85×10^{-5}	8.905×10^{-4}	4.635×10^{-3}
Surface Tension, σ [N/m]		7.255×10^{-2}	9.152×10^{-2}

Implicit in the assumption of the constant properties stated above is the assumption that the flow is incompressible and Newtonian. This allows a standard form of the Navier-Stokes equations to be used as discussed in the next section.

4.2 Governing Equations and the Volume-of-Fluid (VOF) Method

Conservation of mass, the so-called continuity equation, can be derived by applying Reynolds' Transport Theorem (RTT) to any material volume. Noting that the mass, m, within the volume is constant, that is the derivative of the mass with respect to time, t, must be zero:

$$\frac{dm}{dt} = 0 \qquad (4.1)$$

and applying RTT leads to the general continuity equation which can be written in many ways, for instance:

$$\frac{\partial \rho}{\partial t} + \nabla \bullet (\rho \vec{v}) = 0 \qquad (4.2)$$

where ρ is the density, $\vec{v}$ is the velocity vector, and ∂ denotes the partial derivative operator. For the case of constant density, (4.2) simplifies to the statement:

$$\nabla \bullet \vec{v} = 0 \qquad (4.3)$$

The divergence operator, $\nabla\bullet$, must be appropriately defined for the coordinate system. In the present work, the coordinates were either cylindrical or Cartesian. In the cylindrical case, axial symmetry was assumed (no swirl velocity permitted), thus reducing the problem to two spatial dimensions. Thus the continuity equation becomes:

Cartesian 3-D

$$\nabla \bullet \vec{v} = \frac{\partial v_x}{\partial x} + \frac{\partial v_y}{\partial y} + \frac{\partial v_z}{\partial z} \qquad (4.4)$$

Axisymmetric Cylindrical Coordinates with No Swirl Velocity

$$\nabla \bullet \vec{v} = \frac{1}{r}\frac{\partial}{\partial r}(rv_r) + \frac{\partial v_z}{\partial z} \qquad (4.5)$$

where the subscripted v's denote the components of the vector $\vec{v}$.

From a statement of Newton's Second Law of Motion, $\vec{F} = m\vec{a}$ where the force, $\vec{F}$, and acceleration, $\vec{a}$, are both vectors, Cauchy derived the general equation of motion for any continuum irrespective of the relationship between applied stress and exhibited rate of strain (Aris, 1962) (p102). For the case of a Newtonian Fluid, where the stress tensor is at most a linear function of the rate of stain tensor, the standard incompressible Navier-Stokes equations can be derived (Bird *et al.*, 1960; Aris, 1962; Bird *et al.*, 2002) resulting in one equation for each spatial dimension:

Cartesian 3-D

$$\left(\frac{\partial v_x}{\partial t} + v_x\frac{\partial v_x}{\partial x} + v_y\frac{\partial v_x}{\partial y} + v_z\frac{\partial v_x}{\partial z}\right) = -\frac{1}{\rho}\frac{\partial p}{\partial x} + \frac{\mu}{\rho}\left(\frac{\partial^2 v_x}{\partial x^2} + \frac{\partial^2 v_x}{\partial y^2} + \frac{\partial^2 v_x}{\partial z^2}\right) + g_x \qquad (4.6)$$

$$\left(\frac{\partial v_y}{\partial t} + v_x\frac{\partial v_y}{\partial x} + v_y\frac{\partial v_y}{\partial y} + v_z\frac{\partial v_y}{\partial z}\right) = -\frac{1}{\rho}\frac{\partial p}{\partial y} + \frac{\mu}{\rho}\left(\frac{\partial^2 v_y}{\partial x^2} + \frac{\partial^2 v_y}{\partial y^2} + \frac{\partial^2 v_y}{\partial z^2}\right) + g_y \qquad (4.7)$$

$$\left(\frac{\partial v_z}{\partial t} + v_x\frac{\partial v_z}{\partial x} + v_y\frac{\partial v_z}{\partial y} + v_z\frac{\partial v_z}{\partial z}\right) = -\frac{1}{\rho}\frac{\partial p}{\partial z} + \frac{\mu}{\rho}\left(\frac{\partial^2 v_z}{\partial x^2} + \frac{\partial^2 v_z}{\partial y^2} + \frac{\partial^2 v_z}{\partial z^2}\right) + g_z \qquad (4.8)$$

Axisymmetric Cylindrical

$$\left(\frac{\partial v_z}{\partial t} + v_r\frac{\partial v_z}{\partial r} + v_z\frac{\partial v_z}{\partial z}\right) = -\frac{1}{\rho}\frac{\partial p}{\partial z} + \frac{\mu}{\rho}\left(\frac{1}{r}\frac{\partial}{\partial r}\left(r\frac{\partial v_z}{\partial r}\right) + \frac{\partial^2 v_z}{\partial z^2}\right) + g_z \qquad (4.9)$$

$$\left(\frac{\partial v_r}{\partial t} + v_r\frac{\partial v_r}{\partial r} + v_z\frac{\partial v_r}{\partial z}\right) = -\frac{1}{\rho}\frac{\partial p}{\partial r} + \frac{\mu}{\rho}\left(\frac{\partial}{\partial r}\left(\frac{1}{r}\frac{\partial}{\partial r}(rv_r)\right) + \frac{\partial^2 v_r}{\partial z^2}\right) + g_r \qquad (4.10)$$

where μ is the viscosity, p is the pressure, and subscripted g is the component of the acceleration of gravity (or any other body force) in the direction of the subscript.

A finite-volume method was employed to translate these coupled, partial differential equations (4.4 – 4.10) into algebraic expressions that can be calculated with a computer. In this process, the equations of motion and continuity are integrated over each cell and then discretized. The advantages of this method are that application to irregular meshes is reasonably straightforward, and that the resulting discretization automatically satisfies the conservative property for mass and momentum (Tannehill *et al.*, 1997). There are several options for performing the discretization of the equations,

but for the current work, a second-order upwind scheme was used. The discretized equations are linearized and solved in a segregated, 1st-order implicit manner. For a given unknown (velocity in one direction, for example) each governing equation is linearized implicitly with respect to that unknown at a future time. The resulting linear system of simultaneous equations (one for each cell in the domain) is then solved using a Gauss-Siedel equation solver in combination with an algebraic multi-grid (AMG) method (which generates coarse level equations using a Galerkin method without actually performing any re-discretization). This is done for each of the unknowns in the system separately, viz. "segregated". The resulting solution may not satisfy the continuity equation to within the convergence tolerance. If this is the case, a pressure correction is calculated and the segregated solver iterates through the solution for each of the unknowns again, and so on until the solution is converged within the specified tolerance. The solution variables are stored at the cell centers. Since cell face values for pressure are required in the discretized form of the momentum equations, an interpolation technique must be used. The so called "body-force-weighted" scheme was used because it is the most appropriate for buoyancy driven flows as in this work. Face fluxes are related to the velocity at the cell centers using a momentum-weighted averaging technique to avoid the "checkerboarding" that can occur with a linear averaging technique (Fluent Inc., 2003). To relate the solution of the continuity equation to the pressure correction, the PISO (Pressure-Implicit with Splitting of Operators) method, a part of the SIMPLE family of algorithms, was used. Since the flow in this application is driven more by body forces than pressure gradients, an "implicit body force" treatment in the PISO algorithm was used. This utilizes the body forces in the flow in the pressure correction step, resulting in a more realistic pressure field at each iteration. The Fluent solver has sophisticated controls for determining the multi-grid cycles (W, V, combined, etc) for obtaining more rapid convergence. Within the scope of this project, the parameters governing the controls of the multi-grid cycles were not modified from their initial settings.

The basic concept of the VOF method was given in section 2.3.2. As was mentioned, the open issues in any implementation of the VOF method are interface reconstruction and cell advection algorithms (sometimes called donor-acceptor schemes) near the interface. In cells that do not contain an interface (i.e. the volume fraction is either 1 or 0) the standard solution method outlined above is used. Many of the various techniques used throughout the literature are summarized by (Rider and Kothe, 1998). The interface reconstruction used in the present work is a piecewise linear scheme adapted for unstructured grids from (Youngs, 1982). Figure 4.1 illustrates what is meant by a piece-wise linear reconstruction. In some recent papers (Rudman, 1997, 1998; Harvie and Fletcher, 2001), the Youngs method has proven to be one of the most accurate at maintaining the interface across arbitrary grid structure even compared with recently developed methods, although it does not necessarily eliminate the problem of fluid "flotsam and jetsam" that may sometimes remain after a thin film or thread ruptures in the simulation (Harvie and Fletcher, 2001). In this application, flotsam

and jetsam[1] refer to "isolated, submesh-size material bodies that separate from the main material body because of errors induced by the volume tracking algorithm" (Rider and Kothe, 1998). These were at times observed during the simulations; sometimes reducing the time step would ameliorate the problem. However, the net result on the overall predictions was small since the size of these aberrations is less than the size of a mesh element, so the occasional flotsam/jetsam in the simulation was deemed acceptable.

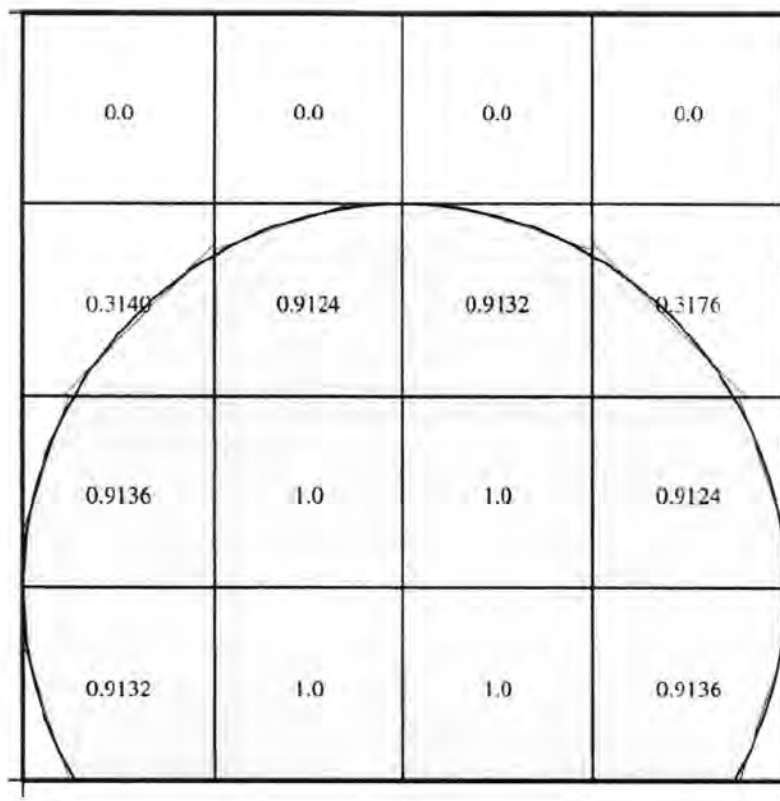

Figure 4.1 Illustration of Piecewise Linear Reconstruction of Interface, adapted from (Rider and Kothe, 1998). Smooth line shows actual interface (circle), numbers represent volume fractions.

[1] From Merriam-Webster, Inc. word of the day 3/4/2002:

flotsam \FLAHT-sum\ (noun)

1 : floating wreckage of a ship or its cargo; broadly: floating debris

2 a : a floating population (as of emigrants or castaways)

b : an accumulation of miscellaneous or unimportant stuff

Did you know?

We started using "flotsam," "jetsam," and "lagan" as legal terms in the 16th and 17th century. (The earliest evidence of "flotsam" dates from circa 1607.) The three words were used to establish claims of ownership to the three types of sea-borne, vessel-originated goods they named. Flotsam was anything from a shipwreck. (The word comes from Old French "floter" -- "to float.") Jetsam and lagan were items thrown overboard to lighten a ship. Lagan was distinguished from jetsam by having a buoy attached so the goods could be found if they sank. In the 19th century when "flotsam" and "jetsam" took on extended meanings, they became synonyms, but they are still very often paired.

Surface tension is handled using the so-called "continuum surface force (CSF)" method of Brackbill et al. (Brackbill *et al.*, 1992; Brackbill and Kothe, 1996). In this, the pressure rise across the interface due to surface tension is converted to a source term in the momentum equations. This source term is a body force similar to the way gravity appears in the equations. To compute the magnitude of this force, the local curvature (sum of the inverse of the two principal radii of curvature) is computed. The normal vector at the interface is defined by the gradient of the volume fraction. The divergence of the unit normal is, from differential geometry, the curvature. With the curvature known, the surface tension force can be described in terms of the jump in pressure across the interface which, in turn, can be expressed as a volume force using the divergence (also referred to as Green's, Gauss's Divergence, LaGrange's, and Ostrogradsky's) theorem (Aris, 1962). In addition, a wall contact angle can be specified which is used to adjust the surface normal in the cells near the wall. In most cases, walls were specified to have a 0° contact angle to ensure complete wetting in the simulation.

In the VOF formulation, the momentum equations are identical and solved in the same manner as described earlier (i.e. a single equation spans the entire solution domain, irrespective of the location of the phases). The continuity equation is slightly modified to be solved for one phase:

$$\frac{\partial \alpha_2}{\partial t} + \vec{v} \bullet \nabla \alpha_2 = 0 \qquad \textbf{(4.11)}$$

where α_2 is the volume fraction of phase 2. The solution for the volume fraction for phase 1 is simply:

$$\alpha_1 = (1 - \alpha_2) \qquad \textbf{(4.12)}$$

The dependence upon the volume fraction in the other equations enters simply through the evaluation of the fluid properties. For instance, the density in any cell can be expressed by:

$$\rho = \alpha_2 \rho_2 + (1 - \alpha_2)\rho_1 \qquad \textbf{(4.13)}$$

where ρ is the evaluated density within the cell, ρ_1 and ρ_2 are the densities of phase 1 and phase 2, respectively. This leads to one limitation of the VOF method: large gradients in velocity across the interface are not accurately recreated (of course, as is almost always the case in computational work, the more refined the grid, the easier it is to accurately capture steep gradients). Fortunately, in the present work, this situation does not arise.

A final important capability provided by the Fluent solver environment is the ability to run on parallel processor machines with shared or distributed memory. Several methods are available for grid partitioning. The computer used for most of the analyses was a SUN FIRE V480 with four 900 MHz cu SPARC CPU's (and 16 GB of RAM). When the fully three dimensional simulation was run

in parallel on four processors, the speed-up was nearly fourfold, indicating that the overhead of parallel communication was quite low.

4.3 Computational Geometry and Grid Generation

The fixed grids used in the present work were made up of quadrilateral (2-D) or hexagonal (3-D) volumes. Quads and hexagonal cells are known to be slightly more accurate when surface tension is an important force (Fluent Inc., 2003), as is the case here (section 22.2.8 of the Fluent 6.1 Users Guide). The grids were generated using the program GAMBIT (Fluent Inc., 2003). In order to parameterize the grid generation process, the commands were coded as journal/script files using variables for parameters such as tube diameters, tube spacing, and mesh size. The details of the individual meshes will be given with the discussion of the results in the following sections. Four basic geometries were considered in the present work:

1. A 3.2 mm diameter (2.0 mm ID) vertical capillary tube
2. A 5.0 mm diameter (4.0 mm ID) vertical capillary tube 20 mm above a flat plate
3. A column of 15.9 mm diameter spheres (15.9 mm spacing)
4. A column of 15.9 mm diameter horizontal tubes (15.9 mm spacing)

These are shown to scale in Figure 4.2.

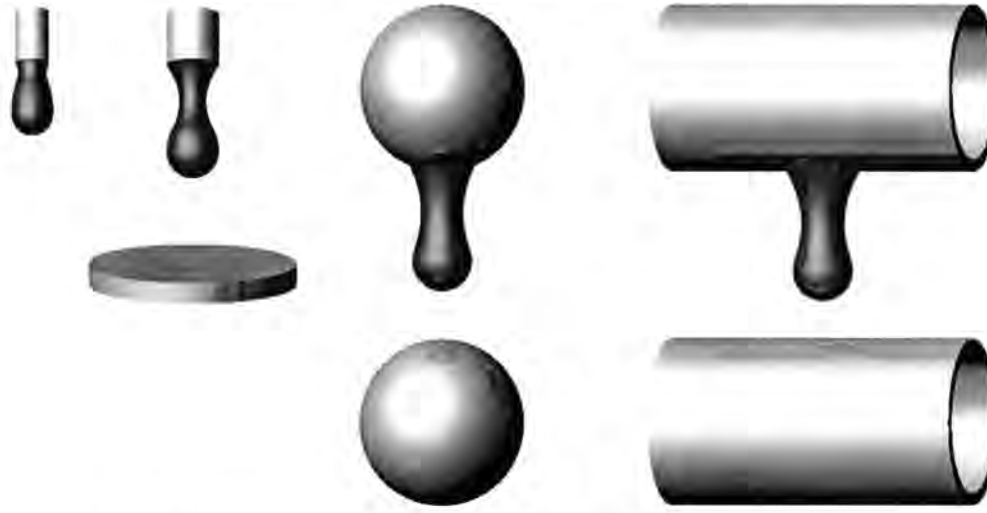

Figure 4.2 Four Basic Geometries used in Computational Analysis

The 3.2 mm capillary tube was considered for comparison with the literature. The larger capillary tube was used to generate droplets closer to the size observed in the horizontal tube experiments and to observe wave formation upon impact with a thin film covering a flat plate placed below the capillary tube. The conditions under which a droplet forms in a capillary tube are fairly different from those in falling films around a solid body. In the case of a capillary tube, fluid enters the drop at the centerline of the drop and the radial extent of the drop is confined by the tube diameter; in

formation from falling films, fluid enters as a film at the edges of the forming drop and there is no geometrical feature which pins the edge of the forming drop. It is, therefore, expected that the droplet evolution and internal circulation patterns would also be different in the two cases. The column of spheres was an intermediate step between the capillary tube and the column of horizontal tubes. Like the capillary tube, it is axisymmetric and thus can be modeled in two spatial dimensions; but like the horizontal tubes, it provides drop formation underneath a solid circular object over which a film falls by the force of gravity.

In the axisymmetric cases, only one half of the cross-section of the tubes or spheres was modeled and an axis-type symmetry boundary condition was used along the centerline. The horizontal tubes were modeled with three spatial dimensions. It was assumed that the drop was mirror-symmetric about the plane of the centerline of the tubes and the perpendicular plane containing the centerline of the droplet. This allowed the model to include only ¼ of the forming drop with appropriate symmetry boundary conditions on the two centerline planes.

4.4 Validation of Method – Capillary Tube

Zhang (1999b) previously simulated the formation of a water droplet from a capillary tube into quiescent air with various tube diameters and flow rates using the VOF method. Excellent agreement was shown with experiments (see Figure 4.3). Zhang used the RIPPLE program (Kothe and Mjolsness, 1992) on a grid with 62 tessellations in the radial direction and 202 in the axial direction.

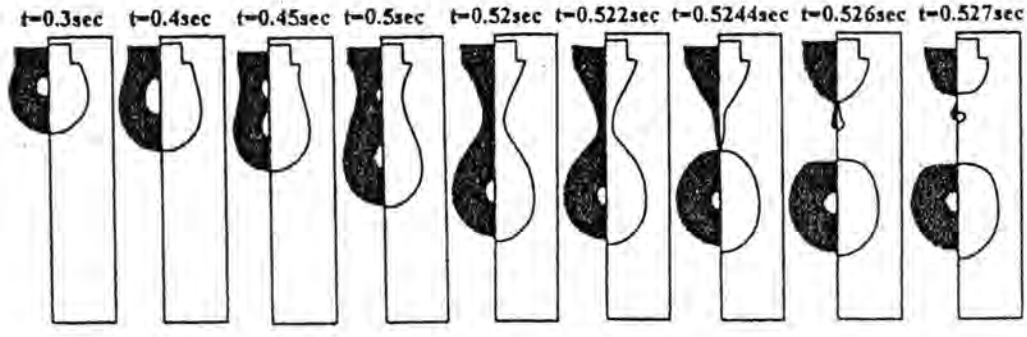

Figure 4.3 From Zhang (1999b): Water Droplet Formation from a Capillary Tube, 3.2mm OD, 2.0 mm ID, 10 mL/min, (experiments shown in dark left-halves, computational results in light right-halves)

The simulation suggested in Figure 4.3 was repeated in the present work using the analysis procedure outlined above. By comparing the results, it was hoped that the present method could be rigorously validated. Unfortunately, as will be shown, precise agreement was not obtained. The results, however, appeared to be plausible as they predicted similar behavior, albeit with some differences in the details.

The tube diameter and thermophysical properties were taken to be the same as listed in (Zhang, 1999b): ρ_{water} = 1000 kg/m^3, μ_{water} = 0.001 kg/m-s, σ = 0.07255 N/m. Zhang did not state the properties of the gas phase used; in the current work they were taken to be ρ_{air} = 1.225 kg/m^3, μ_{air} = 1.7894×10^{-5} kg/m-s. As in (Zhang, 1999b), the grid employed had 62 radial tessellations. The exact dimensions of the solution domain were not stated in (Zhang, 1999b) so they were estimated from other known lengths in the results. The outer radius of the domain was taken to be 3.0 mm resulting in mesh elements with lengths of about 4.8×10^{-5} m. The height of the solution domain was taken to be 15 mm. The tube OD was 3.2 mm and the ID 2.0 mm. The meshed solution domain used in the current work is shown in Figure 4.4. The stated incoming liquid flow rate was 10 mL/minute and a fully-developed, laminar parabolic velocity profile was used (Zhang, 1999b); at time zero, the interface was flat across the opening of the capillary tube and the fluid throughout the solution domain was quiescent. The boundaries surrounding the solution domain were taken to be constant pressure inlet/outlets.

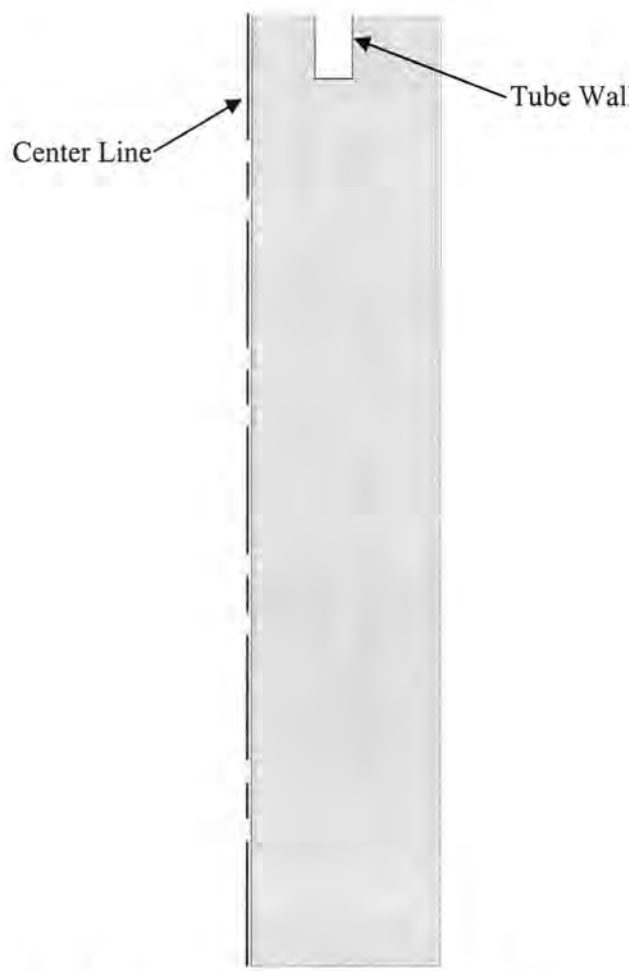

Figure 4.4 Grid Used in Capillary Tube Validation Analysis, Left Edge is Centerline/Axis of Symmetry

The boundary condition at the tube wall requires some explanation. In the CSF method described previously (Brackbill *et al.*, 1992), wall adhesion is specified using a prescribed contact angle. Zhang claims to have used the CSF method, but apparently modified it at the tube wall based on experimental observations. In experiments, the fluid appears to remain pinned to the outer diameter of the tube at all times. Zhang claims that this implies that "no contact angle needs to be specified in this problem" though it is not entirely clear then how the CSF formulation was applied in the region of the wall. In the present work, the "pinned" condition was originally created by specifying a contact angle of 0° (complete wetting, included angle through liquid phase) on the bottom face of the tube and 179° (completely non-wetting) on the outer surface of the tube. In this way the liquid would fully wet the bottom surface of the tube but would not have any impetus to wick up the outside of the tube. With this configuration, at the beginning of the simulation, the interface would undergo severe oscillations as it spread to the outer diameter requiring very small time-steps to maintain convergence. Some researchers have artificially raised the fluid viscosity to "a very high value" for a period of time after the simulation starts to avoid this kind of behavior (Eggers and Dupont, 1994). In a second simulation with the same geometry, the contact angle at the tube face was set to 95° (slightly resistant to wetting) at t=0. At start up, the oscillations were significantly reduced (the same time-step could be used during the whole simulation) since the liquid film was not forced to stretch across the face of the film immediately, but was allowed to proceed more "naturally" as the nascent drop formed. The problem with this method is that, if the contact angle specification is left unchanged throughout the simulation, the point of contact will drift between the inner and outer diameters during the droplet evolution. When the diameter of the thinning liquid bridge becomes less that the OD of the tube, the direction of the force of surface tension is inward, thus pulling the unpinned contact point to the inner diameter. During most of the other periods of formation, the contact point tends to remain at the outer diameter. The moving contact point was seen to have an effect on the necking and eventual detachment of the droplet since it allowed the parent material attached to the tube to take a smaller diameter. This issue was resolved as follows: during the first few tenths of a second of initial droplet formation from a flat interface spanning the ID, the contact angle at the tube face was set to be 95° on the tube face to allow the droplet to spread across the face with minimal oscillations. Sometime after the liquid interface reached the outer diameter, but before the droplet began to pull away forming a thinning neck, a contact angle of 20° was assigned to the tube face, a representative value for water on high-energy surfaces such as glass and metal (Carey, 1992) (p 70). This pinned the interface to the outer diameter.

As was intimated above, the model set up to replicate the results of Zhang (1999b) did not agree well as shown in Figure 4.5 for three times. As can be readily seen in Figure 4.5, in the current work, the droplet extended farther down and grew significantly faster. In addition, the droplet detached sooner in time and was stretched further from the tube at the point of detachment. These observations suggest a discrepancy in the applied fluid flow rates, especially in light of the effect of flow rate

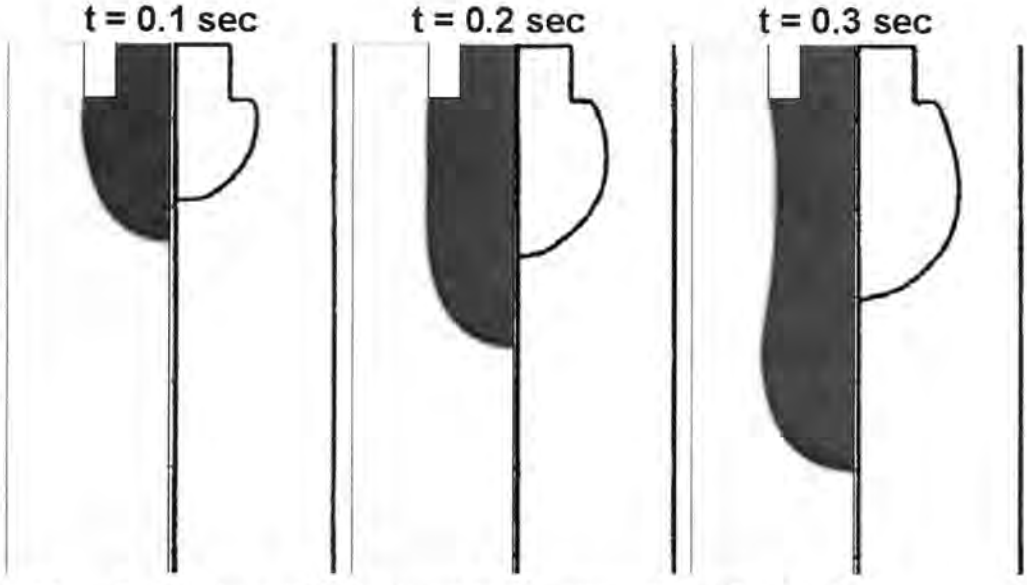

Figure 4.5 Comparison of Early Droplet Formation at Q = 10 mL/min, Current Work – Left, Zhang - Right

documented by Zhang (increasing flow rate led to longer break-off lengths at earlier times). The flow rate in the current model was checked several ways: the velocity profile applied at the inlet was numerically integrated over each boundary element to determine the actual inlet flow rate, the total volume of the fluid phase versus time was determined by integrating the volume fraction over the entire solution domain at each time step, and the image files produced were analyzed using IMAN to estimate the change in droplet size as a function of time. All three of these methods agreed that the applied flow rate in the current work was 10 mL/min ±1%. In fact, the value calculated from image analysis of the frames (purposefully stated here with too many significant figures) was 10.021 mL/min, attesting to the accuracy of the method. This apparent discrepancy was investigated further by analyzing the droplet profiles provided in the figures of (Zhang, 1999b) using IMAN (obtained from a PDF version of the paper). Using 5 frames spaced 0.1 sec apart in time, the calculated flow rate turned out to be approximately 7-8 mL/min; significantly lower than the 10 mL/min claimed. There is, of course, greater uncertainty in this estimate than when analyzing the high-resolution image frames in the present work due to the potential for distortions during the reproduction of the image and the generally lower resolution of the image. To account for this, four reference lengths in the images were used for calibration: the inner and outer radii of the tube, and the horizontal and vertical tick-marks on the plots. The results are sensitive to the calibration value (which has units of pixels/mm, for example) since volume estimates must be scaled by this value cubed (see Appendix A); thus, the calibration value was calculated many times for each reference length (since they are reproduced on each frame presented) and the droplet volumes reanalyzed. From these, the average flow rate from 0.1 to 0.5 seconds in Zhang's results was estimated to be 7.43 mL/min. From the

repeatability using the various calibration values, the uncertainty in this estimate could be as high as ±1.5 mL/min, but even the outside bounds of this do not include the stated flow rate of 10 mL/min. Finally, some of these same profiles appear in another figure in the paper that was also analyzed in a similar manner with nearly identical results. Therefore, in the present work, another simulation was conducted with a flow rate of 7.5 mL/min. The same comparison is shown in Figure 4.6.

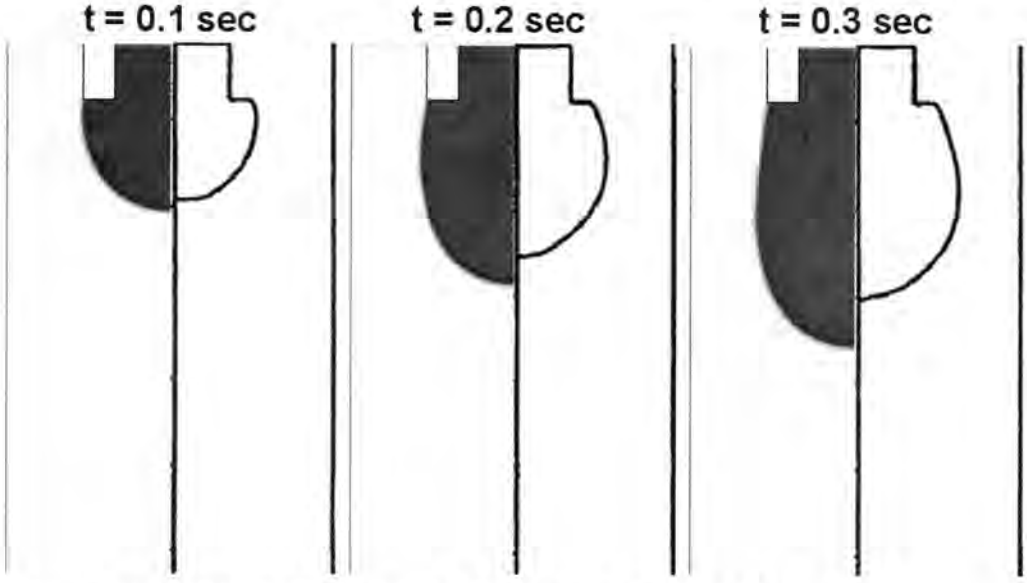

Figure 4.6 Comparison of Early Droplet Formation at Q = 7.5 mL/min, Current Work – Left, Zhang - Right

The comparison shown in Figure 4.6 is certainly more favorable than the one in Figure 4.5, corroborating the evidence for the lower flow rate. In fact, it appears that the flow rate in (Zhang, 1999b) might actually be lower still. However, the comparison at early formation times does not illustrate the whole story. In droplet of Figure 4.3, between 0.52 and 0.53 seconds, the neck thins and breaks forming a single, upward-moving satellite drop around 0.5 mm in diameter or smaller. The break-off corresponding to the simulation shown in Figure 4.6 occurred at a time between 0.46 and 0.47 seconds. The profiles of some of the shapes predicted during the detachment are shown in Figure 4.7 (1 ms between frames) along with corresponding profiles from (Zhang, 1999b), synchronized at the time of the break, not the initiation of the simulation. It can be seen that in the present work, the liquid neck was predicted to be significantly larger at the time of the break resulting in a satellite drop of significantly greater volume. In addition, the collapsing liquid bridge imparted a significant amount of energy to this satellite drop resulting in shape oscillations. Though the break occurred earlier, the droplet was further away from the capillary and the liquid neck was much longer. Qualitatively, the agreement is good; the common features of necking, bifurcation, oscillation of the primary drop, flattening of the retained drop, and satellite formation are predicted. It is also possible that further adjustment of the flow rate in the current work could lead to better agreement. It should also be noted that the specific timing of events, satellite drop sizes and behavior are strongly

influenced by very small scale phenomena at the point of bifurcation (Peregrine *et al.*, 1990; Eggers, 1997). Accurately predicting the behavior of satellite droplets has proven to be quite challenging (Notz *et al.*, 2001). Thus it seems quite possible that phenomena strongly determined by the bifurcation events may have particularly high grid sensitivity. The conclusion from this validation step is that the current technique appears to have potential for predicting the observed behavior but may be limited in precision by the grid sensitivity of small-scale events that have a large impact on the flow patterns observed.

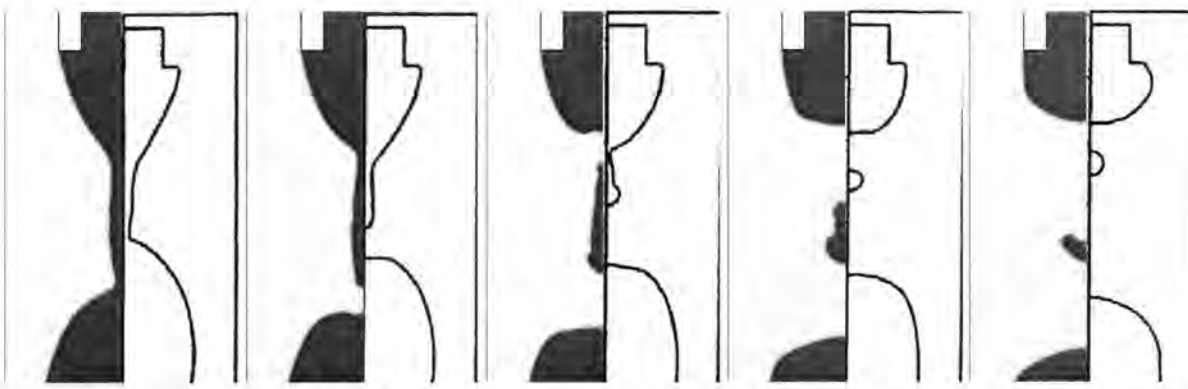

Figure 4.7 Comparison of Droplet Detachment at Q = 7.5 mL/min, Current Work – Left, Zhang – Right, synchronized at rupture point, 1 ms between frames

4.5 Model results

After validation, the reason for considering geometric models other than the fully three-dimensional horizontal tube is to determine if the behavior of the droplets in horizontal tubes could be approximated well enough using a simplified (computationally less expensive) geometry. Even on the relatively modern, high powered computer used for the current study (see section 4.2), analyzing the development cycle of one droplet in 3-D required over 30 hours of wall clock time (on four parallel processors – thus the computational time is even greater) on what is arguably too coarse of a grid. By contrast, the 2-D cases could usually be completed in a time on the order of 3 hours (depending on the time-step limitations imposed by the problem conditions and mesh size).

As was mentioned in the previous section, there is a large potential for grid dependence in these models. Grid dependence tests were not performed in all cases, but only for the axisymmetric spheres. This model captures some of the effects of drop formation under horizontal tubes without the computational expense of the 3-D model, so it was the most suitable choice for assessing grid dependence. All models discussed from this point forward were modeled with aqueous LiBr and the properties listed in Table 4.1

4.5.1 Analysis with Digital Image Processing Routines

The image analysis routines described in section 3.3 can easily be applied to the images of the droplets generated from the computational results. It is true that many parameters such as surface area and volume could be computed directly from the numerical results. However, utilizing the same tool for analysis of both experimental and computational results eliminates many possible sources of error. The images from the computational work are particularly easy to analyze because there are no issues with shadows, glare, background noise, etc. in the images and reference lengths for calibration are easily selected. Consequently, after identifying the location of the interface in the first frame and selecting appropriate edge detection algorithm and thresholds, the analysis proceeds virtually automatically, only requiring the user to click through the frames and occasionally double check the fit.

4.5.2 Capillary Tube with Droplet Impact

The droplets observed in the experimental work were almost always 5 to 6 mm in diameter the moment before impact. In most capillary tubes, the diameter of the primary drop is slightly larger than the tube diameter. It was hoped that simulating a 5mm OD capillary tube would give droplet sizes in the range observed in the experiments. The tube ID was taken to be 4 mm. A circular flat plate was placed 20 mm below the bottom of the capillary tube. The plate was covered with a quiescent film of LiBr initially 0.3 mm thick. The meshed solution domain is shown in Figure 4.8; the darker areas indicate the initial location of the liquid. Note that the solution domain extends upward 5 mm from the plate diameter. This region accommodates the waves and the deforming droplet during impact. The mesh comprises 20806 elements with a typical element edge length of 8×10^{-5} m. The contact angle on the plate was taken to be 0° to ensure complete wetting. A fully developed laminar velocity profile was again prescribed at the inlet. The remaining boundaries were constant pressure inlet/outlets. It should be noted that the initial distribution of the liquid film is unstable with the given boundary conditions. The pressure boundary is treated like an ambient gas surrounding. Therefore, the location where the initially uniform film touches this boundary is treated like a liquid-vapor interface. Thus the initially cylindrical film transitions to the equilibrium shape for a sessile drop (more like a dome) the diameter of the plate.

Three flow rates were considered, from $25< Re <50$. Figures 4.9-4.11 contain selected frames from each of the simulations (not equally spaced in time). The results are described next. At Re = 25, a 5.1 mm primary drop forms and detaches completely from the liquid thread before impacting with the film. The recoiling thread breaks at the top and forms a large (almost 2 mm diameter) oscillating satellite drop. The spreading lamella forms a wave front approximately 1 mm high; the impact of the satellite drop also creates a notable lamella. At Re = 37.5, the primary droplet also detaches just before impact, and is nearly spherical with a diameter of 5.3 mm. The wave front of the advancing lamella reaches 1.2 mm high. The recoiling bridge breaks near the droplet, and a 2.4 mm

Figure 4.8 Meshed Solution Domain for 5 mm Capillary Tube over a Flat Plate

satellite droplet is formed. The volume of liquid remaining attached to the tube is significant and the recoiling liquid quickly takes the shape of a pendant drop. The analysis was run a bit further to show that, due to this large attached volume of liquid, another droplet approximately the same size as the original primary drop detaches in rapid succession. For the Re = 50 case, the 5.4 mm diameter primary drop does not detach from the trailing neck before impacting the film. As was often seen in the experimental work, the thread does detach shortly after impact, due in part to the impact impulse propagating back up toward the eventual pinch point. The liquid thread does not recoil greatly in this case. It is rather large, ranging in diameter from 1.6 smoothly up to the tube diameter of 5.0 mm. The bottom of the broken thread forms a spherical shape that is repeated back up the thread in a string-of-pearls configuration as was seen in much of the video as well though typically in smaller diameter bridges. The wave height near the front of the advancing lamella approaches 1.3 mm. Not only does the size of the primary droplet increase slightly with increasing flow rate, but the width and endurance of the liquid trail does also. It can be seen that no splashing is predicted but the spreading liquid lamellae are very wavy and quickly carry a significant amount of fluid away from the point of impact.

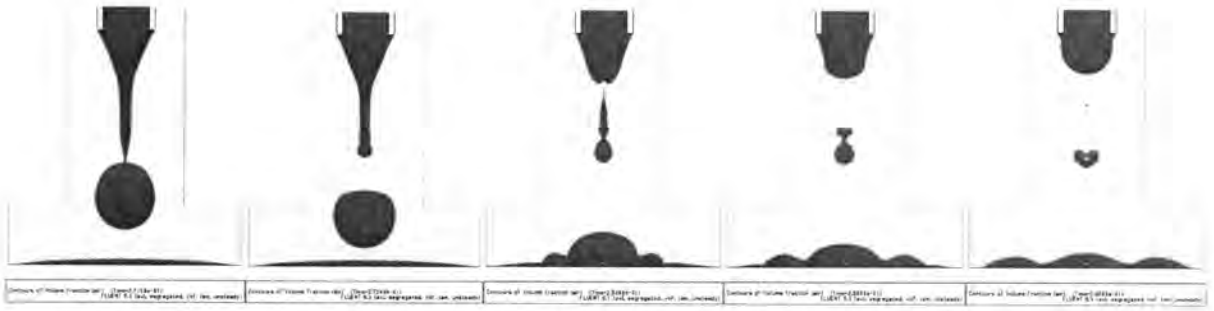

Figure 4.9 Selected Stages of Droplet in 5 mm Capillary Tube over a Flat Plate at Re = 25

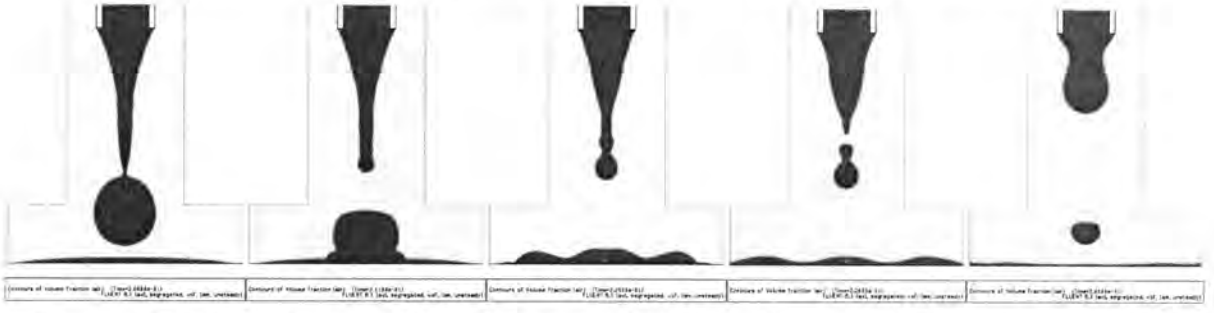

Figure 4.10 Selected Stages of Droplet in 5 mm Capillary Tube over a Flat Plate at Re = 37.5

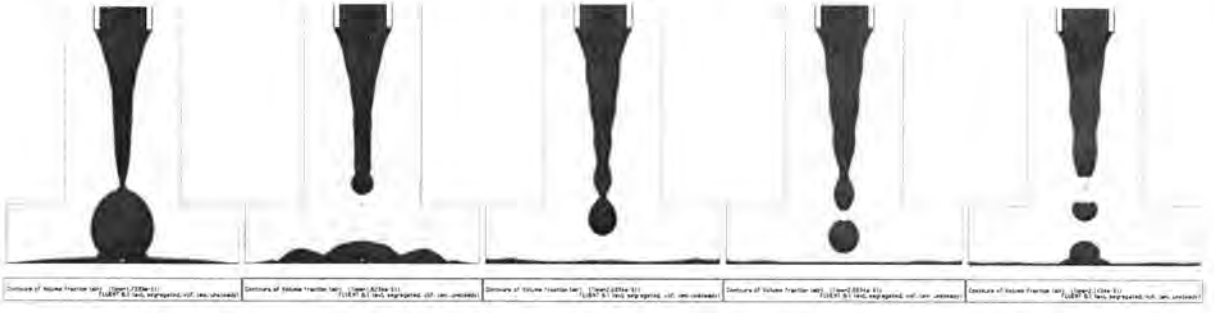

Figure 4.11 Selected Stages of Droplet in 5 mm Capillary Tube over a Flat Plate at Re = 50

4.5.3 Column of Spheres

The 5 mm capillary tube was more a point of interest for validation than a real candidate for a simplified model of droplet formation under horizontal tubes. In theory, a bank of spheres, though physically not practical, provides a much better approximation to the conditions found under horizontal tubes. In addition, they provide a suitable platform for grid independence tests. As will be seen however, the convergence of the film to the bottommost *point* on the sphere causes droplet formation to be accelerated versus the case of a horizontal tube where the flow convergence is to a *line*, not a point.

There was no "flow rate" prescribed in the following simulations. Instead, the spheres started with an initially stagnant, smooth, uniform film surrounding them which eventually sagged and formed a droplet. Only one sphere was included in the solution domain, but the top and bottom

boundaries were translationally periodic so that the flow that exited the bottom boundary entered the top with the same conditions. This model represents following a droplet through an infinite bank of spheres each starting with a uniform film at the same time. In theory, the appropriate volume fractions could simply be assigned to each cell in the mesh to create the initial film distribution. In practice, because of the finite resolution of the grid, this resulted in films with slightly non-uniform thickness and somewhat rough interface profiles. This was because the assignment algorithm was limited to using the coordinates of the centroid of each cell to evaluate the appropriate volume fraction. If an assignment function defined the interface sharply, then its value within the cells near the interface would depend strongly on whether the centroid was just inside or outside this sharp boundary. This would lead to jagged interface definitions. If the assignment function defined the interface with a gradual transition, then the interface would be diffused over multiple cells, a highly undesirable condition. Thus, to begin with a smooth film, free from disturbances and spurious currents and of a known initial thickness, the film was "grown" on the surface of the spheres. That is, for the first 0.01 seconds of the simulation, the sphere wall boundary was changed to a uniform-velocity inlet of the liquid phase. The flow rate was set to obtain the desired film thickness. At the end of the growing period (which was purposefully quick in model time to avoid any significant sagging of the film due to gravity), a zero velocity field was patched to the entire solution domain. Thus t=0.01 is the effective start time of the simulations.

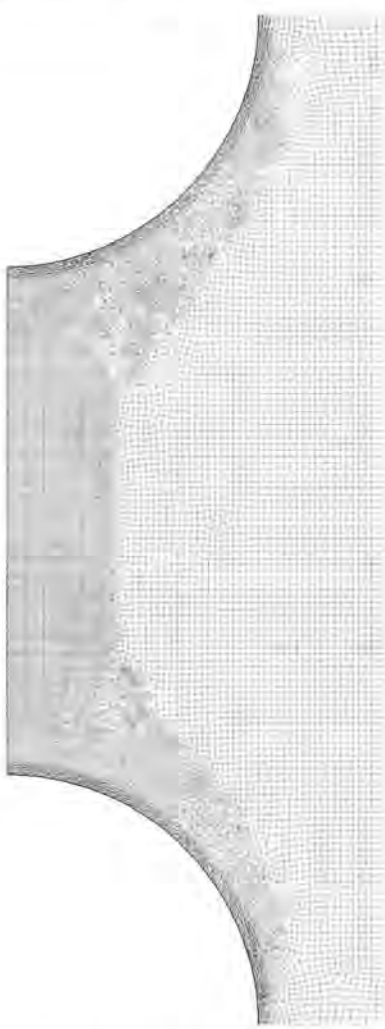

Figure 4.12 Meshed Solution Domain for 15.9 mm Spheres

The spheres modeled were 15.9 mm diameter with a vertical gap of 15.9 mm, following after the tube bank used with the LiBr experiments. A challenge of both this model and the model of the horizontal tubes was that the tube diameter is about three times the typical droplet diameter. Thus the extent of the domain is considerable compared to the capillary tube case. A non-uniform grid was constructed in such a way that the elements near the sphere walls and between the spheres in the path of the droplet fall were significantly smaller than the elements near the boundaries. A typical element length near the wall was 8×10^{-5} m; near the far boundary, it was 2×10^{-4}. The meshed solution domain shown in Figure 4.12 is made up of 19,740 quadrilaterals. The sphere was split across the periodic

boundary at its centerline to ease visualization of the droplet behavior.

Initial film thicknesses in the range of 0.2 to 0.5 mm were considered. With 0.2 mm initial thickness, not enough liquid was available to form an unstable drop. With 0.5 mm, after the initial transient, the liquid flowed essentially as a column between the tubes. Within the range 0.23 to 0.4 mm initial thickness, droplets would form and fall with differing timing, diameters, and trailing bridge dynamics. Interestingly, the diameter of the primary drop did not necessarily increase with increasing initial thickness, but the trailing bridge diameter did. The insensitivity of droplet diameter to film thickness is likely due to the relative constancy of the maximum size of a stable pendant drop under these conditions. In addition, and perhaps intuitively, the time required for the droplet to impact the tube below decreased as the initial film thickness increased. Note that an initial film thickness of 0.23 mm is approaching the minimum that will drip in this situation; over half a second of film sagging occurred before the droplet formed enough to begin to pull away. This behavior is summarized in Table 4.2.

Table 4.2 Summary of Effect of Film Thickness on Droplet Dynamics in Spheres Model

Initial Film Thickness [mm]	Diameter of Primary Droplet at Impact [mm]	Minimum Diameter of Bridge at Impact [mm]	Time to First Impact [msec]
0.20	No droplet falls		
0.23	5.09	1.3	611
0.25	5.03	1.6	158
0.30	4.88	1.9	124
0.35	4.89	2.2	112
0.40	5.18	2.7	98
0.50	Fluid flowed as continuous column		

Figure 4.13 provides a comparison of the behavior of the droplets and trailing liquid bridges for the five initial thicknesses from 0.23 to 0.40. The frames were chosen to be near the same point in the evolution of the drop and are **not** spaced equally in time (after the impact, time can be estimated by noting the distance that the lamella has traversed around the sphere). There are several things to note. In the first two columns, it is clear that the early shape of the drop is fairly independent of the film thickness, except perhaps the second column with the 0.40 mm initial thickness where the falling drop looks significantly thicker through the short bridge. By the time the droplets impact the tubes, the varying thicknesses of the liquid bridges are apparent (column 3). This gives rise to varying degrees of persistence of the bridge (columns 4-6). In the thinnest case, the bridge breaks well before the primary droplet has completely spread onto the tube below. For the thickest case, a stable column is established that persists for a comparatively long time. In the last three rows of the thickest film case, the bulk of the fluid from the primary drop has traveled all the way around the sphere and actually

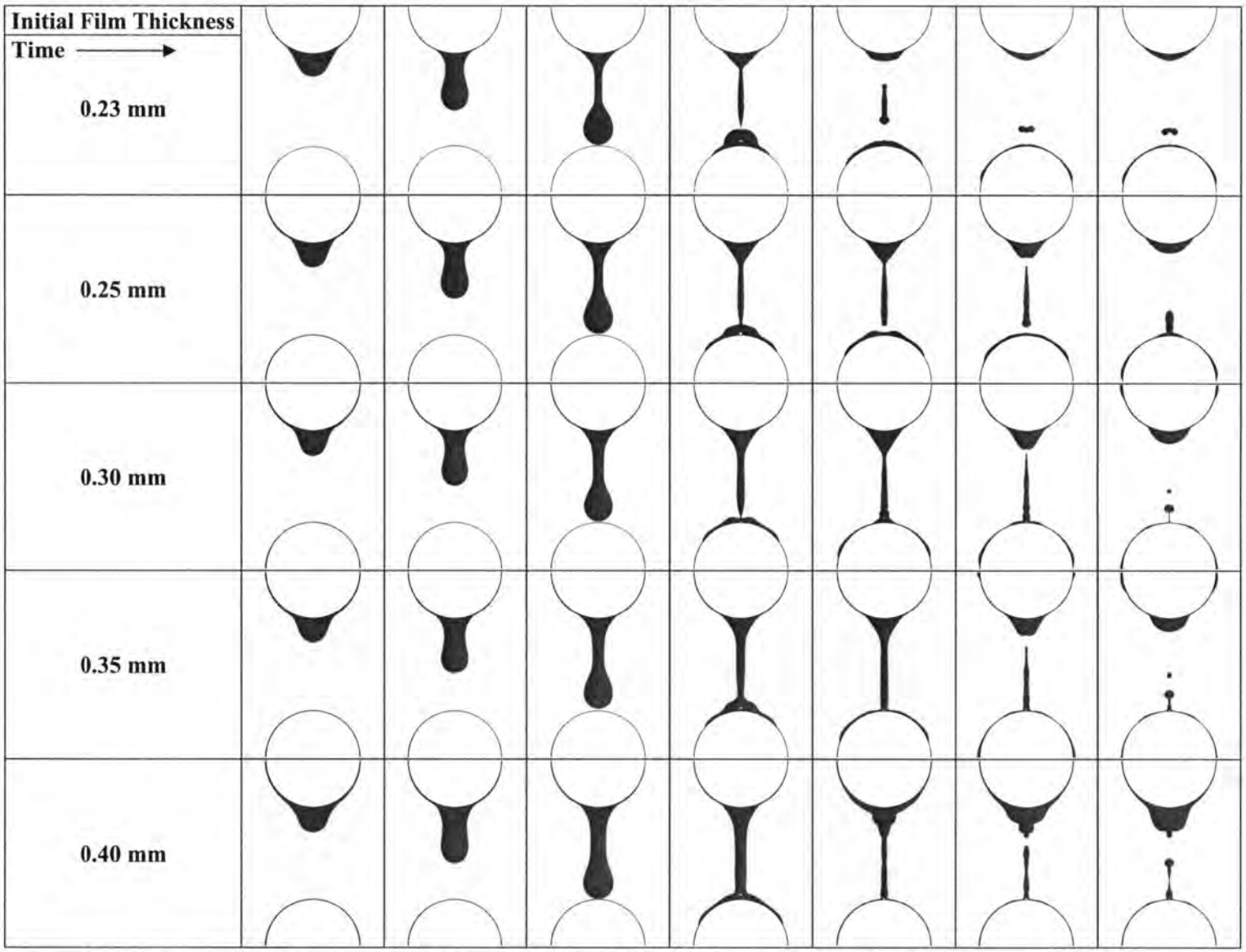

Figure 4.13 Comparison of Computed Droplet Behavior with Changing Initial Film Thickness

causes or at least affects the break of the bridge. At the bottom of the liquid bridge in the 0.30 mm case, there is alternating breaking and coalescence of the bottom of the bridge with the film on the tube: within milliseconds of a break, the whole column falls down far enough that contact is reestablished between the bridge and film. The 0.30 mm case is the transition between the cases with less liquid, where the liquid thread breaks at the bottom first and later at the top, and the cases with more liquid, where the thread remains attached at the bottom the entire time and eventually breaks at the top first. Tube spacing would likely also affect this transition. Finally, the shape of the satellite drops and liquid bridges shown in the last columns are certainly interesting, but also suggest how violent the shape transitions may be during the collapse of the bridge. The implications for heat and mass transfer are that satellites may be particularly effective due to the attendant mixing and fresh surface generation.

Not shown in Figure 4.13 is the fact that, in particular with the thicker films, the second and subsequent droplets formed are substantially altered. This is because the fluid from the first drop as it flows around the sphere quickly becomes inextricably engaged in the formation of the next droplet. This is what has created the strange shape of the pendant drop in the last two columns of the 0.4 mm case in Figure 4.13. Usually this expedites the formation of the next drop significantly and results in a droplet with significant downward velocity and waviness very early in the formation process.

The spherical model was planned as a stepping stone to the fully three-dimensional case, and as a candidate for capturing essential phenomena with less computational expense. As such, it is important to understand the sensitivity of the results to the details of the mesh. There is a strong impetus to find the coarsest acceptable grid, since when adding another spatial dimension, each grid point in the 2-D model is protracted through the third dimension resulting in many offset copies of the original mesh. To study the effect of mesh density, the 0.35 mm initial film thickness condition was simulated on meshes of with elemental lengths 0.8^{-1} and 0.8 times the original, (the original mesh had elemental lengths of 8×10^{-5} m for the finest cells close to the spheres; characterized the same way, the two meshes used to study grid sensitivity are 10×10^{-5} m and 6.4×10^{-5} m, respectively). This resulted in meshes with 15,425 and 24,893 quadrilateral cells, respectively, versus the original mesh which had 19,740.

Unfortunately, the results of the three models show significant grid dependence. In results not presented here, two finer meshes were also utilized and there did not appear to be a converging trend. There are several ways to examine these differences: timing of certain events, size of droplets at impact, break-up pattern of the liquid thread, and so on. Much of this information is depicted through an analysis of the inter-tube surface area and volume performed using IMAN. Figure 4.14 shows the volume, surface area and area/volume ratio for the three models. On the plot, the three models have been synchronized using the impact event for clarity. The maximum values of surface area and volume are also displayed. The volume differs between the three models by almost 6% and the surface area by over 3%. What is more noteworthy, however, is the slope of the curves leading up to

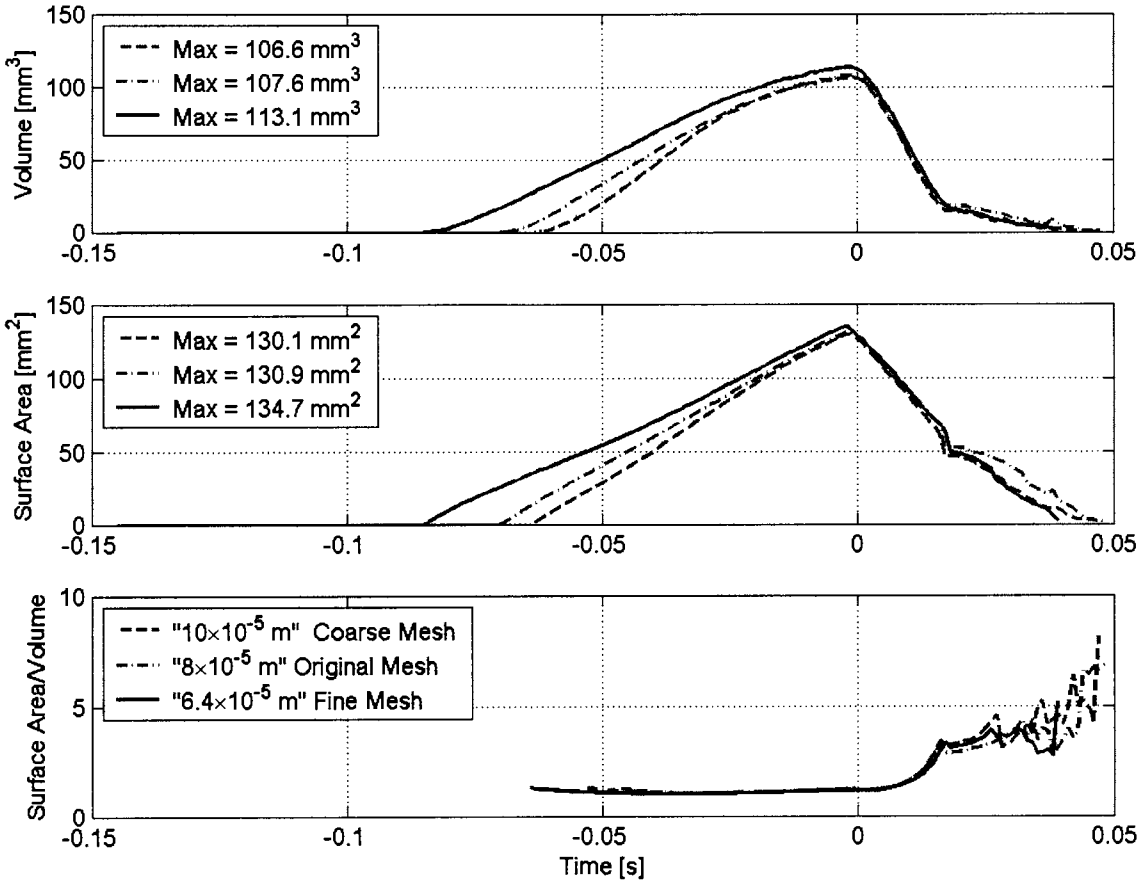

Figure 4.14 Analysis of Grid Dependence

the maximum. These indicate (and a synchronized video playback clearly shows) that the droplet falls more slowly as the mesh-size becomes smaller (also see first two rows of Figure 4.15). In all three simulations, the droplets crossed a line 2.9 mm under the upper tube between 62 and 63 ms after the simulation began (this was the upper limit in the image analysis of Figure 4.14). The elapsed times from that moment until the droplets hit the tubes were 62, 68, and 83 ms for the 10×10^{-5}, 8×10^{-5}, and 6.4×10^{-5} m meshes, respectively. This is a discrepancy on the order of 25 to 33%; a troublesome result. The simulations were run through two droplet cycles and the trend remained the same (thus the models were even further out of synch after the second drop. Finally, the break-up of the liquid jets was seen to vary as well, as can be seen by examining the plots in Figure 4.14 at times beyond about 0.02. The bridge in the finest mesh collapsed most quickly and did not form any satellite droplets; the bridge in the coarsest mesh was the second quickest to collapse and one satellite was formed midway through the process and another near the end; the bridge collapse in the middle of the three meshes took the longest and generated satellites in a similar pattern to the coarser model. More details can be seen in Figure 4.15. According to almost any metric, the middle mesh gave results closer to the coarse mesh than the fine mesh.

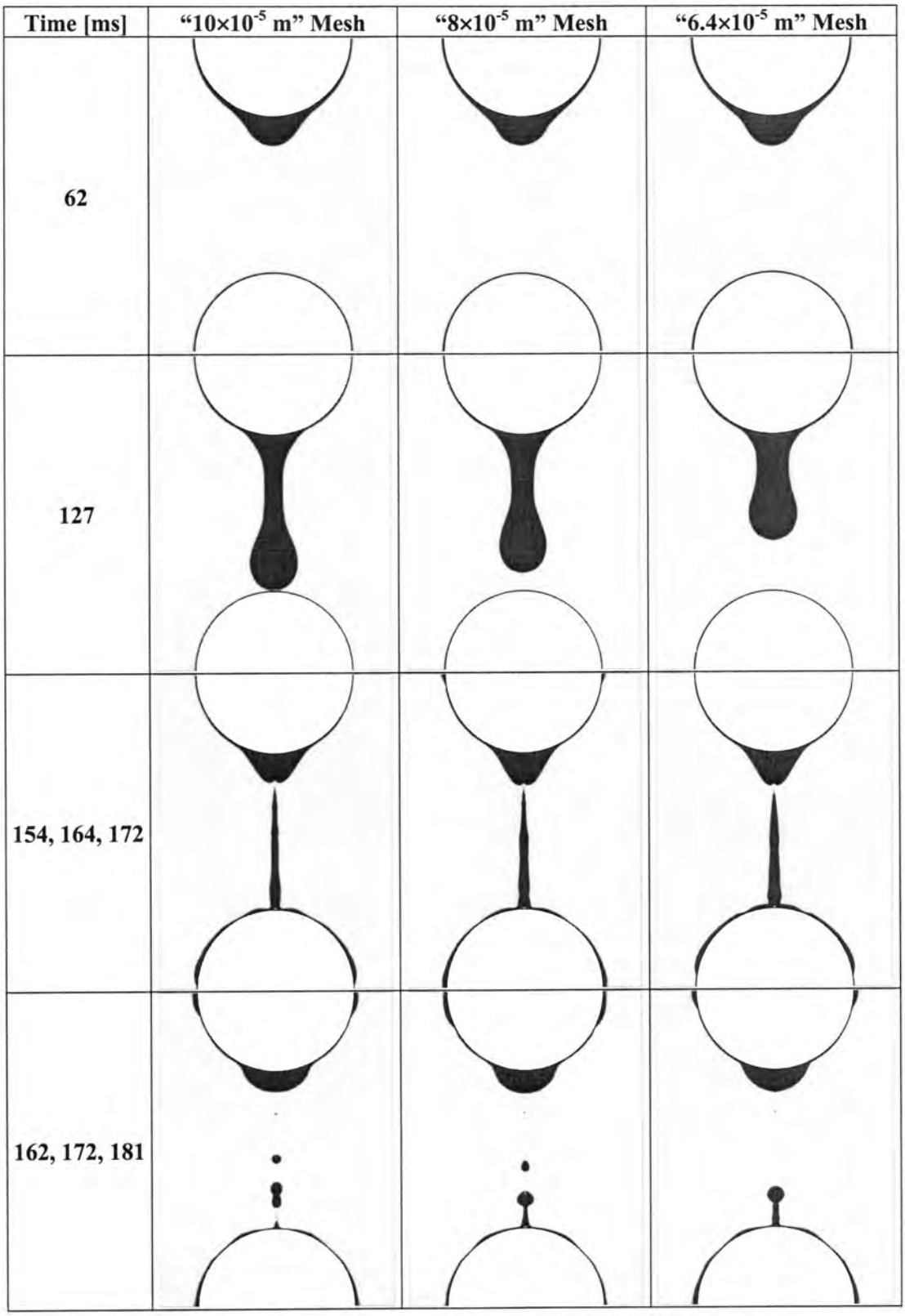

Figure 4.15 Details of Grid Dependence for Spheres Model

Although grid independence was not proven, a comparison between the results of droplet formation under spheres with the results of the experimental video was undertaken with the aid of the image processing methods developed. Figure 4.16 summarizes the results. Again, the droplet impact event has been synchronized to time 0 for clarity of comparison. In Figure 4.16, the solid line represents the droplet analyzed in section 3.3. Three of the spherical models are compared with this result: the 0.30, 0.35, and 0.40 mm initial thicknesses. The thickest film comes closest in terms of inter-tube volume and surface area at the moment of impact. However, it also exhibits the quickest droplet pull-away from the tube, although the slope from t = -0.05 until impact appears very close to the slope of the experimental line during that same period. Simply based on the dynamics observed in the simulations, one could have predicted that the 0.4 mm initial thickness would come the closest because it was the only condition that gave rise to the persistent liquid bridge that was observed in the experimental work. As a result of this stable, thinning bridge, the curve for the 0.4 mm case also follows the experimental line at times greater than +0.05 where the liquid bridge in the other models has already completely collapsed. The lack of agreement at early formation times is probably closely related to the lack of agreement in total magnitude of the drop. With spheres, the falling film must all converge to a single point. With a horizontal tube, the liquid is drawn to a line, but the geometry of the tube does not promote formation at any particular point along this line; a droplet is free to form at any position along the bottom of the tube. Thus other influences, such as film instability, must drive the collection of liquid into a particular formation site. This means that the liquid collection process early in the formation is not as strongly driven by the geometry as in the spherical case. Moreover, due to surface tension, the droplets are stretched in the direction of the axis of the tube. Droplet fall volume depends primarily on the maximum equilibrium volume that can be suspended (Middleman, 1995). The stretching of the droplet in the direction of the axis of the tube is indicative of the larger surface tension forces in this direction. These larger forces likely can support a somewhat larger equilibrium volume than in the spherical case. Thus, it is sensible that the droplet volume for the spherical case would be smaller than in the case of horizontal tubes. This is borne out in the simulation results presented in the next section as well. In this study, typical droplet diameters (measured in the horizontal direction just before impact) predicted for the spheres case were around 5.0 mm, whereas predicted and measured droplet diameters for the horizontal tube case were nearer to 6.0 mm. It seems plausible then that the rapid early growth of the droplets and the lack of an axial stretch accounts for the underestimates in the spherical models of both evolution time and the maximum droplet volume.

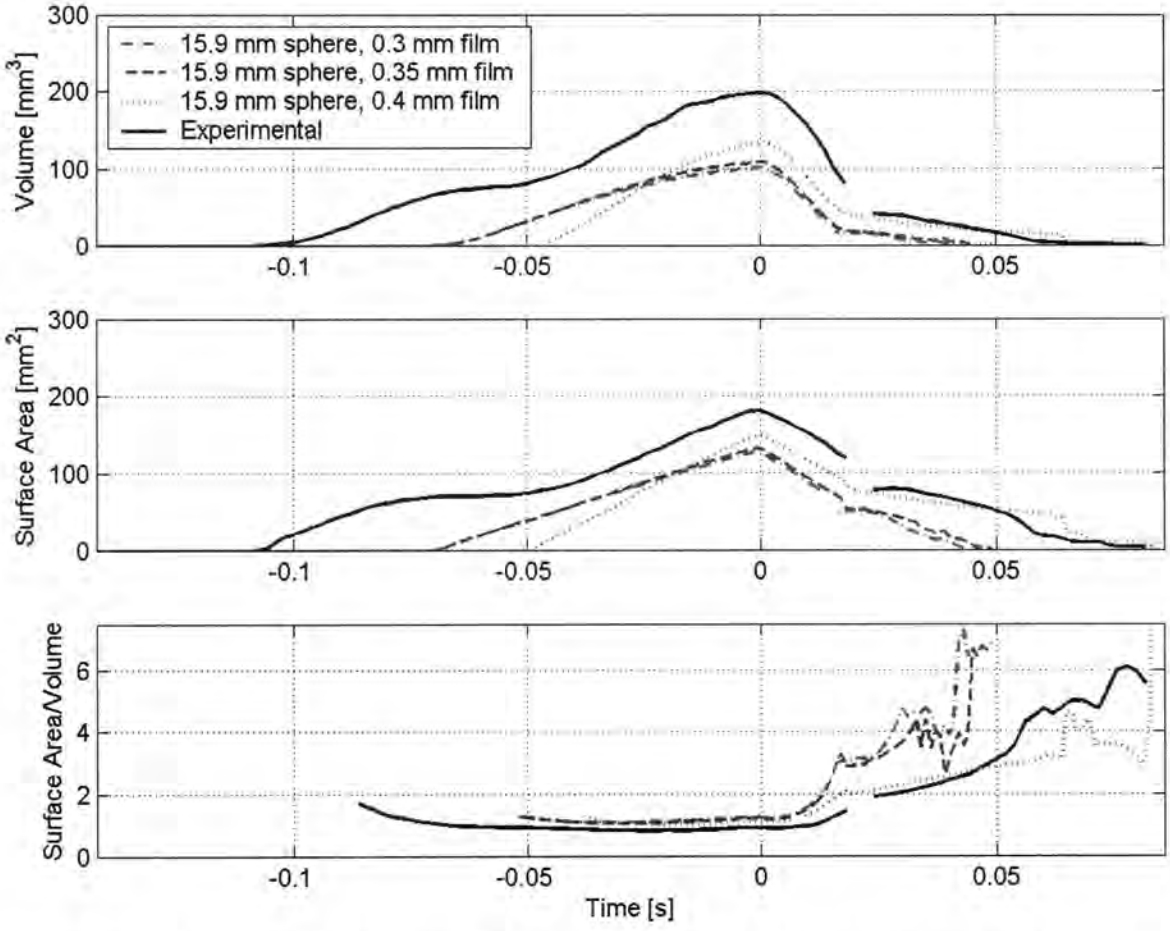

Figure 4.16 Comparison of Results of Analysis of Inter-Tube Liquid Volume and Surface Area for Experimental Work and "Spheres" Model with Three Different Initial Conditions

4.5.4 Horizontal Tubes

For the horizontal tube model in three spatial dimensions, symmetry about two vertical planes was assumed. The planes pass through the centerlines of the tubes and, in a perpendicular direction, through the centerline of the droplet. In this way only ¼ of the droplet and tube had to be included in the solution domain. As in the case of the model for the spheres, the top and bottom boundaries were taken to be translationally periodic, effectively making a column of tubes out of the one in the solution domain. It was desirable to use simple boundary conditions for all of the other boundaries as well to minimize computational expense. At the ends of the tube, periodic boundary conditions were applied. This is the same as having duplicate, synchronized droplets on either side of the main droplet that, upon impact, will have spreading lamellae that perfectly mirror that within the solution domain. Although it is not generally the case that two drops will fall in perfect unison at neighboring

sites, interference wave patterns are frequently observed in practice, so this formulation of the model is in fact derived from and closely represents observed phenomena.

The minimum elemental length in the model is 10×10^{-5} m; however as in the grid used for the spheres, the grid was finer near and between the tubes. The mesh comprises 1,185,870 hexagonal elements. It was created using the Cooper meshing technique where one face is essentially repeated at constant intervals from the "front" to the "back" of the model. The repeated mesh contained 16,590 quadrilaterals and is shown in Figure 4.17. The model was solved on a four-processor parallel computer. The shading in Figure 4.17 corresponds to the partitioning for the parallel solution. The cells in each shade were assigned to an individual processor. Each processor has two neighbors.

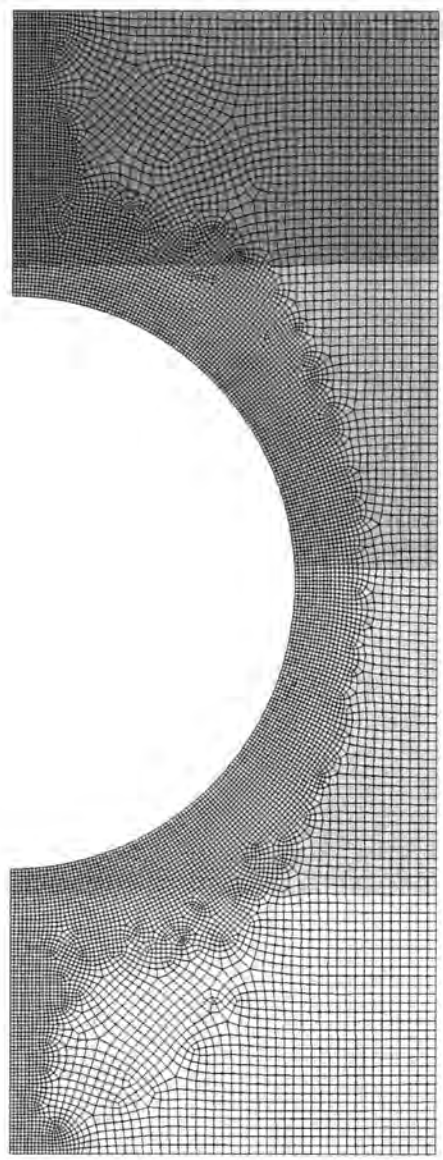

Figure 4.17 Mesh Used for Three-Dimensional Model of Tubes, Shades of Gray Indicate Partitioning for Parallel Computing

As in the case of the spheres, there is no fluid inlet. An initial film was "grown" on the tube by changing the tube to a velocity inlet at the beginning of the simulation. It was not known ahead of time how thick this fluid film needed to be to generate a typical droplet; the only point of reference was that it would need to be somewhat thicker than the spherical case due to the line-convergence of the sagging film discussed previously. In order to establish a droplet on one of the periodic boundary conditions, a sinusoidal film distribution was utilized. One end of the tube received significantly more fluid initially, but the slope of the film thickness at both boundaries was 0. Four periodic repetitions (two sine waves) of this profile can be seen in the upper left frame in Figure 4.18. The initial thickness profile settled upon varied from 0.53 mm at the end where the drop was to form to 0.20 mm at the outer edge. The results of this simulation are summarized in the series of frames in Figure 4.18. In these frames, the model has been reflected to appear as four simultaneous droplets. This aids in the visual interpretation of the interference patterns that arise on the surface of the tube due to the interaction of the spreading lamellae.

Qualitatively, these results are in excellent agreement with the observations made in section 3. All of the critical phenomena identified in the experimental work can be observed in the figures above. This includes contraction of the droplet in the lengthwise direction during early formation, the transition to a more axisymmetric droplet shape as the droplet pulls away from the tube, The formation of a thinning liquid bridge, the extremely high initial propagation speed of the spreading lamella, the impact impulse propagation back up into the liquid bridge, the characteristic saddle wave made by the spreading lamella, the fast recoil of the bridge after bifurcation, the eventual break-up into a number of oscillating satellite droplets, the interaction of the saddle waves, including the stationary wave formed between two such waves, the fast recoil of the material still attached to the tube and the associated excitation of the film, the large axial motion imparted by droplet impact, the large amount of liquid that quickly reaches the underside of the tube subsequent to impact, etc.

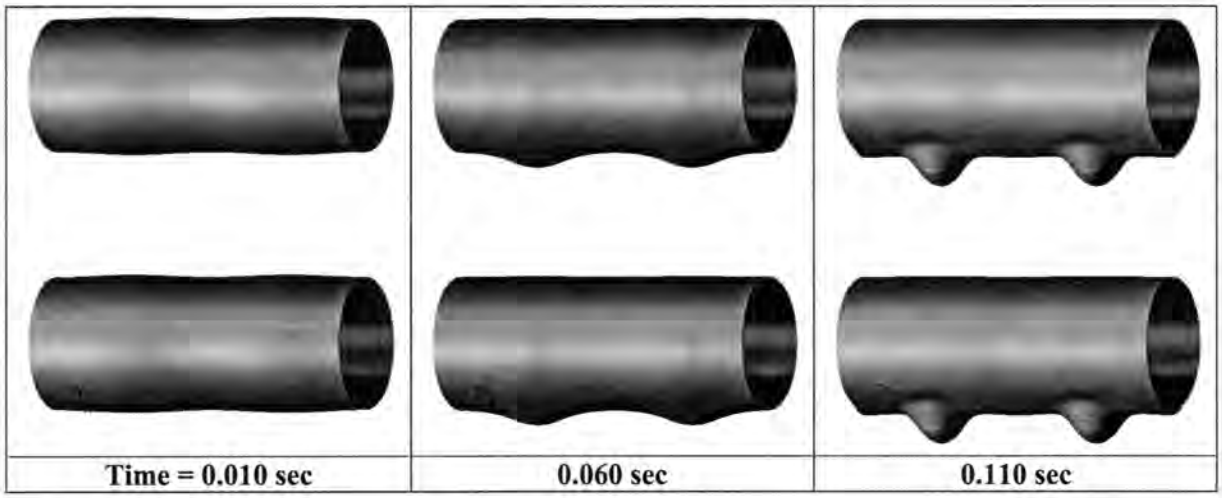

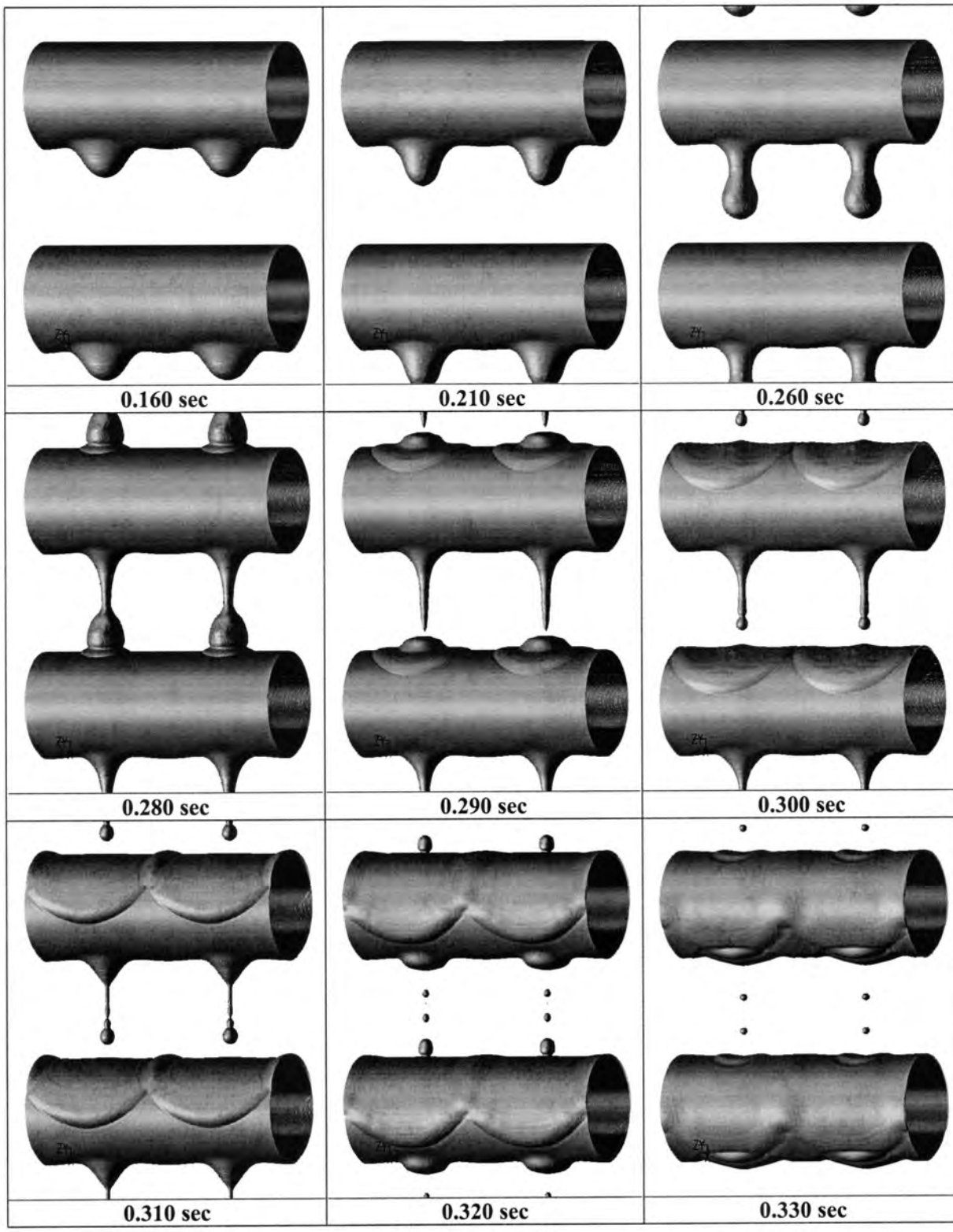

Figure 4.18 3D Simulation of Droplets and Falling Films on Horizontal Tubes

To quantitatively assess the results, the same images as in Figure 4.18, but viewed from the side, were analyzed with IMAN for comparison with the experiment. Figure 4.19 shows the resulting comparison. There are several things that should be noted from this plot. Starting at the left, the simulated 3D drop took considerably longer to reach the 75 mm^3 threshold, but at that point, it was not only in good agreement with the experiment in magnitude, but also in time elapse from this stage until impact. The early formation discrepancy is easy to understand if one recalls that, more often than not, in the experiments, the early stages of the droplet formation are forced along by the arrival of a significant amount of fluid from a droplet impact above (see, for example, the last frame in Figure 4.18). In fact, it is difficult to find in the video any time where a relatively smooth film was allowed to proceed unaffected into a droplet formation site. This accounts for the initially steep curves seen in the experiments since the arrival of extra fluid is a kind of one-time event that gives an initial unsustainable boost in droplet growth rate. Also, the initial conditions in the simulation were somewhat arbitrary and may have had a spurious effect on the timing of this early stage of development.

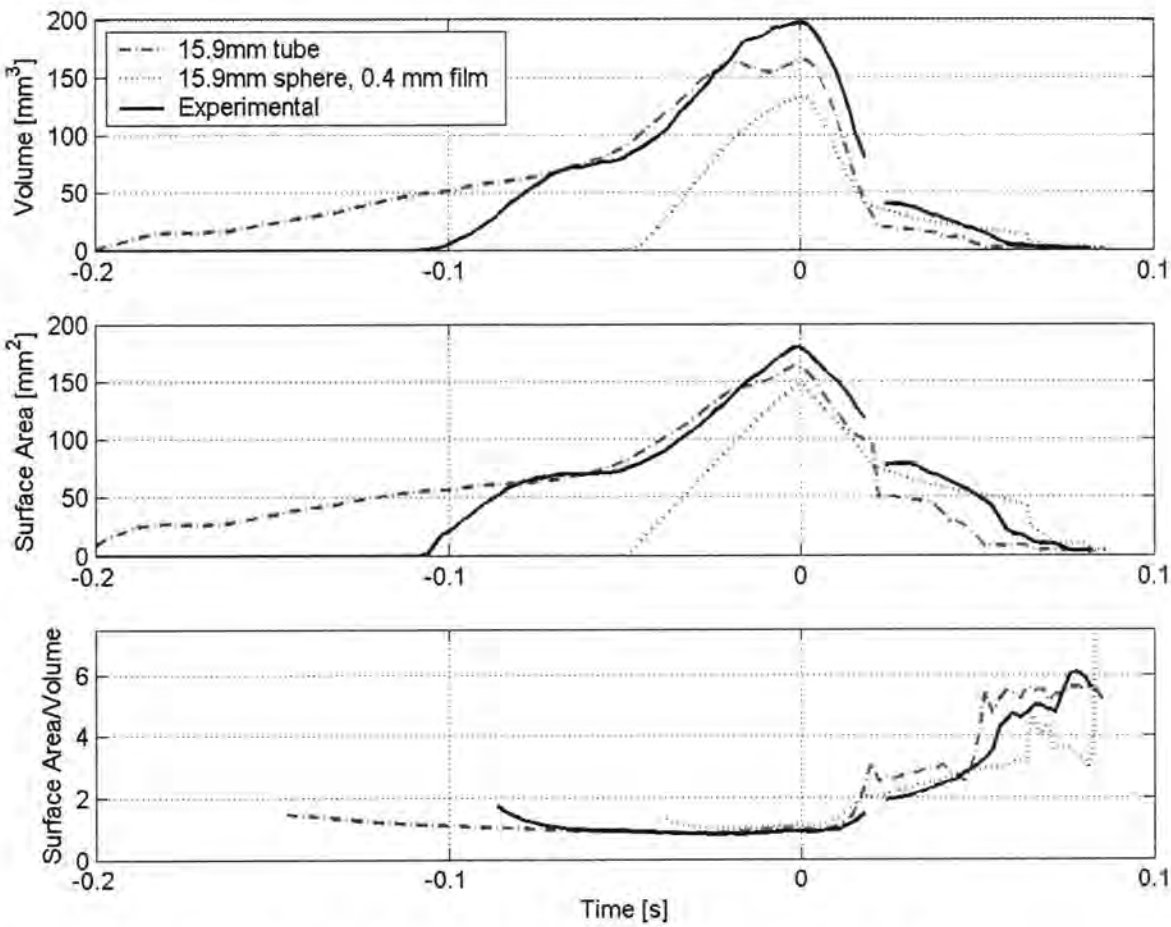

Figure 4.19 Comparison of Experiment and 3-D VOF Model in terms of Inter-Tube Volume and Surface Area

The 3D simulation tracked with the experiments very well from the time they reached approximately 75 mm^3 until just before the impact. It appears (see Fig 4.18) that the droplet ran into a short supply of liquid from the tube above at this critical moment. The images in Figure 4.18 reveal that, indeed, the liquid trail was slightly starved and started to pinch off earlier than in the experiments. It is likely that the initial film thickness was at the lower limit of what was needed to duplicate the experiments. This continues to play out after impact as well, since, in the simulation, the liquid bridge breaks into satellites more quickly than the experimental bridge that persists for a longer period of time. The curves after impact still exhibit the two characteristic slopes: the initial steep drop due to the primary droplet merging into the film around the tube and the later, less steep portion due to the thinning liquid bridge and eventually the satellite droplets. The rather significant offset in the curves (but nearly identical slopes) in this region suggest that the simulated drop might have followed the experimental curves even more closely if the film feeding it could keep up.

4.6 Summary and Conclusions of Computational Work

The stated objective of the computational work was to develop a model that could accurately predict the behavior of droplets and falling films observed in the experimental work. Some success in meeting this was achieved. Agreement with some models and experiments from the literature proved challenging, although plausible explanations for the discrepancies were developed and tested with favorable results. Two "simplified" geometry models were considered for their potential to give insight into the 3D case at a much lower computational expense. The conclusions were that capillary tubes do not provide the flow conditions sought, and for the case of spheres, it was found that the natural convergence of the liquid film to the droplet formation site speeds up the early formation of the droplet considerably. In addition, the axial lengthening of the droplet in the case of horizontal tubes appears to lead to slightly larger droplets and longer development times. The results of the three dimensional model capture most, if not all, of the behavior observed in the experimental work, and also compared well with a quantitative analysis of experimental results. The remaining discrepancies are probably due to differences in the oversimplified initial conditions used in computational work and the actual conditions in the experiments. Also, some modification of the assumed flow-rates/fluid inventories, particularly in the 3D model, might address some of the observed discrepancies.

Grid independence is still very much an open issue in this work. It was proposed at the outset that phenomena with very small length and time scales that can have a profound impact on the overall flow pattern, as is also the case in droplet formation, could prove to be challenging to capture with a grid of finite resolution. Grid independence was investigated using three meshes for the axisymmetric spheres considered in the present work. The most troublesome result of this was that the droplet was predicted to fall fastest through the coarsest grid. The reason for this result remains unknown.

5 CONCLUSIONS

> There will be but few of my readers who have not, in some heavy shower of rain, beguiled the tedium of enforced waiting by watching, perhaps half-unconsciously, the thousand little crystal fountains that start up from the surface of pool or river; noting now and then a surrounding coronet of lesser jets, or here and there a bubble that floats for a moment and then vanishes.
>
> It is to this apparently insignificant transaction, which always has been and always will be so familiar, and to others of a like nature, that I desire to call the attention of those who are interested in natural phenomena; hoping to share with them some of the delight that I have myself felt, in contemplating the exquisite forms that the camera has revealed, and in watching the progress of a multitude of events, compressed indeed within the limits of a few hundredths of a second, but none the less orderly and inevitable, and of which the sequence is in part easy to anticipate and understand, while in part it taxes the highest mathematical powers to elucidate.
>
> WORTHINGTON, 1908 "A Study of Splashes," Chapter 1

In the application of a horizontal-tube falling-film absorber, the "apparently insignificant transactions" of droplet formation, impact and waves play a pivotal role. The objective of this study was to investigate and elucidate the fluid phenomena in falling films over horizontal-tube banks to provide a foundation from which the coupled heat and mass transfer processes may be studied in greater detail.

In the first part of this study, a review of the literature was conducted in three areas: mathematical modeling of falling-film absorption, experimental investigations on the performance of horizontal-tube falling-film absorbers, and the dynamics of droplet formation and impact. It was shown that mathematical models of falling-film absorption have grown increasingly sophisticated from the initial works that assumed laminar, smooth films with uniform velocity. Models that have included the effects of various velocity profiles, variable thermophysical properties, coolant heat transfer conditions, and film waviness were reviewed. In addition, several models specifically developed for the horizontal tube case were reviewed. It was concluded that even the most sophisticated models include significant simplifications in terms of assumed flow patterns. Only in recent efforts has appropriate attention been paid to the role of droplets, but the understanding of droplet behavior in this situation is only rudimentary. Thus, the modeling effort will be advanced through improved understanding of the details of the flow patterns, and in particular, the behavior and role of droplets. The experimental investigations into falling-film absorption on horizontal tubes revealed that, though many parameters such as tube diameter and spacing affect absorption rates, the fundamental mechanism by which they do is not well understood. Furthermore, issues such as inconsistent

definitions for transfer coefficients, low resolution of measured data, and lack of comparable operating conditions and geometric parameters made comparison between the results of different researchers difficult. This lack of commonality meant that conclusions drawn by different investigators were not always consistent. Experimental investigations also pointed to further understanding of film and droplet behavior as key to capturing the effects of the various parameters on performance. A review of droplet formation and impact studies revealed that these are significant topics in recent literature. The work in this area has been bolstered by the growing accessibility to high-performance computers and high-resolution, high-speed cameras. Almost all of this work has considered situations that are axisymmetric such as the formation of droplets from capillaries and jets or the impact of spherical droplets on flat plates. One of the noteworthy conclusions of this, however, was that the dynamics near the point of rupture of a liquid thread are virtually independent of the macroscopic details of the method by which it was formed. The implication of this is that, even in the three dimensional case of interest in the present study, the recent advancements in understanding droplet formation and impact are quite relevant. From this review, the Volume-of-Fluid method was identified as particularly suitable for the current problem because of its ability to handle three dimensions with arbitrary geometry, break-up and coalescence in a straightforward manner.

Flow visualization experiments were conducted on two horizontal-tube banks with water and aqueous LiBr flowing in droplet mode. A high-speed digital video camera was used to capture the evolution of pendant drops, droplet detachment and satellite droplet formation, and droplet impact and film waviness at frame rates of 500 frames per second. Qualitative analysis of the resulting images identified many of the common features and also illustrated differences between the current case and the axisymmetric cases considered in the literature. In the case of horizontal tubes, the early stages of droplet formation were marked by significant elongation of the droplet formation site in the direction of the axis of the tubes. The spreading lamella formed upon impact created a characteristic saddle wave containing significant circumferential and axial velocity components. The oscillatory nature of satellite droplets and the complexities that arise when droplets interact during formation and impact were also illustrated.

Using a combination of digital image processing techniques and the mathematics of splines, a program was developed to facilitate the expedient and accurate quantitative analysis of the flow visualization results. A semi-automated interface detection algorithm that utilized an initial input of interface location from the user was used to develop mathematical representations of the shape and location of the liquid-vapor interface throughout a sequence of video frames. This allowed the estimation of droplet volume and surface area within the space between the tubes. The image analysis program was validated with simple images of known volumes generated from the computational results and was shown to be very accurate. The quantitative analysis of the droplet formation process was used to compute the progression of volume and surface area versus time. Both the volume and surface area steadily rose to maximum values at the moment of impact, after which

steep declines in both occurred as the primary droplet joined the film around the tube. After the initial steep decline, a period of slower decay of the thinning liquid bridges was shown to be a period when the surface area to volume ratio increased significantly. Increasing surface area versus fluid volume generally increases the absorption rate, thus these results suggest that satellite droplets and the trailing liquid bridge may perform a proportionally large amount of absorption.

Computational models utilizing the VOF method were developed and validated with the literature for the case of water droplets forming from an axisymmetric capillary tube into air. Exact agreement with the literature was not achieved, but some plausible reasons for the discrepancies were proposed. The validation case was extended to a larger capillary tube above a flat plate for the case of aqueous LiBr. The results showed some of the characteristics of the spreading lamella during droplet impact and the thinning liquid bridge, but it was clearly evident that the large capillary tube was a poor approximation of the horizontal tube case. An intermediary 2D model of a column of spheres, the same diameter as the horizontal tubes, was then developed. The results reveal the interesting change in dynamics as the liquid inventory changes. The liquid thread trailing the droplet could break at impact or persist as a thinning liquid bridge depending on the initial amount of liquid on the spheres. Applying the same image analysis techniques developed in the experimental work to the computational results, it was shown that droplet development in the case of spheres proceeds significantly more rapidly than in the horizontal tube case, especially with large liquid inventories, that the droplet and thread volume was significantly smaller in the case of spheres, and that, except for the case of maximum liquid inventory, the droplet trail break-up generally proceeded more quickly than in the horizontal tube case as well. In addition, grid independence tests were done with the sphere models. The results showed that a coarse and medium sized mesh agreed reasonably well with each other, but the results were not convergent toward the results with the finest grid. The effects of grid size manifested themselves primarily in the speed of the droplet fall (faster for coarser grids) and the break up of the liquid thread, which was qualitatively different in each case.

Finally, a fully three dimensional model of droplet formation under a horizontal tube was developed. The results revealed good qualitative agreement with the experimental results, exhibiting many of the characteristic features, including the elongation of the drop during early formation and the saddle wave upon impact. Some differences could be observed in the predicted break-up of the liquid bridge. Quantitative analysis revealed that the 3D model agreed well with the experimental results after an initially slow development period. It was suggested that the slow early development was due to the unrealistic initial conditions of a quiescent, uniform film used in the computations versus the experimental case where early droplet formation is often driven by the arrival of liquid from a preceding droplet impact event. The droplet volume and surface area predictions by the 3D model also agreed with the experimental results better than the spherical case, although the model slightly under-predicted the experimental results. It is thought that a slightly low initial liquid inventory in the model was the reason for this discrepancy.

The current study has laid a solid foundation for developing a more thorough understanding of heat and mass transfer in falling-film absorption in horizontal-tube banks. There is some assurance now that the important fluid flow phenomena have been identified and that the computational techniques developed here are able, with a fair to good measure of accuracy, to predict these fluid flow patterns. This allows the coupled heat and mass transfer problem to be revisited under much more realistic conditions. The computational models developed provide a framework in which heat and mass transfer may be modeled simultaneously without neglecting significant fluid flow dynamics. In addition, these results suggest the possibility of including the two-way influence between absorption heat and mass transfer and the fluid dynamics problem through the inclusion of thermophysical property variations and surfactant models. Validation of the results of these predictions will require a level of resolution in experimental data that is not currently available in the literature. Of paramount importance will be the measurement of local, droplet and tube-level transfer rates that can be used to validate models of single droplets on a section of tube. More systematic parametric studies are required to capture the effect of tube geometry and thermophysical properties at the level of detail just described. With a validated droplet-level model, the complex interaction of operating conditions, absorber geometry and fluid properties could be investigated. In addition, accurate component-level models that would capture the effects that current models are unable to capture could be developed. The result of these improved design tools would be optimized absorber designs and, in turn, much more marketable absorption heat pump technology, ultimately resulting in a positive impact on the global environment.

REFERENCES

Al-Durrah, M. M. and J. M. Bradford (1982), "Mechanism of Raindrop Splash on Soil Surfaces," *Soil Science Society of America Journal* Vol. 46(5) pp. 1086-1090.

Ambravaneswaran, B., S. D. Phillips and O. A. Basaran (2000), "Theoretical Analysis of a Dripping Faucet," *Physical Review Letters* Vol. 85(25) pp. 5332-5335.

Ambravaneswaran, B., E. D. Wilkes and O. A. Basaran (2002). *Drop Formation from a Capillary Tube: Comparison of One-Dimensional and Two-Dimensional Analyses and Occurrence of Satellite Drops*. Physics of Fluids, American Institute of Physics Inc., Vol. 14 pp. 2606-2621.

American Society of Heating Refrigeration and Air-Conditioning Engineers Inc. (1997). *Ashrae Handbook, Fundamentals*. Atlanta, GA., American Society of Heating, Refrigeration, and Air-Conditioning Engineers, Inc.

Andberg, J. W. (1986). *Absorption of Vapors into Liquid Films Falling over Cooled Horizontal Tubes*. Austin, University of Texas.

Andberg, J. W. and G. C. Vliet (1983), "Nonisothermal Absorption of Gases into Falling Liquid Films," *ASME-JSME Thermal Engineering Joint Conference Proceedings* Vol. 2 pp. 423-431.

Andberg, J. W. and G. C. Vliet (1987a), "Absorption of Vapors into Liquid Films Flowing over Cooled Horizontal Tubes," *Second ASME-JSME Thermal Engineering Joint Conference*, Honolulu, Hawaii, pp. 533-541.

Andberg, J. W. and G. C. Vliet (1987b), "A Simplified Model for Absorption of Vapors into Liquid Films Flowing over Cooled Horizontal Tubes," *ASHRAE Transactions* Vol. 93(2) pp. 2454-2463.

Aris, R. (1962). *Vectors, Tensors, and the Basic Equations of Fluid Mechanics*. Englewood Cliffs, N.J., Dover 1989 (Prentice-Hall).

Armbruster, R. and J. Mitrovic (1994), "Pattens of Falling Film Flow over Horizontal Smooth Tubes," *Proceedings of the Xth International Heat Transfer Conference*, pp. 275-280.

Armbruster, R. and J. Mitrovic (1998), "Evaporative Cooling of a Falling Water Film on Horizontal Tubes," *Experimental Thermal and Fluid Science* Vol. 18(3) pp. 183-194.

ASHRAE (1997). *1997 Ashrae Handbook - Fundamentals*, American Society of Heating, Refrigerating and Air-Conditioning Engineers, Inc.

Atchley, J. A., H. Perez-Blanco, M. J. Kirby and W. A. Miller (1998), "An Experimental and Analytical Study of Advanced Surfaces for Absorption Chiller Absorbers," *Gas Research Institute Report GRI.*

Benjamin, T. B. (1957), "Wave Formation in Laminar Flow Down an Inclined Plane," *Journal of Fluid Mechanics* Vol. 2 pp. 554-574.

Besl, P. J. (1988). *Surfaces in Range Image Understanding*. New York, Springer-Verlag.

Beutler, A., I. Greiter, A. Wagner, L. Hoffman, S. Schreier and G. Alefeld (1996a), "Surfactants and Fluid Properties," *International Journal of Refrigeration* Vol. 19(5) pp. 342-346.

Beutler, A., L. Hoffman, F. Ziegler, G. Alefeld, K. Gommed, G. Grossman and A. Shavit (1996b), "Experimental Investigation of Heat and Mass Transfer in Film Absorption on Horizontal and Vertical Tubes," *Ab-Sorption 96, International Ab-sorption Heat Pump Conference*, Montreal, Quebec, Canada, pp. 409-419.

Beutler, A., F. Ziegler and G. Alefeld (1996c), "Falling Film Absorption with Solutions of a Hydroxide Mixture," *Ab-Sorption 96, International Ab-sorption Heat Pump Conference*, Montreal, Quebec, Canada, pp. 303-309.

Bird, R. B., W. E. Stewart and E. N. Lightfoot (1960). *Transport Phenomena*. Wiley, New York.

Bird, R. B., W. E. Stewart and E. N. Lightfoot (2002). *Transport Phenomena*. 2nd Ed. New York, J. Wiley.

Blake, J. R., J. M. Boulton-Stone and R. P. Tong (1995). Boundary Integral Methods for Rising, Bursting and Collapsing Bubbles. *Boundary Element Applications in Fluid Mechanics*. H. Power, Computational Mechanics Publications, WIT Press p. 31/376.

Blanchard, D. C. and A. H. Woodcock (1957), "Bubble Formation and Modification in the Sea and Its Meteorological Significance," *Tellus* Vol. 9(2) pp. 145-158.

Bogy, D. B. (1979), "Drop Formation in a Circular Liquid Jet," *Annual Review of Fluid Mechanics* Vol. 11 pp. 207-228.

Boulton-Stone, J. M. (1993), "Comparison of Boundary Integral Methods for Studying the Motion of a Two-Dimensional Bubble in an Infinite Fluid," *Computer Methods in Applied Mechanics and Engineering* Vol. 102(2) pp. 213-234.

Brackbill, J. U. and D. B. Kothe (1996), "Dynamical Modeling of Surface Tension," *Proceedings of the 1996 3rd Microgravity Fluid Physics Conference,Jul 13-15 1996*, Cleveland,OH,USA, NASA,Cleveland,OH,USA, pp. 693-698.

Brackbill, J. U., D. B. Kothe and C. Zemach (1992), "A Continuum Method for Modeling Surface Tension," *Journal of Computational Physics* Vol. 100(2) pp. 335-354.

Brauner, N. (1989), "Modelling of Wavy Flow in Turbulent Free Falling Films," *Int. J. Multiphase Flow* Vol. 15(4) pp. 505-520.

Brauner, N. (1991), "Non-Isothermal Vapour Absorption into Falling Film," *International Journal of Heat and Mass Transfer* Vol. 34(3) pp. 767-784.

Brauner, N., A. Dukler and D. Moalem Maron (1985), "Interfacial Structure of Thin Falling Films: Piecewise Modelling of the Waves," *Physico-Chemical Hydrodynamics* Vol. 6 pp. 87-113.

Brauner, N. and D. Moalem Maron (1982), "Characteristics of Inclined Thin Films, Waviness and the Associated Mass Transfer," *International Journal of Heat and Mass Transfer* Vol. 25(1) pp. 99-110.

Brauner, N. and D. Moalem Maron (1983), "Modeling Wavy Flow in Inclined Thin Films," *Chemical Engineering Science* Vol. 38(5) pp. 775-788.

Brauner, N., D. Moalem Maron and H. Meyerson (1988), "The Effect of Absorbate Concentration Level in Hygroscopic Condensation," *International Communications Heat and Mass Transfer* Vol. 15(3) pp. 269-279.

Brauner, N., D. Moalem Maron and H. Meyerson (1989), "Coupled Heat Condensation and Mass Absorption with Comparable Concentrations of Absorbate and Absorbent," *International Journal of Heat and Mass Transfer* Vol. 32(10) pp. 1897-1906.

Brenner, M. P., J. Eggers, K. Joseph, S. R. Nagel and X. D. Shi (1997), "Breakdown of Scaling in Droplet Fission at High Reynolds Number," *Physics of Fluids* Vol. 9(6) p. 1573.

Burdukov, A. P., N. S. Bufetov, N. P. Deriy, A. R. Dorokhov and V. I. Kazakov (1980), "Experimental Study of the Absorption of Water Vapor by Thin Films of Aqueous Lithium Bromide," *Heat Transfer Soviet Research* Vol. 12(3) pp. 118-123.

Burdukov, A. P., N. S. Bufetov and A. R. \Dorokov (1979), "Absorption on a Falling Liquid Film," *Izv. Sib. Otd. Akad. Nuak SSSR, seriya tekhn. Nauk* Vol. 13(3) pp. 48-52.

Canny, J. (1986), "A Computational Approach to Edge Detection," *IEEE Transactions on Pattern Analysis and Machine Intelligence* Vol. PAMI-8(6) pp. 679-698.

Carey, V. P. (1992). *Liquid-Vapor Phase-Change Phenomena : An Introduction to the Thermophysics of Vaporization and Condensation Processes in Heat Transfer Equipment*. Washington, D.C., Taylor & Francis Series, Hemisphere Pub. Corp.

Cavallini, A., L. Doretti, E. Fornasieri and C. Zilio (2001), "Heat and Mass Transfer and Flow Patterns During Absorption of Steam in LiBr + Water Falling Film," *IIF-IIR - Commission B1*, Paderborn, Germany

Cazabat, A. M. and M. A. Cohen Stuart (1987), "Some Experiments on Wetting Dynamics," *PCH, PhysicoChemical Hydrodynamics, 6th Int Conf, Dedicated to the Memory of Veniamin Levich, Apr 6-8 1987*, Oxford, Engl, pp. 23-31.

Chapman, D. S. and P. R. Chritchlow (1967), "Formation of Vortex Rings from Falling Drops," *Journal of Fluid Mechanics* Vol. 29 pp. 177-185.

Chen, L., S. V. Garimella, J. A. Reizes and E. Leonardi (1997), "Motion of Interacting Gas Bubbles in a Viscous Liquid Including Wall Effects and Evaporation," *Numerical Heat Transfer; Part A: Applications* Vol. 31(6) pp. 629-654.

Chen, M. M. (1961), "An Analytical Study of Laminar Film Condensation: Part 2 - Single and Multiple Horizontal Tubes," *Journal of Heat Transfer* Vol. 83 p. 55.

Ching, B., M. W. Golay and T. J. Johnson (1984), "Droplet Impacts Upon Liquid Surfaces," *Science* Vol. 226(4674) pp. 535-537.

Choudhury, S. K., A. Nishiguchi, D. Hisajima, T. Fukushima, T. Ohuchi and S. Sakaguchi (1993), "Absorption of Vapors into Liquid Films Flowing over Cooled Horizontal Tubes," *Proceedings of the 1993 Annual Meeting of the American Society of Heating, Refrigerating and Air-Conditioning Engineers, Inc.,Jun 27-30 1993*, Denver,CO,USA, Publ by ASHRAE,Atlanta,GA,USA, pp. 81-89.

Clift, R., J. R. Grace and M. E. Weber (1978). *Bubbles, Drops, and Particles*. New York, Academic Press.

Cohen, E., R. F. Riesenfeld and G. Elber (2001). *Geometric Modeling with Splines: An Introduction*. Natick, Mass., AK Peters.

Conlisk, A. T. (1992), "Falling Film Absorption on a Cylindrical Tube," *AIChE Journal* Vol. 38(11) pp. 1716-1728.

Conlisk, A. T. (1993), "The Use of Boundary Layer Techniques in Absorber Design," *ASME Proceedings of the International Absorption Heat Pump Conference*, pp. 163-170.

Conlisk, A. T. (1994a), "Semi-Analytical Design of a Falling Film Absorber," *Journal of Heat Transfer* Vol. 91 pp. 391-396.

Conlisk, A. T. (1994b), "Structure of Falling Film Heat and Mass Transfer on a Fluted Tube," *AIChE Journal* Vol. 40(5) pp. 756-766.

Conlisk, A. T. (1995a), "Analytical Solutions for the Heat and Mass Transfer in a Falling Film Absorber," *Chemical Engineering Science* Vol. 50(4) pp. 651-660.

Conlisk, A. T. (1995b), "The Effect of Coolant Flow Parameters on the Performance of an Absorber," *ASHRAE Transactions* Vol. 101(2) pp. 73-80.

Conlisk, A. T. (1996a), "A Model for the Prediction of the Performance of a Splined-Tube Absorber - Part 2: Model and Results," *ASHRAE Transactions* Vol. 102(1) pp. 128-137.

Conlisk, A. T. (1996b), "Prediction of the Performance of a Splined-Tube Absorber - Part 1: Governing Equations and Dimensional Analysis," *ASHRAE Transactions* Vol. 102(1) pp. 116-127.

Conlisk, A. T. and J. Mao (1996), "Nonisothermal Absorption on a Horizontal Cylindrical Tube - 1. The Film Flow," *Chemical Engineering Science* Vol. 51(8) pp. 1275-1285.

Cosenza, F. and G. C. Vliet (1990), "Absorption in Falling Water/LiBr Films on Horizontal Tubes," *ASHRAE Transactions* Vol. 96(1).

Cosenza, F. B. (1989). *Experimental Study of Absorption in Falling Aqueous Lithium Bromide Films on Horizontal Tubes*. Department of Mechanical Engineering. Austin, University of Texas p. 93.

Cossali, G. E., A. Coghe and M. Marengo (1997), "The Impact of a Single Drop on a Wetted Solid Surface," *Experiments in Fluids* Vol. 22(6) pp. 463-472.

Cram, L. E. (1983), "A Numerical Model of Droplet Formation," *1983 Conference on Computational Techniques and Applications (CTAC-83)*, University of Sydney, Australia, Elsevier Science, pp. 182-188.

de Boor, C. (1978). *A Practical Guide to Splines*. New York, Springer-Verlag.

Delancey, G. B. and S. H. Chiang (1968), "Dufour Effect in Liquid Systems," *AIChE Journal* Vol. 14(4) pp. 664-665.

Dickson, A. N. and A. J. Addlesee (1984). *Liquid Aerosol Filter with Mechanical Removal of the Collected Liquid*, Vol. 21 pp. 189-190.

Dooley, B. S., A. E. Warncke, M. Gharib and G. Tryggvason (1997), "Vortex Ring Generation Due to the Coalescence of a Water Drop at a Free Surface," *Experiments in Fluids* Vol. 22(5) pp. 369-374.

Douglas, P. L. and S. Ilias (1987), "On the Deposition of Aerosols on Cylinders in Turbulent Cross Flow," *Particulate and Multiphase Processes. Volume 2: Contamination Analysis and Control.*, Miami Beach, FL, USA, Hemisphere Publ Corp, Washington, DC, USA, pp. 181-194.

Durst, F. (1996), "Penetration Length and Diameter Development of Vortex Rings Generated by Impacting Water Drops," *Experiments in Fluids* Vol. 21(2) pp. 110-117.

Dussan V., E. B. (1979), "On the Spreading of Liquids on Solid Surfaces: Static and Dynamic Contact Lines," *Annual Review of Fluid Mechanics* Vol. 11 pp. 371-400.

Edgerton, H. E. (1937). *Milk Drop Coronet*. Cambridge, MA, http://web.mit.edu/museum/exhibits/flashes5.html (date retrieved: June 16, 2003).

Edgerton, H. E., E. A. Hauser and W. B. Tucker (1937), "Studies in Drop Formation as Revealed by the High-Speed Motion Camera," *Journal of Physical Chemistry* Vol. 41 pp. 1017-1028.

Eggers, J. (1993), "Universal Pinching of 3d Axisymmetric Free-Surface Flow," *Physical Review Letters* Vol. 71 p. 3458.

Eggers, J. (1995), "Theory of Drop Formation," *Physics of Fluids* Vol. 7(5) p. 941.

Eggers, J. (1997), "Nonlinear Dynamics and Breakup of Free-Surface Flows," *Reviews of Modern Physics* Vol. 69(3) pp. 865-929.

Eggers, J. and T. F. Dupont (1994), "Drop Formation in a One-Dimensional Approximation for the Navier-Stokes Equation," *Journal of Fluid Mechanics* Vol. 262 pp. 205-221.

Emmert, R. E. and R. L. Pigford (1954), *Chemical Engineering Progress* Vol. 50 p. 87.

Enderby, J. E. (1983), "Neutron Scattering from Ionic Solutions," *Annual Reviews of Physical Chemistry* Vol. 34 pp. 155-185.

Engel, O. G. (1955), "Waterdrop Collisions with Solid Surfaces," *Journal of Research of the National Bureau of Standards* Vol. 54(5) pp. 281-298.

Esmailizadeh, L. and R. Mesler (1986), "Bubble Entrainment with Drops," *Journal of Colloid and Interface Science* Vol. 110(2) pp. 561-574.

Fagerquist, R. (1996), "Jet, Wave, and Droplet Velocities for a Continuous Fluid Jet," *Journal of Imaging Science and Technology* Vol. 40(5) pp. 405-411.

Field, J. E. and I. M. Hutchings (1984), "Impact Erosion Processes," *Mechanical Properties at High Rates of Strain, 1984, Proceedings of the Third Conference*, Oxford, Engl, Inst of Physics, Bristol, Engl, pp. 349-371.

Fluent Inc. (2003). *Fluent*. Lebanon, NH.

Frohn, A. and N. Roth (2000). *Dynamics of Droplets*. New York, Springer.

Fujii, T. (1992), "Overlooked Factors and Unsolved Problems in Experimental Research on Condensation Heat Trasfer," *Experimental Thermal and Fluid Science* Vol. 5(5) pp. 652-663.

Fujita, I. and E. Hihara (1999), "Surface Tension-Driven Instability of Thin Liquid Film of LiBr Aqueous Solution Absorbing Water Vapor," *Proceedings of the International Sorption Heat Pump Conference*, Munich, Germany, pp. 367-373.

Fujita, T. (1993), "Falling Liquid Films in Absorption Machines," *International Journal of Refrigeration* Vol. 16(4) pp. 282-294.

Fukai, J., Y. Shiiba, T. Yamamoto, O. Miyatake, D. Poulikakos, C. M. Megaridis and Z. Zhao (1995), "Wetting Effects on the Spreading of a Liquid Droplet Colliding with a Flat Surface. Experiment and Modeling," *Physics of Fluids* Vol. 7(2) p. 236.

Fukai, J., Z. Zhao, D. Poulikakos, C. M. Megaridis and O. Miyatake (1993), "Modeling of the Deformation of a Liquid Droplet Impinging Upon a Flat Surface," *Physics of Fluids A Fluid Dynamics* Vol. 5(11) p. 2588.

Fulford, G. D. (1964), "The Flow of Liquids in Thin Films," *Adv. Chemical Engineering* Vol. 5 p. 151.

Gander, W. and W. Gautschi (2000). Adaptive Quadrature - Revisited. BIT, Vol. 40, 2000, pp. 84-101. This document is also available at http:// www.inf.ethz.ch/personal/ganderp.

Gommed, K., G. Grossman and M. Koenig (1999), "Numerical Model of Ammonia-Water Absorption inside a Vertical Tube," *Proceedings of the International Sorption Heat Pump Conference*, Munich, Germany, pp. 275-281.

Greiter, I., A. Wagner, V. Weiss and G. Alefeld (1993), "Experimental Investigation of Heat and Mass Transfer in a Horizontal-Tube Falling-Film Absorber with Aqueous Solutions," *International Absorption Heat Pump Conference*, New Orleans, Louisiana, The Advanced Energy Systems Division, ASME, pp. 225-232.

Grigoryeva, N. I. and V. E. Nakoryakov (1977), "Exact Solution of Combined Heat and Mass Transfer Problems During Film Absorption," *Journal of Engineering Physics* Vol. 33(5) pp. 1349-1353.

Groshart, E. (1985), "Thermal Sprayed Coatings," *Metal Finishing* Vol. 83(12) pp. 49-55.

Grossman, G. (1982), "Simultaneous Heat and Mass Transfer in Absorption/Desorption of Gases in Laminar Liquid Films," *AIChE Winter Annual Meeting*, Orlando, Florida

Grossman, G. (1983), "Simultaneous Heat and Mass Transfer in Film Absorption under Laminar Flow," *Int. J. Heat and Mass Transfer* Vol. 26(3) pp. 357-371.

Grossman, G. (1986). Heat and Mass Transfer in Film Absorption. *Handbook of Heat and Mass Transfer, Chapter 6*. Houston, Gulf Publishing, Vol. 2 pp. 211-257.

Grossman, G. (1987), "Analysis of Interdiffusion in Film Absorption," *International Journal of Heat and Mass Transfer* Vol. 30(1) pp. 205-208.

Grossman, G. and G. Alefeld (1996). Investigation of Heat and Mass Transfer in Absorption Heat Pumps. Technion - Israel Institute of Technology and TUM - Technische Universität München, Final GIF Report, GIF Contract No. I-0187-100.10/91, 103 p.

Grossman, G. and K. Gommed (1997), "Heat and Mass Transfer in Film Absorption in the Presence of Non-Absorbable Gases," *International Journal of Heat and Mass Transfer* Vol. 40(15) pp. 3595-3606.

Gueyffier, D. (2000). *Doctoral Dissertation: Etude De L'impact De Gouttes Sur Un Film Liquide Mince. Développement De La Corrolle Et Formation De Projections (in French)*. Mécanique. Paris 6, Université Pierre et Marie Curie p. 177.

Gueyffier, D., J. Li, A. Nadim, R. Scardovelli and S. Zaleski (1999), "Volume-of-Fluid Interface Tracking with Smoothed Surface Stress Methods for Three-Dimensional Flows," *Journal of Computational Physics* Vol. 152(2) pp. 423-456.

Haar, L., J. S. Gallagher, G. S. Kell and National Standard Reference Data System (U.S.) (1984). *Nbs/Nrc Steam Tables : Thermodynamic and Transport Properties and Computer Programs for Vapor and Liquid States of Water in Si Units*. Washington, D.C., Hemisphere Pub. Corp.

Habib, H. M. and B. D. Wood (1990), "Simultaneous Heat and Mass Transfer for a Falling Film Absorber - the Two Phase Flow Problem," *Solar Energy Engineering, Proceedings of the 12th Annual International Solar Energy Conference, ASME*, pp. 61-67.

Hajji, A. and Z. Lavan (1990), "Effect of Film Depth and Interfacial Convection on Transient Heat and Mass Transfer in Film Absorption," *International Heat Transfer Conference*, Hemisphere Publishing Corp., pp. 347-352.

Hajji, A. and W. M. Worek (1992), "Transient Heat and Mass Transfer in Film Absorption of Finite Depth with Nonhomogeneous Boundary Conditions," *International Journal of Heat and Mass Transfer* Vol. 35(9) pp. 2101-2108.

Harvie, D. J. E. and D. F. Fletcher (2001), "A New Volume of Fluid Advection Algorithm: The Defined Donating Region Scheme," *International Journal for Numerical Methods in Fluids* Vol. 35(2) pp. 151-172.

Hauser, E. A., H. E. Edgerton, B. M. Holt and J. T. Cox, Jr. (1936), "The Applicationof the High-Speed Motion Picture Camera to Research on the Surface Tension of Liquids," *Journal of Physical Chemistry* Vol. 40 p. 973.

Healy, W. M., J. G. Hartley and S. I. Abdel-Khalik (2001), "On the Validity of the Adiabatic Spreading Assumption in Droplet Impact Cooling," *International Journal of Heat and Mass Transfer* Vol. 44(20) pp. 3869-3881.

Heertjes, P. M., L. H. de Nie and H. J. de Vries (1971), "Drop Formation in Liquid-Liquid Systems - I Prediction of Drop Volumes at Moderate Speed of Formation," *Chemical Engineering Science* Vol. 26 pp. 441-449.

Herold, K. E., R. Radermacher and S. A. Klein (1996). *Absorption Chillers and Heat Pumps*. Boca Raton, CRC Press LLC.

Hihara, E. and T. Saito (1993), "Effect of Surfactan on Falling Film Absorption," *International Journal of Refrigeration* Vol. 16(5) pp. 339-345.

Hobbs, P. V. and Osheroff (1967), "Splashing of Drops on Shallow Liquids," *Science* Vol. 158(3805) pp. 1184-1186.

Hoffman, L., I. Greiter, A. Wagner, V. Weiss and G. Alefeld (1996), "Experimental Investigation of Heat Transfer in a Horizontal Tube Falling Film Absorber with Aqueous Solutions of LiBr with and without Surfactants," *International Journal of Refrigeration* Vol. 19(5) pp. 331-341.

Hozawa, M., M. Inoue, J. Sato and T. Tsukuda (1991), "Marangoni Convection During Steam Absorption into Aqueous LiBr Solution with Surfactant," *Journal of Chemical Engineering, Japan* Vol. 24(2) pp. 209-214.

Hsiao, M., S. Lichter and L. G. Quintero (1988), "The Critical Weber Number for Vortex and Jet Formation for Drops Impinging on a Liquid Pool," *Physics of Fluids* Vol. 31(12) pp. 3560-3562.

Hu, X. and A. M. Jacobi (1996a), "The Intertube Falling Film: Part 1 - Flow Characteristics, Mode Transitions, and Hysteresis," *Journal of Heat Transfer* Vol. 118(3) pp. 616-625.

Hu, X. and A. M. Jacobi (1996b), "The Intertube Falling Film: Part 2 - Mode Effects on Sensible Heat Transfer to a Falling Liquid Film," *Journal of Heat Transfer* Vol. 118(3) pp. 626-633.

Hu, X. and A. M. Jacobi (1998), "Departure-Site Spacing for Liquid Droplets and Jets Falling between Horizontal Circular Tubes," *Experimental Thermal and Fluid Science* Vol. 16(4) pp. 322-331.

Huang, C.-H. and C.-J. Tsai (2003), "Mechanism of Particle Impaction and Filtration by the Dry Porous Metal Substrates of an Inertial Impactor," *Aerosol Science and Technology* Vol. 37(6) pp. 486-493.

Hyman, J. M. (1983), "Numerical Methods for Tracking Interfaces," *Physica D: Nonlinear Phenomena* Vol. 12D(1-3) pp. 396-407 (also in Fronts, Interfaces and Patterns, Proc of the 393rd Annu Int Conf of the Cent for Nonlinear Stud, May 392-396 1983).

Ibrahim, G. A. and G. A. Vinnicombe (1993), "A Hybrid Method to Analyse the Performance of Falling Film Absorbers," *International Journal of Heat and Mass Transfer* Vol. 36(5) pp. 1383-1390.

Incropera, F. P. and D. P. DeWitt (1990). *Fundamentals of Heat and Mass Transfer*. 3rd Ed. New York, John Wiley & Sons.

Inoue, N., Y. Nagaoka, N. Nishiyama and H. Yabase (1986a), "Absorber of Absorption Refrigeration Machine, 1st Report," *20th Japan Joint Conference on Air-Conditioning and Refrigeration (in Japanese)*, pp. 1-4.

Inoue, N., Y. Nagaoka, N. Nishiyama and H. Yabase (1986b), "Absorber of Absorption Refrigeration Machine, 2nd Report," *SHASE (Society of Heating, Air-Conditioning and Sanitary Engineering Japan) Annual Meeting (in Japanese)*, pp. 141-144.

Inoue, N., Y. Nagaoka, N. Nishiyama and H. Yabase (1987), "Absorber of Absorption Refrigeration Machine, 3rd Report," *21st Japan Joint Conference on Air-Conditioning and Refrigeration (in Japanese)*, pp. 85-88.

Islam, M. R., N. E. Wijeysundera and J. C. Ho (2003), "Simplified Models for Coupled Heat and Mass Transfer in Falling-Film Absorbers," *International Journal of Heat and Mass Transfer* Vol. Forthcoming.

Isshiki, N. and K. Ogawa (1996), "Enhancement of Heat and Mass Transfer by Ccs Tubes," *Ab-Sorption 96, International Ab-sorption Heat Pump Conference*, Montreal, Quebec, Canada, pp. 335-341.

Jalalzadeh-Azar, A. A. (2003), "Quantifying Potential of Integrated Energy Systems with a Varying Level of Nationwide Deployment," *International Mechanical Engineering Conference and Exposition*, Washington, D.C., November 15-21, ASME

Jayanti, S. and G. F. Hewitt (1997), "Hydrodynamics and Heat Transfer of Wavy Thin Film Flow," *International Journal of Heat and Mass Transfer* Vol. 40(1) pp. 179-190.

Jeong, S. and S. Garimella (2002), "Falling-Film and Droplet Mode Heat and Mass Transfer in a Horizontal Tube LiBr/Water Absorber," *International Journal of Heat and Mass Transfer* Vol. 45(7) pp. 1445-1458.

Jernqvist, A. and H. Kockum (1996), "Simulation of Falling Film Absorbers and Generators," *International Ab-Sorption Heat Pump Conference*, Montreal, Canada, pp. 311-318.

Kang, B., Z. Zhao and D. Poulikakos (1994), "Solidification of Liquid Metal Droplets Impacting Sequentially on a Solid Surface," *Journal of Heat Transfer, Transactions ASME* Vol. 116(2) pp. 436-445.

Kapitza, P. L. (1965). Wave Flow of Thin Layers of a Viscous Fluid. *Collected Papers of P. L. Kapitza*. Oxford, Pergamon Press.

Kashiwagi, T., Y. Kurosaki and H. Shishido (1985), "Enhancement of Vapor Absorption into a Solution of Using the Marangoni Effect," *Nihon Kikai Gakkai Ronbunshu* Vol. 51(B) p. 463.

Kawae, N., T. Shigechi, K. Kanemaru and T. Yamada (1989), "Water Vapor Evaporation into Laminar Film Flow of a Lithium Bromide-Water Solution (Influence of Variable Properties and Inlet Film Thickness on Absorption Mass Transfer Rate)," *Heat Transfer Japanese Research* Vol. 18(3) pp. 58-70.

Keenan, J. H., J. Chao and J. Kaye (1983). *Gas Tables : International Version : Thermodynamic Properties of Air Products of Combustion and Component Gases Compressible Flow Functions, Including Those of Ascher H. Shapiro and Gilbert M. Edelman*. 2nd Ed. New York, Wiley.

Kelecy, F. J. and R. H. Pletcher (1997), "The Development of a Free Surface Capturing Approach for Multidimensional Free Surface Flows in Closed Containers," *Journal of Computational Physics* Vol. 138(2) p. 939.

Kelkar, K. M. and S. V. Patankar (1994), "Numerical Method for the Prediction of Two-Fluid Flows in Domains with Moving Boundaries," *Proceedings of the 1994 ASME Fluids Engineering Division Summer Meeting. Part 7 (of 18), Jun 19-23 1994*, Lake Tahoe, NV, USA, Publ by ASME, New York, NY, USA, pp. 169-176.

Keller, J. B. and M. J. Miksis (1983), "Surface Tension Driven Flows," *SIAM (Society of Industrial and Applied Mathematics) Journal of Applied Mathematics* Vol. 43 pp. 268-277.

Kholpanov, A. P., V. Y. Shkadov and N. M. Zhavoronkov (1967), "Mass Transfer in a Wavy Liquid Film," *Teor. Osnovy khim. Tekhn.* Vol. 1(1) pp. 73-75.

Kholphanov, L. P. (1987), "Heat and Mass Transfer and Fluid Mechanics in Thin Liquid Films," *Theoretical Foundations of Chemical Engineering (English Translation of Teoreticheskie Osnovy Khim)* Vol. 21(1) pp. 55-62.

Kholphanov, L. P. (1990), "Heat and Mass Transfer in Systems with a Phase Interface," *Fluid Mechanics - Soviet Research* Vol. 19(1) pp. 109-118.

Killion, J. D. and S. Garimella (2001), "A Critical Review of Models of Coupled Heat and Mass Transfer in Falling-Film Absorption," *International Journal of Refrigeration* Vol. 24(8) pp. 755-797.

Killion, J. D. and S. Garimella (2002), "Visual Documentation of Departures from Idealized Falling Films over Horizontal Tube Banks," *Proceedings of the International Sorption Heat Pump Conference*, Shanghai, China, pp. 326-334.

Killion, J. D. and S. Garimella (2003a), "Behavior of Aqueous Lithium-Bromide Drops Pendant from Horizontal Tube Banks," *Journal of Heat Transfer* Vol. Accepted for publication.

Killion, J. D. and S. Garimella (2003b), "Gravity-Driven Flow of Liquid Films and Droplets in Horizontal Tube Banks," *International Journal of Refrigeration* Vol. 26(5) pp. 516-526.

Killion, J. D. and S. Garimella (2003c), "A Review of Experimental Investigations of Absorption of Water Vapor in Liquid Films Falling over Horizontal Tubes," *HVAC&R Research* Vol. 9(2) pp. 111-136.

Kim, K. J., N. S. Berman, D. S. C. Chau and B. D. Wood (1995), "Absorption of Water Vapour into Falling Films of Aqueous Lithium Bromide," *International Journal of Refrigeration* Vol. 18(7) pp. 486-494.

Kim, K. J., N. S. Berman and B. D. Wood (1994), "Surface Tension of Aqueous Lithium Bromide + 2-Ethyl-1-Hexanol," *Journal of Chemical Engineering Data* Vol. 39(1) pp. 122-124.

Kim, K. J., N. S. Berman and B. D. Wood (1996), "The Interfacial Turbulence in Falling Film Absorption: Effects of Additives," *International Journal of Refrigeration* Vol. 19(5) pp. 322-330.

Kinnell, P. I. A. (2001), "Particle Travel Distances and Bed and Sediment Compositions Associated with Rain-Impacted Flows," *Earth Surface Processes and Landforms* Vol. 26(7) pp. 749-758.

Kirby, M. J. and H. Perez-Blanco (1994), "A Design Model for Horizontal Tube Water/Lithium Bromide Absorbers," *ASME Heat Pump and Refrigeration Systems Design, Analysis and Applications* Vol. 32 pp. 1-10.

Klein, S. A. and F. L. Alvarado (2000). *Ees-Engineering Equation Solver*, F-Chart Software, www.fchart.com.

Klinker, G. J. (1993). *A Physical Approach to Color Image Understanding*. Wellesley, Mass., A.K. Peters.

Koenig, M. S., G. Grossman and K. Gommed (1999), "Additive-Induced Enhancement of Heat and Mass Transfer in a Static Absorber: A Numerical Study," *Proceedings of the International Sorption Heat Pump Conference*, Munich, Germany, pp. 359-366.

Kothe, D. B. and R. C. Mjolsness (1992), "Ripple: A New Model for Incompressible Flows with Free Surfaces," *AIAA Journal* Vol. 30(11) pp. 2694-2700.

Kowalewski, T. A. (1996), "On the Separation of Droplets from a Liquid Jet," *Fluid Dynamics Research* Vol. 17(3) pp. 121-145.

Kulankara, S. and K. E. Herold (2000), "Theory of Heat/Mass Transfer Additives in Absorption Chillers," *International Journal of Heating, Ventilating, Air Conditioning and Refrigeration Research* Vol. 6(4) pp. 369-380.

Kulankara, S. and K. E. Herold (2002), "Surface Tension of Aqueous Lithium Bromide with Heat/Mass Transfer Enhancement Additives: The Effect of Additive Vapor Transport," *International Journal of Refrigeration* Vol. 25(3) pp. 383-389.

Kulankara, S., V. S. and K. E. Herold (1999), "Theory of Heat/Mass Transfer Additives in Absorption Chillers," *ASME Advanced Energy Systems Division*, pp. 199-206.

Kumar, R. and N. R. Kuloor (1970), "The Formation of Bubbles and Drops," *Advances in Chemical Engineering* Vol. 8 pp. 255-368.

Kyung, I. S. and K. E. Herold (2000), "Experimental Investigation of Absorber Performance with and without 2-Ethyl-Hexanol in H2o-LiBr Absorption Cycle," *Proceedings of the 34th National Heat Transfer Conference*, Pittsburgh, PA, ASME

Kyung, I.-S. and K. E. Herold (2002), "Performance of Horizontal Smooth Tube Absorber with and without 2-Ethyl-Hexanol," *Journal of Heat Transfer* Vol. 124(1) pp. 177-183.

Lee, R. J., R. M. DiGuilio, S. M. Jeter and A. S. Teja (1990), "Properties of Lithium Bromide-Water Solutions at High Temperatures and Concentrations - Part Ii: Density and Viscosity," *ASHRAE Transactions* Vol. 86 pp. 220-226.

Lesser, M. B. (1981), "Analytic Solutions of Liquid-Drop Impact Problems," *Proceedings of the Royal Society of London. Series A, Mathematical and Physical Sciences* Vol. 377(1770) pp. 289-308.

Levin, Z. and P. V. Hobbs (1971), "Splashing of Water Drops on Solid and Wetted Surfaces, Hydrodynamics and Charge Separation," *Phil Trans Roy Soc London Ser A. Math Phys Sci* Vol. 269(1200) pp. 555-585.

Loehr, K. F. (1990). *Doctoral Dissertation: Etalement Et Éclatement De Gouttes*. Paris 6, Université Pierre et Marie Curie.

Lu, Z., D. Li, S. Li and B. Yu-Chi (1996), "A Semi-Empirical Model of the Falling Film Absorption Outside Horizontal Tubes," *International Ab-Sorption Heat Pump Conference*, pp. 473-480.

Mariotte, E. (1686). *Traite' Du Mouvement Des Eaux Et Des Autres Corps Fluids*. Paris, E. Michallet.

McNeely, L. A. (1979), "Thermophysical Properties of Aqueous Solutions of Lithium Bromide," *ASHRAE Transactions* Vol. 85(413-434).

Meacham, J. M. and S. Garimella (2002), "Experimental Demonstration of a Prototype Microchannel Absorber for Space-Conditioning Systems," *Proceedings of the International Sorption Heat Pump Conference*, Shanghai, China

Michaels, C. and S. L. Goren (1987), "Aerosol Capture in Particle Laden Granular Beds in the Impaction Dominated Regime," *Aerosol Science and Technology* Vol. 7(1) pp. 31-46.

Middleman, S. (1995). *Modeling Axisymmetric Flows : Dynamics of Films, Jets, and Drops*. San Diego, Academic Press.

Miller, W. A. (1998). *The Experimental Analysis of Aqueous Lithium Bromide Vertical Falling Film Absorption*. Knoxville, University of Tennessee.

Miller, W. A. (1999), "The Synergism between Heat and Mass Transfer Additive and Advanced Surfaces in Aqueous LiBr Horizontal Tube Absorbers," *International Sorption Heat Pump Conference*, Munich, Germany, pp. 307-321.

Miller, W. A. and M. Keyhani (1999), "The Experimental Analysis of Local Heat and Mass Transfer Data for Vertical Falling Film Absorption," *Proceedings of the ASME Advanced Energy Systems Division*, 1999 ASME International Mechanical Engineering Conference and Exposition, Nashville, TN, pp. 189-197.

Morioka, I. and M. Kiyota (1991), "Absorption of Water Vapor into a Wavy Film of an Aqueous Solution of LiBr," *JSME International Journal Series II* Vol. 34(2) pp. 183-188.

Morioka, I., M. Kiyota and R. Nakao (1993), "Absorption of Water Vapor into a Film of Aqueous Solution of LiBr Falling Along a Vertical Pipe," *JSME International Journal Series B* Vol. 36(2) pp. 351-356.

Mudawar, I. and R. A. Houpt (1993), "Measurement of Mass and Momentum Transport in Wavy-Laminar Falling Liquid Films," *International Journal of Heat and Mass Transfer* Vol. 36(17) pp. 4151-4162.

Mundo, C., M. Sommerfeld and C. Tropea (1995), "Droplet-Wall Collisions: Experimental Studies of the Deformation and Breakup Process," *International Journal of Multiphase Flow* Vol. 21(2) pp. 151-173.

Nagaoka, Y., N. Nishiyama, K. Ajisaka, O. Kawamata and T. Tadaki (1987a), "Study on Heat Transfer Tubes for an Absorber of the Absorption Refrigerator," *24th National Heat Transfer Symposium of Japan (in Japanese)*, pp. 507-509.

Nagaoka, Y., N. Nishiyama, K. Ajisaka and M. Nakamura (1987b), "Absorber of Absorption Refrigeration Machine (Enhancement of Heat and Mass Transfer in Falling Film Absorbers by Surface Configuration)," *XVIIth International Congress of Refrigeration*, pp. 990-995.

Nakoryakov, V. E. and N. I. Grigor'eva (1977), "Combined Heat and Mass Transfer During Absorption in Drops and Films," *Journal of Engineering Physics* Vol. 32(3) pp. 243-247.

Nakoryakov, V. E. and N. I. Grigor'eva (1980), "Calculation of Heat and Mass Transfer in Nonisothermal Absorption of the Initial Portion of a Downflowing Film," *Theoretical Foundations of Chemical Engineering (English Translation of Teoreticheskie Osnovy Khim)* Vol. 14(4) pp. 483-488.

Nakoryakov, V. E. and N. I. Grigor'eva (1995), "Heat and Mass Transfer in Film Absorption with Varying Liquid-Phase Volume," *Theoretical Foundations of Chemical Engineering (English Translation of Teoreticheskie Osnovy Khim)* Vol. 29(3) pp. 223-228.

Nakoryakov, V. E. and N. I. Grigoryeva (1992), "Heat and Mass Transfer in Film Absorption," *Russian Journal of Engineering Thermophysics* Vol. 2 pp. 1-16.

Nakoryakov, V. Y., N. S. Bufetov and N. I. Grigor'yeva (1982a), "Heat and Mass Transfer in Film Absorption," *Fluid Mechanics - Soviet Research* Vol. 11(3) pp. 97-115.

Nakoryakov, V. Y., A. P. Burdukov, N. S. Bufetov, N. I. Grigor'eva and A. R. Dorokhov (1982b), "Coefficient of Heat and Mass Transfer in Falling Wavy Liquid Films," *Heat Transfer - Soviet Research* Vol. 14(3) pp. 6-11.

Nakoryakov, V. Y. and N. I. Grigor'yeva (1980), "Combined Heat and Mass Transfer in Film Absorption," *Heat Transfer Soviet Research* Vol. 12(3) pp. 111-117.

Nearing, M. A. and J. M. Bradford (1987), "Relationships between Waterdrop Properties and Forces of Impact," *Soil Science Society of America Journal* Vol. 51(2) pp. 425-430.

Nearing, M. A., J. M. Bradford and R. D. Holtz (1986), "Measurement of Force vs. Time Relations for Waterdrop Impact," *Soil Science Society of America Journal* Vol. 50(6) pp. 1532-1536.

Nomura, T., N. Nishimura, S. Wei, S. Yamaguchi and R. Kawakami (1993), "Heat and Mass Transfer Mechanism in the Absorber of Water/LiBr Conventional Absorption Refrigerator: Experimental Examination by Visualized Model," *International Absorption Heat Pump Conference*, New Orleans, Louisiana, The Advanced Energy Systems Division, ASME, pp. 203-208.

Notz, P. K., A. U. Chen and O. A. Basaran (2001), "Satellite Drops: Unexpected Dynamics and Change of Scaling During Pinch-Off," *Physics of Fluids* Vol. 13(3) pp. 549-552.

Nusselt, W. D. o. d. W., " VDI Zeitschrift, Vol. 60, pp. 541-546, 569-575. (1916), "Die Oberflaechenkondensateion Des Wasserdampfes," *VDI Zeitschrift* Vol. 60 pp. 541-546, 569-575.

Office of Energy Efficiency and Renewable Energy (2003). 2002 Buildings Energy Databook. U.S. Department of Energy. http://buildingsdatabook.eren.doe.gov, 112 p.

Oguz, H. N. and A. Prosperetti (1993), "Dynamics of Bubble Growth and Detachment from a Needle," *Journal of Fluid Mechanics* Vol. 257 pp. 111-145.

Papageorgiou, D. T. (1995), "On the Breakup of Viscous Liquid Threads," *Physics of Fluids* Vol. 7(7) p. 1529.

Patnaik, V. and H. Perez-Blanco (1993), "A Counterflow Heat-Exchanger Analysis for the Design of Falling-Film Absorbers," *ASME International Absorption Heat Pump Conference*, pp. 209-216.

Patnaik, V. and H. Perez-Blanco (1996a), "Roll Waves in Falling Films: An Approximate Treatment of the Velocity Field," *International Journal of Heat and Fluid Flow* Vol. 17(1) pp. 63-70.

Patnaik, V. and H. Perez-Blanco (1996b), "A Study of Absorption Enhancement by Wavy Film Flows," *International Journal of Heat and Fluid Flow* Vol. 17(1) pp. 71-77.

Patnaik, V., H. Perez-Blanco and W. A. Ryan (1993), "A Simple Analytical Model for the Design of Vertical Tube Absorbers," *ASHRAE Transactions* Vol. 99(2) pp. 69-80.

Peck, B. and L. Sigurdson (1994), "The Three-Dimensional Vortex Structure of an Impacting Water Drop," *Physics of Fluids* Vol. 6(2) pp. 564-576.

Peck, B. and L. Sigurdson (1995), "Vortex Ring Velocity Resulting from an Impacting Water Drop," *Experiments in Fluids* Vol. 18(5) pp. 351-357.

Peck, B., L. Sigurdson, B. Faulkner and I. Buttar (1995), "Apparatus to Study Drop-Formed Vortex Rings," *Measurement Science & Technology* Vol. 6(10) p. 1538.

Penev, V., S. V. Krylov, C. H. Boyadjiev and V. P. Vorotilin (1968), "Wavy Flow of Thin Liquid Film," *International Journal of Heat and Mass Transfer* Vol. 15 pp. 1389-1406.

Peregrine, D. H., G. Shoker and A. Symon (1990), "The Bifurcation of Liquid Bridges," *Journal of Fluid Mechanics* Vol. 212 pp. 25-39.

Photron USA Inc. San Diego, CA; Distributed by Motion Engineering Company, www.motionengineering.com, Indianapolis, Indiana, www.photron.com.

Pitts, E. (1974), "The Stability of Pendant Liquid Drops. Part 2. Axial Symmetry," *Journal of Fluid Mechanics* Vol. 63 pp. 487-508.

Plateau, J. (1849), *Acad. Sci. Bruxelles Mem.* Vol. 23(5).
Prosperetti, A. and H. N. Oguz (1993), "Impact of Drops on Liquid Surfaces and the Underwater Noise of Rain," *Annual Review of Fluid Mechanics* Vol. 25 p. 577.
Pumphrey, H. C. and P. A. Elmore (1990), "Entrainment of Bubbles by Drop Impacts," *Journal of Fluid Mechanics* Vol. 220 pp. 539-567.
Qiao, Y. M. and S. Chandra (1998), "Spray Cooling Enhancement by Addition of a Surfactant," *Journal of Heat Transfer, Transactions ASME* Vol. 120(1) pp. 92-98.
Rayleigh, L., J. W. S. (1879a), *Proceedings of the London Mathematics Society* Vol. 10 p. 4.
Rayleigh, L., J. W. S. (1879b), *Proceedings of the Royal Society of London: A* Vol. 29 p. 94.
Rein, M. (1993), "Phenomena of Liquid Drop Impact on Solid and Liquid Surfaces," *Fluid Dynamics Research* Vol. 12(2) pp. 61-93.
Reynolds, O. (1881), "On the Floating of Drops on the Surface of Water Depending Only on the Purity of the Surface," *Proceedings of the Manchester Literary and Philosophical Society*, Manchester, England, (also in Reynolds, O. (1900) Papers on mechanical and physical subjects 1870-1880. Collected Work, Volume I, 413-414, Cambridge University Press)
Richards, J. R. (1994). *Doctoral Thesis: Fluid Mechanics of Liquid-Liquid Systems*. Chemical Engineering, University of Delaware p. 241.
Richards, J. R., A. N. Beris and A. M. Lenhoff (1995), "Drop Formation in Liquid-Liquid Systems before and after Jetting," *Physics of Fluids* Vol. 7(11) pp. 2617-2630.
Rider, W. J. and D. B. Kothe (1998), "Reconstructing Volume Tracking," *Journal of Computational Physics* Vol. 141(2) p. 112.
Rieber, M. and A. Frohn (1999), "Numerical Study on the Mechanism of Splashing," *International Journal of Heat and Fluid Flow* Vol. 20(5) pp. 455-461.
Rodriguez, F. and R. Mesler (1985), "Some Drops Don't Splash," *Journal of Colloid and Interface Science* Vol. 106(2) pp. 347-352.
Rodriguez, F. and R. Mesler (1988), "Penetration of Drop-Formed Vortex Rings into Pools of Liquid," *Journal of Colloid and Interface Science* Vol. 121(1) pp. 121-129.
Rudman, M. (1997), "Volume-Tracking Methods for Interfacial Flow Calculations," *International Journal for Numerical Methods in Fluids* Vol. 24(7) pp. 671-691.
Rudman, M. (1998), "Volume-Tracking Method for Incompressible Multifluid Flows with Large Density Variations," *International Journal for Numerical Methods in Fluids* Vol. 28(2) pp. 357-378.
Ruheman, M. (1947), "The Transfer of Heat and Matter in an Ammonia Absorber," *Transactions of the Institute of Chemical Engineers* pp. 17-20.
Russ, J. C. (2002). *The Image Processing Handbook*. 4th Ed. Boca Raton, Fla., CRC Press.
Rutland, D. F. and G. J. Jameson (1971), *Journal of Fluid Mechanics* Vol. 46(Reproduced in Eggers, 1997, "Nonlinear Dynamics and Breakup of Free-Surface Flows, Reviews of Modern Physics, Vol. 69, pp. 865-929) p. 267.
Sabir, H., K. O. Suen and G. A. Vinnicombe (1996), "Investigation of Effects of Wave Motion on the Performance of a Falling Film Absorber," *International Journal of Heat and Mass Transfer* Vol. 39(12) pp. 2463-2472.
Savart, F. (1833), *Annal. Chim.* Vol. 53 p. 337 (with additional plates in Vol 354).
Scheele, G. F. and B. J. Meister (1968), "Drop Formation at Low Velocities in Liquid-Liquid Systems: Part 1. Prediction of Drop Volume," *AIChE Journal* Vol. 14(1) pp. 9-19.
Schulkes, R. M. S. M. (1994), "The Evolution and Bifurcation of a Pendant Drop," *Journal of Fluid Mechanics* Vol. 278 pp. 83-100.
Seul, M., L. O'Gorman and M. J. Sammon (2000). *Practical Algorithms for Image Analysis : Description, Examples, and Code*. Cambridge, U.K. ; New York, Cambridge University Press.
Shi, X. D., M. P. Brenner and S. R. Nagel (1994), "Cascade of Structure in a Drop Falling from a Faucet," *Science* Vol. 265(5169) p. 219.

Shin, J. and T. A. McMahon (1990), "The Tuning of a Splash," *Physics of Fluids* Vol. 2(8) pp. 1312-1317.

Shultz, K. (2001). *Personal Communication: Description of the Trane Horizontal Tube LiBr Absorber Test Apparatus*. LaCrosse, WI, Trane, a business of American Standard Companies.

Sigurdson, L. and B. Peck (1994), "Three-Dimensional Transition of the Vorticity Created by an Impacting Water Drop," *Proceedings of the 1994 5th European Turbulence Conference, Jul 5-8 1994*, Siena, Italy, p. 470.

Sobel, I. E. (1970). *Doctoral Thesis: Camera Models and Machine Perception*. Dept. of Electrical Engineering. Palo Alto, Stanford University pp. 89 (also in Stanford Computer Science Dept. Artificial Intelligence Laboratory. AIM-121 technical report).

Stow, C. D. and M. G. Hadfield (1981), "An Experimental Investigation of Fluid Flow Resulting from the Impact of a Water Drop with an Unyielding Dry Surface," *Proceedings of the Royal Society of London. Series A, Mathematical and Physical Sciences* Vol. 373(1755) pp. 419-441.

Stultz, D. and Stultz Photography (2003). *Water Drop for Harrison Advertising*. Chicago, IL, http://www.stultzphoto.com/water_drop_.htm (date retrieved: June 16, 2003).

Sundaram, A. (1992), "Influence of Surfactant Concentration on Foliar Retention of Pesticides Used in Forestry," *Journal of Environmental Science and Health, Part B: Pesticides, Food Contaminants, and Agricultural Wastes* Vol. 27(5) pp. 591-620.

Sundaram, A. and K. M. S. Sundaram (1991), "Role of Physical Factors on Pesticide Performance in Foresty: An Overview," *Journal of Environmental Science and Health, Part B: Pesticides, Food Contaminants, and Agricultural Wastes* Vol. 26(1) pp. 115-146.

Sundaram, A., K. M. S. Sundaram, J. W. Leung and L. Sloane (1994), "Droplet Size Spectra and Deposits of Two Aerially Sprayed Bacillus Thuringiensis Formulations on Artificial Samplers and Live Foliage," *Journal of Environmental Science and Health, Part B: Pesticides, Food Contaminants, and Agricultural Wastes* Vol. 29(4) pp. 697-738.

Sussman, M., E. Fatemi, P. Smereka and S. Osher (1998), "Improved Level Set Method for Incompressible Two-Phase Flows," *Computers & Fluids* Vol. 27(5-6) pp. 663-680.

Sussman, M., P. Smereka and S. Osher (1994), "A Level Set Approach for Computing Solutions to Incompressible Two-Phase Flow," *Journal of Computational Physics* Vol. 114(1) pp. 146-159.

Suzuki, T., K. Mitachi and A. Fukuda (1998), "Numerical Analysis of Free Surface Motion Ensuing Burst of Bubble Dome," *Proceedings of the 1998 ASME/JSME Joint Pressure Vessels and Piping Conference, Jul 26-30 1998*, San Diego, CA, USA, ASME, Fairfield, NJ, USA, pp. 235-241.

Taghavi-Tafreshi, K. and V. K. Dhir (1980), "Taylor Instability in Boiling, Melting and Condensation or Evaporation," *International Journal of Heat and Mass Transfer* Vol. 23 p. 1433.

Takle, E. S. (2003). *Global Change Course*, Iowa State University, http://www.iitap.iastate.edu/gccourse/ (date retrieved: June 16, 2003).

Tannehill, J. C., D. A. Anderson and R. H. Pletcher (1997). *Computational Fluid Mechanics and Heat Transfer*. 2nd Ed. Washington, DC, Taylor & Francis.

The Mathworks Inc. (2002a). *Matlab Spline Toolbox, Ver. 3.1.1*. Natick, MA, Matlab Version 6.5.0.180913a Release 13.

The Mathworks Inc. (2002b). *Matlab Version 6.5.0.180913a Release 13*. Natick, MA, http://www.mathworks.com (date retrieved: June 16, 2003).

Thomson, J. J. and H. F. Newall (1885), "On the Formation of Vortex Rings by Drops Falling into Liquids, and Some Allied Phenomena," *Proceedings of the Royal Society of London* Vol. 39 pp. 417-436.

Thoroddsen, S. T. and J. Sakakibara (1998), "Evolution of the Fingering Pattern of an Impacting Drop," *Physics of Fluids* Vol. 10(6) pp. 1359-1374.

Tropea, C. and M. Marengo (1999), "Impact of Drops on Walls and Films," *Multiphase Science and Technology* Vol. 11(1) pp. 19-36.

Tsai, B. and H. Perez-Blanco (1998), "Limits of Mass Transfer Enhancement in Lithium Bromide-Water Absorbers by Active Techniques," *International Journal of Heat and Mass Transfer* Vol. 41(15) pp. 2409-2416.

Tsvelodub, O. Y. (1989), "Nonisothermal Absorption of a Gaseous Impurity in a Wavy Liquid Film," *Soviet Journal of Applied Physics* Vol. 3(4) pp. 54-59.

Uddholm, H. and F. Setterwall (1988), "Model for Dimensioning a Falling Film Absorber in an Absorption Heat Pump," *International Journal of Refrigeration* Vol. 11 pp. 41-45.

Unverdi, S. O. and G. Tryggvason (1992a), "Computations of Multi-Fluid Flows," *Physica D: Nonlinear Phenomena*

Proceedings of the 11th Annual International Conference of the Center for Nonlinear Studies, May 20-24 1991 Vol. 60(1-4) p. 70.

Unverdi, S. O. and G. Tryggvason (1992b), "A Front Tracking Method for Viscousm Incompressible Multi-Fluid Flows," *Journal of Computation Physics* Vol. 100 p. 25.

van der Wekken, B. J. C. and R. H. Wassenaar (1988), "Simultaneous Heat and Mass Transfer Accompanying Absorption in Laminar Flow over a Cooled Wallx," *Int. J. Refrig.* Vol. 11 pp. 70-77.

Verelst, J. and J. Berghmans (1981), "Surface Tension Effects During Condensation on a Horizontal Tube," *20th Joint ASME/AIChE National Heat Transfer Conference*, Milwaukee, Wisconsin, American Society of Mechanical Engineers, Heat Transfer Division, 81-HT-26, p. 7.

Vliet, G. C. and F. Cosenza (1991), "Absorption Phenomena in Water-Lithium Bromide Films," *Japanese Absorption Heat Pump Conference*, Tokyo, Japan

Walzel, P. (1980), "Zerteilgrenze Beim Tropfenprall (in German)," *Chem,-Ing.-Tech.* Vol. 52(4) pp. 338-339.

Wang, H.-C. and G. Kasper (1991), "Filtration Efficiency of Nanometer-Size Aerosol Particles," *Journal of Aerosol Science* Vol. 22(1) pp. 31-41.

Wang, K. (1996), "An Experimental Study of Heat and Mass Transfer for Absorption of LiBr Solution Film Falling over Horizontal Circular Tubes," *1995 International Conference on Energy and Environment, ICEE*, Shanghai, China, Begell House Inc. New York, NY, pp. 304-309.

Wasden, F. K. and A. E. Dukler (1989), "Insights into the Hydrodynamics of Free Falling Wavy Films," *AIChE Journal* Vol. 35(9) pp. 1379-1390.

Wasden, F. K. and A. E. Dukler (1990), "A Numerical Study of Mass Transfer in Free Falling Waves," *AIChE Journal* Vol. 36(9) pp. 1379-1390.

Wassenaar, R. H. (1996), "Measured and Predicted Effect of Flowrate and Tube Spacing on Horizontal Tube Absorber Performance," *International Journal of Refrigeration* Vol. 19(5) pp. 347-355.

Wassenaar, R. H. and J. J. W. Westra (1992), "Dynamic Model of a Film Absorber with Coupled Heat and Mass Transfer," *International Journal of Heat and Mass Transfer* Vol. 35(1) pp. 87-99.

Weiss, D. A. and A. L. Yarin (1999), "Single Drop Impact onto Liquid Films: Neck Distortion, Jetting, Tiny Bubble Entrainment and Crown Formation," *Journal of Fluid Mechanics* Vol. 385 pp. 229-254.

Wilkes, E. D., S. D. Phillips and O. A. Basaran (1999), "Computational and Experimental Analysis of Drop Formation," *Physics of Fluids* Vol. 11(12) pp. 3577-3860.

Worthington, A. M. (1881), "On Pendent Drops," *Proceedings of the Royal Society of London* Vol. 32 pp. 362-377.

Worthington, A. M. (1908). *A Study of Splashes*. London, New York, Bombay, Calcutta, Longmans Green and Co.

Yang, R. and D. Jou (1993), "Heat and Mass Transfer on the Wavy Film Absorption Process," *Canadian Journal of Chemical Engineering* Vol. 71 pp. 533-538.

Yang, R. and D. Jou (1995), "Heat and Mass Transfer of Absorption Process for the Falling Film inside a Porous Medium," *International Journal of Heat and Mass Transfer* Vol. 38(6) pp. 1121-1126.

Yang, R., D. Jou and J. H. Chen (1991), "Numerical Study of Heat and Mass Transfer on the Wavy Film Absorption Process," *Intersociety Energy Conversion Engineering Conference*, pp. 559-565.

Yang, R. and B. D. Wood (1992), "A Numerical Modeling of an Absorption Process on a Liquid Falling Film," *Solar Energy* Vol. 48(3) pp. 195-198.

Yao, W., H. Bjurström and F. Setterwall (1991), "Surface Tension of Lithium Bromide Solutions with Heat-Transfer Additives," *Journal of Chemical Engineering Data* Vol. 36(1) pp. 96-98.

Yarin, A. L. (1993). *Free Liquid Jets and Films: Hydrodynamics and Rheology*, Longman Publishing Group.

Yarin, A. L. and D. A. Weiss (1995), "Impact of Drops on Solid Surfaces: Self-Similar Capillary Waves, and Splashing as a New Type of Kinematic Discontinuity," *Journal of Fluid Mechanics* Vol. 283 pp. 141-173.

Yoshikawa, T., Y. Murai and F. Yamamoto (1997), "Numerical and Experimental Investigations of Bursting Bubble on Free Surface," *Proceedings of the 1997 ASME Fluids Engineering Division Summer Meeting, FEDSM'97. Part 13 (of 24), Jun 22-26 1997*, Vancouver, Can, ASME, New York, NY, USA, p. 6.

Youngs, D. L. (1982). Time-Dependent Multi-Material Flow with Large Fluid Distortion. *Numerical Methods for Fluid Dynamics*. K. W. Morton and M. J. Baines, Academic Press.

Zhang, D. F. and H. A. Stone (1997), "Drop Formation in Viscous Flows at a Vertical Capillary Tube," *Physics of Fluids* Vol. 9(8) pp. 2234-2242.

Zhang, X. (1999a), "Dynamics of Drop Formation in Viscous Flows," *Chemical Engineering Science* Vol. 54 pp. 1759-1774.

Zhang, X. (1999b), "Dynamics of Growth and Breakup of Viscous Pendant Drops into Air," *Journal of Colloid and Interface Science* Vol. 212(1) pp. 107-122.

Zhang, X. and O. A. Basaran (1995), "An Experimental Study of Dynamics of Drop Formation," *Physics of Fluids* Vol. 7(6) pp. 1184-1203.

Zhbankova, S. L. and A. V. Kolpakov (1990), "Collision of Water Drops with a Plane Water Surface," *Fluid Dynamics (English Translation of Izvestiya Akademii Nauk SSSR, Mekhanika Zhidkosti i Gaza)* Vol. 25(3) pp. 470-473.

Zhuang, W. H., K. Etemadi, D. M. Benenson and N. Ashgriz (1999), "Sensitivity of the Spreading Rate of a Liquid Droplet on a Surface to the Approximation of the Contact Angle," *International Journal of Modelling and Simulation* Vol. 19(2) pp. 184-193.

Ziegler, F. and G. Grossman (1996), "Heat-Transfer Enhancement by Additives," *International Journal of Refrigeration* Vol. 19(5) pp. 301-309.

Ziegler, F., L. Hoffman, A. Beutler and G. Grossman (1999), "Heat and Mass Transfer Enhancement by Additives," *Entropie*(220/221) pp. 12-16.

APPENDIX: GEOMETRIC ANALYSIS OF SPLINES

The image processing routine, IMAN, was described in detail in section 3.3. The main result of the image analysis process is a mathematical representation of the position and shape of the liquid-vapor interface. The advantage of using a functional representation for the interface rather than simply a set of coordinates lies in the accuracy with which surfaces and volumes of revolution can be computed. Numerical integration is still used, as would be the case with a list of coordinates; however, the evaluation is performed using accurate, recursive, adaptive Simpson quadrature. The details of this technique, developed by Gander and Gautschi, are given in (Gander and Gautschi, 2000). Essentially, the "resolution" of the numerical integration is automatically increased in areas of complex behavior of the function, i.e. high curvature in this case. In this way, the integral can, within practical limits, be evaluated with any desired precision. In the present case, where the function is essentially a curve-fit of experimental data, the precision need not be exceedingly high. However for the relatively small computational expense involved, there was no strong motivation to change the tolerance from the default value of 1×10^{-6} suggested (The Mathworks Inc., 2002b) (see help for the "quad" function).

The integrands to be evaluated are combinations of the spline functions from the image analysis and, from basic principles of differential geometry, functions that result in appropriate differential surface areas and volumes for the required revolution operation. To assess the accuracy of this method, the routines were applied to spline approximations of spheres. The test case is written into the function itself so that, if called with no arguments, the test is run automatically. A complete listing of the routine can be found at the end of this appendix. Also contained in the listing is an algorithm for calculating the curvature at any point. This allowed even more rigorous evaluation of the quality of the curve fit for the test case, but is not currently utilized for evaluating arbitrary splines. It should also be noted that the values of surface area and internal volume returned by the routines are in the units of the spline (which in the case of IMAN is pixels). The calibration step is handled in the IMAN procedure (see Appendix B), not here in the analysis of the revolutions.

The heart of the technique is the functional form of the differential area and volume. (A superb resource on these topics is "Eric Weisstein's World of Mathematics" web-site, available at http://mathworld.wolfram.com/; a useful search term is surface of revolution.) Cylindrical coordinates are assumed, and the (x;y) image-coordinates of the spline are converted to/treated as (r;z). This requires determining an x-axis which may be passed as an argument to the routine along with the spline and the limits of integration. It is assumed that the axis of revolution is always vertical. When not passed as an argument, an arc-length-weighted average of the spline x-coordinates is taken to be the axis of rotation. Thus, for any x, r = abs(x-xa), where xa is the x-coordinate defining the position of the axis of rotation. In cylindrical coordinates, the differential surface area of any surface is:

$$dA = r d\Theta ds \tag{A.1}$$

where ds is the differential arc length of the curve. Since we assume axial symmetry, the integration with respect to $d\Theta$ simply results in a factor of 2π. The differential surface area is related to the x and y coordinates as follows:

$$ds = \sqrt{(dx)^2 + (dy)^2} \tag{A.2}$$

dx and dy are easily evaluated from the definition of the spline. Therefore the functional form of dA is specified as follows for use in the quadrature routine:

$$dA = 2\pi * \left[(dx)^2 + (dy)^2\right]^{0.5} * abs(x - xa) \tag{A.3}$$

which is the differential area of a circular band of a differential length along the spline. It should be noted that when revolving through 2π, the two halves of the spline are additive. Thus a factor of 0.5 must be used to convert to the average of the two halves.

In cylindrical coordinates, the differential volume is:

$$dV = r\,dr\,d\Theta\,dz \tag{A.4}$$

Again, due to axial symmetry, the integration with respect to Θ results in 2π and rdr becomes $0.5r^2$. Therefore the differential volume slice associated with a differential length along the curve is:

$$dV = \pi(x - xa)abs(x - xa)\,dy \tag{A.5}$$

Note that for dV to always be positive, due to the sign of dy in the direction of parameterization of the spline, one of the values of r must be the signed difference between x and xa while the other taken to be the absolute value.

The results of the "test case" with 20 points and no padding points (see code) are shown in Figure A.1 and listed below. In the figure, the small circles represent the control points for the spline and the solid line is the spline itself.

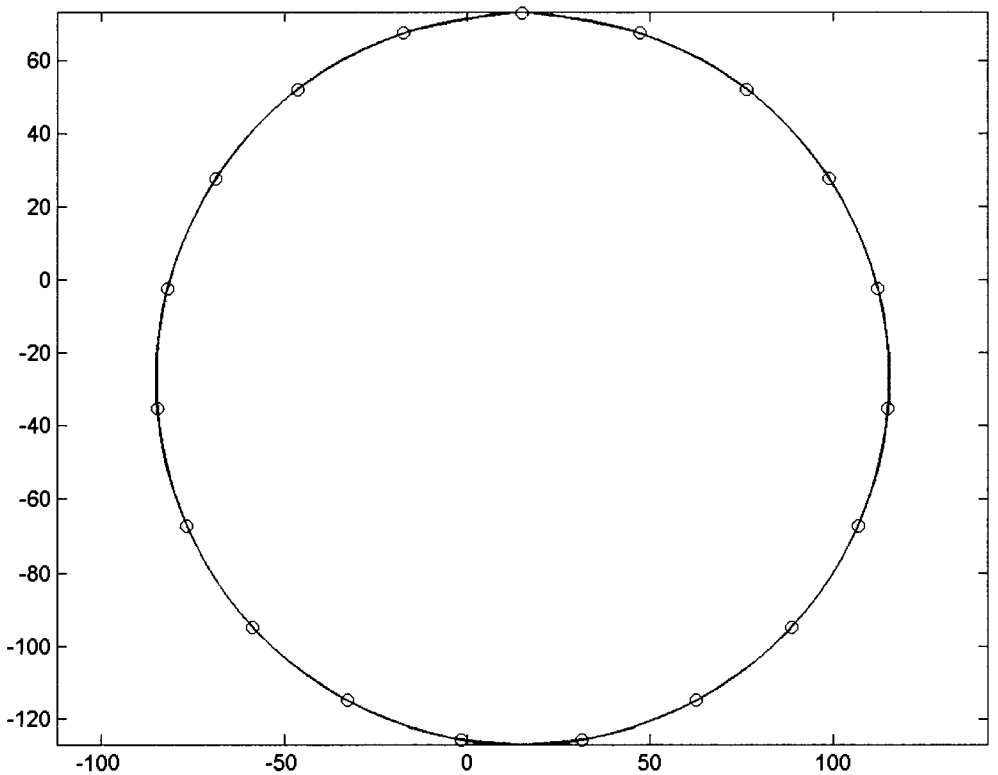

Figure A.1 Smoothing Cubic Spline Approximation to Sphere

```
percent_error_area =  -0.0657 %
percent_error_vol =  -0.1004 %
curvature analysis, exact radius, r = 100
min(r) = 87.3137
mean(r) = 108.4117
max(r) = 4.070834e+017
```

The agreement in calculated surface area and volume are clearly excellent, virtually within a tenth of a percent of the exact values. The curvature (output in terms of radius of curvature, effectively the reciprocal of curvature) does not fare as well. The reason for this can be seen near the topmost point in Figure A.1. This point represents the end-point of the spline. As the spline approaches the end points, without extra padding points, the curvature goes to zero. This appears as a slight discontinuity in slope at the top of the circle and is reflected in the maximum value of the radius of curvature. This illustrates simply that in calculating the curvature, the end points of a spline should be avoided. It is

remarkable how little this affects the computed values of surface area and volume, however, which is a fortuitous result for the technique developed here.

Below is a listing of the function "surf_analyze" which is invoked from a button press in IMAN after fitting a spline through the interface pixels in a droplet image:

```
function [sar,vol,xa] = surf_analyze(inputs)
%test volume and surface area algorithms
%
%  [sar,vol] = surf_analyze(inputs)
%
% inputs should be a structured array containing:
% inputs.spline    - definition of spline
%                    spline should return [x;y] coordinates
% inputs.arclength - array of parameters over which spline should be
%                    analyzed - range defines limits of analysis
% inputs.xa        - x-coordinate of axis of symmetry
%                    assumed that axis of sym. is a vertical line
%   if xa is not defined it will be calculated from the average of x
%   coordinates corresponding to the points in arclength
%
% sar = surface area in (spline units)^2
% vol = internal volume in (spline units)^3

if nargin
    % do couple checks of input, could expand greatly
    if isstruct(inputs)
        if ~isfield(inputs.spline,'form') | ~isfield(inputs.spline,'form') |
~isfield(inputs.spline,'form')
            %doesn't look like spline
            error('inputs.spline must contain valid spline')
        end
    else
        warning('see help surf_analyze for correct form of inputs')
        return
    end
    if ~isfield(inputs,'xa')
        xa = fnval(inputs.spline,inputs.arclength);
                xa = mean(xa');
                inputs.xa = xa(1);
        end
    test = 0;
else
    % run test case - sphere
    test = 1;
    numpts = 20; % different values used to see effect on results
        pad = 0; %can be used to add extra points and beginning and end

    % make spline control points on circle
        s = linspace(0,2*pi,numpts);
        s = [-2*pi/(numpts-1)*[pad:-1:1], s, 2*pi+2*pi/(numpts-1)*[1:pad]];
        radius = 100;
        xy=[radius*sin(s)+15 ; radius*cos(s)-27];  % offest from origin

    % create spline
```

```
        cir.points=xy;
        cir.diff = diff(cir.points')';
        cir.lengths = ([1 1]*cir.diff.^2).^0.5;
        cir.arclength = cumsum([0 cir.lengths]);

    % tried many forms of spline fit to see results, some better than
    % others
        %w = ones(size(cir.arclength));w([1 end])=100;
        %cir.spline = spaps(cir.arclength,cir.points,0.001,w,3);
        %cir.spline = csape(cir.arclength,cir.points,[0 0;0 0]); % cs with periodic ends
        %cir.spline = csape(cir.arclength,cir.points);      % cubic spline with knots on points
        %cir.spline = spapi(4,cir.arclength,cir.points);     % cubic spline with knots not on points
        inputs.spline = spaps(cir.arclength,cir.points,10);    % cubic spline approx, smoothest

        % need value for x-axis to calculate r vector
        xa = fnval(inputs.spline,linspace(0,cir.arclength(end),301));
        xa = mean(xa');
        inputs.xa = xa(1); %pass as extra argument
        inputs.arclength = cir.arclength(1+pad:end-pad);    % padded points just control shape,
                                                           % but they're not revolved
end

if test;disp('calculating surface area');end
% evaluate surface area using differential area function, da
sar = 0.5*quad(@da,inputs.arclength(1),inputs.arclength(end),[],[],inputs.spline,inputs.xa);
 % spline is on both sides so factor of 0.5 arises

if test;disp('calculating volume');end
% evaluate volume using differential volume function, dv
vol = 0.5*abs(quad(@dv,inputs.arclength(1),inputs.arclength(end),[],[],inputs.spline,inputs.xa));
 % spline is on both sides so factor of 0.5 arises

if test;disp('calculating curvature');
    kappa = curvature(inputs.spline,inputs.arclength);
end

if test  % output some extra results to screen and make a plot
        cla;plot(xy(1,:),xy(2,:),'bo');hold on;fnplt(inputs.spline,'r');axis equal
        percent_error_area = (sar-4*pi*radius^2)/(4*pi*radius^2)*100
        percent_error_vol = (vol-4/3*pi*radius^3)/(4/3*pi*radius^3)*100
        disp(['curvature analysis, exact radius, r = ' num2str(radius)])
        if min(kappa)   % no 0 curvature
                r = 1./[max(kappa) mean(kappa) min(kappa)];
        disp(['min(r) = ' num2str(r(1))])
        disp(['mean(r) = ' num2str(r(2))])
        disp(['max(r) = ' num2str(r(3))])
        %    [tmp,j]=min(kappa);
        %    disp(num2str(j/length(kappa)))
        else  % zero curvature gives infinite radius so skip
                r = 1./[max(kappa) mean(kappa)];
        disp(['min(r) = ' num2str(r(1))])
        disp(['mean(r) = ' num2str(r(2))])
        end
end
xa = inputs.xa;  % send to outputs

function out = da(t,fg,xa)
```

```
        % fg is a spline fun: fg(t) = (f(t),g(t)) = (x,y) = [x;y]
        % where t is a parameter - it's close to arc-length but not quite
        % since t was calculated point-to-point without spline curvature
        % in reality, (x,y) is (r,z)
        % differential surface area is r dtheta ds where s is arc-length
        % since r and s are independent of theta, we can do the dtheta intergral
        % which leaves SAR = integral(r ds) so r*ds is integrand
        % r is abs(f-xa)
        % ds = sqrt( (f')^2 + (g')^2 ) dt = arc length relative to parameter t

        fg_prime=fnder(fg);          % this is [f';g']
        fgs = fnval(fg,t);           % evaluated at the point(s) s
        fg_primes = fnval(fg_prime,t);
        out = 2*pi*(sum(fg_primes.*fg_primes)).^(0.5).*abs(fgs(1,:)-xa);


function out = dv(t,fg,xa)
        % fg is a spline fun: fg(t) = (f(t),g(t)) = (x,y) = [x;y]
        % where t is a parameter - it's close to arc-length but not quite
        % since t was calculated point-to-point without spline curvature
        % in reality, let (f(t),g(t))=(x,y) be (r+xa,z) of a cylindrical coord
        % differential surface area is r dtheta ds where s is arc-length
        % centered along xa, then dv = r dr dtheta dz
        % since r and s are independent of theta, we can do the dtheta intergral
        % and the r integral => 0.5*r^2
        % which leaves integrand pi*r^2*g' dt
        % r is abs(f-xa)
        % ds = sqrt( (f')^2 + (g')^2 ) dt = arc length relative to parameter t

        fg_prime=fnder(fg);                                          %
        fgs = fnval(fg,t);                                           %
        fg_primes = fnval(fg_prime,t);                               %
        out = pi*(fgs(1,:)-xa).*abs(fgs(1,:)-xa).*(fg_primes(2,:)); %


function kappa = curvature(fg,t)
        % kappa = curvature(t,fg)
        % fg is spline fuction fg(t) = (x,y)

        fg_prime=fnder(fg);
        fg_primes=fnval(fg_prime,t);
        fg_pps=fnval(fnder(fg_prime),t);
        kappa = -(fg_primes(1,:).*fg_pps(2,:)-
        fg_primes(2,:).*fg_pps(1,:))./(sum(fg_primes.^2)).^(3/2);
```